



FACULTEIT LANDBOUWKUNDIGE EN  
TOEGEPASTE BIOLOGISCHE  
WETENSCHAPPEN



---

Academiejaar 2001-2002

# MODELLING FOR OPTIMISATION OF BIOFILM WASTEWATER TREATMENT PROCESSES: A COMPLEXITY COMPROMISE

## MODELBOUW VOOR OPTIMALISATIE VAN BIOFILM- WATERZUIVERINGSPROCESSEN: EEN COMPLEXITEITSCOMPROMIS

door

**ir. Henk VANHOOREN**

Thesis submitted in fulfilment of the requirements  
for the degree of Doctor (Ph.D.) in Applied Biological Sciences

Proefschrift voorgedragen tot het bekomen van de graad  
van Doctor in de Toegepaste Biologische Wetenschappen

op gezag van

Rector: **Prof. Dr. ir. J. WILLEMS**

Decaan:

**Prof. Dr. ir. O. VAN CLEEMPUT**

Promotor:

**Prof. Dr. ir. P.A. VANROLLEGHEM**



The author and the promotor give the authorisation to consult and to copy parts of this work for personal use only. Any other use is limited by the Laws of Copyright. Permission to reproduce any material contained in this work should be obtained from the author.

De auteur en de promotor geven de toelating dit doctoraatswerk voor consultatie beschikbaar te stellen en delen ervan te kopiëren voor persoonlijk gebruik. Elk ander gebruik valt onder de beperkingen van het auteursrecht, in het bijzonder met betrekking tot de verplichting uitdrukkelijk de bron te vermelden bij het aanhalen van de resultaten van dit werk.

De promotor:

De auteur:

Prof. Dr. ir. Peter Vanrolleghem

ir. Henk Vanhooren



# Woord vooraf

---

Jawel, er komt veel kijken bij een doctoraat. Vooral op het einde moeten er zoveel kleine dingen geregeld worden dat je haast zou vergeten dat aan dit stukje proza vier jaar voorafgegaan zijn. Of moet ik zeggen vijf...? Ik herinner me immers als de dag van gisteren dat Bob en ik op zoek gingen naar een onderwerp voor onze ingenieursthesis bij Peter Vanrolleghem. Peter was toen nog vrij “vers” in de job van doctorassistent. Wij waren inderdaad de eerste lichting die van hem oefeningen procesregeling te slikken kregen. Na die traumatische ervaring getuigde het zoeken naar een thesisonderwerp aan diezelfde vakgroep natuurlijk van pure doodsverachting. Maar goed, de modelmicrobe had ons gebeten en dus...

Nadat we Peter hadden weten te strikken voor een gesprek en een onderwerp hadden vastgelegd, kwamen we terecht in een kleine maar leuke groep mensen die zichzelf BIOMATH had gedoopt. De vrouwelijke kant van de maatschappij werd vertegenwoordigd door Britta en verder waren er Filip, Filip, Bas en Hans. Ook Geert was er, al viel die nauwelijks op in zijn minuscuul hoekje tussen de AD5 en de AD10. Deze ploeg heeft zowat het fundament gelegd voor mijn interesse voor modellering, controle en niet te vergeten ... unix-systeembeheer. Tijdens mijn thesis en later, tijdens de eerste jaren van mijn doctoraat, heb ik hen ontelbare keren lastiggevallen met mijn vragen. Ik kan me niet een keer herinneren dat er geen tijd gemaakt werd om te overleggen en te antwoorden. Daarvoor ben ik deze mensen heel dankbaar.

Na deze eerste periode is BIOMATH vrijwel uit zijn voegen gearsten. Het zou te ver leiden om alle personen die op een of andere manier met dit werk te maken hebben, op te noemen. Toch wil ik enkele mensen speciaal bedanken. De samenwerking met Geert bij het ontwerpen en het bouwen van de pilootinstallatie was fantastisch en gelukkig had ik Lieven om mij de weg te wijzen bij het interpreteren van de titraties. Verder zijn er ook de mensen van EPAS en Janssen Pharmaceutica: hun hulp bij de meetcampagnes was onontbeerlijk.

Helemaal los van het onderzoek, moet ik ook een woordje van dank richten aan Martijn en Bart met wie ik het roemruchte A-team vormde. Jawel, ze kunnen ons misschien nabootsen, maar evenaren zullen ze nooit! In feite heeft dit team nog een ferme taart tegoed, maar wie had ons dat ook alweer beloofd?

En dan waren er natuurlijk nog de thesisstudenten: Frederik, Tom, Patrick, Diedert en Dirk en daarnaast Nancy uit Quebec en Annalisa uit Cagliari. Zij hebben een onmisbare bijdrage geleverd aan dit werk. Zelfs het benchmark-werk van Diedert is zeer waardevol gebleken, hoewel dat oorspronkelijk niet te verwachten was. Inderdaad, een benchmark voor de simulatie van actief slibsystemen heeft op het eerste gezicht niets te maken met biofilms, maar toch was dit precies een van de leukste projecten uit mijn BIOMATH-tijd. De buitenlandse verplaatsingen, namelijk mijn verblijf in Ottawa en de COST-meetings hebben mijn blik op de (model- en controle)wereld verruimd en hebben ervoor gezorgd dat ik heel wat boeiende mensen ontmoet heb. Hiervoor wil ik Peter toch eens speciaal bedanken.

Natuurlijk moet ik Peter voor nog heel wat dingen bedanken, niet in het minst omdat hij mij de kans gaf dit doctoraat te beginnen en te voltooien bij BIOMATH. Soms is zijn enthousiasme misschien wat overweldigend en moet je zijn vele voorstellen en ideeën een beetje in toom houden. Aan de andere kant krijg je wel de gelegenheid om enorm veel verschillende facetten van labotesten, meettechnieken, modellen en controle te leren kennen.

En geleerd heb ik, met vallen en opstaan. Vooral in de lente van 1999 deed het even pijn. Nooit gedacht dat ik zo'n moeite zou hebben met het idee "ziek te zijn". Maar alles went en heeft zijn positieve kant. Ik denk dat ik mezelf en mijn grenzen nu veel beter ken dan voordien. Ik ben heel veel dank verschuldigd aan de mensen die mij in die zoektocht geholpen en gesteund hebben. Daarbij denk ik dan vooral aan mijn vrienden van het KUC, mijn familie en schoonfamilie en natuurlijk aan Els. Zonder haar liefde en steun was dit, zeker weten, niet gelukt.

Gent, november 2001

Henk

# Contents

---

<b>1</b>	<b>Introduction and problem statement</b>	<b>1</b>
<b>2</b>	<b>Literature review</b>	<b>5</b>
2.1	Introduction	5
2.2	Overview of the different biofilm reactor types	6
2.3	Mass transport in biofilm systems	9
2.4	Kinetics of microbial conversions in biofilms	13
2.5	Modelling of biofilm systems	16
1.6	In situ parameter estimation in biofilm systems	36
1.7	Aim of this thesis	45
<b>3</b>	<b>WEST: Modelling biological wastewater treatment</b>	<b>47</b>
3.1	Modelling wastewater treatment: benefits and practical use	47
3.2	Introducing the WEST modelling and simulation environment	48
3.3	The model specification language MSL-USER	50
3.4	Building the model base	52
3.5	The modelling environment: building a graphical configuration and a coupled model	65
3.6	Parsing from MSL-USER to MSL-EXEC	68
3.7	Working with the model: the experimentation environment	70
3.8	Conclusions	72
<b>4</b>	<b>A simplified mixed-culture biofilm model</b>	<b>75</b>
4.1	Introduction	75
4.2	General modelling concept	76
1.3	Diffusion limitation in a multiple substrate/species system	80
1.4	Description of biokinetic processes in the biofilm - Process matrix: an example	87
1.5	Proposed parameter set	88
1.6	Extended model description	89
1.7	Conclusions	101
<b>5</b>	<b>Development and characterisation of a pilot-scale trickling filter</b>	<b>103</b>
5.1	Introduction	103
5.2	Design and development	103
5.3	On-line sensors	108
5.4	Biofilm and suspended solids characterization	108
5.5	Hydraulic characterization	111
5.6	Preliminary COD removal experiments	115
5.7	Off-gas measurement results	116
5.8	Conclusions	117

<b>6</b>	<b>Monitoring off-gas O<sub>2</sub> and CO<sub>2</sub> concentrations and their use in the model description of a pilot-scale trickling filter</b>	<b>119</b>
6.1	Introduction	119
6.2	The use of off-gas analysis in wastewater treatment	119
6.3	Model extension for off-gas measurements	123
6.4	Experiment set-up	125
6.5	Results	125
6.6	Model development in WEST	128
6.7	Model description of the filter before the load shift	130
6.8	Model description of the filter after the load shift	133
1.9	Conclusions	139
<b>7</b>	<b>Induction of denitrification in a pilot-scale trickling filter by adding nitrate at high loading rate</b>	<b>141</b>
7.1	Introduction	141
7.2	Incorporation of <i>pH</i> control in the filter set-up	141
7.3	Set-up of the nitrate addition test	143
7.4	Modelling of the nitrate addition test	145
1.5	Increased conversion capacity	149
1.6	Conclusions	150
<b>8</b>	<b>Measurement and modelling of COD removal in a full-scale industrial trickling filter system</b>	<b>153</b>
8.1	Introduction	153
8.2	Description of the trickling filter plant under study	155
8.3	Design of the measurement campaign	156
8.4	Measurement campaign results	157
8.5	Dynamic biodegradation modelling	165
8.6	Phosphorus dosing	173
8.7	Conclusions	176
<b>9</b>	<b>Modelling VOC stripping in a trickling filter</b>	<b>179</b>
9.1	Introduction	179
9.2	Non-equilibrium steady-state modelling	180
9.3	Conclusions	187
<b>10</b>	<b>Performance evaluation of nitrogen removal suspended-carrier biofilm systems using dynamic simulation</b>	<b>189</b>
10.1	Introduction	189
10.2	The benchmark, an objective performance evaluation procedure	191
1.3	Reference benchmark plants	198
1.4	Attached growth processes: suspended carriers in the aerobic phase	203
1.5	Attached growth processes: suspended carriers in the complete reactor	211
1.6	Conclusions	218

<b>11</b>	<b>Conclusions and perspectives</b>	<b>219</b>
11.1	The WEST simulator	219
11.2	Mixed-culture biofilm modelling: a complexity compromise	220
11.3	Model applications in a pilot-scale trickling filter	223
11.4	Modelling a full-scale industrial trickling filter system	226
11.5	Simulation of suspended-carrier biofilm systems	228
11.6	General conclusions	230
	<b>References</b>	<b>231</b>
	<b>Notation</b>	<b>241</b>
	<b>Summary</b>	<b>245</b>
	<b>Samenvatting</b>	<b>249</b>







# 1 Introduction and problem statement

---

Biofilms are omnipresent in our environment and play an important role both in nature and in technological processes. Microorganisms attach to every surface in contact with water and can cause phenomena as corrosion, fouling of filter material, tooth decay, etc. Although biofilms are widely considered to be a plague, they are also very useful. Biofilms grow in the ocean and on riverbeds, eliminating quite some organic matter from the water. This capability of biofilms is also frequently used in water and wastewater treatment. The technology using biofilms for this goal is receiving increasing attention since a high volumetric biomass density can be obtained. Biofilm systems also have some other advantages. The older process configurations like trickling filters and rotating biological contactors are robust and need only limited maintenance and control. They are therefore well suited for small-scale wastewater treatment plants. More modern configurations like submerged filters and fluidised beds do need a well performing control system but they can offer conversion capacities beyond the ones that can be obtained in traditional activated sludge wastewater treatment.

Since the end of the 70's, models have been developed to obtain a better understanding of the structure and functioning of biofilms. A wide range of biofilm models is currently available in literature (Noguera *et al.*, 1999). In chapter 2, some of these models will be described. Many of these biofilm models are relatively complex. Not only the microbial conversion of substrate needs to be considered but also the diffusive transport of soluble substrates inside the biofilm. Early modelling approaches consequently neglected the aspect of biomass growth by assuming a predefined microbial distribution and biofilm thickness (Williamson and McCarty, 1976; Harremoës, 1978). Later on, Kissel *et al.* (1984) and Wanner and Gujer (1986) introduced a more accurate description of the system behaviour, both in time and in space, which made it possible to predict microbial species development over the depth of the biofilm as a function of substrate flux. Recent advances in biofilm research (Lewandowski *et al.*, 1994; Bishop, 1997) conclude that also the heterogeneity of the biofilm must be taken into account. Describing this quantitatively has been attempted in the revised mixed-culture biofilm model of Wanner and Reichert (1996). Very recently, also following the findings on the heterogeneity of the biofilm, 3D modelling is getting a lot of attention among biofilm researchers. These models are particularly interesting to gain understanding about how biofilms develop under different environmental conditions. Researchers intensively use them to study attachment and detachment mechanisms in biofilms and the colonisation of substrates (Picioreanu *et al.*, 1998).

Now, the question arises what the models described above can be used for. Noguera *et al.* (1999) classified the use of models into two broad categories. First of all, models can be interesting research tools. Using them, further understanding can be developed on certain phenomena such as biofilm structure, population dynamics and biofilm heterogeneity. Morgenroth *et al.* (2000) described such use of biofilm models as being qualitative. On the other hand, mathematical models can also be used as practical engineering tools. The aim of such model use is found in quantitatively describing the dynamics of a plant as good as possible. Mainly its response to influent variations is of importance. This way, off-line optimisation via scenario-analysis can be performed. A good way to use biofilm models might indeed be to give the operator of a plant an answer to practical questions on how the

plant should be operated. Models may also be helpful tools in reactor design. In this application, they are used to predict full-scale operation after evaluating pilot plant data. In the future on-line control and optimisation using biofilm models might even become possible.

The use of mathematical biofilm models in practical applications, as described above, is up to now fairly limited (Morgenroth *et al.*, 2000). It should however be noted that, apart from the general belief that models are merely interesting research tools, modelling should be considered to be an inherent part of the design, the engineering and operation of each wastewater treatment system. In the most fundamental modelling approach, the engineer reduces the complex system he is dealing with to a conceptual image of how it functions. Often, however, it is recognised that the conceptual model alone does not provide sufficient information for design or operation and thus a physical model is constructed, such as a lab-scale reactor or a pilot plant, on which various ideas can be tested. However, limitations of time and money mostly prevent exploration of all potentially feasible solutions. Consequently, the use of mathematical models becomes interesting. Empirical models which incorporate a statistical approach can be developed or, if the conceptual process understanding expands sufficiently, mechanistic models may be formulated.

It is obvious that when a mathematical biofilm model is to be selected, the selection-criterion should depend on the objective of the modelling or a specific model application. One might argue that a mechanistic model can never include enough phenomena that occur in practice since otherwise the model is not a good representation of reality. Following this approach, biofilm modellers have over the past years tended to include almost all processes thought to be taking place. However, integrating that much micro-scale knowledge in a biofilm model has quite some shortcomings. First of all, it leads to the use of a lot of empirical relations to describe dynamic processes that are not fully understood (yet). Also of importance is the required computational effort and time for solving the resulting set of partial differential equations. This factor often leads to simulation times too long to permit practical use of the model for design, process optimisation and operation. The high complexity of the model also increases the number of unknown parameters and the possible dependencies between them. These factors make the accurate estimation of parameter values very difficult.

Therefore, simpler models should be used whenever their limited complexity is sufficient to perform the task the model is aimed at. This is certainly the case for models that should be used as practical engineering tools. It is undoubtedly true that a simple model will never be able to describe all the dynamics of the system precisely because of simplifications. However, in the current situation, where measurement equipment for wastewater treatment purposes is still under every-day development, it is an illusion to be able to even measure these dynamics in practical situations on a pilot-scale or a full-scale biofilm treatment plant. Hence, rather than following the trend to include more and more phenomena in the model, the aim of this work is to use simpler models.

So the basic question remains: "What is the purpose of the model". In this research, the emphasis is not on understanding the exact mechanisms which cause a biofilm to develop itself in a certain shape. It is rather on using models for the understanding of the overall biofilm process and subsequently to use these models to optimise the process where possible. It is obvious that a model used for this purpose should be surveyable, not be too detailed and enable a relatively fast simulation. Furthermore,

it should be possible to couple the model to other existing and well-accepted models used to describe other unit processes in wastewater treatment systems.

In this thesis, a model is developed that attempts to be such a complexity compromise. It is relatively simple, since it is based on the analytical solution of the substrate profiles in the biofilm. This factor is very important for the application of the model in practical situations and in combination with other widely accepted models in wastewater treatment. On the other hand, the model is able to calculate the conversion rates of different processes in the biofilm performed by different biomass species. Thus, despite of its simplifications, it can be used to describe processes occurring in different depths of the biofilm.

The aim of the second part of this thesis is to apply and test this model under different circumstances using data obtained from measurement campaigns in a pilot-scale and a full-scale system. Although the model is rather simple, it still includes quite some conversion processes and a considerable set of parameters needs to be calibrated. To gather the data needed for a successful calibration, the use of on-line measurement techniques is explored. Where needed, the model is extended to be able to describe the results from the on-line sensors. Using the available set of data, the model is calibrated such that it gives a reasonably good description of the dynamics of the plants under study and it is further used to propose process optimisations.

As a last application, the simplified mixed-culture biofilm model is used in a simulation study investigating suspended carrier biofilm systems. Although not supported with measurements, data from literature is found sufficient here to obtain and investigate a realistic description of the dynamic behaviour of such systems.



# 2 Literature review

---

## 2.1 Introduction

Biofilms play an important role in natural as well as in technological processes. They are present in about every system where microorganisms are present. Whenever water is flowing over a solid surface, microbial organisms will attach to this surface from the water. They will grow and multiply, producing a structured matrix composed of extracellular polysaccharides (EPS), so as to produce a biofilm (Characklis and Marshall, 1990). This kind of bacterial film can be formed on about every surface. A classical example is the layer of microorganisms that is formed on the teeth and that can give rise to caries. Biofilm growing on river beds and in seas and oceans are generally seen as very useful, because they have a big contribution in eliminating a lot of chemicals out of the water. Also in wastewater treatment, biofilms can have beneficial uses. They are used by man especially to oxidise and/or further treat organic and inorganic compounds. On the other hand, biofilms are known to cause big problems and economic losses. For example, a lot of attention is devoted to biofilms in water distribution systems. In that case the biofilm causes a significant health risk to the consumer. Apart from that, they deteriorate the quality of the water in terms of colour, taste, odour and turbidity. In industry, biofilms can block pipes, and are sometimes responsible for corrosion and increased flow resistance. In the case of heat exchanges, they increase thermal resistance.

The technology using biofilms for wastewater treatment processes is currently receiving a lot of attention, especially in places where the space available is small. There, a biofilm-based system is interesting because a high biomass density can be guaranteed. This way the necessary volume needed for the wastewater treatment can be minimised. Growing urbanisation has led to wastewater treatment plants located in densely populated areas where extension can be very difficult, both physically and economically. The optimisation of biofilm systems in these areas is therefore of big importance. Another important factor in favour of biofilm reactors is that in traditional biofilm reactor processes, like trickling filters, the need for control is very limited. Also, these configurations can easily survive shock load and short toxic waste shocks because of the relatively short hydraulic retention time in the reactor. This basically means that only the organisms on the biofilm surface will be affected (Grady and Lim, 1980). The operation of biofilm plant is further simplified by the limited need for sludge sedimentation and sludge recirculation (Henze *et al.*, 1995). Even effluent recirculation can often be omitted. However, in the most recent process configurations, like fluidised beds, the retention time is so short that the process would be too sensitive to short time influent variations without effluent recirculation.

Applications for biofilm processes extend far beyond the aerobic treatment of sewage. Some of the most promising applications include nitrification and denitrification of wastewaters and drinking waters and detoxification of water containing hazardous organic chemicals. The short hydraulic retention times and excellent biomass retention in biofilm reactors make them especially attractive when the compounds to be treated are inhibitory or slowly degraded (Jeppsson, 1996).

The description of biofilms via mathematical models can help to develop understanding about how biofilms grow, what limits their development and degradation capacity and how their operation can be optimised. When a biofilm is described mathematically, the transport of substrates and reaction products in and out of the biofilm is mostly treated as the rate-limiting step. This particular physical step seems to be crucial in describing the behaviour of biofilm reactors and it can be seen as the biggest distinction between systems based on biofilms and systems based on micro-organisms growing in suspension (Jeppsson, 1996).

In aerobic wastewater treatment, one of the substrates needed in the biofilm is oxygen. Mostly, oxygen is supplied to the bulk water via exchange at the air/water interface. At this interface, also gaseous products like CO<sub>2</sub> are formed, which are exchanged with the air phase. The biological phenomena in the biofilm – growth and decay – are mostly treated in a way similar to recent activated sludge models. However, the description based on Monod kinetics may not be valid in all cases. (Hamilton & Characklis, 1989). In general, biofilms are very porous structures, so inorganic as well as organic compounds can be captured by the biofilm matrix (Jeppsson, 1996). As a last point, parts of the biofilm can be eroded at the surface or entire pieces of biofilm can be detached (Bishop *et al.*, 1995).

In short: the thickness, composition and structure of a biofilm are caused by a complicated ensemble of different interacting processes. It is obvious that a biofilm is composed of several micro-niches, so that a complex microbial community can develop. As an example, it is possible that in the same biofilm, aerobic, anoxic and anaerobic zones are present.

The physical and biological phenomena described above, give rise to systems that can roughly be subdivided into a set of compartments (Characklis and Marshall, 1990).

- A carrier material, a non-porous material or a membrane as it is often used in medical and industrial applications. The carrier material is mostly inert but can sometimes be used as a substrate for the biomass;
- the base film, strongly structured and dense;
- the surface film with an irregular morphology;
- the bulk liquid;
- and the gas phase.

The structure of each of these compartments is highly dependent on the way the biofilm has started growing and the condition that it is subject to. It is important to note that every compartment consists of at least one chemical phase (solid, liquid or gas). The biofilm compartment itself is almost entirely made up out of water, however, it is possible that gas inclusions are present due to aeration.

## **2.2 Overview of the different biofilm reactor types**

Different reactor types have been developed for the beneficial use of biofilms in wastewater treatment. The oldest ones are the traditional biofilters. They were initially used as purely physical filters. After some time it became clear that the most important mechanism of purification was not the physical filtration, but the biological degradation (Jeppsson, 1996).

As mentioned before, it is accepted that biofilm systems, because of their high biomass density, have a smaller footprint than conventional activated sludge systems. This explains the success of these systems at places where only limited space is available. On the other hand, biofilm systems have some shortcomings. A lower flexibility and controllability is inherent to biofilm systems. An uncontrolled increase of the biofilm thickness can lead to limitations of the mass transport from bulk liquid to biofilm. This might lead to massive sloughing of biomass (Characklis and Marshall, 1990). The more recent configurations have dealt with this problem via filter backwashing or limited biomass growth due to high shear forces in the system. As mentioned before, these configurations mostly need recirculation to be implemented, because due to their short hydraulic retention times, they are more vulnerable to sudden changes in the influent load (Jeppsson, 1996).

The major reactor types are shortly described below in Table 2.1.

**Table 2.1. Characteristics of some biofilm reactors (Tijhuis *et al.*, 1994)**

	<i>specific surface area (m<sup>2</sup>/m<sup>3</sup>)</i>	<i>biofilm thickness (mm)</i>	<i>hydraulic surface loading (m/h)</i>	<i>conversion capacity (kg<sub>02</sub>/m<sup>3</sup>d)</i>
trickling filter	150	5-10	0.5-2.5	1.5
rotating biological contactor	200	5	-	2
submerged filter	700	0.5-1	10-15	7
fluidised bed reactor	2000	0.2	30	5
biofilm airlift suspension reactor	2000	0.2	30	20

The trickling filter is a reactor where the water is flowing over a plastic or stone carrier material. To date, the construction of trickling filters is usually done using plastic media, that are contained in a cylindrical tower with a maximum height of 12 m (Figure 2.1). The medium has, on the one side, to provide a big attachment surface for the biofilm biomass and, on the other side, a high pore volume to assure easy liquid flow and sufficient oxygen transfer. For the oxygen transfer, the chimney effect can be used or ventilators can provide the biomass with fresh air. The water to be treated is sprinkled on top of the filter bed by rotating arms. To assure a minimal flow rate for the biomass wetting, effluent recirculation is sometimes implemented. Higher flow rates through the filter can be obtained this way, so as to avoid filter blocking by higher biofilm erosion (Bishop and Kinner, 1986). Trickling filters are mostly used to treat organic pollutants, but quite some applications of tertiary nitrogen removal by nitrifying trickling filters are known (Characklis and Marshall, 1990). Trickling filters can withstand high peak loads and toxicity very well (Grady and Lim, 1980). For reasons of robustness, they are especially suitable for application in small communities (Characklis and Marshall, 1990).

The rotating biological contactor dates from a little while later than the trickling filter. In this mechanism, parallel plates attached to a horizontally turning axis are partially exposed to the wastewater (Figure 2.1). This allows for a biofilm to grow on the plates. This biofilm is also exposed to air while the axis is turning at a relatively slow rate of about 1 rpm. This in turn allows for the necessary oxygen to be transferred to

the biofilm, so as to assure aerobic biofilm growth (Bishop and Kinner, 1986). The advantages of this system are amongst others the extremely low cost for mixing and oxygen provision. The system is also less vulnerable to low or fluctuating flow rates as compared to the trickling filter system.

More recent process configurations are the submerged filters (Figure 2.1). They can be used in a downflow or an upflow mode. In these systems, the carrier material is completely submerged in the wastewater to be treated (Jeppsson, 1996). In most cases, air is provided through nozzles underneath the filter medium. These filter configurations have to be backwashed regularly to avoid high pressure drop and eventually clogging by the biofilm growth. About 10% of the treated water is re-used during this backwash process. Submerged filters are known with a wide variety of fixed and floating carrier material types.

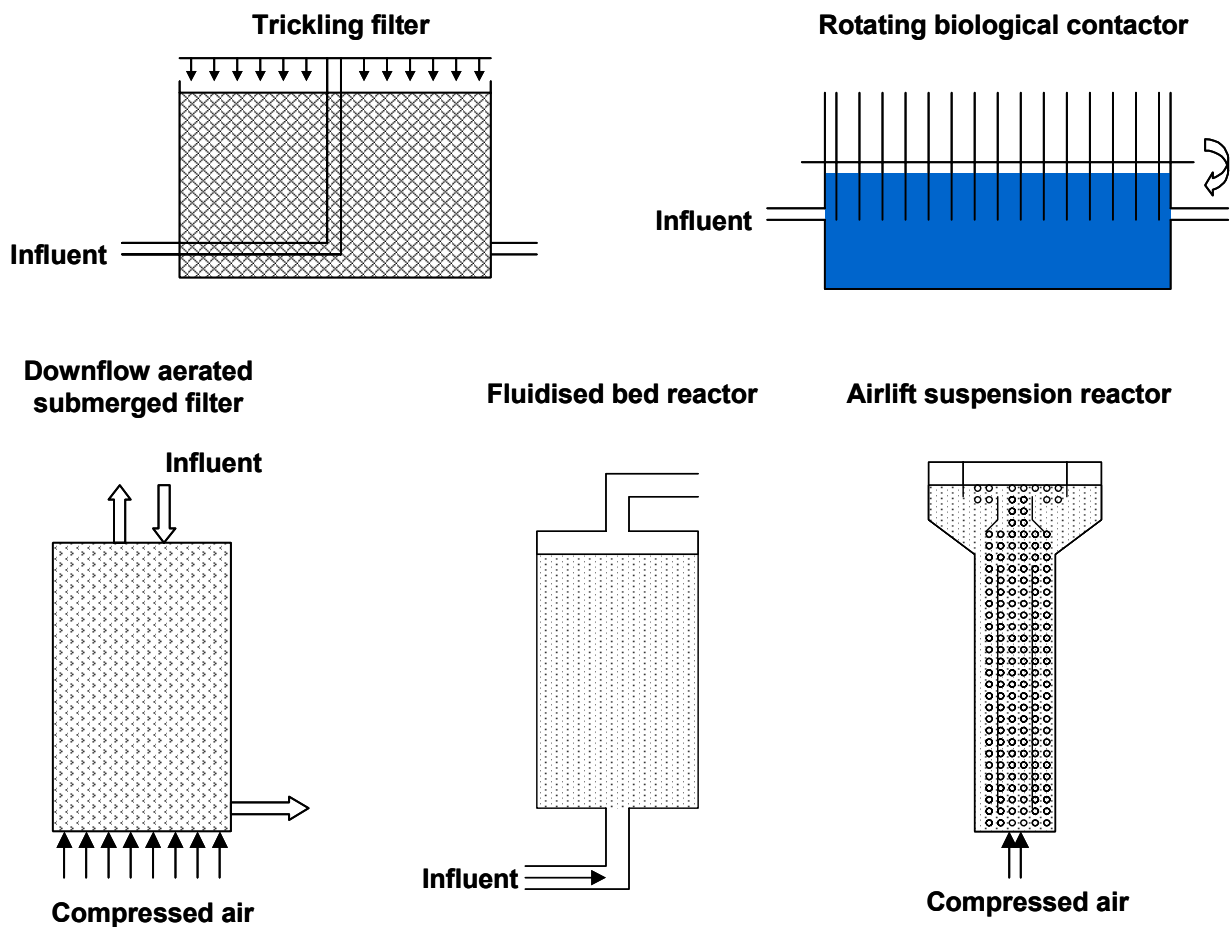


Figure 2.1: Five types of regularly used biofilm system configurations

In the fluidised bed process, particles (0.2 – 0.5 mm) grown with biofilm are fluidised in an upward liquid flow or a mixed air-liquid flow. This way of operation – the small particle size and the fluidisation – assures a big biological activity per unit volume, so that small retention times and thereby relatively small reactor volumes can be used (Bishop and Kinner, 1986). The aeration of the wastewater is done together with the fluidisation or in the recirculation loop. The pumping capacity needed for the fluidisation is different during the life cycle of the reactor: a bigger capacity is usually needed during start-up. This and other practical problems sometimes hinder the application of fluidised bed reactors at full scale (Henze *et al.*, 1995).

The airlift suspension reactor is essentially made up of two concentric tubes. Air is blown into the inner tube, so that a constant density difference exists between the contents of the two tubes, hereby causing the complete reactor contents to circulate. On top of the two tubes, a phase separator is constructed. Here, the particles grown with biofilm are led back to the bottom of the reactor. Recent studies show the great potential of this reactor set-up in wastewater treatment, mainly because of its big conversion capacity. In the Netherlands, some full-scale installations are operational.

## 2.3 Mass transport in biofilm systems

The degradation of organic matter in a biofilm can only take place when bacteria are provided with an electron donor, an electron acceptor and nutrients. Each of these three components can be rate limiting in the conversion process in a biofilm. The mass transfer resistance to be overcome between the different phases in a biofilm system cause concentration gradients to exist for each of the components needed in conversion (Figure 2.2).

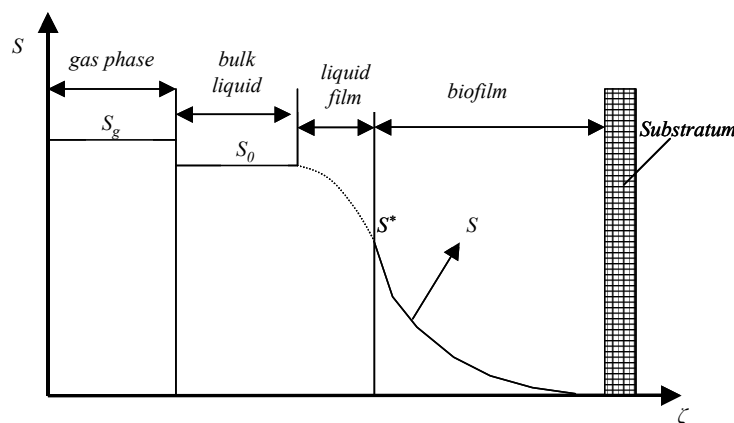


Figure 2.2: Different phases in biofilm systems and resulting concentration gradients

### 2.3.1 Interphase transport: gas to liquid

Before oxygen can diffuse into the biofilm, the barrier between gas and liquid has to be taken. The major part of the oxygen needed for conversion is coming from the gas phase rather than from the limited amount of oxygen available in the bulk liquid. For other (volatile) compounds too, the exchange between gas and liquid can be of major importance, especially when biofilters are used for waste gas treatment processes. As a last point, part of the  $\text{CO}_2$  formed by aerobic and anaerobic conversion processes is removed via the gas phase.

### 2.3.2 Intraphase transport: liquid

When laminar flow in a tube or over a tilted plate is described, an analytical solution to the problem of substrate transport in the liquid phase is still possible. In this case, velocity and concentration profiles can be calculated (Bird *et al.*, 1960). In a turbulent flow regime, the phenomena taking place are a lot more complicated and an exact solution can not be found. In normal cases, averages of all the quantities of interest can be taken. Transport coefficients found will be dependent on the properties of the liquid phase and the substrate, but also on the degree of turbulence. However, close to the wall of a pipe, a laminar flow zone can be distinguished, where friction forces dominate the flow regime. The thickness of the laminar flow layer decreases with increasing flow velocity.

### 2.3.3 *Interphase transport: liquid to wall - liquid to biofilm*

Whenever concentration profiles are measured in a turbulent flow regime, it is obvious that the largest concentration gradients are situated close to the wall of the pipe and are very small in the turbulent core. The greatest resistance for mass transport to a biofilm will be present close to the biofilm itself. The most obvious way to model this kind of system is to assume that all mass transport resistance is concentrated close to the wall or the upper biofilm boundary (Characklis and Marshall, 1990). For this reason, a boundary layer is defined in which the mass transport from the bulk liquid to the biofilm can be entirely explained by the mass transport laws for stagnant fluids – a modified Fick law – while in the rest of the liquid phase, a homogeneous concentration distribution is assumed (Figure 2.2).

- Quite some researchers use pure water diffusion coefficients in this layer (Williamson and McCarty, 1976; Rittmann and McCarty, 1980b; Wanner and Gujer, 1986; Wanner and Reichert, 1996). It is important to note here that the thickness of this fictitious boundary layer is not the same as the thickness of an eventual laminar boundary layer. Indeed, the thickness of the boundary layer in biofilm models is defined as the thickness of a stagnant liquid film, through which each transport can be described as molecular diffusion (Characklis and Marshall, 1990). This modelling methodology implicitly states that the fluid velocity at the liquid-biofilm boundary is zero. This is in reality not always the case (see among others Lewandowski *et al.*, 1995).
- Other modellers define this stagnant liquid layer as a surface film of the biofilm, for which a mass transfer coefficient is calculated using the following formula:

$$N_{int} = h \cdot (S_0 - S^*) \quad (2.1)$$

where  $N_{int}$  is the mass flux through the liquid-biofilm interface,  $S_0$  denotes the substrate concentration in the bulk liquid phase and  $S^*$  is the substrate concentration at the interface between the surface film and the biofilm. The external mass transfer coefficient  $h$  is strongly dependent on the liquid flow velocity. This is linked to a thinner boundary or surface layer, but possibly also with a bigger portion of advective transport through the pores of the biofilm at higher flow velocities.

### 2.3.4 *Intraphase transport: biofilm*

#### 2.3.4.1 **Description of the transport**

Transport of substrates through the biofilm is mostly described as a process alike molecular diffusion governed by the Fick law. Most models assume no advective transport is present, so only a new diffusion coefficient replaces the one in the liquid phase (Williamson and McCarty, 1976; Rittmann and McCarty, 1980b; Wanner and Gujer, 1986; Wanner and Reichert, 1996). This so-called effective diffusion coefficient is used as a kind of *lumping* parameter. This way, an highly heterogeneous diffusion-reaction system can be described as a homogeneous system. The concentration gradients in the biofilm are determined by this effective diffusion process description as well as by the rate of reaction and the stoichiometry in the biofilm.

#### 2.3.4.2 Determination of the effective diffusion coefficient

A lot of authors have stated that the value of the effective diffusion coefficient in a biofilm should be about 80% of the value in pure water. Different values are however stated for different substrates (Williamson and McCarty, 1976; Characklis and Marshall, 1990). Techniques to determine these coefficients also differ from one study to another, so the results can differ quite significantly. Measurements can be done using filtered biomass on a membrane in a diffusion cell. Next to this measurement method, data-fitting techniques can be used (Zhang and Bishop, 1994b). The diffusion coefficient can be fitted using a diffusion-reaction model where of course measurements or estimates of the kinetic and stoichiometric coefficients are needed. Alternatively these reaction and diffusion coefficients can be fitted using concentration profiles measured in the biofilm – mostly using micro-electrodes.

The use of micro-electrodes is relatively new in biotechnology (Revsbech, 1989). The last decade, enormous progress has been made in the application of micro-electrodes in biofilm research. Electrodes for the measurement of  $O_2$ ,  $N_2O$ ,  $pH$ ,  $NH_4^+$ ,  $NO_3^-$ ,  $S^{2-}$ ,  $H_2S$ ,  $NO_2^-$ ,  $CH_4$  and  $CO_2$  are available (de Beer and Schramm, 1999). Some years ago, only the  $O_2$  sensor was relatively stable and could be used outside the laboratory. Nowadays, increased shielding (Jensen *et al.*, 1993) and the use of protein coatings (de Beer *et al.*, 1997) introduce solutions to these problems.

Zhang and Bishop (1994) determined the diffusion coefficients with techniques developed for porous catalysts, for which only a value for the porosity is needed. However, this method has some inherent errors. With this method, Zhang and Bishop (1994) notice a lower diffusion coefficient in the lower and denser parts of the biofilm. Using data collected by Fu *et al.* (1994), they calculated a diffusion coefficient amounting to 75% of the pure water coefficient at the top of the biofilm and only 40% at the bottom of the film. Their calculation agrees quite well with the measurements of Fu *et al.* (1994), who used a micro-electrode technique with oxygen concentration measurements every 10  $\mu m$  in the biofilm.

Stewart (1998) published a review on the experimental methods used to measure effective diffusivity in biofilms. He concludes that the measurements of effective diffusivity in biofilms vary widely, but that most of the variation can be attributed to differences in solute physical chemistry and in biofilm density. Three categories of solute physical chemistry could be distinguished. In order of descending relative effective diffusivity, these were ionic solutes (inorganic anions or cations), small solutes (nonpolar solutes with molecular weights of 44 or less), and large solutes. A theory is proposed that large solutes are effectively excluded from microbial cells, that small solutes partition into and diffuse within cells and that ionic solutes are excluded from cells but have an increased effective diffusivity due to their sorption capabilities to the biofilm matrix.

#### 2.3.4.3 Conceptual models of biofilm structure - factors influencing mass transport

Clearly, several factors influence the effective diffusion coefficient and, consequently, the mass transport to the biofilm. Siegrist and Gujer (1985) report a small increase of the coefficient with increasing biofilm age and a decrease with increasing biofilm thickness. According to the authors, this last part has mainly to do with the virtual absence of a laminar boundary layer with biofilm thicknesses exceeding 100  $\mu m$ . Also according to Siegrist and Gujer (1985), a diffusion coefficient higher in the biofilm than in pure water is perfectly possible. This might have to do with the presence of eddy-diffusion at the liquid-biofilm

interface or even in the biofilm pores themselves. This effect can be visualised by moving filaments in the biofilm. This effect is however highly dependent on the growth conditions of the biofilm which have an important influence on the morphological structure of the biofilm. Based on these findings, Siegrist and Gujer (1985) propose a biofilm to be represented as a number of layers parallel to the substratum. A surface layer in which eddy-diffusion is possible, followed by a base layer where molecular diffusion is the main transport phenomenon.

However, the image representing the biofilm as a homogeneous flat surface, has changed dramatically over the last decade thanks to the confocal scanning laser microscopy (CSLM). This technique enables researchers to produce images of a fully functional biofilm *in vivo*, even incorporating liquid flow (Lawrence *et al.*, 1991). On the basis of this technique, the image of biofilms was changed to a three-dimensional structure with a porous nature (Figure 2.3). The building blocks of this structure are bacterial clusters or microcolonies that are separated by a network of channels, linked to the biofilm surface (Lewandowski *et al.*, 1994).

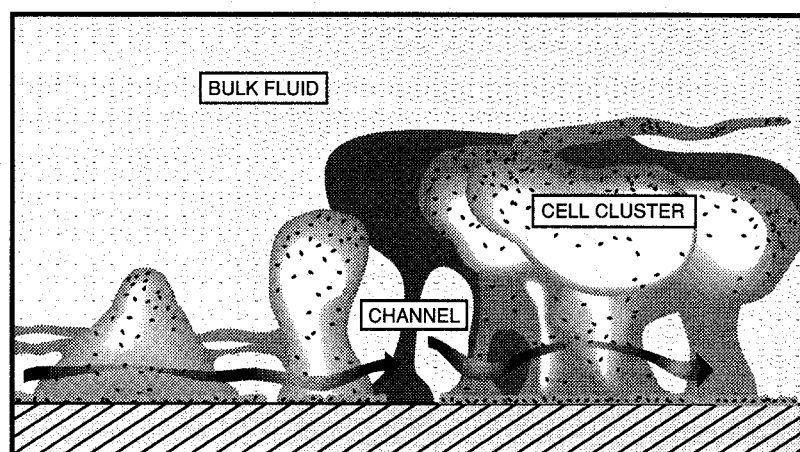


**Figure 2.3: Structure of a hypothetical biofilm drawn from a number of Confocal Scanning Laser Microscopy (CSLM) examinations of biofilms (Lewandowski *et al.*, 1995)**

The presence of these channels led to the hypothesis of advective transport in the biofilm. Nuclear Magnetic Resonance (NMR) has been successfully applied by Lewandowski *et al.* (1993) to visualise this transport. However, relating the data with the actual local biofilm structure remained a problem (Stoodley *et al.*, 1994). A more powerful technique was used by de Beer *et al.* (1994) and Stoodley *et al.* (1994). They were able to follow the movement of fluorescent latex particles using particle image velocimetry with CLSM. The flow velocity in the biofilm turned out to be closely related to the local structure of the biofilm. A result of these findings is that bacteria in deeper layers of the biofilm could be a lot more active than thought before, since the conversion in deeper layers of the biofilm need not be diffusion limited.

A fourth technique can be used to quantify liquid flow in a biofilm, namely the limiting current technique. This technique is based on micro-electrodes sensitive to fluid current (Xia *et al.*, 1998). Yang and Lewandowski (1995) used this technique in combination with a mobile micro-electrode to measure local mass transport coefficients in the biofilm. The limiting current technique uses electrodes parallel to the substratum and an electro-active species. Thanks to a number of assumptions, the reaction rate at the electrode tip can be assigned completely to the mass transport.

Yang and Lewandowski (1995) were able to connect the measured limiting current  $I$  of the electro-active species ferricyanide to its diffusion coefficient  $D$  and the thickness of the mass transfer boundary layer  $\delta_{bl}$ :

$$i = \frac{I}{A_{electrode}} = \frac{n_e \cdot F \cdot S_0 \cdot D}{\delta_{bl}} \quad (2.2)$$

where  $A_{electrode}$  is the active surface of the micro-electrode and  $n_e$  denotes moles of transferred electrons in the reaction.  $F$  is the Faraday constant and  $S_0$  is the bulk liquid concentration of the electro-active species. A constant ferricyanide concentration in the bulk liquid makes it possible to evaluate the mass transfer coefficient  $D/\delta_{bl}$ . Since the boundary layer thickness is determined by the local fluid velocity, also a relation between the local current density  $i$  and the local flow velocity  $u$  could be found (Xia *et al.*, 1998). This way it was found that the flow velocity in channels parallel to the substratum is larger than in channels perpendicular to the substratum. In a cluster of micro-organisms the fluid velocity is zero.

Based on the above finding, de Beer and Stoodley (1995) proposed a different model. They started from a biofilm that can be represented as an ensemble of clusters of micro-organisms and big pores, in which the liquid can flow. The flow in the pores is assumed to be laminar, but diffusion as well as advective transport is possible. In the clusters, only stagnant water is present, so only molecular diffusion is possible. They verified their model with micro-electrode measurements for oxygen, proving that the oxygen concentration is higher in pores than in cell clusters at a given depth in the biofilm. Their conclusion is that convective transport in the biofilm is dependent on the liquid flow velocity, that is then also partly governing the substrate removal in a biofilm.

In contrast to this conceptual biofilm model, research using CSLM and transition electron microscopy on biofilm in dental plaque tend to find biofilms with a very dense matrix with no indications for pores or channels. However, there was clearly some structural organisation, since numerous micro-colonies of uniformly shaped cells were found.

## 2.4 Kinetics of microbial conversions in biofilms

### 2.4.1 Metabolic reactions in biofilm

Several layers can be distinguished in a biofilm. It is perfectly possible that aerobic conditions are present only in the upper layer of the film. In the lower parts of the biofilm, oxygen transport can be insufficient and anoxic or anaerobic conditions can be present. Micro-electrode measurements showed that these conditions are possible only 100  $\mu\text{m}$  deep in the biofilm (Bishop *et al.*, 1995). This value is of course only an indication since big fluctuations are possible, dependent on the oxygen and substrate concentrations in the bulk liquid, the mass transfer to the biofilm and the conversion speed. At different depths in the biofilm micro-organisms will thus develop that use different electron donors and acceptors. Reduced organic substances can serve as donors next to ammonium (for nitrification). A wide variety of acceptors are possible: oxygen (aerobic metabolism), nitrate (denitrification), sulphate (sulphate reduction), hydrogen (methanogenesis) and other organic molecules (fermentation). In most domestic wastewaters, nutrients will be available abound, in some industrial wastewaters however, this might not be the case.

The aerobic metabolism is the most efficient one from an energetic point of view. Other metabolic processes should however not be neglected, since they can contribute significantly to the conversion of organic matter from wastewaters. Bishop and Kinner (1986) constructed a theoretical model about the micro-organisms that can possibly be predominant in a biofilm at a certain loading condition. As mentioned before, the aerobic metabolism will be present at the surface of the biofilm. In deeper – but still aerobic – layers of the biofilm, slower growing nitrifiers may be present. The nitrate formed by these organisms may be used by denitrifiers in anoxic conditions. In an anaerobic part of the biofilm,  $H_2S$  might be formed by sulphate reductions and even methanogenesis and fermentations processes may be present. These processes in the biofilm can be followed using micro-electrode measurements of, among others, oxygen,  $pH$ , ammonium and nitrate (Bishop *et al.*, 1995).

It is important to note here that even in a biofilm that is not thick enough to sustain a fully developed anaerobic layer, still anaerobic niches are likely to be present. This way, anaerobic organisms can survive even in assumed fully aerobic biofilms (Lens *et al.*, 1995a). The presence of these niches gives rise to a cycle of sulphur, whereby sulphate is reduced in anaerobic conditions and is oxidised again in the aerobic parts of the biofilm. Even this cycle can be the driving force of organic matter removal in a biofilm.

### 2.4.2 Kinetic equations

When microbial transformations are described, two factors are of major importance: the speed of reaction and the stoichiometry. Kinetic equations are thus of big importance in biological systems modelling. The form of this equations can be the result of a theoretical analysis on the basis of a mechanistic model, or it can be derived using an empirical curve-fitting technique. The parameters used in kinetic equations should be determined by experiments, since they are highly dependent on the specific condition under which the microbial conversion is taking place. Only when the exact reaction mechanism is known, extrapolation can be done to regions for which no experimental information is available. Since this involves a lot of experiments and statistical uncertainty and since it is almost impossible to do in any practical case, quite some simplified kinetic expressions are commonly used. An example of this simplification is the  $n^{\text{th}}$ -order kinetic equation:

$$r = k \cdot S^n \quad (2.3)$$

where  $r$  is the volumetric reaction rate,  $k$  is the reaction rate coefficient,  $S$  is the local substrate concentration and  $n$  is the order of the reaction. This kinetic equation can be written more generally as:

$$r = k \cdot \prod_i S_i^{n_i} \quad (2.4)$$

The equations tend to give a good statistical fit for experimental data over a limited range.

The growth of micro-organisms is usually proportional to the amount of biomass present, so one can write:

$$r = \mu \cdot X \quad (2.5)$$

where  $X$  denotes the biomass concentration. The specific growth rate  $\mu$  is often introduced as a saturation equation as a function of the substrate concentration  $S$ .

$$\mu = \frac{\mu_{\max} \cdot S}{K_S + S} \quad (2.6)$$

where  $\mu_{\max}$  is the maximal specific growth rate and  $K_S$  is the half-saturation coefficient. As an alternative, the logistic expression can be used for this purpose in which  $X_{\max}$  is the maximal attainable biomass concentration:

$$r = \mu_{\max} \cdot X \cdot \left(1 - \frac{X}{X_{\max}}\right) \quad (2.7)$$

It is of course possible that two or more substrates or nutrients are limiting or influencing the growth. Several mathematical representations of such a situation have been developed, like for example (Characklis and Marshall, 1990):

$$r = \left(1 + \sum_j \frac{k_j \cdot S_{Sti,j}}{K_{S,Sti,j} + S_{Sti,j}}\right) \left(\prod_i \frac{\mu_{\max,i} \cdot S_{Ess,i}}{K_{S,Ess,i} + S_{Ess,i}}\right) \cdot X \quad (2.8)$$

where  $S_{Ess,i}$  is the concentration of the  $i^{\text{th}}$  essential substrate or nutrient and  $S_{Sti,j}$  is the concentration of the  $j^{\text{th}}$  not essential but growth stimulating substrate or nutrient. Especially the following expression for double substrate limitation is often used:

$$r = \left(\frac{\mu_{\max} S_1 S_2}{(K_{S,1} + S_1)(K_{S,2} + S_2)}\right) X \quad (2.9)$$

Also the endogenous metabolism needs attention. When micro-organisms receive no substrate, they start to metabolise substances from their own cells. This metabolism can play an important role in the survival of a biofilm under substrate limiting conditions. The endogenous metabolism is mostly modelled as follows:

$$r_{end} = k_{end} X \quad (2.10)$$

where  $r_{end}$  denotes the rate of endogenous metabolism and  $k_{end}$  is the maximal specific rate of endogenous metabolism.

## 2.5 Modelling of biofilm systems

### 2.5.1 Introduction

A wide range of biofilm models is currently available in literature (Noguera *et al.*, 1999). In the following paragraph, some of these models are described. After discussing the simplifications often used in modelling biological systems, the biofilm models are structured according to their complexity. First, the attention is drawn to one-dimensional biofilm models. Some examples of one-dimensional models are treated that describe substrate gradients assuming a uniform biomass distribution in the biofilm. The major advantage of these models is the resulting set of relatively simple analytical equations (Harremoës, 1976; LaMotta, 1976). Other modellers gradually started to introduce stratification of biomass considering multiple substrates and multiple species in one-dimensional models (Rittmann and McCarty, 1980b; Namkung and Rittmann, 1987; Rittmann and Manem, 1992). This finally resulted in the development of the state-of-the-art 1D model by Wanner and Reichert (1996). The solution of these models has to be done using dedicated software, since the stratification in the models gives rise to partial differential equations. An important aspect in the previous models is the description of attachment and detachment of biomass at the liquid-biofilm interface. At this moment this is mostly done using empirical formulas. It is however important to realise that these processes are highly dependent on the biofilm structure. The modelling of this structure is the subject of the last class of models treated in this review. Multi-dimensional models with heterogeneous biomass and substrate distributions in two or three dimensions are focussed upon. The modelling of the biofilm structure in these models is mostly accomplished by the implementation of cellular automaton models.

### 2.5.2 Simplifications in modelling biological systems

#### 2.5.2.1 Functional homogeneity in the populations

Individual cells in a population aren't always in the same state, but a distribution of states is present like for example age, size, morphology, physiology... While modelling a biological system, this heterogeneity is neglected and the population is described using the properties of a "typical" individual. This also happens when biofilm models are developed, although it is known that over very short distances gradients of  $pH$ , temperature and substrate concentration exist that have an influence on the physiological state of the micro-organisms.

#### 2.5.2.2 Homogeneity in space

A population is distributed into different entities, the cells. A lot of models make the assumption that such distribution can be neglected. The exact amount of cells is not seen as a model parameter, but the biomass is assumed to be distributed homogeneously and only the total mass or concentration of the biomass is considered. It is clear that these types of models can not be used to describe the initial processes in the formation of a biofilm, since only a very small number of cells are involved at that stage of the biofilm development. These cells will certainly form a non-uniform distribution over the carrier material.

### 2.5.2.3 Homogeneity in time

The life time of an individual cell is not uniform over the complete population too, but it is distributed along a mean value. Despite this knowledge, the growth of bacteria is most often treated as a deterministic process.

There is a big difference among the time constants of the processes that are taking place inside a microbial system. This can sometimes simplify the analysis of a complicated biological process. Short term variations of the influent concentration can be treated and modelled with a microbial distribution in steady-state. Also in case a process of interest reacts slower than another process in the system, this last process can be assumed to be in a steady-state. Changes in the species distribution can therefore be modelled with a (pseudo-)steady-state substrate concentration profile. Kissel *et al.* (1984) give the following overview of the most important time constants involved in biofilm systems modelling (Table 2.2).

**Table 2.2. Time constants of some important biofilm processes**

<i>Process</i>	<i>Time scale</i>
Sloughing of the biofilm	Instantaneous
Diffusion of soluble components into the biofilm	Seconds to minutes
Growth and erosion of biomass	Days
Changes in species distribution in a biofilm	Weeks to months

### 2.5.3 One-dimensional biofilm models

Most biofilm models which have been developed up to now are one-dimensional models or pseudo-one-dimensional models in space. One-dimensional means that only the space coordinate perpendicular to the substratum is considered in the model and that all quantities are averaged in planes parallel to the substratum. Pseudo-one-dimensional means that the biofilm surface is divided into a series of sections which are all modelled in a one-dimensional way. The only way these sections are coupled is by coupling to the bulk liquid phases (Wanner, 1995).

#### 2.5.3.1 1D diffusion-reaction models without biomass growth

Notwithstanding the non-uniform nature of the biofilm, most authors treat the biofilm as a uniform plane in space. Some authors also describe the biofilm as being a reactive surface. In these types of models, abstraction is made of microbial growth and only substrate conversion is modelled. LaMotta (1976) was the first to treat the biofilm as a porous catalyst. He started from the mass balance for the rate limiting substrate in which convective terms were neglected. This mass balance describes simultaneous diffusion and reaction relative to the time  $t$ :

$$\frac{\partial S}{\partial t} = D_f \cdot \nabla^2 S + r \quad (2.11)$$

where  $D_f$  is the effective diffusion coefficient of the substrate  $S$  in the biofilm. This way the biofilm is in fact treated as a gel in which the micro-organisms are uniformly distributed. In other words, the

reactive spots are distributed as in a porous catalyst. Simplifying this equation, only including a 1D-geometry, the steady-state equation becomes:

$$D_f \cdot \frac{\partial^2 S}{\partial \zeta^2} = r \quad (2.12)$$

where  $\zeta$  is an indication of the place in the biofilm. The boundary conditions to solve this equation differ from situation to situation. In the case of a fully penetrated – shallow – biofilm, the boundary condition (next to the boundary condition at the biofilm surface ( $\zeta = 0$ )) becomes:

$$\zeta = L, \quad \frac{dS}{d\zeta} = 0 \quad (\text{no penetration of the substrate through the substratum}) \quad (2.13)$$

where  $L$  indicates the thickness of the biofilm. In the case of partial penetration of the biofilm, this condition becomes:

$$\zeta = z, \quad \frac{dS}{d\zeta} = 0 \quad (\text{no penetration of the substrate deeper than } z) \quad (2.14)$$

An expression for the rate of substrate consumption can then be found by calculating the amount of substrate that has diffused through the liquid-biofilm interface  $N_{\text{int}}$ . In the case of a fully penetrated biofilm, this becomes:

$$N_{\text{int}} = A_F \cdot k_{0v} \cdot L \quad (2.15)$$

where  $A_F$  is the biofilm surface area and  $k_{0v}$  is the true volumetric substrate consumption rate, a zero-order reaction constant. In the case of partial penetration, this becomes:

$$N_{\text{int}} = A_F \cdot (2 \cdot D_f \cdot k_{0v})^{1/2} S^{1/2} \quad (2.16)$$

In case of partial penetration, an intrinsic zero-order reaction in the biofilm can be translated into a half-order reaction at the liquid-biofilm interface. Harremoës (1978) pointed out that the specific growth rates of bacteria can be assumed zero-order with respect to the concentration of the substrate  $S$  in the biofilm. The reason is that the saturation coefficients (assuming Monod-type kinetics) are very small for most substrates at hand (dissolved oxygen, soluble organic matter, ammonium and nitrate). Hence, the biofilm volume where the assumption of zero-order kinetics does not hold is very small and can be conveniently neglected. Note that the substrate removal has become independent of the biofilm thickness. The depth in the biofilm to which the substrate penetrates is given by:

$$z = \sqrt{\frac{2 \cdot D_f \cdot S}{k_{0v}}} \quad (2.17)$$

so that equation 2.16 can be simplified to:

$$N_{\text{int}} = A_F \cdot k_{0v} \cdot z \quad (2.18)$$

Harremoës (1976) also treats the biofilm as a porous medium. He uses the half-order kinetic equation because it makes a good, fast and easy simulation of the biofilm conversion processes possible. For the development of his model, the biofilm is treated as an ensemble of cylindrical pores with radius  $R$  and length  $L$  (Figure 2.4).

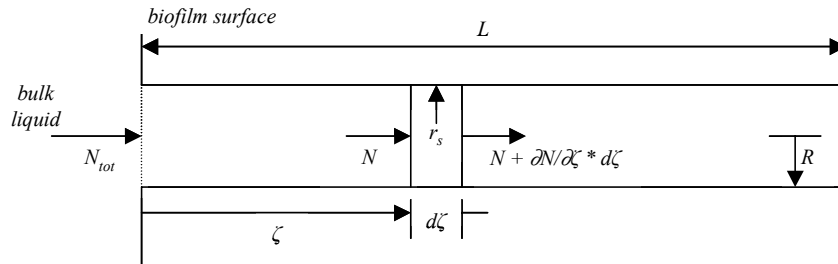


**Figure 2.4: Idealised pore into which the substrate has to diffuse in order to react at the pore walls (Harremoës, 1976)**

The reactions and conversions take place on the walls of these pores with a conversion rate  $r_s$ . A mass balance of these pores can be written as follows:

$$\frac{\partial N_{\text{tot}}}{\partial \zeta} = -2 \cdot \pi \cdot R \cdot r_s, \text{ because } N_{\text{tot}} = \left( N_{\text{tot}} + \frac{\partial N_{\text{tot}}}{\partial \zeta} \cdot d\zeta \right) + 2 \cdot \pi \cdot R \cdot r_s \cdot d\zeta \quad (2.19)$$

The model is based upon the assumption that the complete transport  $N_{\text{tot}}$  is due to diffusive transport of substrate  $S$  through the pore, or:

$$N_{\text{tot}} = -\pi \cdot R^2 \cdot D_f \cdot \frac{\partial S}{\partial \zeta} \quad \text{or} \quad \frac{\partial^2 S}{\partial \zeta^2} = \frac{2}{R \cdot D_f} r_s \quad (2.20)$$

In case a zero-order reaction is taking place on the reactive walls of the pore, then  $r_s$  can be written as  $r_s = k_{0s}$ , where  $k_{0s}$  is the zero-order reaction constant based on the pore surface. This equation can be integrated. In case the substrate penetrates to the end of the pore, the total transport into the pore, calculated at the surface of the biofilm, becomes:

$$N_{0,\text{tot}} = 2 \cdot \pi \cdot R \cdot L \cdot k_{0s} \quad \text{or} \quad k_{0a} = n_p \cdot 2 \cdot \pi \cdot R \cdot L \cdot k_{0s} \quad (2.21)$$

where  $N_{0,\text{tot}}$  is the total transport through the pore entrance,  $n_p$  is the number of pores per surface area of biofilm and  $k_{0a}$  is the zero-order reaction constant but now based on the surface area of biofilm. Here, obviously, the zero-order reaction at the pore walls is replaced by again a zero-order reaction at the biofilm surface. This, however, is not the case if the substrate can not diffuse completely up to the substratum. In this case a fraction  $\beta$  is used, representing the active fraction of the pore, where

$$\beta = \sqrt{\frac{R \cdot D_f \cdot S_0}{L^2 \cdot k_{0s}}} \quad (2.22)$$

and  $S_0$  denotes the concentration of the substrate in the bulk liquid phase.

The total transport into the pore then becomes:

$$N_{0,tot} = 2 \cdot \pi \cdot R \cdot L \cdot \beta \cdot k_{0s} = 2 \cdot \pi \cdot R \cdot \sqrt{k_{0s} \cdot R \cdot D_f} \cdot S_0^{1/2} \quad (2.23)$$

$$\text{or } N_{0,tot} = k_{1/2a} \cdot S_0^{1/2}$$

Here, the zero-order reaction constant at the pore walls is replaced by a half-order reaction at the biofilm surface, represented by  $k_{1/2a}$ . In this equation again the biofilm thickness does not play a role. Harremoës (1976) also implemented this half-order reaction kinetics to a complete filter instead of to a small fraction of it. For this application, the only extra parameter in the model is the specific biofilm surface in the reactor. This hypothesis was tested using methanol profiles in biofilm reactors. The profiles found followed the half-order approximation very well. However, no attempts were done to fit the reaction constants in the formulas above to the measurements. Experiments by Christiansen *et al.* (1995) showed comparable results. Harremoës (1976) theoretically showed that when all the pores in the filter are completely penetrated with a substrate, an overall zero-order kinetic reaction will prevail. At low substrate concentrations, the reaction rate will tend towards a first order reaction. In this case the analogy with the classical Monod kinetics appears.

### 2.5.3.2 The 1D Williamson-McCarty-Rittmann model

#### *The basis of the model*

The next model was originally developed by Williamson and McCarty (1976). Initially, the model was only oriented toward substrate transport and degradation in a steady-state biofilm. However, over the past twenty years, changes have often been applied to the model, aiming at describing different possible situations in a biofilm. In the model, however, a steady-state situation is always modelled. Even when adaptations to the model structure were implemented, instantaneous steady-state concentration profiles were always used. This means the fast dynamics of the biofilm system are not considered.

The model is based on the assumption that the biofilm is a flat surface and that the conversion is limited by a single limiting substrate  $S$ . The model divides the biofilm reactor into a bulk liquid compartment, a transient film between liquid and biofilm modelled as a stagnant liquid layer, an active and a non-active biofilm compartment. The model is based on the application of Fick's diffusion law combined with Monod kinetics.

Using Fick's law, the thickness of the stagnant liquid layer can be expressed as:

$$\delta_{bl} = \frac{A_F \cdot D \cdot (S_0 - S^*)}{N_{int}} \quad (2.24)$$

When a mass balance in steady-state is used, considering only the substrate removal in the biofilm with a Monod kinetic function, this mass balance becomes:

$$\frac{d^2S}{d\zeta^2} = \frac{\mu_{\max}}{Y} \frac{S \cdot X}{D_f \cdot (K_S + S)} \quad (2.25)$$

where  $Y$  is the substrate yield coefficient for growth.

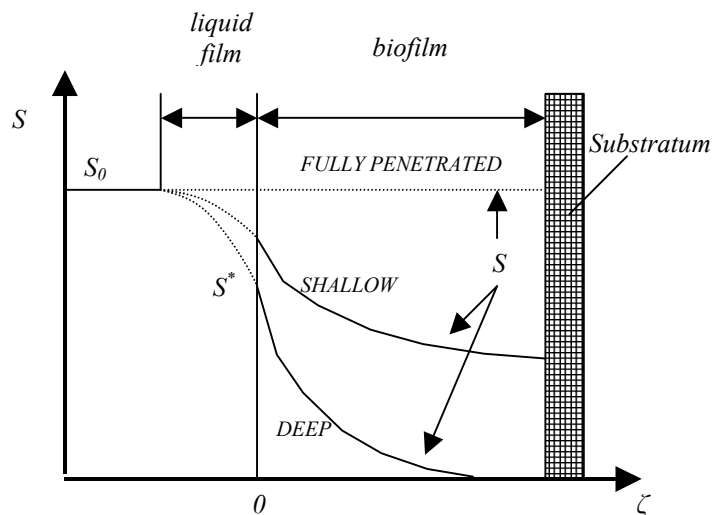


**Figure 2.5: Conceptual model for the 1D Williamson-McCarty-Rittmann model.**

To solve this diffusion-reaction problem, two boundary conditions are necessary. At the biofilm surface it is clear that  $S = S^*$ . When considering a 'deep' biofilm (Figure 2.5), the boundary conditions at  $\zeta = z$  are:

$$\frac{dS}{d\zeta} = 0 \quad \text{and} \quad S = \omega \quad (2.26)$$

where  $\omega$  is a limiting substrate concentration (not necessarily 0) and  $z$  is called the effective thickness of the biofilm. In order to find this effective biofilm thickness, the integration of equation 2.25 is translated into an optimisation problem. Therefore, equation 2.25 is integrated backwards several times starting from different points in the biofilm where the substrate concentration  $S$  is assumed to be  $\omega$ . These integrations proceed towards the biofilm surface. After each integration, the substrate gradient and concentration at the biofilm surface are calculated and compared to  $S^*$ . The optimisation procedure stops when for a chosen starting point  $\zeta$  the calculated substrate concentration at the biofilm surface equals the surface substrate concentration  $S^*$ , at which point the value for the biofilm thickness may be determined. In the case the substrate concentration in the biofilm remains significantly above  $\omega$ , in other words if the biofilm is 'shallow', then the boundary conditions have to be adapted to this fact.

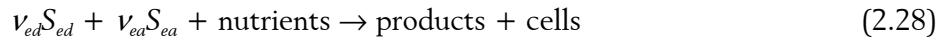
Because the model only uses a single limiting substrate, care has to be taken with the choice whether this is the electron donor with concentration  $S_d$  or the electron acceptor with concentration  $S_a$ . This can be done by making a comparison between the concentrations of both substrates on the relative reaction rate. For both substrates, this influence is given by the term  $S/(S+K_S)$ .

This analysis, and the fact that Monod kinetics are used in this model, leads to the conclusion that the electron acceptor is limiting if

$$S_{ea} < \left( \frac{K_{S,ea}}{K_{S,ed}} \right) \cdot S_{ed} \quad (2.27)$$

In the opposite case, the electron donor is limiting. The possibility that one substrate is limiting at the top of the biofilm and another is limiting at the bottom of the biofilm is not treated at this stage of the model development as opposed to the model of Wanner and Reichert (1996) described further.

Next to substrate limitation, also flux limitation can play a role. With this, the authors mean that it is important to know if the substrate diffusion through the surface film of the biofilm is limiting. For that, a general metabolic reaction rate is considered:



where  $S_{ed}$  and  $S_{ea}$  are respectively the electron donor and acceptor, and  $\nu_{ed}$  and  $\nu_{ea}$  are the stoichiometric coefficients. To fulfil the reaction stated above, the fluxes of electron donor and acceptor should be linked as:

$$\frac{N_{\text{int},ed}}{\nu_{ed} \cdot MW_{ed}} = \frac{N_{\text{int},ea}}{\nu_{ea} \cdot MW_{ea}} \quad (2.29)$$

where  $MW_{ed}$  and  $MW_{ea}$  are the molecular weights of the electron donor and acceptor. On the basis of Fick's law, at each depth in the biofilm one can write:

$$\frac{S_{ed}^* - S_{ed}}{S_{ea}^* - S_{ea}} = \frac{D_{f,ea} \cdot \nu_{ed} \cdot MW_{ed}}{D_{f,ed} \cdot \nu_{ea} \cdot MW_{ea}} \quad (2.30)$$

The species of which the concentration approaches zero the fastest is flux limiting. This indicates that the concentration of the electron acceptor is limiting in the case that

$$S_{ea}^* < \frac{D_{f,ed} \cdot \nu_{ed} \cdot MW_{ed}}{D_{f,ea} \cdot \nu_{ea} \cdot MW_{ea}} S_{ed}^* \quad (2.31)$$

This equation can be reformulated in terms of the bulk liquid concentrations of donor and acceptor. The authors state that in most cases the electron acceptor (oxygen in the case of aerobic metabolism)

will be limiting. This model can only be used if one single substrate is both flux limiting and substrate limiting.

### *Extension of the model with growth and decay of biomass*

In a next step, the model was extended to a model that includes growth and decay of biomass. This was done despite the fact that in steady-state conditions, no net growth and decay can be present (Rittmann and McCarty, 1980a, b). It is clear that different substrate concentrations will result in different biofilm thicknesses. There is also a minimal substrate concentration below which no biofilm development is possible. The thickness of the biofilm is governed by the flux of substrate to the biomass, the growth and the decay of the micro-organisms. The equation introducing growth and decay in the model is:

$$\frac{\partial A_F X d\zeta}{\partial t} = \frac{\mu_{\max} S}{K_S + S} A_F X d\zeta - b A_F X d\zeta \quad (2.32)$$

where  $b$  is the specific biomass decay rate. Note that in this model formulation, the biomass losses due to erosion and sloughing are neglected, so the calculated biofilm thickness should be seen as an overestimation of the real value of the biofilm thickness. To calculate the steady-state biofilm thickness, the assumption is made that in such a situation the amount of biomass that can be sustained by the calculated substrate flux is equal to the biomass associated with the steady-state biofilm thickness. The energy transferred to the biofilm in the form of substrate is  $N_{int} Y$ ; the energy needed to sustain a biofilm of thickness  $L$  is  $XLb$ , so the steady-state biofilm thickness can be written as:

$$L = \frac{N_{int} Y}{bX} \quad (2.33)$$

Rittmann and McCarty, 1980b also deduce a minimal concentration under which no biofilm can develop or in other terms  $\frac{\partial A_F X d\zeta}{\partial t} = 0$ , this concentration is given by:

$$S_{\min} \cong S_{\min}^* = K_S \frac{b}{\mu_{\max} - b} \quad (2.34)$$

where the assumption is made that the minimal concentration in the bulk liquid is about equal to the minimal concentration at the liquid-biofilm interface.

In order to use this model, quite some parameters need to be known; being  $\mu_{\max}$ ,  $K_S$ ,  $Y$ ,  $b$ ,  $X$ ,  $D$ ,  $D_f$  and  $L$  (Table 2.3). The first four parameters were estimated by the authors in systems with suspended micro-organisms, while the density  $X$  was estimated using biofilm thickness and weight measurements. The other parameters were gathered from different literature sources or calculated via empirical formulas ( $L$ ). The method proposed by the authors to solve this model calculates values for  $N_{int}$ ,  $S$  and  $L$  that are valid for a certain steady-state biofilm system. Based on their experiments to validate the model, the authors conclude that

- the persistence of compounds with very low concentrations in wastewater treatment facilities is partially due to the fact the microbial populations can not gather enough energy to sustain growth;
- there is a minimal substrate concentration under which no noticeable biofilm growth is present;
- the calculated biofilm thickness is an overestimation of the measured thickness of the biofilm during experiments.

**Table 2.3. Parameter values for use in the steady-state biofilm model (Rittmann and McCarty, 1980a)**

<i>Parameter</i>	<i>Unit</i>	<i>Value</i>
$k (= \mu_{\max}/Y)$	mg / (mg C . d)	$20 \pm 4.4$
$K_S$	mg/cm <sup>3</sup>	$0.0039 \pm 0.00058$
$X$	mg C/cm <sup>3</sup>	2.5
$Y$	mg C/mg	$0.071 \pm 0.007$
$b$	1/d	$0.205 \pm 0.049$
$D$	cm <sup>2</sup> /d	1.09
$D_f$	cm <sup>2</sup> /d	0.87

### ***Extension of the model with biomass losses due to erosion and sloughing***

To cope with the limitations of the original model – only one substrate, one species and a steady-state situation – other extensions were made to generate a more adequate description of the biofilm. Rittmann and Brunner (1984) developed a variant of the original model that is capable to describe the biofilm dynamically. Together with this, a new biomass decay coefficient  $b'$  is used that also includes the biomass losses due to erosion and sloughing. In their further developments, the authors did not take the fast dynamic processes in the biofilm into account, because still an instantaneous steady-state concentration profile is used, while the growth of the bacteria is modelled dynamically using the equation:

$$\frac{dXL}{dt} = YN_{\text{int}} - b'XL \quad (2.35)$$

This way the model is capable of describing transients in the growth of a biofilm. Indeed, the integration of equation 2.35 is used to adjust the biofilm thickness in finite time steps  $\Delta t$ .

### ***Extension of the model with two substrates***

The model was further extended with the possibility to model the conversion of two substrates (Namkung & Rittmann, 1987). It is possible that a substrate is available in a too low concentration to sustain the biofilm, but it is used anyway because another substrate provides for the bulk amount of energy needed by the biofilm. In this case, however, the model only considers a single species in a steady-state situation. The essential difference between this description and the original model is the formulation for the biofilm thickness  $L$ .

$$L = \frac{N_{\text{int},1}Y_1 + N_{\text{int},2}Y_2}{b'X} \quad (2.36)$$

Using this model, the authors conclude the following:

- When a spore element is present in very small concentrations, the kinetics of its removal will be highly dependent on the kinetics of the element that is available to the biomass in higher concentrations.
- In case the concentration of the element is somewhat higher and about equal to  $S_{min}$ , its removal is more and more governed by its own kinetic parameters.

### ***Extension of the model with two competing species***

The next step in the model development was the integration of two competing species in the biofilm (Rittmann and Manem, 1992). From their analysis, it becomes clear that a slower growing organism has some advantages as well as disadvantages. The slower growing species takes advantage of the fact that it is less affected by erosion losses by friction with the bulk liquid phase. However, since they grow in deeper layers of the biofilm, the resistance for substrate transport to these species is relatively big.

In this model description, again an instantaneous steady-state concentration profile is used. The steady-state mass balances for the different competing species in a fixed control volume of biofilm are calculated as:

$$(\text{biomass flux out})_j = (\text{biomass flux in})_j + (\text{net growth})_j \quad (2.37)$$

The flux of biomass is proportional to the integrated growth of all biomass deeper in the biofilm and the fraction of species  $j$  at that position.

$$(\text{biomass flux in})_j = f_j \int_0^z (\text{net growth rate of all species}) d\zeta \quad (2.38)$$

The net growth rate of a species  $j$  is equal to  $(\mu_j - b_j)f_jX$  for the species  $j$  out of a total of  $n$  species, where  $\mu_j$  is the specific growth rate of species  $j$  and  $b_j$  is its specific decay rate. The fraction of the total microbial mass made up by the species  $j$  is represented by  $f_j$ . The growth rate of inert material in the biofilm is equal to:

$$(\text{net growth rate})_{\text{inerts}} = \sum_{i=1}^n b_i (1 - f_i) f_i X \quad (2.39)$$

where  $(1 - f_d)$  denotes the fraction of the microbial mass that gives rise to inert particulates when decaying. When the growth rate of all species is integrated from the substratum to a position  $z$  and is summed for all species also including the inert particulate matter, equation 2.38 becomes:

$$(\text{biomass flux in})_j = f_j X \sum_{j=1}^{n_x} \int_0^z (\mu_j - b_j f_d) f_j d\zeta \quad (2.40)$$

Knowing this, and after rewriting equation 2.37 as:

$$d(\text{biomass flux})_j = (\text{net growth})_j \quad (2.41)$$

it can be concluded that:

$$df_j F_x = (\mu_j - b_j f_d) f_j X d\zeta \quad (2.42)$$

in which  $F_x$  is the summation of fluxes of all species  $n_x$  at position  $z$ .  $F_x$  is found by dividing equation 2.40 by  $f_j$ . Application of the chain rule to equation 2.42 yields:

$$f_j \frac{dF_x}{d\zeta} + F_x \frac{df_j}{d\zeta} = (\mu_j - b_j f_d) f_j X \quad (2.43)$$

After substitution of  $F_x$  and its derivative in 2.43, the final form of the mass balance in species  $j$  is found:

$$\frac{df_j}{d\zeta} \sum_{i=1}^n \int_0^z (\mu_j - b_j f_d) f_j d\zeta = (\mu_j - b_j f_d) f_j - f_j \sum_{j=1}^n (\mu_j - b_j f_d) f_j \quad (2.44)$$

Solving this mass balance generates a steady-state solution of the species distribution in the biofilm, also incorporating the inert products formed by decay.

### 2.5.3.3 The state-of-the-art 1D model of Wanner and Reichert (1996)

The biofilm model that is widely considered state-of-the-art in 1D biofilm modelling, is the model developed by Wanner and Gujer (1986) and further extended and refined in Wanner and Reichert (1996). It is a mixed model in which mechanistic equations (mass balances...) as well as empirical parts (equations for attachment and erosion, ...) are present (Figure 2.6). The recent changes are mostly the result of new experimental findings (Wanner, 1995), namely

- the transport of soluble components in a biofilm is not always the direct result of molecular diffusion;
- the transport of particulates can not always be related to the net growth of biomass;
- the volume of the liquid fraction (porosity) in the biofilm is not constant;
- the attachment and erosion of particles to the surface of the biofilm should be included as essential processes.

In the publication of Wanner and Reichert (1996), the model has been developed with boundary conditions valid for an ideally mixed bulk liquid phase. An empirical mass transfer coefficient is included to describe the mass transfer resistance from bulk liquid to biofilm.

The model is quite complex in terms of its capability to differentiate within the biofilm between different species and substrates at different sites in the biofilm. However, still, functional homogeneity is assumed within one species. The non-homogeneous distribution of the species in space, however, makes it possible to model the species composition of the biofilm at different depths. This way, it becomes clear that slower growing autotrophs can not stand the higher erosion forces at the biofilm surface and therefore are

forced to develop in deeper layers of the biofilm where, however, the oxygen concentration easily becomes limiting to nitrification.

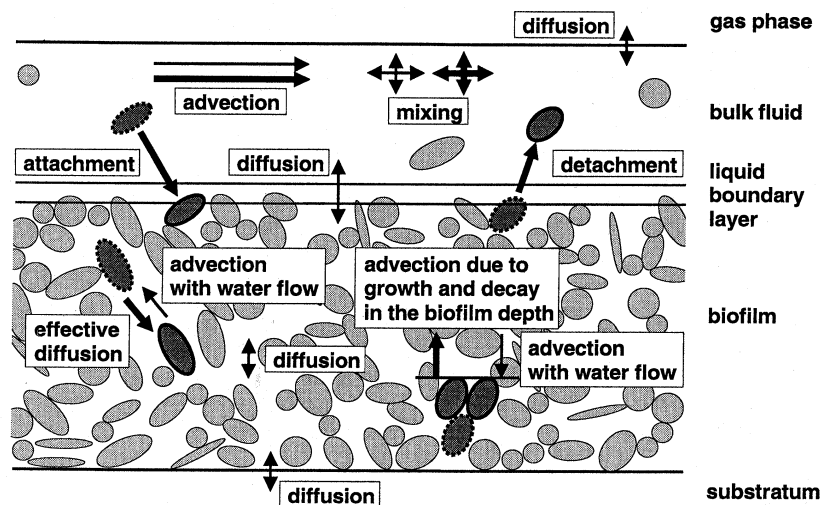


Figure 2.6: Transport processes considered in the mixed-culture biofilm model. Thick arrows refer to particulates, thin arrows to dissolved components (Wanner and Reichert, 1996)

The model is based on the mass conservation law formulated as a partial differential equation.

$$\frac{\partial D(\zeta, t)}{\partial t} + \frac{\partial J(\zeta, t)}{\partial \zeta} = \mathcal{R}(\zeta, t) \quad (2.45)$$

In this equation  $D$  is vector of one-dimensional variables that describe quantities per unit of length.  $J$  is a vector of variables describing quantities per unit of time, while  $R$  represents the production rates of the different components in the biofilm, defined per unit of length and time. The length coordinate  $\zeta$  is taken perpendicular to the substratum and is defined with  $\zeta = 0$  at the substratum.

The state variables in the model are subdivided into several particulate ( $X_j$ ) and soluble ( $S_j$ ) components. Their concentration is averaged over a plane parallel to the substratum. The components  $X_j$  are represented per unit of total volume, whereas the components  $S_j$  are represented per unit of the water phase. If  $\rho_j$  is the density of the particles of type  $j$  in the biofilm, the volume of the water phase in the biofilm can be defined as:

$$\varepsilon_l = 1 - \sum_{k=1}^{n_x} \frac{X_k}{\rho_k} \quad (2.46)$$

The model assumes that the growth of particulate matter (biomass) in the film leads to an advective displacement – thus an increase – of the biofilm thickness. Also, a change of the total water volume in the biofilm gives rise to an increase of the biofilm thickness. The advective velocity of the biofilm at any coordinate  $\zeta$  is given by the sum of both.

$$u_F = \frac{1}{A_F} \int_0^{\zeta} \left( \sum_{k=1}^{n_X} \frac{r_{X,k}}{\rho_k} + r_{\varepsilon_l} \right) A_F d\zeta \quad (2.47)$$

In many cases, the porosity of the biofilm – the water fraction inside the biofilm – is assumed to be constant. The production of water is in that case proportional to the volumetric production of particulate matter, or:

$$r_{\varepsilon_l} = \frac{\varepsilon_l}{1 - \varepsilon_l} \sum_{k=1}^{n_X} \frac{r_{X,k}}{\rho_k} + r'_{\varepsilon_l} \quad (2.48)$$

Here the last term accounts for an eventual change of the porosity of the biofilm. This term can for example be modelled dependent on the distance to the substratum, the growth rate...

The one-dimensional densities defined in the mass conservation law can now further be refined as:

$$\mathcal{D} = \begin{bmatrix} X_j \\ \varepsilon_l \cdot S_i \\ \varepsilon_l \end{bmatrix} \cdot A_F \quad (2.49)$$

The corresponding fluxes are modelled as:

$$j = \begin{bmatrix} u_F X_j - D_{f,X,j} \frac{\partial X_j}{\partial \zeta} \\ -(1 - \varepsilon_l) u_F S_i + \sum_{k=1}^{n_X} \frac{D_{f,X,k}}{\rho_k} \frac{\partial X_k}{\partial \zeta} S_i - \varepsilon_l D_{f,S,i} \frac{\partial S_i}{\partial \zeta} \\ \varepsilon_l u_F + \sum_{k=1}^{n_X} \frac{D_{f,X,k}}{\rho_k} \frac{\partial X_k}{\partial \zeta} \end{bmatrix} \cdot A_F \quad (2.50)$$

The first row of this set of equations represents the flux of particulate matter in the biofilm. The first term describes the advective transport through the biofilm caused by the growth processes taking place. The second term describes the displacement of the particular components that can be modelled using a diffusive process with an effective diffusion constant. This displacement is introduced to account for “mixing” of cells or particles in the biofilm matrix as a result of mechanical deformation of the matrix by hydraulic forces.

The second row describes the flux of soluble matter. The first two terms introduce a flux that is indirectly caused by the growth processes in the biofilm. These processes also cause a water displacement in the film, that compensates for the volume changes caused by these growth processes. The third term again models a diffusive transport of the soluble components in the pores of the film. This diffusive transport is, however, not necessarily caused by molecular diffusion, but it can also include eddy-diffusion. In all cases an effective diffusion constant should be used instead of a molecular diffusion constant.

The last row describes the flux of the volume of free water in the biofilm. The first term again describes the advective movement, while the second term compensates for the diffusive flux of particulate components in the film.

To complete the conservation law, the transformation processes still need to be given. They are represented as:

$$\mathcal{R} = \begin{bmatrix} r_{X,j} & r_{S,i} & r_{\varepsilon_l} \end{bmatrix}^T \cdot A_F \quad (2.51)$$

These reaction rates describe processes of mass transformation per unit of total biofilm volume, including the particulate components. For the further elaboration of the transformation term, it is possible to rely on an approach very much alike the Activated Sludge Model No. 1 of the IWA (Henze et al., 1987). As an example only aerobic processes are included here, but other processes like denitrification can be included very easily (Table 2.4). A matrix format is chosen here for the representation of the model. In the first row of the matrix, the components of relevance in the model are identified. In the first column, the biological processes occurring in the system are listed, whereas their respective process rates are given in the last column. The elements within the matrix are the stoichiometric coefficients, which set out the mass relationships between the components in the individual processes. More information on this matrix format representation is given in section 3.4.4.2 of this thesis

**Table 2.4. Microbial kinetics and stoichiometry (Wanner and Reichert, 1996)**

Process	$X_H$	$X_A$	$X_I$	$S_S$	$S_{NH_4}$	$S_O$	Process rate
heterotrophic growth	1	-	-	$-1/Y_H$	-	$-\frac{\alpha_H - Y_H}{Y_H}$	$\mu_H \frac{S_S}{K_S + S_S} \frac{S_O}{K_{O,H} + S_O} X_H$
heterotrophic inactivation	-1	-	1	-	-	-	$k_H X_H$
heterotrophic respiration	-1	-	-	-	-	-1	$b_H \frac{S_O}{K_{O,H} + S_O} X_H$
autotrophic growth	-	1	-	-	$-1/Y_A$	$-\frac{\alpha_A - Y_A}{Y_A}$	$\mu_A \frac{S_{NH}}{K_{NH} + S_{NH}} \frac{S_O}{K_{O,A} + S_O} X_A$
autotrophic inactivation	-	-1	1	-	-	-	$k_A X_A$
autotrophic respiration	-	-1	-	-	-	-1	$b_A \frac{S_O}{K_{O,A} + S_O} X_A$

Integration of the above equations into mass balance equations, yields the following description:

$$\begin{aligned}
\frac{\partial X_j}{\partial t} &= -u_F \frac{\partial X_j}{\partial \zeta} + \frac{1}{A_F} \frac{\partial}{\partial \zeta} \left( A_F D_{f,X,j} \frac{\partial X_j}{\partial \zeta} \right) - r'_{\varepsilon_l} X_j \\
&\quad + \left( r_{X,u} - \frac{X_j}{1 - \varepsilon_l} \sum_{k=1}^{n_X} \frac{r_{X,k}}{\rho_k} \right) \\
\frac{\partial S_i}{\partial t} &= \frac{1 - \varepsilon_l}{\varepsilon_{l,F}} u_F \frac{\partial S_i}{\partial \zeta} + \frac{1}{\varepsilon_{l,F}} \sum_{k=1}^{n_X} \frac{r_{X,k}}{\rho_k} S_i \\
&\quad + \frac{1}{A_F \varepsilon_l} \frac{\partial}{\partial \zeta} \left( A_F \sum_{k=1}^{n_X} \frac{D_{f,X,k}}{\rho_k} \frac{\partial X_k}{\partial \zeta} \right) \\
&\quad + \frac{1}{A_F \varepsilon_l} \frac{\partial}{\partial \zeta} \left( \varepsilon_l D_{f,S,i} \frac{\partial S_i}{\partial \zeta} \right) + \frac{1}{\varepsilon_l} r_{S,i} \\
\frac{\partial \varepsilon_l}{\partial t} &= -u_F \frac{\partial \varepsilon_l}{\partial \zeta} - \frac{1}{A_F} \frac{\partial}{\partial \zeta} \left( A_F \sum_{k=1}^{n_X} \frac{D_{f,X,k}}{\rho_k} \frac{\partial X_k}{\partial \zeta} \right) + (1 - \varepsilon_l) r'_{\varepsilon_l}
\end{aligned} \tag{2.52}$$

The first of these three equations describes the evolution in time of the concentration of the particulate components in the biofilm at a certain depth  $\zeta$ . The first term on the right hand side describes the effect of the advective transport between the substratum and the position  $\zeta$  caused by growth processes. The second term models the diffusive transport of the particulate components in the biofilm. The third term describes the eventual porosity change, while the last term incorporates the growth processes in the biofilm.

The second equation does the same for the soluble components. The first term incorporates the advective transport of solubles together with the water flux in the biofilm caused by particulates growing in the film. The second term describes the direct effect of the growth of particulate components on  $S_{F,i}$ . The next two terms include diffusive transport of particulates and solubles causing concentration changes, and the last term describes the transformation processes that include the consumption or the production of soluble components by the biomass.

The last equation describes the change of the free water volume inside the film. The first two terms describe respectively the influences of advective and diffusive transport of particulates in the film, while the last term includes possible porosity changes.

The evolution in time of the biofilm thickness is given by:

$$\frac{dL}{dt} = u_T \tag{2.53}$$

In this formula, the advective velocity of the liquid-biofilm interface is not equal to  $u_F(L)$ . The difference is caused by processes of attachment and detachment at the biofilm surface.

$$u_T = u_F(L) - u_{dt} + u_{at} \quad (2.54)$$

In this formula,  $u_{dt}$  en  $u_{at}$  are respectively the attachment and erosion velocities. For these velocities Wanner and Reichert (1996) propose functions of the different particulate components concentrations:

$$\begin{aligned} u_{dt} &= \frac{1}{1 - \varepsilon_l} \sum_{k=1}^{n_x} \frac{k_{dt,k} X_k}{\rho_k} \\ u_{at} &= \frac{1}{1 - \varepsilon_l} \sum_{k=1}^{n_x} \frac{k_{at,k} X_k^*}{\rho_k} \end{aligned} \quad (2.55)$$

The superscript \* at  $X_k$  here denotes the concentration at the liquid-biofilm interface. As mentioned before, erosion is most likely also dependent on the fluid velocity and other factors in the reactor. Most studies up to now however treat erosion in steady-state conditions. The empirical formulas resulting from these studies do not contain enough information to adequately introduce this into the model description (Rittmann, 1982; van Loosdrecht *et al.*, 1995).

To be able to solve the above set of equations, appropriate boundary conditions are necessary. For particulate components, the boundary condition at the substratum states that no particulate material is exchanged between substratum and biofilm, or  $dX_k/d\xi = 0$  at the substratum. For soluble components, an impermeable substratum can be modelled, but also diffusion through or sorption at the substratum can be included in the boundary conditions.

At the biofilm surface, the flux of particulate components out of the biofilm should be equal to the interfacial transfer rate from biofilm to liquid phase. This interfacial transfer rate is caused by detachment and attachment processes. For dissolved components, the concentration at the biofilm surface is equal to the concentration directly outside the biofilm.

## 2.5.4 Modelling erosion and sloughing in biofilm reactors

### 2.5.4.1 Causes of biofilm loss

Bryers (1988) distinguished five different causes for sloughing in biofilm reactors: erosion, abrasion, sloughing, grazing by predators and human intervention. In practice, however, the exact reason is very hard to find. Mostly a combination of these phenomena will be the reason for biomass loss in a biofilm reactor.

#### **Erosion**

Erosion can be defined as the loss of individual cells or smaller cell groups at the biofilm surface. It is a continuous process that is closely related to the fluid dynamics in the reactor (Chang and Rittmann, 1988). The physical causes for erosion are Brownian motion and the friction forces coming from the flowing fluid. Erosion is said to increase with increasing biofilm thickness and with increasing fluid shear (Figure 2.7). Biofilms that are subject to high friction forces are normally characterised by a relatively smooth surface compared to biofilms undergoing sloughing (Characklis and Marshall, 1990).

Biofilms growing under circumstances of high erosion can be subject to adaptations of the microbial biomass. A more concentrated growth and an increase of the extracellular polymeric substances (EPS) is possible so as to attain a stronger biofilm (Gjaltema, 1996).

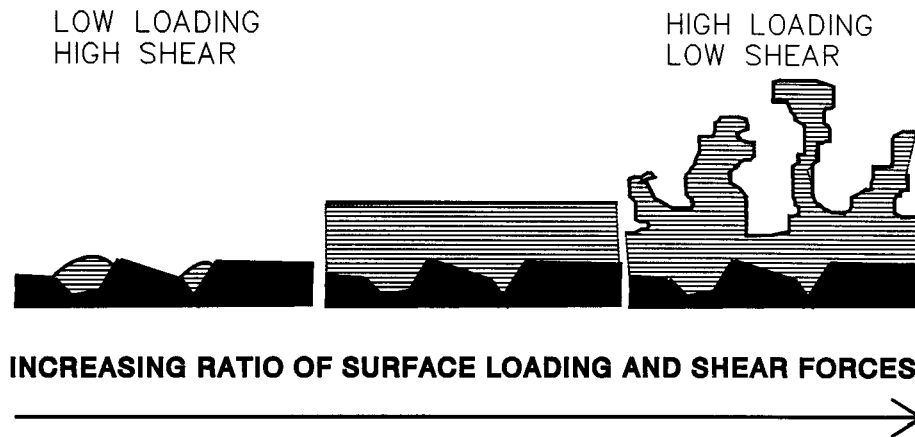


Figure 2.7: Schematic representation of the influence of surface loading and shear forces on the structure of a biofilm (van Loosdrecht *et al.*, 1995)

### **Abrasion**

Abrasion is the loss of biofilm due to the collisions of biofilm particles to other (biofilm) particles or the reactor wall. This is a factor of importance when modelling biofilm reactors with a moving carrier material such as fluidised beds or biofilm airlift suspension reactors. In the case of low concentrations of carrier material, abrasion may not be the major source of biofilm loss. Turbulent eddies in the reactor can cause much more damage to the biofilm structure. At higher carrier concentrations, however, abrasion becomes the major source of biomass loss.

### **Sloughing**

Sloughing can be described as the sudden loss of big pieces of biofilm due to suddenly changing conditions in the biofilm system (Characklis and Marshall, 1990). As opposed to erosion and abrasion, sloughing is not a continuous process, and therefore it can be a reason for frequent variations in the removal efficiencies of biofilm reactors (Howell and Atkinson, 1976). A wide range of physico-chemical and biological factors can induce sloughing of the biomass. Several factors can also interact, so a strict distinction can not be made.

#### 1. Physical causes of sloughing

In the first place erosion and abrasion can be the basis for sloughing. Sometimes not only small cell clusters will be lost during these processes, but the entire biofilm may come off the carrier material because of damage to the biofilm structure (Tijhuis *et al.*, 1994; Gjaltema, 1996). Another possible explanation for sloughing is the vortex street, which is an induced vibration characterised by a Reynolds number of several hundreds (Lewandowski and Stoodley, 1995). This vortex street causes biofilm extrusions to move, causing the complete biofilm to oscillate and eventually break off. Also gas formation in the deeper layers of the biofilm may cause sloughing (Characklis and Marshall, 1990). Even temperature and substrate concentration changes may play a role.

## 2. Biological and cell related causes of sloughing

Biological processes resulting in sloughing are, amongst others, microbial production of surfactants and cell division. Also the lysis of bacteria as a result of substrate limitation can lead to irregularities in the biofilm matrix (Gantzer *et al.*, 1989). Proteinases and polysaccharide polymerases are capable of hydrolysing and depolymerising a range of components. This might cause a weakened biofilm matrix or morphological changes in the biofilm.

## 3. Chemical and biochemical causes of sloughing

Chemical causes of sloughing can be related to the destabilisation of the polymer matrix of the biofilm. Among others cation exchange, *pH* changes, a changing substrate concentration or a changing ionic strength can play a role (Gantzer *et al.*, 1989). Sloughing is more obvious in thick biofilms in a rich environment (Chang and Rittmann, 1988). A sudden increase of the nutrient concentration in the bulk liquid or a toxic shock can cause sloughing to happen (Trulear and Characklis, 1982).

### ***Grazing by predators***

The amount of studies investigating the role of protozoa in biofilm studies is rather limited. However, biofilms can be an important source of nutrition for protozoa like ciliates, flagellates... Stimulating the grazing by protozoa is considered as a promising tool in controlling biomass accumulation in biotrickling filters (Cox and Deshusses, 1999). Mostly the interest in grazing is limited to the microscopic level. However, also large populations of macro-invertebrates, like insects, arachnids, worms, ... can live in percolating filters and give rise to a considerable loss of biomass in the biofilm.

### ***Human intervention***

The addition of chemical substances can cause a lot of damage to the biofilm structure and give rise to an increased biomass loss rate. For example the presence of calcium specific chelants (*e.g.* EDTA) in the water phase will cause the biofilm to come off the substratum. Again, this underlines the essential role of calcium in the biofilm integrity (Turakhia *et al.*, 1983). Other possible methods to combat unwanted biofilms are oxidising biocides, surfactants and non-oxidising biocides (Characklis and Marshall, 1990).

#### **2.5.4.2 Modelling biofilm loss in biofilm reactors**

Despite its importance for the formation and stability of a biofilm, biofilm loss through erosion, sloughing and abrasion is still one of the least understood phenomena in biofilm research. However, during the last two decades, quite some mathematical expressions to describe the rate of biofilm loss have been formulated (Peyton and Characklis, 1993; Stewart, 1993; Tjihuis *et al.*, 1994; Gjaltema, 1996). Peyton and Characklis (1993) carried out a statistical analysis of some of these formulas. It turned out that the correlation with the data was better in case the model formulation was biofilm growth related. Models depending on fluid shear did not give an equally good result. These authors state that (1) the fluid shear is not of very significant importance in the rate of erosion and (2) a formula containing the product of the substrate removal rate, the yield coefficient and the biofilm thickness gave the best result with their data set.

Stewart (1993) developed a more general mathematical framework for the modelling of biofilm loss, based on a mass balance of the biomass. He proposes an equation that calculates the biofilm loss based on the product of the biofilm loss frequency with the mass of the loosening particles:

$$r_d = \int_0^L f_e(\zeta) \cdot (L - \zeta) \cdot A_F \cdot X_i(\zeta) \cdot d\zeta \quad (2.56)$$

where  $X_i$  represents the local density of component  $i$  and  $f_e$  is the local erosion or biofilm loss frequency. The total biomass loss frequency  $F_e$  is then given by:

$$F_e = \int_0^L f_e(\zeta) \cdot d\zeta \quad (2.57)$$

### 2.5.5 *Mathematical Modelling biofilm structure - cellular automaton models*

Cellular automata can be described as discrete systems in space and time. The state of an automaton is hereby determined by a set of logical rules that have a local influence, but are globally valid. Although they are apparently simple, cellular automata are capable of simulating highly complex systems that have a high degree of non-linearity and thus are very difficult to represent by a set of differential equations (Wolfram, 1984; Lazlo and Silman, 1993; Wimpenny and Colasanti, 1997).

Essentially, the characteristics of a cellular automaton are:

- its state, a number or a property that differs from cell to cell;
- its surroundings, the ensemble of cells that interacts with the cell in question;
- its program, a set of rules that define how the state of the cell will change dependent on its current state and the state of the surrounding cells.

A one-dimensional cellular automaton is defined by a row of cells, each having a value of 0 or 1 or more generally a value 0, 1, ...,  $k - 1$ . The value  $a_i$  of each cell  $i$  can be changed in discrete time steps according to a deterministic set of rules  $\Phi$  and dependent on the value of the surrounding cells.

$$a_i^{(t+1)} = \Phi[a_{i-r}^{(t)}, a_{i-r+1}^{(t)}, \dots, a_{i+r}^{(t)}] \quad (2.58)$$

Even when  $k = 2$  and  $r = 1$  or  $2$ , the behaviour of a CA can be quite complex. Only recently, this technique was used in modelling biofilm systems, and more specifically in the framework of investigations to the theoretical relationship between environmental conditions and the biofilm structure.

#### 2.5.5.1 **An adapted DLA-model**

Wimpenny and Colasanti (1997) based their CA on an existing model (Colasanti, 1992) that adds biological rules to a diffusion limited aggregation (DLA) model. This type of model tries to mimic a system in which a component can diffuse and aggregate to cells in a growing structure. They are part of a subset of CA, known as gas-lattice systems. They differ from traditional CA in that particles can move between the grid cells following predefined rules.

In this case, stationary microbial cells each occupy a square cell and are capable of reproducing themselves. Each action of the microbial cell is governed by substrate conversion. However, taking into account only substrate conversion in biofilm formation provoked quite some reaction from other authors, among which van Loosdrecht *et al.* (1997). Next to the availability of substrate, also biomass loss phenomena play an important role in forming the biofilm structure.

### 2.5.5.2 A CA model for two-dimensional biofilm morphology

Hermanowicz (1998) too developed a simple two-dimensional CA model. In this modelling approach, each grid cell is occupied by biomass that grows or detaches every time step. The other cells are filled with water. Outside the boundary layer, the substrate concentration is kept constant ( $S=S_0$ ). Inside the biofilm it is subject to diffusional processes. The probability for a cell to reproduce and grow is indicated by the expression:

$$\frac{S}{1+S} \quad (2.59)$$

When a cell grows, this happens in the direction where the smallest resistance is present, this is the direction with the smallest distance to the biofilm surface. All other cells in that direction move one cell by this growth. A cell at the biofilm surface can erode due to the fluid shear stress  $\tau$ . The probability for a cell to come off the biofilm surface is:

$$\frac{1}{1+\frac{\sigma}{\tau}} \quad (2.60)$$

where  $\sigma$  is a measure for the biofilm strength. Simulations were carried out by Hermanowicz (1998) for different substrate concentrations, substrate diffusion coefficients and kinetic parameters. Only the boundary layer thickness and the strength of the biofilm was changed. The results of these simulations are summarised in Table 2.5.

**Table 2.5. Influence of a variation of boundary layer thickness and biofilm strength on the biofilm structure and the mass transport in the biofilm (Hermanowicz, 1998)**

VARYING PARAMETER VALUES	PREDICTED BIOFILM STRUCTURE BY THE CA-MODEL AND EVENTUAL CONSEQUENCES FOR MASS TRANSPORT
1. Small boundary layer thickness Intermediate biofilm strength	Development of a compact, homogeneous biofilm Formation of a relatively flat surface
2. Large boundary layer thickness Intermediate biofilm strength	Development of an extremely stratified biofilm Diffusion is dominant, despite the open structure, convective transport is limited by the large boundary layer thickness
3. Large boundary layer thickness Limited biofilm strength	Growth of a biofilm in a mushroom-like structure (de Beer <i>et al.</i> , 1994) or tulips (Hermanowicz <i>et al.</i> , 1995) A relatively high substrate penetration thanks to the open structure of the biofilm, despite the thickness of the boundary layer

### 2.5.5.3 A combined differential discrete CA approach

Picioreanu *et al.* (1998a, b) combined the discrete representation of the solid phase (biomass) by means of cellular automata, with continuous methods for soluble components (substrate) to predict possible biofilm structures. Contrary to the model developed by Wimpenny and Colasanti (1997), this model is not only limited to biofilm growth at the surface of the biofilm. Growth can also take place at the inside of the biofilm structure. The pressure caused by the growth of bacteria inside the biofilm leads to an expansion of the microcolonies, so that the biofilm can grow in three dimensions.

While older model approximations produced structures that evolved according to a discrete time, the combination of discrete and continuous models allows to predict the biofilm structure along with a correct description of the concentrations, fluxes and conversion rates in time.

## 2.6 In situ parameter estimation in biofilm systems

### 2.6.1 Introduction

In order to solve the models described above, and to use them for the description and the prediction of the behaviour of biofilm systems, values for the kinetic and stoichiometric parameters have to be chosen. Up to now, no general method has been accepted to estimate or measure the values of these parameters. Most of them cannot be measured in actual treatment plants – and even in controlled laboratory biofilm reactors many parameters are difficult to determine (Morgenroth *et al.*, 2000). Generally, during the calibration of biofilm models, a subset of the complete parameter set is calibrated using measurement results; the rest is taken from literature. It should be investigated which parameters in biofilm systems are significant and also which ones are identifiable. Quite some parameters in complex model descriptions are impossible to accurately determine using the measurements currently available for investigating biofilm systems. In the following, some attempts are described to estimate biofilm parameters, with the focus on the uncertainty and the identifiability problems that have been encountered in this research.

For the determination of parameters in biofilm systems, and more specifically kinetic parameters, quite some influencing factors have to be taken into account (Ellis *et al.*, 1996).

First of all, the estimated parameters will be highly dependent on the circumstance under which the biomass has developed. A classical technique is to derive kinetic parameters from batch experiments with suspended biomass and to use these parameters in biofilm systems (Livingston and Chase, 1989). However, the conditions in suspended growth systems are totally different from the ones in biofilm systems. The bacteria in a biofilm are embedded in a matrix of EPS, with its channels and pores. To bring these organisms in suspension, the complete biofilm matrix has to be broken up. Next to this, the substrate concentration gradients noticed in a biofilm are less obvious in suspended growth cultures. Parameter estimations based on suspended cultures should thus be used with care within biofilm systems modelling (Grady *et al.*, 1996).

Another technique that is often used, is to form pseudo suspended cultures in which biofilms are taken from a biofilm reactor and are examined in a batch test (Cao and Alaerts, 1995). Even in this case, the possibility for disruption of the biofilm matrix is high.

To overcome these problems, it is recommendable to estimate the biofilm parameters “in situ”. This way the biofilm is left intact.

A second factor to be taken care of while doing kinetic tests is the initial substrate to biomass concentration ratio ( $S_{init}/X_{init}$ ) (Grady *et al.*, 1996). Using a large proportion will make the bacteria tune their metabolism to a level that is typical for unlimited growth. Therefore it is possible that the measured kinetic parameters are no longer influenced by the growth history of the bacterial population. These parameters might not be a very good approximation of the growth characteristics of the original population. Kinetic parameters obtained this way are called intrinsic parameter values.

When a low  $S_{init}/X_{init}$  is used, the micro-organisms retain their original physiological state, making the measured parameters a better approximation of the real growth parameters of the population. These extant parameter values are however difficult to obtain, due to the low substrate concentrations needed in the tests. This makes it difficult to measure substrate concentration changes. In the following, it will be explained why respirometry might be a way out of this problematic situation.

## 2.6.2 *Measuring biofilm kinetic parameters using respirometry*

### 2.6.2.1 **An introduction to respirometry**

Respirometric experiments can be used to estimate kinetic parameters on the basis of oxygen uptake rate profiles. This method can serve as an alternative to classical methods based on substrate removal profiles. Indeed, there is a direct stoichiometric relationship between oxygen and substrate removal:



Respirometry has a number of advantages compared to classical substrate removal measurement (Riefler *et al.*, 1998).

1. Electrodes measuring dissolved oxygen are quite sensitive and robust and can work at the low oxygen levels at which small changes in the oxygen concentration should be measured.
2. Dissolved oxygen measurements can be done in situ, which means the reactor need not be disturbed and no biomass has to be removed.
3. Measurements can be performed automatically and continuously.
4. Respirometry can be used to estimate the kinetic parameters of the degradation of different kinds of substrates and also degradation of mixtures of substrates can be monitored.
5. Using respirometry, extant parameters values can be determined, because working at low substrate concentrations is possible.

### 2.6.2.2 **In situ measurement of kinetic parameters using respirometry**

Riefler *et al.* (1998) developed a biofilm model to estimate the kinetics of cell growth, substrate removal and also the substrate diffusion resistance in a biofilm. For their goal, they used a biofilm

model that is an adaptation of the model introduced by Rittmann and McCarty (1980b), explained in paragraph 2.5.3.2.

Transport of oxygen and substrate in the biofilm boundary layer (the modelled stagnant water layer), is described as:

$$\begin{aligned}\frac{\partial S_s}{\partial t} &= D_{f,S_s} \frac{\partial^2 S_s}{\partial \zeta^2} \\ \frac{\partial S_o}{\partial t} &= D_{f,S_o} \frac{\partial^2 S_o}{\partial \zeta^2}\end{aligned}\quad (2.62)$$

However, transport and conversion of oxygen and substrate in the biofilm itself is modelled as:

$$\begin{aligned}\frac{\partial S_s}{\partial t} &= D_{f,S_s} \frac{\partial^2 S_s}{\partial \zeta^2} - \frac{\mu_{\max}}{Y} X \frac{S_s}{K_s + S_s} \\ \frac{\partial S_o}{\partial t} &= D_{f,S_o} \frac{\partial^2 S_o}{\partial \zeta^2} - \frac{1-Y}{Y} \mu_{\max} X \frac{S_s}{K_s + S_s} - bX\end{aligned}\quad (2.63)$$

The research of Riefler *et al.* (1998) had not as a primary goal to find the exact values of the kinetic parameters, but to formulate a general method for the use of respirometry in estimation kinetic parameters. A lot of attention was therefore paid to sensitivity analysis and the influence of measurement error on the values of the estimates. No laboratory experiments were conducted, but the model developed assumed an experimental set-up as described in the following (Figure 2.8).

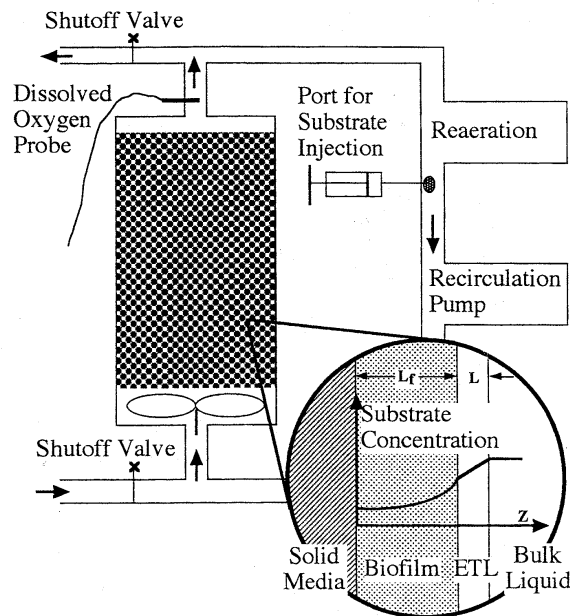


**Figure 2.8: Hypothetical bioreactor and conceptual biofilm model proposed by Riefler *et al.* (1998)**

In order to apply this method in the laboratory, a biofilm should be grown in a reactor under steady-state conditions, while supplying excess oxygen. Once the biofilm has reached steady state, it should

be fed with a solution without substrate or oxygen, and aeration should be stopped. The oxygen uptake in the reactor is then followed up to the point where a constant oxygen consumption rate versus time is found. This means that the oxygen uptake is only due to endogenous respiration of the biofilm. Riefler *et al.* (1998) conclude that at this point, the substrate concentration at each point in the reactor is zero. This way, the initial conditions for substrate is known throughout the system.

After this, the influent should be aerated until a steady-state oxygen concentration in the liquid phase of the reactor is found and thus a steady-state oxygen uptake is attained. The differential equations of the model can at that point be simplified to:

$$\begin{aligned}\frac{\partial^2 S_s}{\partial \zeta^2} &= 0 \\ \frac{\partial^2 S_o}{\partial \zeta^2} &= \frac{b \cdot X}{D_{f,S_o}}\end{aligned}\tag{2.64}$$

Starting from this set of equations, the initial oxygen concentration in the boundary layer and in the biofilm can be found.

Now a small pulse of substrate is injected and the oxygen uptake is measured as a function of time. When the pulse is sufficiently small, the extant kinetic parameters can be estimated using a least squares method (Figure 2.9), minimising

$$f(\hat{\mu}_{\max}, \hat{K}_s) = (y_{obs} - y_{model})^T \cdot W^{-1} \cdot (y_{obs} - y_{model})\tag{2.65}$$

Where  $y_{obs}$  is a vector of observations in the experimental oxygen profile and  $y_{model}$  are the model predicted values.  $W$  is a covariance matrix of the measurement errors on the experimental data. The diagonal elements of this matrix are the variances of the measurements done during the experiments. The covariance between the measurements can be found as the other elements of the matrix.

In order to estimate the uncertainty on the parameter estimates, a sensitivity analysis was carried out in which one model parameter was varied and the other parameters were kept constant so as to check the influence of the parameter on the predicted oxygen profiles. Next to the sensitivity to the values of the parameters  $\mu_{\max}$  en  $K_s$ , also the diffusion coefficients of the substrate, the biofilm thickness and density were evaluated and shown to have a considerable influence on the predicted profiles. It was concluded that correct values for these parameters should be known in order to correctly estimate  $\mu_{\max}$  en  $K_s$ .

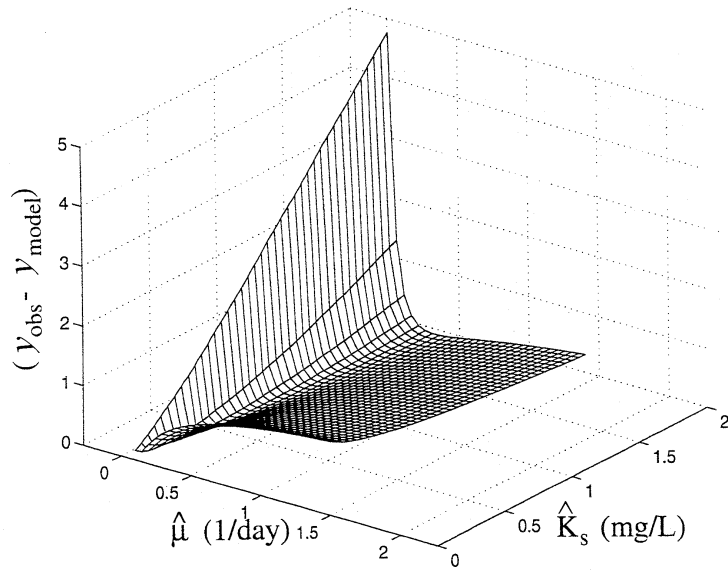


Figure 2.9: Orthographic projection of the parameter estimation response (Riefler *et al.*, 1998)

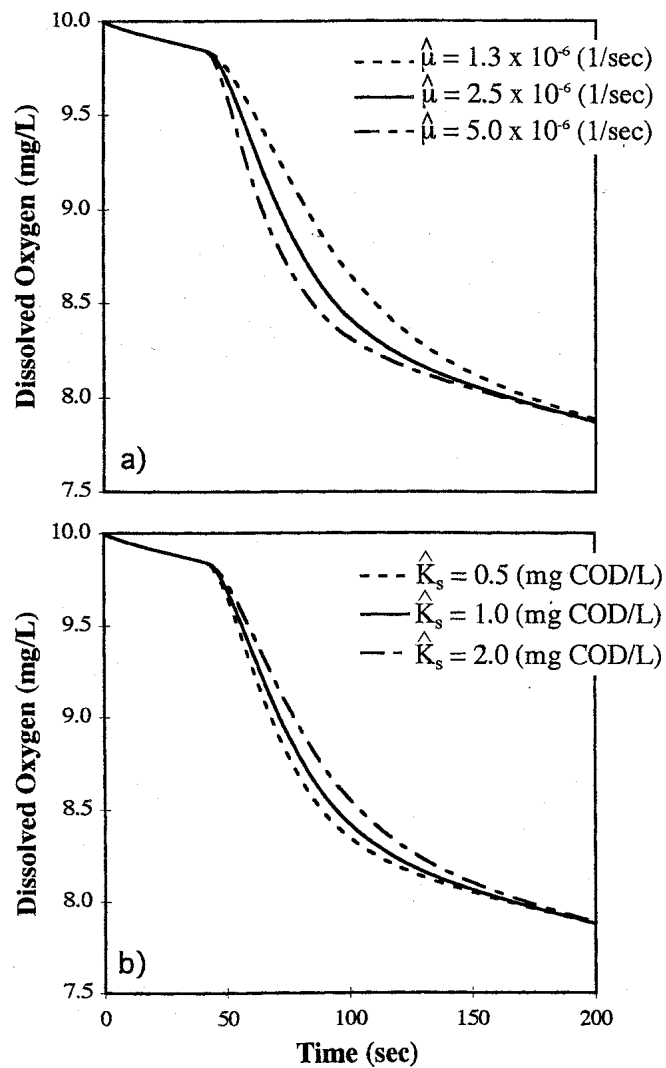


Figure 2.10: Sensitivity of dissolved oxygen profile to  $\mu_{max}$  en  $K_s$  (Riefler *et al.*, 1998)

Parameter identifiability was investigated by determining whether the true parameters were identifiable with data containing typical measurement error. To do this, Riefler *et al.* (1998) first generated a synthetic oxygen profile using the parameters estimated by Rittmann *et al.* (1986). For the maximum specific growth rate a value of  $0.22 \text{ d}^{-1}$  was taken, and the value of  $K_S$  was  $1.0 \text{ mg COD/l}$ . 250 oxygen concentration profiles were now generated adding an uncorrelated, normally distributed error with a standard deviation of  $0.01 \text{ mg/l}$ . The distribution of kinetic parameters estimated using these 250 profiles, gave an indication of the influence of measurement noise on the parameter estimates.

A log-normal distribution for  $K_S$  was a good description of this influence. The mean value of the estimates was  $1.03 \text{ mg/l}$ , the standard deviation was  $0.33 \text{ mg/l}$  and the skew was  $1.26 (\text{mg/l})^{-3}$ . This means the average error caused by the measurement errors on the estimation of  $K_S$  was only 3.3%. In the case of  $\mu$ , this was only 2.3% although the  $\mu_{\max}$  data set failed goodness of fit tests for normal and log-normal distributions. This research showed that estimating biokinetic parameters of biofilms is numerically feasible. However, if only one profile is measured in the laboratory, the uncertainty of the results is rather high. Also, the influence of the numerous assumptions that are made in the model is unclear. In short, quite some additional work needs to be done to determine if this method is effective in the laboratory.

### 2.6.2.3 Estimation of oxygen diffusion coefficients using oxygen uptake profiles

Micro-electrodes are an interesting tool for the estimation of diffusion coefficients in biofilm mass transfer research. These techniques are, however, hard to apply in practical situations. For this reason Khlebnikov *et al.* (1998) developed a technique to estimate the diffusion coefficient of oxygen using oxygen uptake profiles in the bulk liquid phase. For the investigations, a fixed bed biofilm reactor was used with a structured packing made of polypropylene. The concentrations of substrates in the feed were chosen such that the biofilm would be oxygen limited. In the reactor, oxygen electrodes were placed at the top and at the bottom of the carrier material column. After some time of operation, the aeration and the feed to the reactor were stopped and the oxygen concentration as a function of time was determined (Figure 2.11).

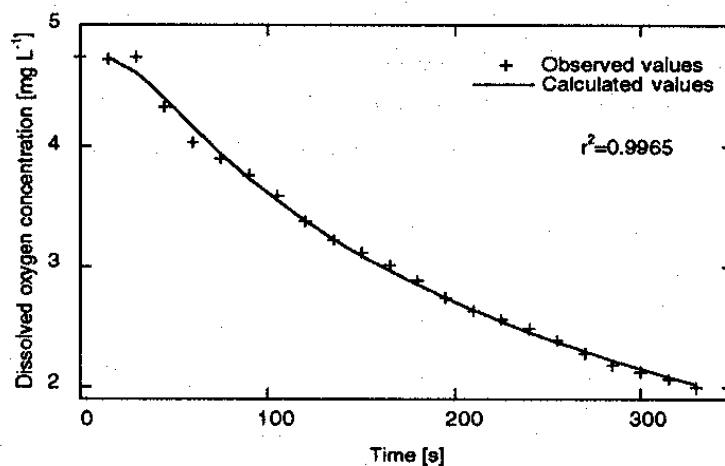


Figure 2.11: Measured and calculated dissolved oxygen profile (Khlebnikov *et al.*, 1998)

The following reaction-diffusion model was used to describe the oxygen concentration profile in the biofilm:

$$\frac{\partial S_O}{\partial t} = D_f \frac{\partial^2 S_O}{\partial \zeta^2} - \frac{V_{\max} S_O}{K_{OH} + S_O} \quad (2.66)$$

where  $V_{\max}$  is the maximal oxygen uptake rate. Using a simple respirometric test, a zero-order reaction was noticed. It meant the oxygen concentration  $S_O$  was considerably larger than  $K_{OH}$ , so the reaction term in the above equation could be simplified. The solution of this simplified equation can be found to be:

$$S_O = A \cdot \operatorname{erf}\left(\frac{\zeta}{2 \cdot \sqrt{D_f \cdot t}}\right) + B - V_{\max} \cdot t \quad (2.67)$$

The unknown parameters  $A$  and  $B$ , should be determined from the boundary conditions (at time 0):

$$\begin{aligned} S_O &= S_{O,L} \text{ at } \zeta = L \\ S_O &= S_{O,0} \text{ at } \zeta = 0 \end{aligned} \quad (2.68)$$

The oxygen concentration at the liquid-biofilm interface as a function of time can then be modelled as:

$$S_O = (S_{O,L} - S_{O,0}) \operatorname{erf}\left(\frac{L}{2 \cdot \sqrt{D_f \cdot t}}\right) + S_{O,0} - V_{\max} \cdot t \quad (2.69)$$

The parameter combination  $L / 2 \cdot D_f^{1/2}$  from the above equation was estimated by the authors using non-linear regression. This allowed the calculation of  $D_f$ . Also, values for  $S_O$  and  $V_{\max}$  are estimated this way. However, in the publication of Khlebnikov *et al.* (1998), the determination of the boundary conditions  $S_{O,0}$  and  $S_{O,L}$  is not discussed. Using the backwashing frequency in the reactor, the thickness of the biofilm was varied. In each of the situations, the diffusion coefficient was estimated, showing a high dependence of the diffusion coefficient to the biofilm thickness (Figure 2.12).

The reliability of this method was not tested against other methods to determine the oxygen diffusion coefficient in the biofilm. It is likely that the results of this method are highly dependent on the experimental conditions. More research and statistical analysis of the results is needed before definitive conclusions about the method and the uncertainty of the results can be drawn.

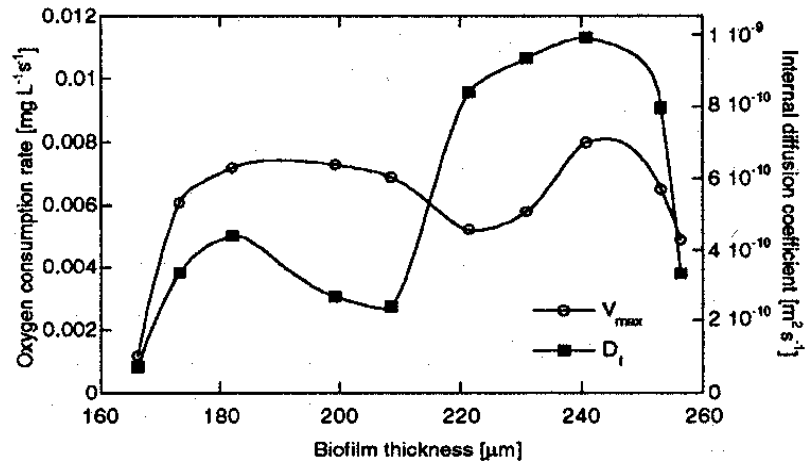


Figure 2.12: Dependency of the oxygen consumption and the diffusion coefficient to the biofilm thickness (Khlebnikov *et al.*, 1998)

### 2.6.3 Estimation of biofilm parameters using substrate monitoring

#### 2.6.3.1 Numerical curve-fitting for the estimation of kinetic parameters

To estimate the kinetic parameters  $K_S$  (saturation coefficient) and  $q_m$  (maximal specific substrate consumption rate) for 2,4-dinitrotoluene (2,4-DNT) and 2,6-dinitrotoluene (2,6-DNT), Smets *et al.* (1999) carried out experiments in a fluidised bed bioreactor. The experiments started from a steady-state situation after which the reactor was subjected to an increased influent concentration. This type of experiments is called a load-shift experiment. The substrate flux and the substrate concentration at the liquid-biofilm interface were calculated from the experimental results:

$$N_{\text{int,measured}} = \frac{Q(S_{\text{in}} - S_0)}{a_{\text{substr}} \cdot M_{\text{substr}}} \quad (2.70)$$

$$S^* = S_0 - \frac{\delta_{\text{bl}} \cdot N_{\text{int}}}{D}$$

where  $Q$  is the influent flow rate to the reactor and  $S_{\text{in}}$  is the influent substrate concentration.  $a_{\text{substr}}$  denotes the biofilm surface area per unit of substratum mass (sand) and  $M_{\text{substr}}$  is the total mass of substratum.

Atkinson and Davies (1974) formulated an equation for the substrate flux  $N_{\text{int}}$  as a function of  $K_S$  and  $q_m$ . A complete description of this function is given in Smets *et al.* (1999).

$$N_{\text{int}} = \frac{\xi \cdot L \cdot S_S \cdot q_m \cdot X}{K_S + S_D} \quad (2.71)$$

In this study – and contrary to the study of Rittmann *et al.* (1986) – no visual techniques were used to find the kinetic parameters, but instead a non-linear optimisation technique was used.  $K_S$  and  $q_m$  were varied in this algorithm until the sum of the squared residual errors was minimised.

$$\min \sum_{i=1}^n (N_{\text{int,measured},i} - N_{\text{int},i}(q_m, K_S))^2 \quad (2.72)$$

The optimisation algorithm was started from different starting points so as to verify the uniqueness of the parameter set. It was found that only one parameter set could be calculated, so a global minimum did exist. Using a statistical F-test, the 95% confidence regions for the estimated parameters were obtained. These confidence regions turned out to be rather large, which means a large number of measurements is needed to accurately estimate kinetic parameters.

In this research too, the impact of measurement errors was investigated using simulations in which calculated sets of  $S_S$  and  $N_{\text{int}}$  data for known parameter combinations were used. Random measurement errors were introduced to these data sets and, subsequently, the algorithm developed was used to estimate the kinetic parameters. In the simulations  $K_S$  deviated 2.7 – 5.9% from the true value and  $q_m$  deviated 1.0 - 2.0%. Again, these deviations can only be used as indications for the confidence in the true parameter values if a large number of measurements is done.

Next to the load-shift experiments,  $K_S$  and  $q_m$  were also estimated from measurements during steady-state conditions. Especially the value of  $K_S$  was underestimated in this case.

### 2.6.3.2 Comparison between a numerical and a visual curve-fitting technique

To investigate whether the results using the least squares method match the results obtained with a visual curve-fitting technique, Smets *et al.* (1999) implemented the technique introduced by Rittmann *et al.* (1986) to fit the kinetic parameters to the same 2,4-DNT and 2,6-DNT data set. With this visual technique, 95% confidence intervals could only be found if different persons were allowed to compare the obtained curve with the set of standard curves shown by Rittmann *et al.* (1986).

In the case of  $q_m$ , the parameter value estimated with the visual technique was on average four times higher than the value obtained with the least-squares method. For  $K_S$  the values obtained by the two techniques were closer together. It was also seen that the visual technique was able to produce parameter values in the case of an experiment where the least-squares algorithm was not able to fit parameters at all. This indicated that a visual technique can produce faulty parameter estimates even if the data set does not carry enough information to support these estimates. The problems with the optimisation algorithm were due to problems with the dissolved oxygen level in this experiments. Also, in the case of a strong correlation between  $K_S$  and  $q_m$ , the visual technique still produced parameters values. This makes clear that visual curve fitting should be used with care, since faulty parameter values could be obtained in quite some cases.

### 2.6.3.3 Parameter estimation for mixtures of unknown substrates

Drinking water as well as wastewater contains several unknown substrates. Zhang and Huck (1996) developed a technique to derive the Monod kinetic parameters  $K_S$ ,  $q_m$  and the diffusion coefficient  $D$  for assimilable organic carbon (AOC) and  $S_{\text{min}}$ , the minimal substrate concentration that can sustain a viable biofilm, in situ. The term AOC is used by Zhang and Huck (1996) to indicate organic substances that can be taken up by micro-organisms as food. The main components of AOC are carboxylic acids, ketoacids and aldehydes (Zhang and Huck, 1996).

The method starts from a dimensionless equation for the flux of substrate into a steady-state biofilm (Saez and Rittmann, 1992). Starting from this equation the four model parameters  $K_S$ ,  $D$ ,  $S_{min}$  and  $X.q_m$  were estimated.

$$N_{int} = \left( 2 \cdot \left[ (S'_0 - N_{int}L/D) - \ln(1 + S'_0 - N_{int}L/D) \right] \right)^{1/2} \cdot \tanh\left\{ \gamma \left( [S'_0 - N_{int}L/D] / S_{min} - 1 \right)^\beta \right\} \quad (2.73)$$

where  $\gamma = 1.557 - 0.4117 \cdot \tanh(\log S_{min})$

$$\beta = 0.5035 - 0.0257 \cdot \tanh(\log S_{min})$$

and  $S'_0 = S_0 / K_S$

$S_0$  = AOC concentration in the bulk liquid

This equation depends on two measured parameters  $N_{int}$  and  $S_0$  and four model parameters  $K_S$ ,  $q_m$ ,  $D$  and  $S_{min}$ . The flux during the experiments of Zhang and Huck (1996) was calculated starting from the influent and effluent concentrations of substrate, using the following equation:

$$N_{int,measured} = \frac{Q \cdot (S_{in} - S_0)}{A_F} \quad (2.74)$$

The bulk liquid concentration was assumed to be equal to the effluent concentration, since the experiments were done in a stirred tank reactor.

Conventional non-linear regression was not used by the authors, since the flux  $N_{int}$  appears at both sides of this implicit equation and also because of the large errors on the AOC measurements in the experiments. These errors can amount to 10% (Zhang and Huck, 1996). Instead, the Error-in-Variables Model (EVM) was used to estimate the parameters. This model does not differentiate between dependent error-containing and independent error-free variables but considers all variables to contain measurement error. This way it is possible not only to estimate the parameter values in the model, but also to obtain an estimate of the *true* values of the measured variables. Reilly and Patino-Leal (1981) developed an algorithm to solve such EVM problem in an iterative way.

Next to this, Zhang and Huck (1996) used the jackknife technique to estimate the confidence intervals of the estimates. From this analysis, it became obvious that only accurate values for  $S_{min}$  could be estimated. For the other parameters, the confidence intervals were too large to consider the EVM model outcome to be good estimates of the true parameter values. The limited number of observations (9 in total) is a possible reason for this outcome.

## 2.7 Aim of this thesis

In the above paragraphs, a description of the experiences in biofilm modelling and parameter estimation has been given. Obviously, a whole range of biofilm models is available, ranging from relatively simple one-dimensional models to comprehensive 3D descriptions of the biofilm structure in

time and space. The first one-dimensional models focussed mainly on mass transport in the biofilm and could be solved analytically. More complex models included equations describing the species distribution in a biofilm and therefore resulted in partial differential equations. Finally, 3D models can only be solved using dedicated hardware because of their computationally intensive nature.

Each of the above models has its value and its possible applications. It is not the aim of this thesis to promote one or the other model structure or complexity. The complexity of the model that is chosen should, however, be relevant for the application it is used for. High complexity models clearly have the advantage of including a lot of the available knowledge about biofilm processes. On the other hand, the high complexity of the model also increases the number of unknown parameters and the possible dependencies between them. These factors make the accurate estimation of parameter values very difficult. Also, even for very complicated models, some biofilm processes – like attachment, detachment, the influence of higher organisms, ... – are still poorly understood and are described by empirical formulas. Based on these findings, combined with the required computational effort and time to solve highly complex models, it becomes clear they are too detailed for use in full-scale on-line applications. On the other hand, low complexity models are not able to describe all the dynamics of the system, since they are simplified. However, their calibration is easier since less parameters need to be estimated. This also explains why the first attempts to estimate model parameters in situ use relatively simple models and why the level of uncertainty in the parameter estimates is still quite high.

In this thesis, a model is developed that attempts to be a complexity compromise. It is relatively simple, since it is based on the analytical solution of the substrate profiles in the biofilm. This factor is very important for the application of the model in practical situations and in combination with other widely accepted models in wastewater treatment. On the other hand, the model is able to calculate the conversion rates of different processes in the biofilm performed by different biomass species in the biofilm. Thus, despite its simplifications, it can be used to describe processes occurring in different depths of the biofilm.

The aim of the second part of this thesis is to apply and test this model under different circumstances using data obtained from measurement campaigns in a pilot-scale and a full-scale system. Although the model is rather simple, it still includes quite some conversion processes and a considerable set of parameters needs to be calibrated. To gather the data needed for a successful calibration, on-line measurement techniques are explored. If needed, the model is extended to be able to describe the results from the on-line sensors. Using the available set of data, the model is calibrated such that it gives a reasonably good description of the dynamics of the plants under study and it is further used to propose process optimisations where possible.

As a last application, the simplified mixed-culture biofilm model is used in a simulation study investigating suspended carrier biofilm systems. Although not supported with measurements, data from literature is found sufficient to obtain and investigate realistic descriptions of the dynamic behaviour of such systems.

# 3 WEST: Modelling biological wastewater treatment

---

## 3.1 Modelling wastewater treatment: benefits and practical use

The problem of modelling and simulation of wastewater treatment plants (WWTP's) has been found important as a result of growing environmental awareness. Compared to the modelling of well-defined (such as electrical and mechanical) systems, modelling of ill-defined systems such as WWTP's is more complex. In particular, choosing the "right" model is a non-trivial task.

Modelling is an inherent part of the design of a wastewater treatment system. At the fundamental level, a design model may be merely conceptual. The engineer reduces the complex system he is dealing with to a conceptual image of how it functions. That image then determines the design approach. Often, however, the engineer recognises that the conceptual model alone does not provide sufficient information for design and thus he constructs a physical model, such as a lab-scale reactor or a pilot plant, on which various design ideas can be tested. Given sufficient time for testing, such an approach is entirely satisfactory. However, the engineer may find that limitations of time and money prevent exploration of all potentially feasible solutions. Consequently, he often turns to the use of mathematical models to further explore the feasible design space. He may devise empirical models, which incorporate a statistical approach to mimic the end results obtained by studies on the physical model or if his conceptual understanding expands sufficiently, he may attempt to formulate models based on mechanistic knowledge. These mechanistic models are the more powerful because they allow extrapolation of the design space to conditions beyond that experienced on the physical model. In this way, many potentially feasible solutions may be evaluated quickly and inexpensively, allowing only the most promising ones to be selected for actual testing in the physical model.

To be able to use mathematical – be it empirical or mechanistic – models, a good software tool to implement and simulate the models is indispensable. Several tools are available that can be applied to the modelling and simulation of wastewater treatment plants. Increasingly, the "system" modelled also transcends the WWTP and includes the "environment" (in the engineering sense). The WWTP model is then integrated in a conceptual model of the wastewater producing plant, the sewer system and the river (with its natural water purification properties or toxicity tolerance) in which the effluent is discharged (Meirlaen *et al.*, 2001).

Wastewater treatment practice has now progressed to the point where the removal of organic matter and nutrient removal by biological nitrification and denitrification and biological phosphorus removal, can be accomplished in a single system. The non-linear dynamics and properties of these biological processes are still not very well understood. As a consequence, a unique model cannot always be identified. This contrasts to traditional mechanical and electrical systems where the model can be uniquely derived from physical laws. Also, the calibration of wastewater treatment models is particularly hard: many expensive experiments may be required to accurately determine model

parameters. Yet, even with the limitations and difficulties stated above, modelling and simulation of wastewater treatment is considered useful (Henze *et al.*, 2000). Models are excellent tools to summarise and increase the understanding of complex interactions in biological systems. More quantitatively, they can be used to predict the dynamic response of the system to various disturbances.

Despite of their promising properties described above, the practical use of dynamic modelling of wastewater treatment is rather limited (Morgenroth *et al.*, 2000). Especially the labour and cost intensive calibration of WWTP models is considered hard to accomplish in practical situations. New methodologies are being developed to overcome this bottleneck (Petersen *et al.*, 2001). In some cases, *e.g.* when modelling biofilm wastewater treatment, the development of models that are able to describe the wastewater treatment system well enough to correctly predict system responses, but that are at the same time having a feasible complexity for simulation, is also problematic. However, the application field for good WWTP models is promising. They could be used to:

1. predict dynamic responses of the system to influent variations so as to develop strategies to optimise treatment plant operation. This can be done either off-line or with on-line 'real-time' simulations that are used for control and optimisation.
2. trouble shoot plant operation. Operators might be interested to use models in finding answers to practical questions.
3. integrate multiple processes. As mentioned above, the removal of organic matter, nitrogen and phosphorus, is accomplished in a single system nowadays. Models are a promising tool to help creating more understanding of the interactions between these processes.
4. design WWTP reactors. Models can be used to evaluate data from pilot-scale reactors and to predict performance of full-scale plants.

## 3.2 Introducing the WEST modelling and simulation environment

WEST (Wastewater Treatment Plant Engine for Simulation and Training) provides the modeller with a user-friendly platform to use existing models or to implement and test new models. Basically, WEST is a modelling and simulation environment for any kind of process that can be described as a structured collection of Differential Algebraic Equations (DAE's). Currently, however, WEST is mainly applied to the modelling and simulation of wastewater treatment plants (Vangheluwe *et al.*, 1998).

WEST is especially aimed at facilitating and optimising the implementation and re-use of knowledge in wastewater treatment models and to maximise the simulation speed and accuracy of simulations with the models used. However, the aims of modelling and simulation are in a sense contradictory. Hence, the WEST modelling and simulation environment makes a strict distinction between a *modelling environment* which aims to enable re-use of model knowledge and the *experimentation environment*, which aims to maximise accuracy and performance.

Next to these two user environments, the *model base* plays a central role in WEST. In this model base, models are described in MSL-USER (MSL stands for *model specification language*), a high level object-oriented declarative language specifically developed to incorporate models. The model base is aimed at maximal re-use of existing knowledge and is therefore structured hierarchically. All re-usable

knowledge – such as mass balances, physical units, default parameter values and applicable ranges – is thus defined centrally and can be re-used by an expert user to build new models. This indicates that WEST has an open structure in that the user is allowed to change existing models and define new ones as needed.

As depicted in Figure 3.1, the model base is loaded and all relevant information for the modeller is extracted from it when the modelling environment is started (step 1). Using the symbolic information in the model base, the ‘atomic’ models available in the model base are linked to a graphical representation. A hierarchical graphical editor (*HGE*) allows for the interactive composition of complex configurations from these basic graphical building blocks. Also the input-output structures (*terminals*) of the models are extracted from the model base so as to decide whether or not two models can be linked together in the HGE. For instance, a model for the activated sludge process can not directly be coupled to a river model, since the set of components used in these models to describe the substrates is not the same. In case such coupling need to be done, an explicit component convertor needs to be used. Next, the parameter set of the different models is loaded so that parameters of different models can be linked. For instance, the same yield coefficient can be used for all activated sludge tanks in a WWTP configuration. Finally, when a configuration has been built, the HGE starts from the information extracted from the model base and creates and outputs a *coupled model* in MSL-USER (step 2), which is automatically added to the model base for further use in new model exercises (step 3).

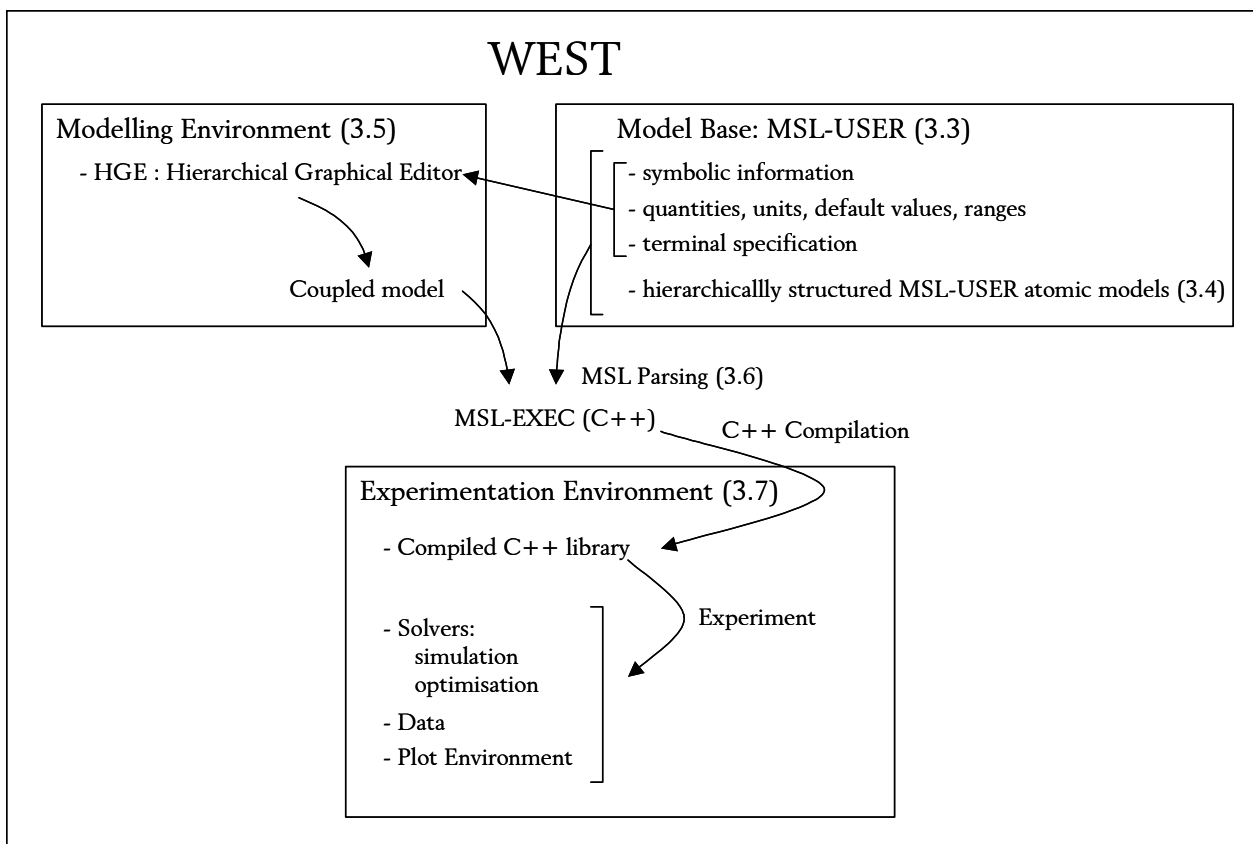


Figure 3.1: Functional WEST architecture

In a next step (step 4), the model parser generates low-level (C++) MSL-EXEC code, which after C++ compilation (step 5) can be used for execution within the experimentation environment. The

parser therefore uses the coupled model together with the atomic model representations in the model base. These steps are especially oriented towards simulation performance and accuracy. Finally, the solvers within the experimentation environment generate data which can be used for plotting, model calibration, process optimisation, output to file, etc. (step 6).

### 3.3 The model specification language MSL-USER

The language MSL-USER that is used in the WEST model base, is an object-oriented language, which allows for the declarative representation of the dynamics of systems. 'Declarative' means that the model (*what*) is presented without specifying *how* to solve it. As mentioned above, a compiler (MSL-parser) is provided to transform MSL-USER model representations into a low level representation (MSL-EXEC based on C++).

The MSL-USER parser is written in lex(flex), yacc(bison) and C++ and makes use of LEDA (Library of Efficient Data structures and Algorithms).

MSL-USER follows the major principles of object-oriented programming in that it uses TYPES, CLASSES and OBJECTS to represent the hierarchy of the items in the model base. The relation between these representations can be visualised like a tree. Basically, types provide a way to describe the structure of an expression in the sense that it is a template to which classes and objects add more information. Indeed, a class is derived from a type definition, further defining the properties of the template. That way, classes provide a way to describe the behaviour of values. For example, a class in MSL-USER is mostly a type to which default values have been assigned. It is clear that one type can have multiple classes derived from it. A class is a template itself for the instantiation of objects that give final values to the structures defined. An object, however, can not only be instantiated from a class, but also directly from a type.

Apart from being object-oriented, MSL-USER is also a multi-abstraction language. It allows one to represent abstract models of the behaviour of systems using different methods of abstraction. This includes the possibility to make use of "abstractions" such as differential and algebraic equations, state transition functions, C++ code, ... (Vangheluwe, 2000).

Other characteristics of MSL-USER are:

- Re-use of models is possible thanks to the EXTENDS inheritance mechanism. This allows for the extension of an existing model. Thus, starting from generic models, a tree of extended models can be built.
- Classification is made possible through the SPECIALISES mechanism. Hereby, it is possible to indicate that a particular type is a sub-type of another type. This not only allows for classification, but also for rigorous type-checking.

Some examples will surely clarify the explanation above. The basic types found in MSL-USER are integer, real, string, char and boolean. Based on these basic types, a number of extended type structures were built. Some type structures are the Record type, the Vector type, the Enumerated

type, ... For example a vector type is used to specify vectors and matrices. A matrix can be specified as a vector of vectors. A column vector is declared as follows:

```
TYPE type_name = type[dimension ];
```

An enumerated type is a type structure consisting of a set of unique identifiers called enumerators, and is declared as:

```
TYPE type_name = ENUM {id_1, id_2, ...,id_n} ;
```

These basic types and structure types can now be used to create user-defined types, such as UnitType, QuantityType and RealIntervalType. The first two are defined as strings while RealIntervalType is defined as a record of two real values and two booleans, describing if the bounds are included in the interval.

```
TYPE UnitType
"The type of physical units"
= String;

TYPE QuantityType
"The different physical quantities"
= String;

TYPE RealIntervalType
"Real Interval"
= RECORD
{
  lowerBound: Real;
  upperBound: Real;
  lowerIncluded: Boolean;
  upperIncluded: Boolean;
};
```

Furthermore, existing types can be extended. For example, the Record type can be extended with extra fields. In the following example, the ExtendedType is a type extended from BasicType.

```
TYPE BasicType "Basic type"
=
RECORD
{
  value: Real;
};
TYPE ExtendedType "Extended type"
EXTENDS BasicType WITH
RECORD
{
  unit: UnitType;
  quantity: QuantityType;
  interval: RealIntervalType;
};
```

The mechanism of specialisation is somewhat different. A class that is specialised from another class or type has the same signature, but the objects in the class are assigned (replaced). For example:

```
CLASS Concentration "A class for concentration" SPECIALISES ExtendedType :=
{:
  quantity <- "Concentration";
  unit      <- "g/m^3";
  interval <- {: lowerBound <- 0; upperBound <- PLUS_INF :};
:};
```

A class such as Concentration, can further be instantiated as an object, where a value is assigned to one of the elements of the vector:

```
OBJ S_O_Sat "Oxygen saturation concentration"
: Concentration := {:value <- 8:};
```

MSL-USER thus allows one to express *physical* knowledge such as units (m, kg, ...), quantity type (Mass, Length, ...), boundary conditions, ... The semantics of these are known by the parser which will check model consistency and, where appropriate, apply this knowledge in the translation to MSL-EXEC. Also some other object attributes are interesting to note here. When the value of a parameter or the initial condition of a variable depends on the value of other parameters, it is possible to declare this parameter or variable as *fixed*. In this case, the user cannot change its value in the experimentation environment. When, in an MSL-USER model, a parameter or variable object has the annotation *hidden* this object is not shown in the experimentation environment.

During the translation from MSL-USER to MSL-EXEC, the different abstractions used in the models created by the user will be translated into C++ representations. Algebraic equations and Differential equations (using the DERIV statement) will be recognised directly by the parser, since they are available in the MSL-USER library. Other built-in statements in MSL-USER are for example FOREACH, SUMOVER and IF-THEN-ELSE structures. Moreover, during the subsequent compilation of the generated MSL-EXEC code, some standard C libraries are automatically linked to the generated model. This way, functions that are not built-in in MSL and that are not defined in the MSL-USER function libraries can be used as long as they are available in these standard libraries. It is even possible to use user defined C++ functions.

### 3.4 Building the model base

To allow for computer aided model building and subsequent simulation/experimentation, a *model base* must be constructed. The models in this model base will be used for modular construction (*i.e.* by connecting component blocks as described above) of complex models describing the behaviour of WWTP's. The steps listed below form a general method for constructing a model base for any application domain:

1. Choose an appropriate level of abstraction.
2. Identify relevant quantities.
3. Identify input-output structures.
4. Build a model class hierarchy starting from general (conservation and constraint) laws and refining these for specific cases.

In the following paragraphs, these steps will be treated in more detail.

### 3.4.1 *Level of abstraction*

As is commonly the case, we will choose an appropriate level of abstraction, upon which Idealised Physical Models (IPM's) will be built. Idealised Physical Models (Broenink, 1990) represent behaviour at a certain level of abstraction. This often means using lumped parameter models (ordinary differential equations or ODE's), even though the physical system has a spatial distribution (which would require partial differential equation or PDE modelling), when the homogeneity assumption is a reasonable approximation.

### 3.4.2 *Relevant quantities*

Secondly, the quantities of interest must be identified. These quantities can be subsequently used to describe the *types* of entities used in modelling: constants, parameters, interface variables and state variables.

In MSL-USER, the type of physical quantities is encoded as a `PhysicalQuantityType`, a structure as given below:

```

TYPE PhysicalQuantityType
"The type of any physical quantity"
=
RECORD
{
  quantity   : QuantityType;
  unit       : UnitType;
  interval   : RealIntervalType;
  value      : Real;
  causality  : CausalityType;
};

```

For numerical computation purposes it is sufficient to specify whether an entity is of real, integer, boolean or string type. When modelling a particular application domain, however, more expert information is available, and it would be very helpful to the modeller if it could be stored (represented) in the model base. For example, information can be available about upper and lower bounds of variables and parameters (*e.g.* stating that concentration, through the definition of its interval, is always positive). Also information about the causality of a quantity (input or output) can be included, since this information is of importance when developing a-causal models. As can be seen in the `PhysicalQuantityType` structure, this information can easily be integrated in MSL-USER. Once represented in a model, the model parser can make use of it to determine the legitimacy of the model (*e.g.* checking if the dimensions of parameters that are coupled match) and to generate efficient code (*e.g.* by means of constraint propagation based on lower and upper bound information). The constraints integrated in MSL-USER are transferred to the symbolic part of the MSL-EXEC representation and is used to protect the user for constraint violations during simulation or user input.

#### 3.4.2.1 **Basic quantities**

Using the methodology introduced earlier, the `PhysicalQuantityType` structure can be specialised as classes for specific quantities. Here, alike the class 'Concentration', the physical quantity 'Area' is defined:

```
CLASS Area
"A class for area"
SPECIALISES PhysicalQuantityType :=
{:
  quantity <- "Area";
  unit <- "m^2";
  interval <- {: lowerBound <- 0; upperBound <- PLUS_INF:};
:};
```

Definitions of physical quantity types are used to instantiate objects of those types. The ISO 1000 standard also defines physical constants such as the universal gravity constant whose MSL-USER description is given as an object declaration below:

```
OBJ UniversalGravityConstant
"Universal gravity constant" : PhysicalQuantityType :=
{:
  quantity <- "G";
  unit <- "m^3/(g*s^2)";
  value <- 6.67259E-11;
:};
```

It should be noted here that in the WEST environment, the units are not only used for dimensional checking during model compilation, but are also passed on to the experimentation environment where the user is presented with variable names, descriptions, values as well as their units. This way, a variable or parameter description, a default value and an interval that have been defined by the expert developing the model, is available for the user. In this way, the user is protected against erroneous parameter values and is warned when a variable evolves out of its boundaries during a simulation run.

### 3.4.2.2 Quantities typical for WWTP's

Simulation of wastewater treatment system behaviour, incorporating phenomena such as carbon oxidation, nitrification, denitrification and phosphorus removal, must necessarily account for a large number of reactions between a large number of components (Henze *et al.*, 2000). Several Activated Sludge Models (ASM 1, 2, 2d and 3) have been developed by the task group on mathematical modelling of the International Water Association (IWA). As will be described in the sequel, each of the variables in these models, denoting a component of the wastewater, indexes a column in the model stoichiometry matrix. In MSL-USER, the components of *e.g.* ASM1 are easily described as an enumerated type:

```
TYPE Components = ENUM {H_2O, S_S, S_O, S_NO, S_ND, S_NH, S_ALK, X_I, X_S, X_BH, X_BA, X_P, X_ND};
```

Thus, the modeller refers to the components by their name, while, where necessary, the corresponding integer index is used. Though WEST's simulator uses the numerical values of the Components indexes to address matrix elements, the experimentation environment presents the symbolic name of the index to the user. This reverse mapping is performed by the model compiler when generating MSL-EXEC code. Note how  $H_2O$  is explicitly modelled as a component.

Other quantities typical for WWTP modelling are stoichiometric and kinetic parameters. Kinetic parameters characterise the rate of reaction of the conversions in the model (*e.g.* maximal specific

growth rate, decay rate, ...); stoichiometric parameters indicate the stoichiometric relations between the different components in the model (e.g. yield coefficient, ...). In MSL, these parameters can easily be declared as objects of a certain, more general, class specification:

```

CLASS Yield
"A class for Yield"
SPECIALISES PhysicalQuantityType :=
{
  quantity <- "Yield";
  unit <- "-";
  interval <- { : lowerBound <- 0; upperBound <- 1:};
:};

CLASS GrowthRate
"GrowthRate"
SPECIALISES PhysicalQuantityType :=
{
  quantity <- "GrowthRate";
  unit <- "1/d";
  interval <- { : lowerBound <- 0; upperBound <- 20:};
:};

CLASS SaturationCoefficient
"Saturation coefficient"
SPECIALISES PhysicalQuantityType :=
{
  quantity <- "K";
  unit <- "-";
  interval <- { : lowerBound <- 0; upperBound <- 100:};
:};

OBJ Y      "Yield For Heterotrophic Biomass"
  : Yield := { :value <- 0.67:};
OBJ mu     "Maximum Specific Growth Rate For Heterotrophic Biomass"
  : GrowthRate := { :value <- 4.00:};
OBJ K_S    "Half-velocity Constant For Heterotrophic Biomass"
  : SaturationCoefficient := { :value <- 20.00:};

```

### 3.4.3 Transferred input-output quantities: terminals

The ultimate goal is to build complex models by connecting more primitive sub-models or blocks, possibly built up of coupled models themselves. In the case of WWTP models, the sub-model types mostly correspond in a 1-to-1 relationship to physical entities such as aeration tanks, clarifiers, pumps, splitters and mixing tanks. This ensures *structural validity* of the assembled models. Note how the building blocks need not match physical objects directly but may rather correspond to abstract concepts such as processes.

To connect sub-models, these sub-models require connection *ports* or *terminals*. This implies that interaction between the sub-models is assumed to *only* occur through the connections made between their terminals. When parsing a coupled model, the connections are replaced by appropriate algebraic equalities.

In our WWTP models, different terminal types are used. DataTerminals represent information to be used in sensor and controller blocks. However, the main terminal type is the WWTPTerminal. In the basic model base discussed here, only flux of biochemical material is considered. Heat flow for

example is not considered. This is one of the modelling assumptions mentioned in the discussion of the ASM1 model and is obvious from the WWTPTerminal definition.

The WWTPTerminal is a vector of mass fluxes for each of the components taken into consideration in the model. The size of the vector is given by the number of identifiers (the cardinality) in the enumerated type 'Components' (section 3.4.2.2) and hence depends entirely on how many components the user includes in this type. Note how the actual Component declaration may be given after all other declarations. MSL-USER interprets the equations and declarations in a model as a set rather than as a sequence of statements. Basically, this means the order in which the declarations or equations are included in the model base is of no importance. This evidently facilitates model base development and may enhance clarity.

```

OBJ NrOfComponents
"
  The number of biological components considered in the WWTP models
"
: Integer := Cardinality(Components);

CLASS WWTPTerminal
"
  The variables which are passed between WWTP model building blocks
"
= MassFlux[NrOfComponents];

```

While the model compiler will check whether (type-)compatible terminals are connected and how many connections are allowed to/from a terminal, the graphical modelling environment will already perform a check during interactive modelling. Normally the same terminals for biochemical transport are used everywhere in a configuration. If other terminals need to be used (*e.g.* for modelling a river system), explicit conversion blocks converting the elements of the different component vectors need to be foreseen. Direct coupling of a river compartment model, using another set of components, to a wastewater treatment model is not possible.

### 3.4.4 *Building a model class hierarchy starting from general laws*

#### 3.4.4.1 **Introduction to the general mass conservation law**

The choice to transfer mass fluxes via the terminals (paragraph 3.4.3) instead of the mostly used concentrations and flow rates has different reasons. In processes where next to water or a water suspension also gasses and carrier materials may be transferred from one unit to another, only the concentration in the water phase is measured in reality. Denoting the concentration in units of  $M \cdot L^{-3}$ , the factor  $L^{-3}$  indicates only the water or the suspension and not the entire transferred volume (including gas and carrier material). This can easily be the source of errors during the model development. Also the easy formulation of mass conservation when masses rather than concentrations are used is an advantage of this choice. The mass conservation law can easily be formulated as  $dM/dt$ . This conservation can be calculated for the different components  $i$  of the WWTPTerminal, so that elemental balances for carbon and nitrogen are easily derived. The user should however still have the possibility to interact with the model through output variables like concentration and flow rather than mass fluxes. For example, a mass balance of an ideally stirred tank reactor (CSTR) with volume  $V$  ( $L^3$ ), components  $i$ , and terminals  $\alpha$ , can be written as:

$$C_i = \frac{M_i}{V} \quad (3.1)$$

$$\frac{dM_i}{dt} = \sum_{\alpha} \Phi_{i\alpha} + R_i V \quad (3.2)$$

$$\frac{dV}{dt} = \sum_i \left( \frac{1}{\rho_i} \sum_{\alpha} \Phi_{i\alpha} \right) \quad (3.3)$$

where  $C_i$  = concentration of a component  $i$  ( $M L^{-3}$ )

$M_i$  = mass of a component  $i$  (M)

$\Phi_{i\alpha}$  = flux of component  $i$  in the flux at terminal  $\alpha$  ( $M T^{-1}$ )

$R_i$  = conversion rate of component  $i$  ( $M L^{-3} T^{-1}$ )

$\rho_i$  = density of component  $i$  ( $M L^{-3}$ )

In the case of an aeration tank with components dissolved at a low concentration in the water phase, the following simplifying assumption can be made:

$$\forall i \neq H_2O : \rho_i = \infty \quad (3.4)$$

stating that it is assumed that only water occupies a finite space. In case the density of the suspensions is different from  $1 \text{ kg/l}$  or  $10^6 \text{ g/m}^3$  ( $= \rho_{H_2O}$ ), this assumption will no longer suffice. In that case the density of the individual components needs to be known.

In case for example heat transport should be modelled, the same assumptions will be used, *i.e.* heat flux will be transferred at the terminals.

### 3.4.4.2 Modelling biochemical conversion: the Petersen matrix

#### *Introduction*

Crucial in modelling the biochemical conversions in a wastewater treatment plant is to realistically model the inter-component biochemical reactions. These reactions must be representative of the most important fundamental processes occurring within the system. Furthermore, the model should quantify both the *kinetics* (rate-concentration dependence) and the *stoichiometry* (relationship that one component has to another in a reaction) of each process. Identification of the major processes and selection of the appropriate kinetic and stoichiometric expressions for each are the major conceptual tasks during development of a mathematical conversion model.

The IWA task group mentioned above (Henze *et al.*, 1987) chose the *matrix format* introduced by Petersen (1965) for the presentation of its models. The first step in setting up this matrix is to identify the *components* of relevance in the model. The second step in developing the matrix is to identify the biological *processes* occurring in the system; *i.e.* the conversions or transformations which affect the components listed.

### A simple example

Consider the situation in which heterotrophic bacteria are growing in an aerobic environment by utilizing a soluble substrate for carbon and energy. In one simple conceptualisation of this situation, two fundamental processes occur: the biomass increases by cell growth and decreases by decay. Other activities, such as oxygen utilization and substrate removal, also occur, but these are not considered to be fundamental because they are the result of biomass growth and decay and are coupled to them through the system stoichiometry. The simplest model of this situation must consider the concentrations of three components: biomass, substrate and dissolved oxygen. The matrix incorporating the fate of these three components in the two fundamental processes is shown in Table 3.1.

**Table 3.1. Process stoichiometry and kinetics for heterotrophic growth in an aerobic environment**

Process $j$	Component $i$			Process Rate $r_j$ (ML <sup>-3</sup> T <sup>-1</sup> )
	1. Biomass $X_B$	2. Substrate $S_S$	3. Oxygen $S_O$	
1. Growth	1	$-\frac{1}{Y}$	$-\frac{1-Y}{Y}$	$\frac{\mu S_S}{K_S + S_S} \cdot X_B$
2. Decay	-1		-1	$b \cdot X_B$
Stoichiometric Parameters: Growth yield $Y$	M(COD).L <sup>-3</sup>	M(COD).L <sup>-3</sup>	M(-COD).L <sup>-3</sup>	Kinetic Parameters: Maximum specific growth rate $\mu$ Half-velocity constant $K_S$ Specific decay rate $b$

As mentioned in the introduction, the first step in setting up the matrix is to identify the *components* of relevance in the model. In this scenario these are biomass, substrate and dissolved oxygen, which are listed, with units, as columns in Table 3.1. In conformity with IWA nomenclature (Grau *et al.*, 1982), particulate constituents are given the symbol  $X$  and the soluble components  $S$ . Subscripts are used to specify individual components:  $B$  for biomass,  $S$  for substrate and  $O$  for oxygen.

The second step in developing the matrix is to identify the *biological processes* occurring in the system; *i.e.* the conversions or transformations which affect the components listed. Only two processes are included in this example: aerobic growth of biomass and its loss by decay. These processes are listed in the leftmost column of the table. The *kinetic expressions* or *rate equations* for each process are recorded in the rightmost column of the table in the appropriate row. Process rates are denoted by  $r_j$  where  $j$  corresponds to the process index.

If we were to use the simple Monod-Herbert model for this situation, the rate expressions would be those in Table 3.1. The Monod equation,  $r_1$ , states that growth of biomass is proportional to biomass concentration in a first order manner and to substrate concentration in a mixed order manner. The expression  $r_2$  states that biomass decay is first order with respect to biomass concentration.

The elements within the table comprise the stoichiometric coefficients,  $\nu_{ij}$ , which set out the mass relationships between the components in the individual processes. For example, growth of biomass (+1) occurs at the expense of soluble substrate ( $-\frac{1}{Y}$ ,  $Y$  is the yield parameter); oxygen is utilized in the metabolic process ( $-\frac{1-Y}{Y}$ ). The coefficients  $\nu_{ij}$  can easily be deduced by working in consistent units. In this case, all organic constituents have been expressed as equivalent amounts of chemical oxygen demand (COD); likewise, oxygen is expressed as negative oxygen demand. The sign convention used in the table is negative for consumption and positive for production.

In matrix form, we obtain a stoichiometry matrix

$$\nu = \begin{pmatrix} 1 & \frac{1}{Y} & \frac{1-Y}{Y} \\ -1 & 0 & -1 \end{pmatrix}$$

and a kinetics vector

$$r = \begin{pmatrix} \frac{\mu S_S}{K_S + S_S} \cdot X_B \\ b \cdot X_B \end{pmatrix}$$

Within a system, the concentration of a single component may be affected by a number of different processes. An important benefit of the matrix representation is that it allows rapid and easy recognition of the fate of each component, which aids in the preparation of mass balance equations. This may be seen by moving down the column representing a component.

As mentioned before, the basic equation for a mass balance within any defined system boundary is equation 3.2. The flux terms are transport terms and depend upon the physical characteristics of the system being modelled. The system reaction term,  $R_i$ , is obtained by summing the products of the stoichiometric coefficients  $\nu_{ij}$  and the process rate expression  $r_j$  for the component  $i$  being considered in the mass balance (*i.e.* the sum over a column):

$$R_i = \sum_j \nu_{ij} r_j \quad (3.5)$$

For example, the rate of reaction,  $R$ , for oxygen,  $S_O$ , at a point in the system would be:

$$R_{S_O} = -\frac{1-Y}{Y} \frac{\mu S_S}{K_S + S_S} X_B - b X_B \quad (3.6)$$

To create the mass balance for each component within a given system boundary (*e.g.* an ideally mixed reactor), the conversion rate would be combined with the appropriate transport terms for the particular system. For instance in an ideally mixed tank reactor with one input, a constant volume  $V$  and an influent flow rate  $Q$ , the following mass balance would emerge for  $S_O$ .

$$V \frac{dS_o}{dt} = \frac{dM_{S_o}}{dt} = \sum_{\alpha} \Phi_{S_o, \alpha} + V \cdot R_{S_o} = Q \cdot S_{o, in} - Q \cdot S_o + V \cdot R_{S_o} \quad (3.7)$$

Another benefit of the Petersen matrix is that continuity may be checked per process by horizontally moving across the matrix. This can only be done provided consistent units have been used, because then the sum of the stoichiometric coefficients must be zero. This can be demonstrated by considering the decay process. Recalling that oxygen is negative COD so that its coefficient must be multiplied by -1, all COD lost from the biomass through decay must be balanced by oxygen utilization. Similarly, for the growth process, the substrate COD lost from solution due to growth minus the amount converted into new cells must equal the oxygen used for cell synthesis.

### 3.4.4.3 Inheritance hierarchy

Using the general mass conservation law introduced above, models must be constructed for each type of building block. This is achieved in the form of a class *inheritance* hierarchy. Hereby, maximum *reuse* and *clarity* is achieved. Clarity is a direct result of the relationship between the inheritance hierarchy on the one hand and the different levels of specificity of the models on the other hand. In the generic model base, GenericModelType is defined:

```
TYPE GenericModelType
=
RECORD
{
  comments    : String;
  interface   : SET_OF (InterfaceDeclarationType);
  parameters  : SET_OF (ParameterDeclarationType);
};
```

It shows how any model has a description (*comments*) part, an *interface* set and a *parameter* set. The interface set describes which terminals serve as an input to the model and which variables are transferred to a subsequent model via an output terminal. The parameters of the model are a set of invariant values that are given a value at the beginning of a simulation.

For basic models in the DAE formalism, PhysicalDAEModelType prescribes the structure:

```
TYPE PhysicalDAEModelType
EXTENDS GenericModelType WITH
RECORD
{
  independent : SET_OF (ObjectDeclarationType);
  state       : SET_OF (PhysicalQuantityType);
  initial     : SET_OF (EquationType);
  equations   : SET_OF (EquationType);
  terminal    : SET_OF (EquationType);
};
```

Time is mostly used as the *independent* variable. In the case of PDE modelling, multiple independent variables can be defined. Dependent (both algebraic and derived) *state* variables are defined in the

*state* section. The *initial* section contains algebraic equations that will be solved only once during simulation. The result of this initial calculations can for example be used to define the initial values of derived state variables used in the *equations* section. This section contains the algebraic equations and ODE's that define the model. Equations in the *terminal* section are only calculated once at the end of the simulation run. The `GenericModelType` can also be extended to describe the essence of coupled models:

```

TYPE CoupledModelType
EXTENDS GenericModelType WITH
RECORD
{
  sub_models : SET_OF (ModelDeclarationType);
  coupling   : SET_OF (CouplingStatementType);
};

```

In a *coupled model*, the *sub\_models* section enumerates the set of models to be coupled. In the *coupling* section, statements are included that describe how to couple these models. This can be done using two statements. The *connect* statement is used to connect the interface variables of the coupled model to the interface of one of the sub-models or to connect the interfaces of two sub-models. The *control* statement is to indicate that a parameter of a sub-model is controlled by an interface variable of a second model. It is important to note that the MSL-USER parser will then automatically transform the controlled parameter into a new interface variable, since this model component will no longer be time-invariant and therefore, by definition, becomes a variable.

Both `CoupledModelType` and `DAEModelType` are extensions of `GenericModelType` which means they inherit its structure (and add to it). The resulting top-level inheritance hierarchy is given in Figure 3.2.

```

GenericModelType
|
|_____ CoupledModelType
|_____ DAEModelType == PhysicalDAEModelType

```

**Figure 3.2: Top level inheritance hierarchy in the WEST model base**

In the WWTP model base hierarchy, some of the model classes are derived directly from `PhysicalDAEModelType` (Figure 3.3). The ones listed directly below are models of the settler. The Takács model, for instance, is a discretised (10-layer) model of the settling process. It should be noted that the dedicated WEST-PDE parser is able to automatically discretise a class of PDE models of, for instance, the settling process using orthogonal collocation (Indrani and Vangheluwe, 1998). Once discretised, these models are of the ordinary `PhysicalDAEModelType` and are fitting in the hierarchy of Figure 3.3.

```

PhysicalDAEModelType
|
|___ Takacs
|___ SecondaryOtterpohlFreund
|---- Generated from PDE with WEST-PDE

```

**Figure 3.3: Settler models directly derived from PhysicalDAEModelType**

Sensor, controller, data filter and transformer models are also derived from PhysicalDAEModelType (Figure 3.4). These models do not describe physical processes involving (transport of) matter and energy and hence do not adhere to physical laws. Though not subject to physical constraints, they do deal with the values of physical variables.

```

PhysicalDAEModelType
|
|___ Sensors
|   |___ Flow
|   |___ DO
|   |___ NH4
|   |___ NO3
|   |___ COD
|   |___ ...
|___ Controllers
|   |___ P
|   |___ PI
|   |___ PID
|   |___ On_Off
|   |___ ...
|___ Data_filters
|   |___ Sample_and_Hold
|   |___ Noise
|   |___ First_Order_Time_Lag
|   |___ TimeDelay
|   |___ ...
|___ Transformers
|   |___ BODCOD
|___ Generators
|   |___ Sinus
|   |___ DoubleSinus
|   |___ Block
|___ Timers
|   |___ ...
|___ Cost_Calculators
|   |___ OperationalCost

```

**Figure 3.4: Models not describing physical processes directly derived from PhysicalDAEModelType**

As mentioned before, WEST is not only used to model wastewater treatment processes but also parts of the environment, in particular the river in which the treated effluent is discharged (Figure 3.5).

```

PhysicalDAEModelType
|
|___ River_models
|       |___ Bulk_Benthic_River
|       |___ BenthicRiver

```

**Figure 3.5: Some river models developed in WEST**

The shallowness of the above inheritance hierarchy reflects the diverse nature of this subset of model types used in wastewater engineering, not allowing for much re-use.

Now we will look into the development of WWTPAtomicModel, derived using the mass conservation law, from which many other model types are derived. This will illustrate the powerful re-use capabilities of the developed system. First of all, note that the matrix of the simple example could be implemented in MSL-USER in the following easy way:

```

TYPE Components = ENUM {H_2O, S_S, S_O, X_B};

TYPE Reactions = ENUM {Growth, Decay};

parameters <-
{
  OBJ Y   "Yield"   : Yield := {:value <- 0.67:};
  OBJ mu  "Maximum Specific Growth Rate" : GrowthRate := {:value <- 4.00:};
  OBJ K_S "SaturationCoeff" : SaturationCoefficient :={:value <- 20.00:};
  OBJ b   "Decay Rate" : DecayRate := {:value <- 0.40:};
};

initial <-
{
  parameters.Stoichiometry[Growth][X_B] := 1;
  parameters.Stoichiometry[Growth][S_S] := - 1/(parameters.Y);
  parameters.Stoichiometry[Growth][S_O] := - (1 - parameters.Y)/parameters.Y;
  parameters.Stoichiometry[Decay][X_BH] := - 1;
  parameters.Stoichiometry[Decay][S_O] := - 1;
};

equations <-
{
  state.Kinetics[Growth] := parameters.mu *
    (state.C[S_S]/(parameters.K_S+state.C[S_S])) * state.C[X_B];
  state.Kinetics[DecayOfHetero] := parameters.b*state.C[X_B];
};

```

The basic mass balance equation 3.2 for each of the components can also be rewritten in MSL format.

First, the flux for each component  $i$  is calculated as  $\sum_{\alpha} \Phi_{i\alpha}$ .

```

{FOREACH Comp_Index IN {1 .. NrOfComponents}:
state.FluxPerComponent[Comp_Index] =
  (SUMOVER In_Terminal IN {SelectByType(interface, InWWTPTerminal)}:
  In_Terminal[Comp_Index]) +
  (SUMOVER Out_Terminal IN {SelectByType(interface, OutWWTPTerminal)}:
  Out_Terminal[Comp_Index]);};

```

Next, the reaction (conversion)  $R_i V = V \cdot \sum_i v_{ij} r_u$  is encoded in a straightforward manner as:

```
{FOREACH Comp_Index IN {1 .. NrOfComponents}:
  state.ConversionTermPerComponent [Comp_Index] =
  SUMOVER Reaction_Index IN {1 .. NrOfReactions}:
    (parameters.Stoichiometry [Reaction_Index] [Comp_Index]
    *state.Kinetics [Reaction_Index])
  *state.V;};
```

Finally, the complete mass balance  $\frac{dM_i}{dt} = \sum_{\alpha} \Phi_{i\alpha} + R_{iV}$  is written for each component:

```
{FOREACH Comp_Index IN {1 .. NrOfComponents}:
  DERIV (state.M [Comp_Index], [independent.t]) =
  state.FluxPerComponent [Comp_Index]
  + state.ConversionTermPerComponent [Comp_Index];};
```

The rate of change of a component's mass thus consists of the net result of incoming and outgoing mass flux augmented with a reaction term due to biochemical interactions between different components. The MSL-USER compiler will expand the above few lines into the appropriate equations based on the matrix given. These equations will subsequently be manipulated to generate correct and efficient simulation code. Note that components which are transported but do not react (*i.e.* only hydraulics, no physico-chemical nor biological processes) have a column of zeroes in the stoichiometry matrix. In MSL-USER, by default, when a variable or a parameter is not given a value, the initial value is 0. Thus, if we don't assign anything to elements of the stoichiometry matrix, it is a matrix of zeroes, which means no biochemical reactions take place.

Note how the use of this matrix representation is not limited to this simple example or even to the ASM1 model. Also the models ASM2, ASM2d, ASM3 and RWQM1 developed by IWA task groups in the mean time have been implemented (Henze *et al.*, 2000; Reichert *et al.*, 2001). The user can also easily implement mass balance models himself using this general approach. Only the component vector, the reaction vector and the stoichiometric and kinetic coefficients need to be specified.

Logically, the next level (below WWTPAtomicModel) of classification would be to distinguish between models without volume (point-model abstractions where no mass is accumulated and hence no reactions occur) and models with volume. For models with volume, the distinction must be made between models where volume is considered constant and those where volume may vary. This class hierarchy is depicted in Figure 3.6.

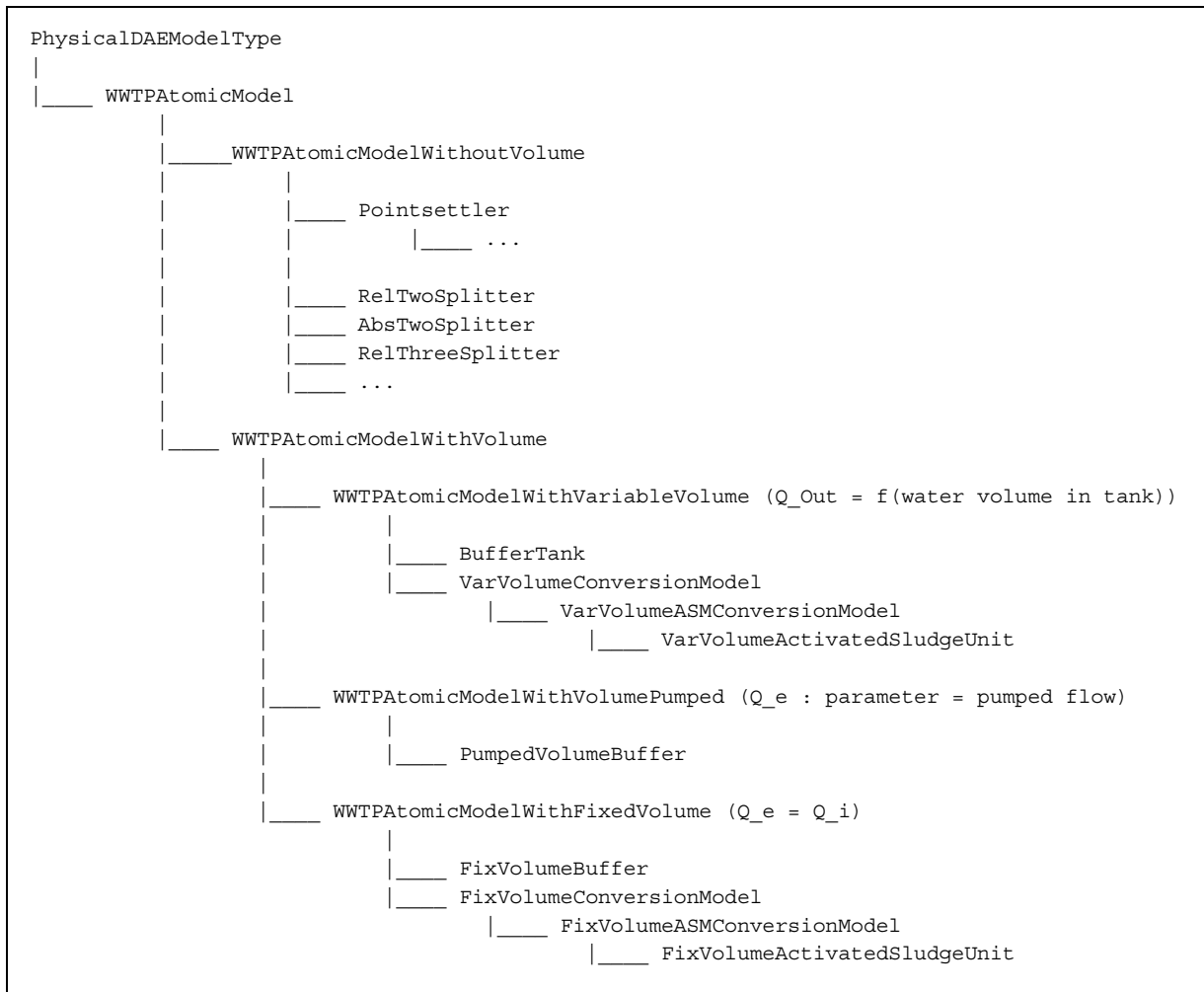


Figure 3.6: Class hierarchy of models without and with volume derived from WWTPAtomicModel

### 3.5 The modelling environment: building a graphical configuration and a coupled model

As mentioned above, the WEST modelling environment allows for graphical component-based modelling. A hierarchical graphical editor (HGE) was especially designed for the interactive building of complex configurations from basic building blocks. The user can entirely rebuild the physical configuration of the wastewater treatment plant in the HGE (Figure 3.7). Each of the components (aeration basins, clarifiers, ...) are symbolically represented by an icon with one or more input and outputs (*terminals*). The program uses two types of terminals: data terminals and physical terminals. Physical terminals represent a physical connection between two components in the configuration. Data terminals on the contrary, represent a dataflow in the system. This can be a measurement signal from a sensor to a control system, or a calculated control action from the control system to the manipulated variable in the configuration.

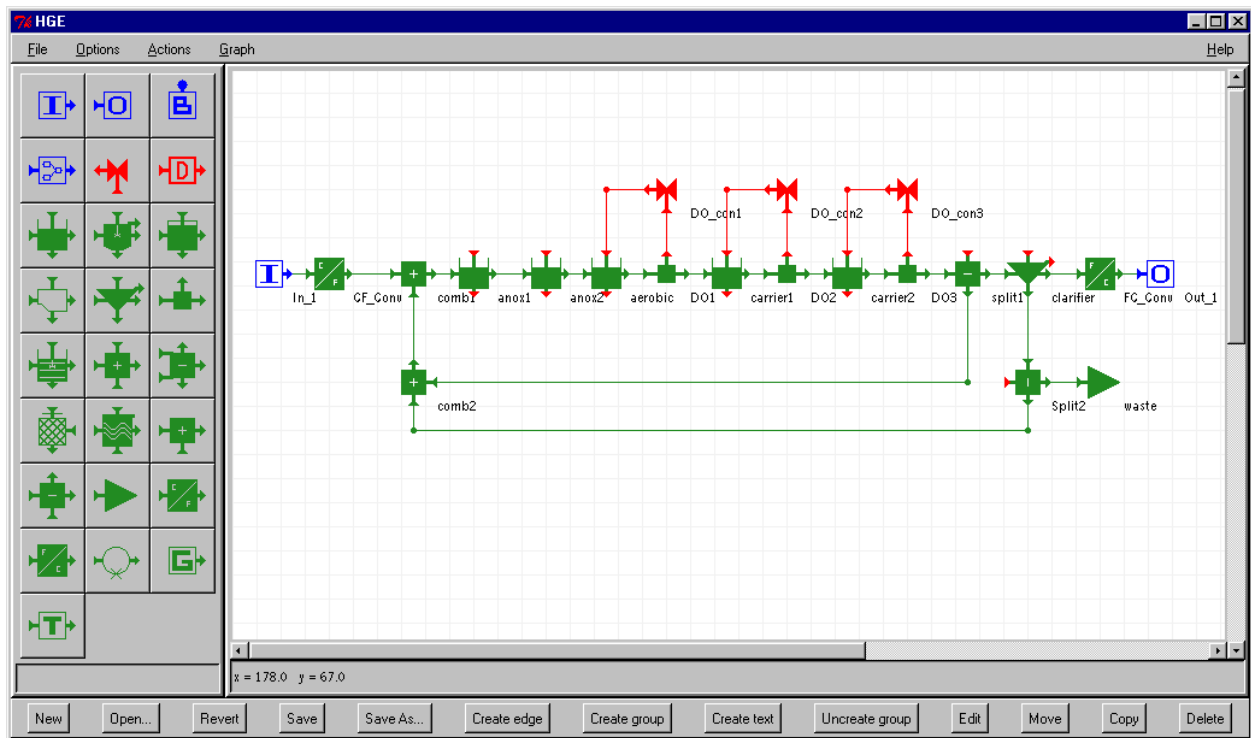


Figure 3.7: Representation of a WWTP model in the HGE (Hierarchical Graphical Editor)

At this point, only a graphical representation has been made of the wastewater treatment plant to be modelled. Nothing has been specified on its behaviour. In a next step, once the configuration has been built graphically, each component of this configuration should be linked to a model from the model base. Each of these models is a structured collection of DAE's representing the time dependent behaviour of the components in question. The complete set of models together with the parameter values chosen by the users then specifies the dynamic behaviour of the model. A model base may contain multiple reasonable candidate models based on model features and user requirements. WEST leaves the final choice to the user, so model selection is mostly done on a manual basis. However, ongoing research tries to find and validate methodologies to accomplish automatic model selection based on measurements performed on the real process (Vanrolleghem and Van Daele, 1994; Cooney and McDonalds, 1995; Takors *et al.*, 1997; Dochain and Vanrolleghem, 2001).

Now from this graphical specification, together with the models chosen from the model base, a coupled model is produced. Some of the MSL-USER code corresponding to the coupled model represented in Figure 3.7 is shown below.

As indicated in paragraph 3.4.4.3, each icon put on the canvas results in the instantiation of an MSL-USER object of the appropriate class in the coupled models *sub\_models* section. If the user decides to define parameters of the coupled model in the HGE, they are stated in the *parameters* section. In the *coupling* section, statements are included that describe how the sub-models are connected to each other. First of all, the relations between the parameters of the sub-models and the user-defined parameters of the coupled model are indicated. Following this, the *connect* and *control* statements are listed. The *connect* statement is used to connect the interface variables of the coupled model to the interface of one of the sub-models or to connect the interfaces of two sub-models. The *control* statement is used to indicate that a parameter of a sub-model is controlled by an interface variable of a

second model. However, parameters are invariant values to be declared at the beginning of a simulation run. In case a controller is used, the parameter serves as a manipulated variable. Therefore, it will automatically be transformed from a parameter to an input variable by the MLS-USER parser.

```

CLASS SuspendedCarrierWWTPClass SPECIALISES CoupledModelType :=
{
  interface <-
  {
    OBJ In_1 (* terminal = "In1" *) "InfluentConc" : InWWTPConcTerminal := {:causality <- CIN:},
    OBJ Out_1 (* terminal = "Out1" *) "EffluentConc" : OutWWTPConcTerminal := {:causality <- COUT:},
  };

  parameters <-
  {
    OBJ Y_A "Autotrophic Yield" : YieldForAutotrophicBiomass := {: value <- 0.24 :},
    OBJ Y_H "Heterotrophic Yield" : YieldForHeterotrophicBiomass := {: value <- 0.67 :},
    ...
  };

  sub_models <-
  {
    OBJ CF_Conv : CtoF,
    OBJ comb1 : TwoCombiner,
    OBJ anox1 : SuspendedCarrierASU,
    ...
    OBJ aerobic : FixVolumeASU,
    OBJ DO1 : DO,
    OBJ DO_con1 : SaturationPI,
    ...
  };

  coupling <-
  {
    // parameter coupling
    ...
    sub_models.anox1.parameters.Y_A.value := parameters.Y_A.value,
    sub_models.anox1.parameters.Y_H.value := parameters.Y_H.value,
    ...
    sub_models.aerobic.parameters.Y_A.value := parameters.Y_A.value,
    sub_models.aerobic.parameters.Y_H.value := parameters.Y_H.value,
    ...
    // sub-model coupling
    connect(interface.In_1, sub_models.CF_Conv.interface.Inflow),
    connect(sub_models.CF_Conv.interface.Outflow, sub_models.comb1.interface.Inflow1),
    ...
    // control statements
    control(sub_models.DO_con1.interface.u, sub_models.aerobic.parameters.Kla),
    ...
  };
};

OBJ SuspendedCarrier "": SuspendedCarrierWWTPClass;

```

The graphical editor and the coupled model introduce a second level of hierarchy in WEST. Indeed, next to the hierarchical structure of the model base, aimed at maximal re-use of knowledge, also coupled models and their graphical representations can be re-used. All coupled model have an interface completely alike the sub-models from which they are composed. Consequently, the user can decide to add a coupled model to the model base and re-use it in yet another coupled model. This way, a model can be structured as a tree of coupled models and atomic models from the original

model base. Again a maximal level of re-usability and transfer of knowledge is obtained here. When coupling the models of the sewer system, treatment plant and receiving water, one can build and test the models separately. Afterwards, they can easily be linked in the graphical editor by re-using the models created before (Figure 3.8). When creating large models, it is very useful to first test the submodels and only afterwards connect them to create the integrated large model.

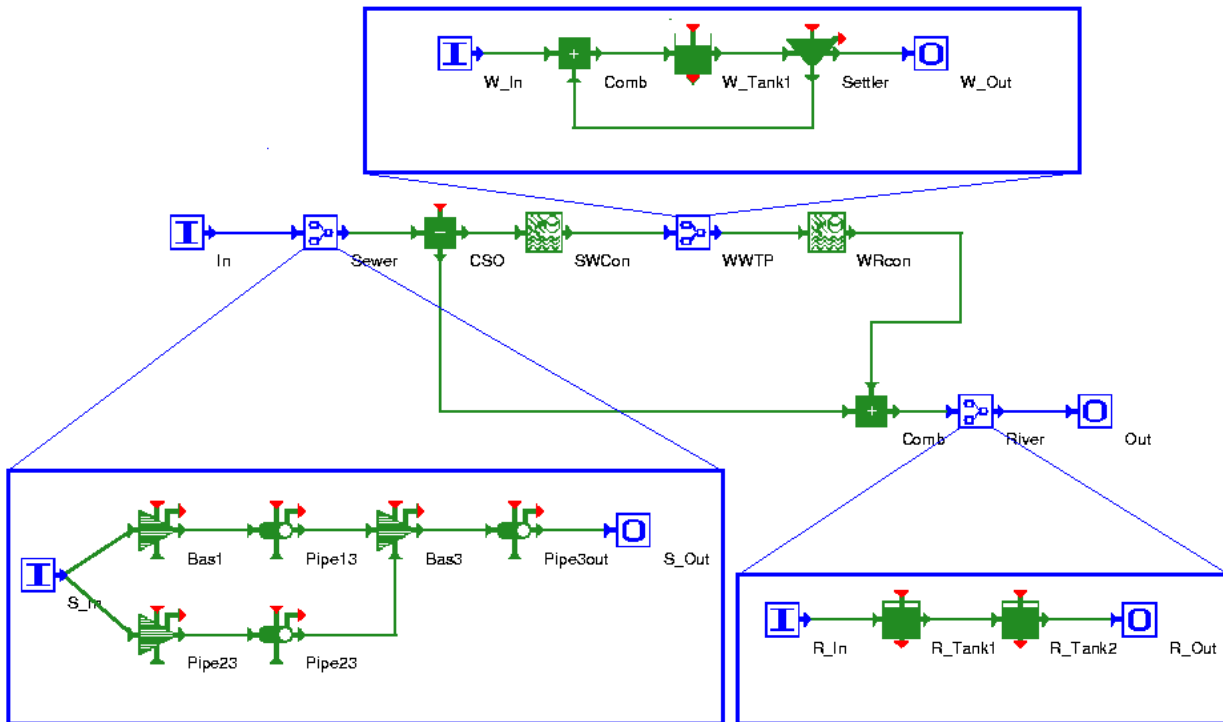


Figure 3.8: Representation of the re-use of models in the graphical editor of WEST

### 3.6 Parsing from MSL-USER to MSL-EXEC

After constructing a coupled model in the HGE, the parser generates MSL-EXEC from this model for use in the experimentation environment of WEST. It therefore uses the coupled model itself along with the models stored in the model base.

During this (parsing) process, the syntax and the semantics of the MSL-USER representation are checked automatically as well as the compatibility of the nature (the units) of the variables passed on between the different sub-models. This way, some model coding errors may be detected here and not only when simulating the model.

MSL-EXEC contains both code to describe dynamics as code to represent the symbolic information (“knowledge”). The model dynamics are specified as a set of ordinary differential equations (ODE’s) and algebraic equations. As the order of the equations is of no importance in MSL-USER, the correct sorting of the differential and algebraic equation has to be done by the parser. The different built-in statements, are recognised by the parser and translated into their equivalent C++ formulations.

The symbolic information is used to display the model information in the WEST experimentation environment. For example, based on the annotations *hidden* and *fixed*, a variable or parameter will not

be shown in the experimentation environment or the user will not be able to change its value. As mentioned before, a controlled parameter will automatically be transformed from a parameter to an input variable by the MLS-USER parser and will therefore no longer be visible in the parameter listing. Also the constraints on variables as integrated in the MSL-USER model base are transferred to the symbolic part of the MSL-EXEC representation and are used to protect the user from constraint violations during simulation or user input. Furthermore default values, units and descriptions are visible in the experimentation environment.

Before the MSL-EXEC code can be used in the experimentation environment, an extra compilation step has to be performed. In this compilation step, a library file (executable code) is generated that can be loaded into the experimentation environment. This compilation step guarantees code that is optimised for simulation performance and accuracy. During this compilation, standard C libraries are linked to the generated model, enabling the user to include all functions available in these libraries in the MSL-USER models. Even user-defined C++ functions can be used and linked during parsing.

During parsing symbolic manipulation can be performed too. Symbolic manipulation is concerned with finding symbolic or exact solutions to mathematical problems. This avoids rounding errors and the need for an error analysis. Exact or symbolic computation has the disadvantage of being more compute-intensive than numerical calculation. However, as symbolic manipulation is performed only once as opposed to numerical code, which gets executed time and again during simulation, the one-time intensive symbolic computation cost at parse time is largely compensated by the performance gain at simulation time.

The following very simple example will illustrate the usefulness of symbolic manipulation. Imagine you are trying to solve an equation for an unknown variable, such as:  $x - 5 = 0$ . An analytical solution is found if the equation can be solved explicitly for the unknown variable. In this case this is easy to see. However, we might develop an *algorithm* on a computer to solve this equation numerically. The algorithm would test various values for  $x$ , and then stop with a solution when the equation is satisfied to some chosen tolerance. For example, we might demand that the computer should solve this equation to an accuracy of 0.5. Then the computer would follow the algorithm until it found a solution. Given an initial guess  $x = 1$ , depending on the algorithm it might come up with the following guesses:  $x = 2.2$ ,  $x = 3.3$ ,  $x = 4.6$ , and return the solution  $x = 4.6$ . Note that if we want to be more accurate, it takes more time to solve this equation to this level of accuracy. If, through symbolic manipulation we were able to find the exact analytical solution  $x = 5$  immediately, an enormous gain at simulation time would result.

When the equations to be solved are large and complex, one has to deal with some issues about how to reach the solution in the most efficient way. Several problems can be tackled both in a numerical and a symbolic way. Getting the solution using one method rather than the other, has advantages and disadvantages. The advantages of symbolic manipulation in the case of WEST are:

- Performance, if you know a quantity analytically, you can avoid some computations and decrease the computation time.
- More accurate numerical results, because by pre-processing data with symbolic manipulations, more advanced numerical techniques can be exploited.

On the other hand, analytical solution methods do not exist for quite some problems. However, symbolic methods can still be used to derive expressions necessary for performing numerical computations – such as gradients and Jacobian and Hessian matrices. Thus, the traditional roles of numerical and symbolic computations are not distinct and many benefits arise from merging the two.

### 3.7 Working with the model: the experimentation environment

The experimentation environment depicted in Figure 3.9 enables the user to perform experiments on compiled models. As such, it is the interface between the user and the “simulator”. During simulation, the solver communicates efficiently with the model dynamics part of the MSL-EXEC model. The simulator as a whole can be asked to perform a numerical simulation. In that case the solver is used to generate a state trajectory for the MSL-EXEC model. Different numerical solvers can be chosen interactively.

The experimentation environment also queries the simulator for symbolic information. This information will be retrieved from the symbolic information part of the MSL-EXEC model. Examples of such symbolic information are the model structure and the parameter listing in Figure 3.9. In this listing, the unit, a description and a default value of the parameter can be found together with its lower and upper bounds.

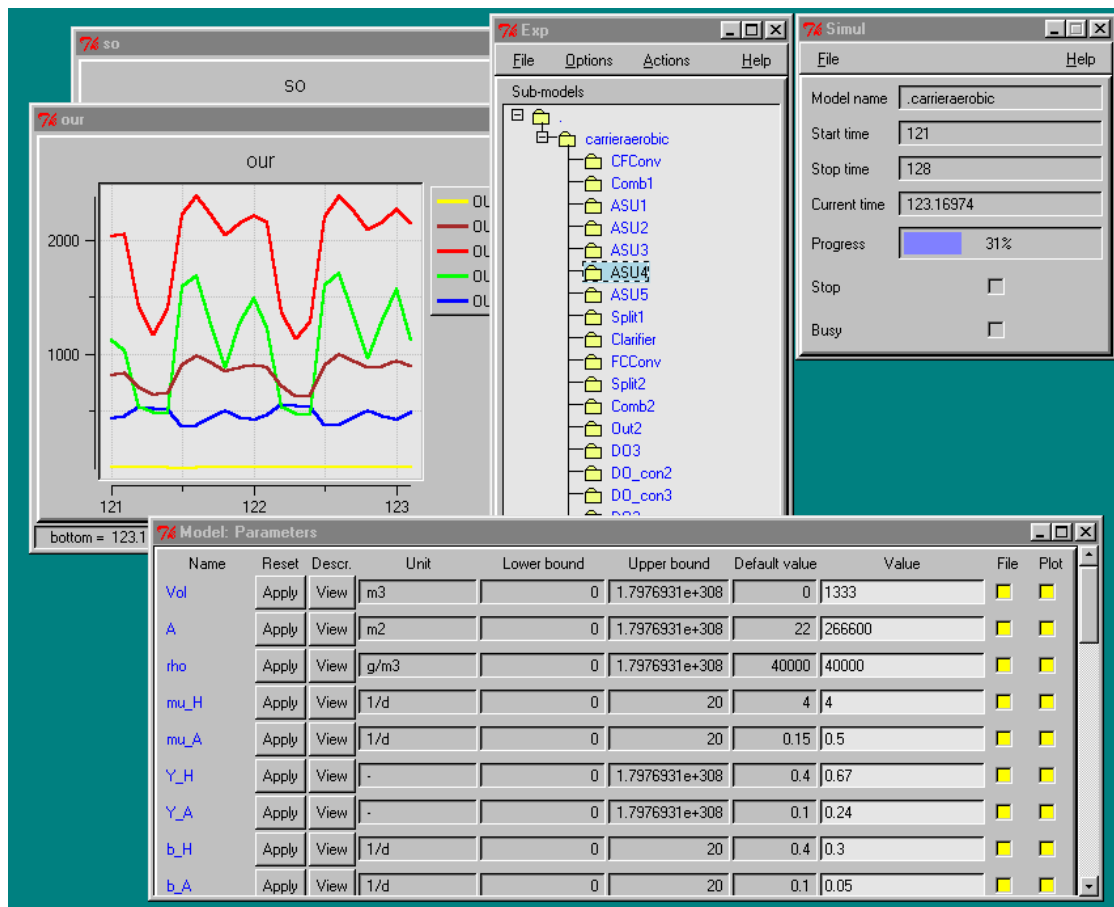


Figure 3.9: The WEST experimentation environment, showing a plot and a parameter listing

The following distinguishes between different *experiment types* as implemented in the WEST environment. The user thinks in terms of different *virtual experiments* with the model of a system. The following experiment types are currently implemented in WEST:

### 1. Simulation experiment

Currently, there are two types of simulation experiments:

- Initial value problem: state variable values are given at time  $t_{ini}$ . The simulator calculates the trajectory over  $[t_{ini}, t_{fin}]$ . This is implemented using a set of forward integrators the user can select among.
- Terminal value, end value or *shooting* problems: state variable values are given at  $t_{fin}$ . The simulator calculates the trajectory over  $[t_{ini}, t_{fin}]$ . Solving the shooting problem is implemented in WEST using an optimisation algorithm whereby the varied entities are the unknown initial conditions and the goal function is the sum of absolute or squared values of differences between simulated end-value and known/specified end-value.

Sometimes it is necessary to “synchronise” with external data. This is for example the case when the input  $u(t)$  is given as a table of measurements, for instance the influent composition or a pump schedule. The integrator can determine its own integration times and when an input value is needed, interpolation is used. When the input is given as a continuous function (via an generator model), no interpolation is required.

### 2. Trajectory optimisation experiment

Certain model parameters are varied by a number of search algorithms the user can select from to minimise the *distance* between a simulated trajectory and a given (measured or desired) trajectory. This is mostly done for (constrained) parameter estimation (model calibration), but it can also be used for controller tuning and process design optimisation. The distance measure is typically a sum of squares of differences between measured and simulated values though absolute values can also be used. The difference between measured and simulated values can be calculated at different points in time: as described above, the simulator can be forced to *synchronise* with external data or interpolation can be used. In general, the differences can be weighted to account for measurement accuracy and possible differences in the order of magnitude of the different values in the objective function. The optimisation experiment also provides confidence information (covariance matrix) about the quality of the parameter estimations. The covariance matrix is calculated with the method of Nelder and Mead (1964). The confidence information can then be used, for instance, to draw confidence ellipses or give parameter confidence bounds.

### 3. End value optimisation experiment

Here the optimiser is used to vary where some parameters (possibly constrained) to extremise a goal function that only evaluates variable at  $t_{fin}$ , for instance total economic cost.

### 4. Sensitivity analysis experiment

The sensitivity of the model with respect to model parameter variations can be investigated. The calculation of sensitivity functions is based on the finite difference method. This method calculates the difference between two experiments, a reference experiment and a perturbation

experiment. The perturbation experiment is performed by perturbing a model parameter by a small factor (the perturbation factor). Dividing the difference in model outputs between these experiments by the parameter change results in the sensitivity function. To make sure the sensitivity functions are calculated properly, a third experiment is performed, the control experiment. For this experiment the parameter perturbation factor is doubled. If the resulting sensitivity function is within an allowed error band it can be assumed that the nonlinearity of the model did not influence the calculations. The error between both sensitivity functions is calculated with different criteria such as the sum of squared errors, the largest absolute difference, etc.

Sensitivity functions form the basis of optimal experimental design because they indicate where the measurements are most sensitive to the parameters. Moreover, the Fisher information matrix which is an important cornerstone of experimental design is calculated using sensitivity functions. This matrix is a measure for the information content of the simulated experiment.

#### 5. Monte Carlo experiment

The uncertainty of the model output due to input (parameter and variable) uncertainty can be calculated in a Monte Carlo experiment. For each model input that is considered to be a random variable, a probability distribution is specified out of a range of possible distributions (normal, log-normal, uniform, triangular, ...). Random samples are taken for each of the input distributions, and the set of samples ('shot') is entered into the deterministic model. The model is then solved as it would be for any deterministic analysis. The model results are stored and the process is repeated until the specified number of model iterations is completed (Cullen and Frey, 1999). From all stored model results, statistical properties (mean and standard deviation) and histograms are produced. These can subsequently be used in decision making, *e.g.* risk analysis (Rousseau *et al.*, 2001)

The experimentation environment can also be controlled via scripting languages (Tcl scripting, Visual Basic scripting). Scripting enables the user to perform several scenarios in an automated way. It is possible to automatically perform a series of experiments using a predefined set of parameter values. Output and integrator options can be controlled interactively. Among others, the Monte Carlo simulation engine has been constructed using such relatively simple scripts.

## 3.8 Conclusions

The mathematical modelling of biological wastewater treatment plants can be used during the design and optimisation phase. WEST is a general modelling and simulation environment and can, together with the developed model base, be used for this task. The model base is written in MSL-USER in which symbolic information can be included in the code. In the graphical modelling environment, the physical layout of the plant can be rebuilt, and each building block can be linked to a specific model from the model base. The graphical information is then combined with the information in the model base to produce MSL-EXEC-code, which can be compiled with a C++-compiler to generate fast, executable code. In the experimentation environment, the user can design different experiments like simulations, optimisations. The main advantages of the use of this software are the following. First, the

modelling and simulation environment are strictly separated since these have different objectives (i.e. flexibility and model re-use vs. accuracy and performance). The MSL-USER language is a high level language which is easy to learn and to use, while information about boundaries and units of parameters and variables can be implemented. Furthermore, an extensive model base for the modelling of WWTP's is available. The parser uses symbolic manipulation to create numerically efficient code. Finally, the experimentation environment can be easily used to perform different types of experiments with the models. The user can extend these experiments by scripting.



# 4 A simplified mixed-culture biofilm model

---

## 4.1 Introduction

The growth of microbial species inside attached biological films causes a significant flux of substrates from the bulk liquid, *i.e.* the water phase outside of the biofilm. As has been denoted before, these processes are of great interest for the aquatic ecology in surface waters, for the treatment of wastewater and in biotechnology. Therefore, considerable effort has been made in the last 25 years to develop adequate mathematical models for the description of substrate utilisation and population dynamics in biofilms. The fact that makes such biofilm models relatively complex is that not only the microbial conversion of substrate needs to be considered, but also the diffusive transport of soluble substrates inside the biofilm. Early modelling approaches consequently neglected the aspect of biomass growth by assuming a predefined microbial distribution and biofilm thickness (see among others: Williamson and McCarty, 1976; Harremoës, 1978; Mueller *et al.*, 1980). It was not before the mid-80's that Kissel *et al.* (1984) and Wanner and Gujer (1986) introduced a more accurate description of the system behaviour, both in time and in space, which made it possible to predict microbial species development over the depth of the biofilm as a function of substrate flux. Recent advances in biofilm research (see among others: Lewandowski *et al.*, 1994; Zhang and Bishop, 1994a; Bishop, 1997) conclude that also the heterogeneity of the biofilm must be taken into account. Describing this quantitatively has been attempted in the revised mixed-culture biofilm model of Wanner and Reichert (1996). Next to the one-dimensional models described above, the heterogeneous structure of biofilm in wastewater treatment led to the development of a multi-dimensional model focussing more on describing the biofilm structure as a result of environmental influences than on quantitative modelling of the substrate removal in the biofilm (Wimpenny and Colasanti, 1997; Hermanowicz, 1998; Picioreanu *et al.*, 1998a, b).

However, such detailed mathematical description of the processes in mixed-culture biofilms has also some shortcomings. Most important among these are the computational efforts required for solving the resulting set of partial differential equations and the high complexity of the model, which makes the accurate estimation of parameter values and initial conditions a tedious task. Hence, rather than following the trend to include more and more phenomena in the model, a simpler model is presented here in order to allow fast but sufficiently accurate simulation of biofilm dynamics. The basic idea of the proposed model is to decouple the modelling of the diffusion process and spatial distribution of bacterial species from the biokinetic conversion. This is done by means of a two step procedure where (1) for each conversion process that is influenced by diffusion, the active fraction of the biomass within the biofilm is computed by means of a simple analytical formula and (2) all conversions within the biofilm are then calculated as if the biofilm were an ideally mixed reactor but with only the active fraction of the species contributing in conversion.

In this chapter, the concept and the equations of the simplified mixed-culture biofilm model are presented. The avoidance of the numerical solution of partial differential equations by using the two-step procedure results in a fairly simple model structure. This aspect makes the proposed model an

attractive alternative to the existing complex models when more emphasis is put on fast predictions of system behaviour than on detailed understanding. The avoidance of partial differential equations also has the advantage of simplifying the connection of the model to other models widely used in wastewater treatment plant simulation. This can be done within standard wastewater treatment plant simulation software without adding extra software for the integration of PDE's.

## 4.2 General modelling concept

### 4.2.1 Background

Figure 4.1 illustrates the ideal biofilm system that is mathematically described in the proposed model. To study the interaction between the biofilm compartment and the bulk liquid compartment it is necessary to distinguish between dissolved and particulate constituents. Dissolved substances are transferred from the bulk liquid into the biofilm (the influence of the liquid film diffusion is here neglected for simplicity, see Christiansen et al. (1995) and then transported by means of molecular diffusion. Particulate components cannot be transferred inside the biofilm but will be adsorbed to the biofilm surface, a process usually denoted as attachment. The reverse phenomenon of displacement of particulate components is consequently addressed as detachment.

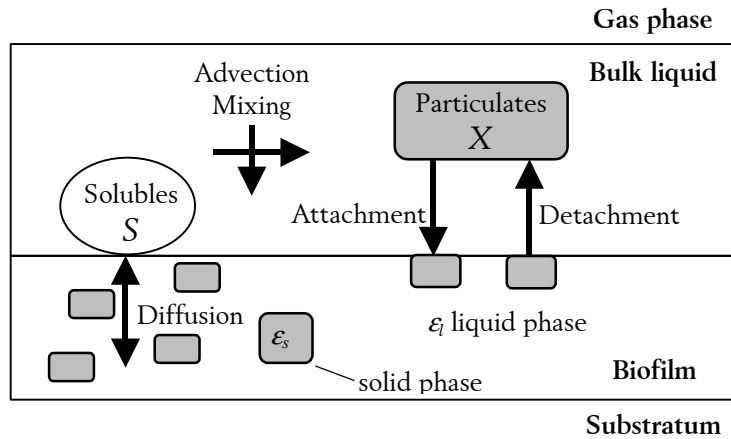


Figure 4.1: Transport processes in an ideal biofilm system

The biofilm compartment consists of two phases, that is (1) the liquid phase, in which the dissolved substances are transported due to the diffusion phenomena and (2) the solid matrix, which consists of several species of bacteria as well as of particulate substrates and inert material. The concentration of particulates and their density in the biofilm is therefore to be expressed as follows:

$$\varepsilon_l + \sum_{j=1}^{n_x} \varepsilon_{sj} = 1 \quad \text{with} \quad \varepsilon_{sj} = \frac{X_j}{\rho_j} = \frac{M_{Fj}}{V_F} \frac{1}{\rho_j} \quad (4.1)$$

where  $\varepsilon_l$  is the volume fraction of the liquid phase,  $\varepsilon_{sj}$  the volume fraction of the particulate component  $j$  in the solid matrix,  $n_x$  the number of particulate components considered and  $\rho_j$  the density of the component. The concentration of a specific component ( $X_j$ ) is given by dividing its mass ( $M_{Fj}$ ) by the entire volume of the biofilm ( $V_F$ ), *i.e.* volume of its liquid and solid phase. The density of

a specific component  $j$ ,  $\rho_j$ , must not be confused with the mean biofilm density  $\rho_m$  which can be measured experimentally.

$$\rho_m = \sum_{j=1}^{n_x} (\varepsilon_{sj} \rho_j) = \frac{\sum_{j=1}^{n_x} M_{Fj}}{V_F} \quad (4.2)$$

For reason of simplification the proposed model is applying the widespread assumption to see the biomass as a continuum (e.g. Wanner and Gujer, 1986), that is  $\rho_j = \text{constant} = \rho_m / (1 - \varepsilon_l)$ .

#### 4.2.2 Concept of active fractions

Soluble substrate from the bulk liquid is transferred inside the biofilm and then transported further by means of molecular diffusion. The substrate is simultaneously utilised in the film by the bacteria for growth. In case the substrate does not fully penetrate the biofilm, the reaction is considered as diffusion limited, *i.e.* the reaction is taking place only over a certain depth of the biofilm.

Harremoës (1978) developed analytical solutions for calculating diffusion limited biofilm reactions by adopting mass balance equations for biofilms with an idealised geometry (Figure 4.2) and steady-state conditions:

$$\frac{\partial^2 S}{\partial \zeta^2} = \frac{r}{D_f} \quad (4.3)$$

where  $S$  is the concentration of the substrate at the location  $\zeta$  in the biofilm,  $D_f$  the diffusion coefficient for the substrate in the biofilm and  $r$  the volumetric reaction rate (positive for substrate removal).

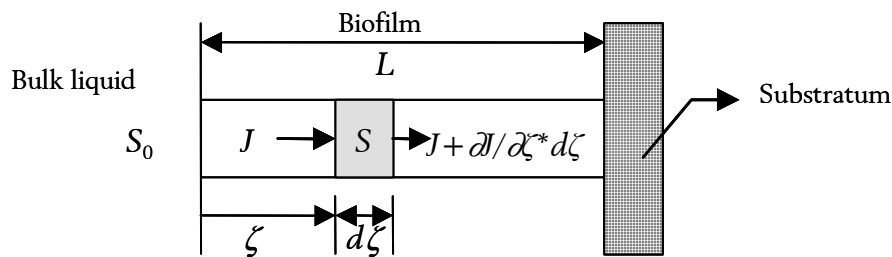


**Figure 4.2: Idealised biofilm system with uniform spatial distribution of microbial species**

To derive an analytical solution to this second order differential equation, the reaction rate needs to be defined. Harremoës (1978) pointed out that the specific growth rates of bacteria can be assumed zero-order with respect to the concentration of the substrate  $S$  in the biofilm. The reason is that the saturation coefficients (assuming Monod-type kinetics) are very small for most substrates at hand (dissolved oxygen, soluble organic matter, ammonium and nitrate). Hence, the biofilm volume where the assumption of zero-order kinetics does not hold is very small and can be conveniently neglected. The volumetric (zero-order) reaction rate of a species with respect to the substrate  $S$  can thus be written as:

$$r = -\mu X \nu \quad (4.4)$$

where  $r$  is the zero-order reaction rate for the bacterial species  $X$  with respect to the substrate  $S$ ,  $\mu$  the (max.) specific growth rate of the species  $X$  and  $\nu$  the stoichiometric coefficient.

The penetration depth  $z$  can be derived from an analytical solution to equation 4.3 (Harremoës, 1978). To derive the penetration depth  $z$ , equation 4.3 must be solved with the appropriate boundary conditions:

$$(S = S_0)_{\zeta=0}, \quad \left( \frac{dS}{d\zeta} \right)_{\zeta=z} = 0 \quad (4.5)$$

where  $S_0$  is the concentration of substrate  $S$  in the bulk liquid.

This leads to the following second order algebraic equation:

$$S = \frac{1}{2} \frac{r}{D_f} \zeta^2 - \frac{r}{D_f} z^2 + S_0 \quad (4.6)$$

And since  $(S = 0)_{\zeta=z}$ :

$$z = \sqrt{\frac{2 D_f S_0}{r}} \quad (4.7)$$

The basic consideration is now whether the biofilm is fully penetrated by the substrate or not. In case the biofilm is fully penetrated (no substrate limitation or  $z \geq L$ ), the solution to the problem is obvious, as the reaction takes place over the full depth of the biofilm  $L$  with a constant (zero-order) maximum rate. However, in case of substrate limitation the reaction is taking place only over a certain depth of the biofilm. Hence, when there is substrate limitation, the biofilm is partitioned in an active (upper) part and an inactive part close to the substratum. This limitation effect can also be expressed by assuming only a certain fraction of the biomass to be active.

From the above reasoning, a solution can be given for the flux of substrate  $S$  into the biofilm:

$$J = -\mu X \nu \phi L \quad \text{and} \quad \phi [0,1] \quad (4.8)$$

where  $J$  is the total transport of the substrate  $S$  through the surface of the biofilm,  $L$  the biofilm thickness and  $\phi$  the active fraction of species  $X$ . The underlying idea is that the active fraction of the biomass  $\phi$  is equal to the dimensionless penetration depth of the limiting substrate  $\beta (= z/L)$ :

$$\phi = \beta = \sqrt{\frac{2 D_f S_0}{r L^2}} \quad (4.9)$$

### 4.2.3 Assumptions underlying the concept

The concept of active fractions forms the basis of the simplified mixed-culture biofilm model. It is therefore essential to be aware of the assumptions this model relies upon: (1) the biofilm is assumed to be of homogeneous structure and density, (2) the microbial species in the biofilm are uniformly distributed, (3) the typically modelled stagnant liquid layer is neglected, (4) reaction rates are of zero-order, (5) soluble components that emerge from conversion processes inside the film are assumed to be subject of immediate out-diffusion at the surface of the biofilm and (6) an instantaneous steady-state substrate profile is assumed.

Assumptions No 1 and 2 can be justified as long as particularly the heterotrophic loading to the system under study is not too high (as in the applications described below). It should be noted that in practice the structure of every biofilm is heterogeneous up to some degree. However, this is highly dependent on the substrate loading and the amount of shear stress the biofilm is subject to during its growth (van Loosdrecht *et al.*, 1997). Therefore, these assumptions should be treated carefully because in some cases they could lead to discrepancies of the simulation results.

The incorporation of a stagnant layer (see assumption No 3) does not affect the basic assumptions of the model required for the analytical solution of the PDE and might therefore be done (paragraph 4.6.3). The possible improvement of the model predictions by including an external diffusion resistance is, however, highly dependent on biofilm loading and fluid velocity. The effect of such effort is most likely rather seen on the decrease of the calculation speed than on the improvement of the predictive power of the model (see Christiansen *et al.*, 1995). As the emphasis of the modelling exercise was on simplification and calculation speed, it was chosen not to incorporate external diffusion resistance at this stage.

The use of zero-order reaction rates (Assumption No 4) is widespread in biofilm modelling, as it is a good description of biofilm kinetics when substrate concentrations are sufficiently high. Other reaction rates can also be used as long as they give rise to analytical solutions for the substrate penetration depth, as this is inherent to the decoupling of diffusion and biokinetic reaction in this approach. Even without the possibility of yielding analytical solutions, this decoupling can also be accomplished for Monod-type kinetics. However, the resulting PDE should then be solved using shooting or finite element methods (Wik, 1999) significantly reducing the gain in calculation speed.

Assumption No 5 is only of importance when a soluble component is produced inside the biofilm due to conversion processes. The assumption of immediate out-diffusion neglects the possible accumulation of the component inside the biofilm. However, due to the principle of homogeneous species distribution in the biofilm (Assumption 2) this effect is partly compensated in the model: the out-diffusion leads to an immediate increase of the concentration of the component in the bulk liquid and, subsequently, to an increase of the substrate flux into the biofilm.

Assumption No 6 is, in principle, violating the mass balances in a dynamic situation and therefore needs to be discussed further. As outlined in Kissel *et al.* (1984) and Wik (1999) the characteristic time of the film diffusion phenomena is about one order of magnitude smaller than the time scale of reactions in the film. From the point of view of the dynamics in the conversion processes it can therefore be assumed that the substrate profile reaches equilibrium very fast. This offers the possibility to omit the consideration of the dynamics of the diffusion process and model diffusion as a steady-state phenomenon within each time step (by means of an analytical solution). Wik (1999) showed that, when simulating the relatively slow dynamics in the biofilm, the error that is introduced to the mass balances in the model by using this approach can be assumed negligible.

### 4.3 Diffusion limitation in a multiple substrate/species system

Applying the theory of diffusion limitation and zero-order substrate utilisation to biological processes (Harremoës, 1978), one must consider that bacteria generally require multiple substances ( $S_i$ ) for growth, usually an electron acceptor, an electron donor and nutrients.

Figure 4.3 outlines the general idea of the theory to the simple example of a 2 substrate / 1 species system. For growth of heterotrophic bacteria in the biofilm two substrates are required, i.e. an electron acceptor (dissolved oxygen  $S_O$ ) and an electron donor (soluble organic matter  $S_S$ ). Both substrates are essential for bacterial growth and, consequently, the whole process stops when one of them is not available. In Figure 4.3 oxygen is considered to be the limiting substrate.

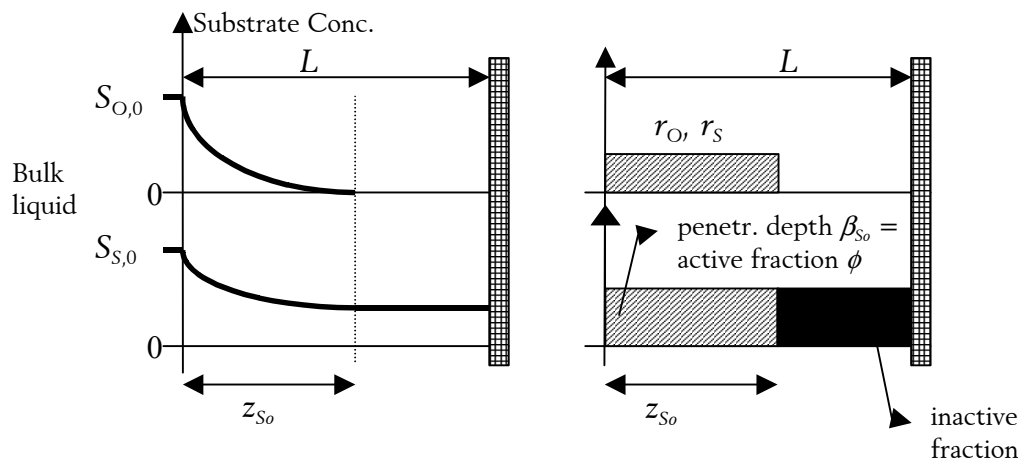


**Figure 4.3:** Illustration of a diffusion limited reaction in a system with two substrates ( $S_O$  oxygen and  $S_S$  organic matter) and one species.  $S_O$  is the limiting substrate.

In this simple system the dependency of the total reaction rate and of the limitation of bacterial growth on the bulk liquid substrate concentration can be derived easily. The active fraction of the biomass  $\phi$  is equal to the dimensionless penetration depth of the limiting substrate  $\beta_{S_0}$  ( $= z_{S_0}/L$  in Figure 4.3). The fluxes of the different substrates  $i$  into the biofilm are then derived directly from:

$$J_i = -\mu X v_i \phi L \quad (4.10)$$

However, the straightforward relation  $\phi = \beta(S_{limiting})$  only holds for very simple systems as in Figure 4.3. Problems arise when this active fraction concept is applied to more complex systems. Indeed, in most cases there are various bacterial species ( $X_j$ ) present in the biofilm, which sometimes compete for the same substrate (*e.g.* both heterotrophic and autotrophic bacteria require oxygen as well as ammonium for aerobic growth). On the one hand, equations for the dimensionless penetration depth  $\beta_i$  can be written that relate to the exhaustion of substrates, while, on the other hand, the active fraction  $\phi_j$  for each biomass species is needed for further calculation. Although there exists a relationship between these two variables, this relation is case specific and requires a thorough analysis of the specific problem at hand, as is illustrated below.

In the following, the basic theory is outlined for a system with substrates  $S_i$  and species  $X_j$ . Based on the considerations above, the volumetric reaction rate of a species with respect to each substrate is written as:

$$r_{ij} = -\mu_j X_j \nu_{ij} \quad (4.11)$$

where  $r_{ij}$  is the zero-order reaction rate for the bacterial species  $X_j$  with respect to the substrate  $S_i$ ,  $\mu_j$  the (max.) specific growth rate of the species  $X_j$ ,  $\nu_{ij}$  the stoichiometric coefficient and  $i,j$  the suffices denoting the substrates and species respectively. In case different species use the substrate  $S_i$ , the total volumetric reaction rate of this substrate becomes:

$$r_i = \sum_j -\mu_j X_j \nu_{ij} \quad (4.12)$$

Now again, in case the biofilm is fully penetrated, all reactions take place over the full depth of the biofilm  $L$  with a constant maximum rate. On the contrary, in case any substrate limitation occurs, the reaction takes place only over a fraction of the total depth of the biofilm.

Given that each reaction is governed by the activity of only one bacterial species, the limitation effect can again be expressed by assuming that only a certain fraction of this particular species is active. Hence, a general solution can be given for the flux of each substrate into the biofilm:

$$J_i = \sum_j -\mu_j X_j \nu_{ij} \phi_j L \quad \text{and} \quad \phi_j \in [0,1] \quad (4.13)$$

where  $J_i$  is the total transport of the substrate  $S_i$  through the surface of the biofilm,  $L$  the biofilm thickness and  $\phi_j$  the active fraction of species  $X_j$ . The calculation of the active fractions is outlined in the following.

#### 4.3.1 Step 1: Active fractions in a multiple substrate - species system

As mentioned in the introduction to this chapter, the proposed model is based on a two step procedure for calculating the conversions in the biofilm reactor. First, the diffusion depth of the substrates into the biofilm is found analytically by assuming pseudo steady-state conditions, zero-order conversion rates and a homogeneous distribution of the bacterial species within the biofilm. The result

of this first step is an estimate of the amount of bacterial mass that is actually active in the conversion processes (active fraction). The other, inactive fraction of the bacterial mass is not exposed to the substrate necessary for performing the conversion processes (the conversion process is diffusion limited). Given this information, the conversion of the substrates in the reactor is then calculated in the second step.

### 4.3.1.1 Analytical derivation of the penetration depth of substrates

As stated above, Figure 4.3 shows the simplest case with respect to diffusion limitation: From the point of view of spatial distribution all processes are stopped when one of the limiting substrates is exhausted. The penetration depth for any substrate, given all other substrates are in excess, can be derived from an analytical solution to equation 4.3:

$$z_i = \sqrt{\frac{2D_{f,i}S_{i0}}{r_i}} \quad \text{and} \quad \beta_i = \sqrt{\frac{2D_{f,i}S_{i0}}{r_i \cdot L^2}} \quad (4.14)$$

$$\text{with } r_i = \sum_j -\mu_j X_j \nu_{ij} \quad (4.15)$$

where  $r_i$  is the zero-order conversion rate of the substrate  $S_i$  (taking into account all bacterial species  $X_j$  that use this substrate under the given environmental condition, *i.e.* aerobic - anoxic),  $\beta_i$  is the dimensionless penetration depth of substrate  $S_i$ ,  $S_{i0}$  the concentration of substrate  $S_i$  in the bulk liquid and  $L$  the biofilm thickness.

However, for a multiple substrate / multiple species system the aspect of diffusion limitation can easily become more complex. Generally, sequential diffusion limitation occurs if a substrate  $S_a$  is used in two (or more) processes and one of these processes is limited earlier than the other by a different substrate  $S_b$ . As a result, the zero-order conversion rate of the substrate  $S_a$  is no longer the same in the whole biofilm. The penetration depth  $z_a$  of the substrate is divided in two parts where the conversion rate in the upper active part ( $r_{ua}$ ) is different (higher) from the one in the lower active part closer to the substratum ( $r_{la}$ ). Indeed, in the upper part two processes consume substrate  $a$ , while in the lower only one process proceeds. This is outlined generally in Figure 4.4.

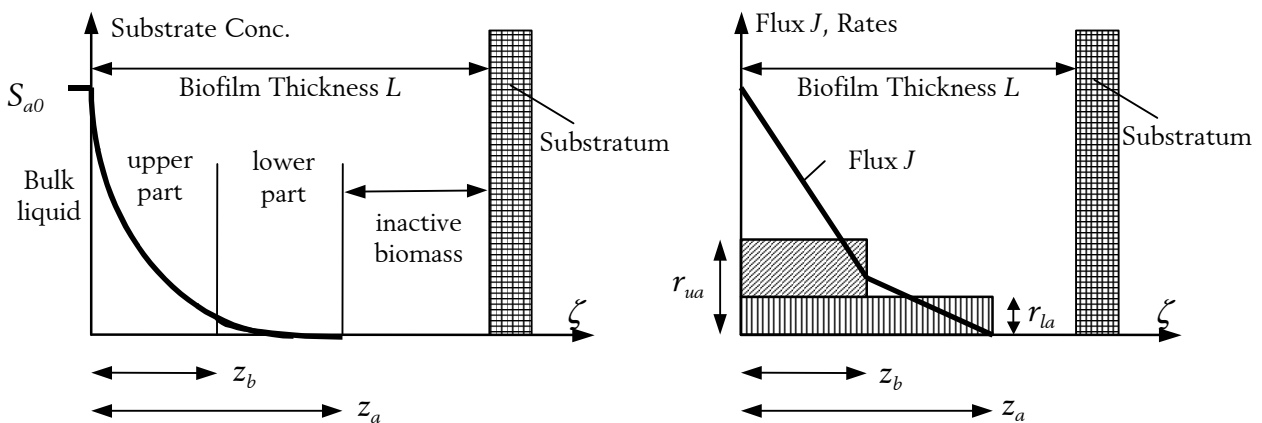


Figure 4.4: General description of sequential diffusion limitation

The depth of the upper part is determined by the penetration depth  $z_b$  of the substrate  $S_b$  that is limiting first. Consequently, the flux of the substrate  $S_a$  deeper into the biofilm is linearly decreasing only within each of the two parts of the biofilm but no longer over the whole penetration depth. Still, the penetration depths  $z_a$  and  $z_b$  can be derived analytically. The differential equations to be solved in this system can be written as:

$$\begin{cases} \frac{\partial^2 S_{ua}}{\partial \zeta^2} = \frac{r_{ua}}{D_{f,a}} \\ \frac{\partial^2 S_{la}}{\partial \zeta^2} = \frac{r_{la}}{D_{f,a}} \end{cases} \quad (4.16)$$

where  $S_{ua}$  is the concentration of substrate  $S_a$  in the upper part of the biofilm.  $S_{la}$  is the concentration in the lower part. Solving these equations leads to two second order algebraic equations. The following boundary conditions can be used to obtain the values of the integration constants:

$$(S_{au} = S_{a0})_{\zeta=0}, \quad \left( \frac{dS_{al}}{d\zeta} \right)_{\zeta=z_a} = 0 \quad (4.17)$$

$$(S_{au} = S_{al})_{\zeta=z_b}, \quad \left( \frac{dS_{au}}{d\zeta} \right)_{\zeta=z_b} = \left( \frac{dS_{al}}{d\zeta} \right)_{\zeta=z_b} \quad (4.18)$$

Furthermore  $(S_{al} = 0)_{\zeta=z_a}$ , yielding the following formula for the penetration depths of substrates  $S_a$  and  $S_b$ :

$$z_b = \sqrt{\frac{2D_{f,b}S_{b0}}{r_b}} \quad \text{and} \quad z_a = \sqrt{z_b^2 \left(1 - \frac{r_{ua}}{r_{la}}\right) + \frac{2D_{f,a}S_{a0}}{r_{la}}} \quad (4.19)$$

where  $r_b$  is the zero-order reaction rate in the upper part with respect to the first limiting substrate  $S_b$  (taking into account all species  $j$  that use this substrate under the given environmental condition),  $r_{ua}$  the zero-order reaction rate in the upper part with respect to  $S_a$  (taking into account all species  $X_j$  that use this substrate under the given environmental condition),  $r_{la}$  the zero-order reaction rate in the lower part with respect to  $S_a$  (taking into account all species  $X_j$  that use this substrate and which are not already limited by another substrate),  $S_{b0}$  the bulk liquid concentration of substrate  $S_b$  that is limiting first and  $S_{a0}$  the bulk liquid concentration of substrate  $S_a$ .

The aerobic growth in a system with both heterotrophic ( $X_H$ ) and autotrophic bacterial species ( $X_A$ ) is an example of this sequential diffusion limitation. Growth of the species requires three substrates, i.e. dissolved oxygen  $S_O$ , soluble organic matter  $S_S$  and ammonium  $S_{NH}$ . If  $S_S$  is limiting, then the growth of heterotrophs stops but the growth of autotrophs proceeds until either oxygen or ammonium gets limiting for them. Hence, this is a sequencing diffusion limitation for oxygen or ammonium. In the

outer part of the biofilm (until  $S_S$  is utilized) both heterotrophic and autotrophic growth take place simultaneously whereas in the next zone (until any other substrate gets limiting) only the autotrophic growth process utilizes  $S_{NH}$  and  $S_O$ . Figure 4.4 expresses this situation in more general terms.

#### 4.3.1.2 Calculation of active fractions of bacterial species: an example

The example used to introduce the approach for the calculation of the active fractions for the penetration depths, considers the main carbon/nitrogen cycles in a biofilm, i.e. carbon removal, nitrification and denitrification (given in Peterson matrix representation (Henze *et al.*, 1987) in Table 4.1). Heterotrophic bacteria are growing under two different environmental conditions in the system, i.e. under both aerobic and anoxic conditions. Other than in continuously stirred tank reactors, a spatial distribution of the oxygen concentration exists in biofilms. Consequently, in biofilms simultaneous nitrification and denitrification can occur, where the top layers of the biofilm are nitrifying whereas the deeper layers denitrify. The spatial distribution is taken into account by means of the anoxic active fraction coefficient  $\phi_H^*$  for heterotrophic bacteria. However, note that heterotrophic bacteria have a preference for oxygen. As a result nitrate can never be the substrate that is limiting heterotrophic activity in the first place, but only after all oxygen is utilised. Furthermore, the biokinetic model outlined in Table 4.1 assumes that species growth limitation by nitrogen is only due to ammonium exhaustion. The anoxic growth rate is denoted as  $\mu_H^*$ .

**Table 4.1. Matrix representation of aerobic/anoxic growth of heterotrophic/autotrophic bacteria**

Process	$S_O$ $ML^{-3}$	$S_S$ $ML^{-3}$	$S_{NO}$ $ML^{-3}$	$S_{NH}$ $ML^{-3}$	Process rate $ML^{-3}T^{-1}$
aerobic het. growth	$1-1/Y_H$	$-1/Y_H$		$-i_x$	$\mu_H \cdot X_H$
anoxic het. growth		$-1/Y_H$	$-(1-Y_H)/2.86Y_H$		$\mu_H^* \cdot X_H$
aerobic aut. growth	$1-4.57/Y_A$		$1/Y_A$	$-1/Y_A \cdot i_x$	$\mu_A \cdot X_A$

With respect to utilisation and production of nitrate in the biofilm, two aspects need to be considered: First, a problem arises when more nitrate is produced via nitrification than utilised due to denitrification. As a consequence, a nitrate flux occurs in the opposite direction, i.e. from the biofilm back into the bulk liquid. The transport of the net produced nitrate through the nitrification zone is subject to diffusion. A second problem arises for nitrate utilisation that usually occurs in the deeper layers of the biofilm. Here too, nitrate is transported through a non-reactive layer. The proposed simplified model gives no direct opportunity to consider these diffusion processes and an instantaneous transport of the soluble products is assumed in both cases (assumption No 5). Hence, produced nitrate does not accumulate in the biofilm but is considered only by means of the net flux transport through the biofilm surface.

A general procedure to derive the active fractions of the species in the biofilm for each specific situation of substrate can be outlined as follows for this heterotrophic/autotrophic biofilm:

1. For each of the substrates  $S_O$ ,  $S_S$ ,  $S_{NO}$  and  $S_{NH}$  the dimensionless penetration depth  $\beta_i (= z_i/L)$  is calculated from equation 4.14. If none of the substrates is limiting, the biofilm is fully penetrated and all active fractions  $\phi_j$  are equal to one. If not, the substrate with the smallest value  $\beta_i$  is limiting first.

- The actual case of substrate limitation is derived from Figure 4.5 where the order of limitation is listed together with the active fractions of the relevant species. Unless  $S_{NH}$  is limiting, another substrate might cause a sequential diffusion limitation that has to be taken into account.
- If there is no  $S_{NH}$  limitation the penetration depths of the substrates are calculated from equation 4.19 based on the possible order of limitations.
- If any of these dimensionless penetration depths is smaller than one, the corresponding substrate is limiting in the second place and the active fraction is obtained from Figure 4.5.

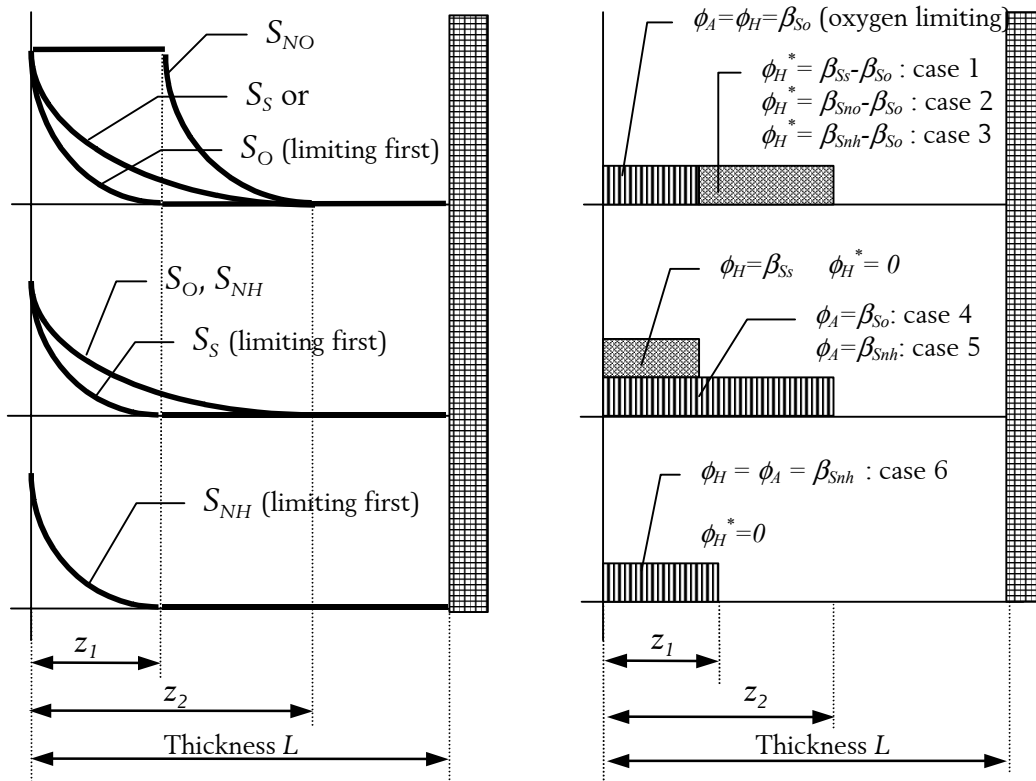


**Figure 4.5:** Six possible situations for substrate limitation in the competition of heterotrophic and autotrophic growth in an idealised biofilm. Left: Substrate profiles and right: active fraction of bacteria species based on zero-order kinetics. From top to bottom: case 1,2,3 = oxygen limiting in the first place and then organic matter (1), nitrate (2) or ammonium (3) limiting, case 4,5 = organic matter limiting in the first place and then either oxygen (4) or ammonium (5) limiting and case 6 = ammonium limited.

#### 4.3.1.3 General algorithm for calculating active fractions

The following algorithm is generally applicable for determining the active fractions in multiple species/substrate systems:

- Make the process matrix, indicate all negative stoichiometric values and evaluate the sequence of switching from one substrate to another for processes that are “on” or “off” (e.g. anoxic growth is not operational as long as oxygen is “on”, assimilation of nitrate as nitrogen source is “off” as long as ammonium is “on”...);
- Calculate the dimensionless penetration depth  $\beta_i$  for each of the relevant components and for all reactions that are “on” assuming zero-order reaction rates and no limitation by any other substrate;
- The smallest  $\beta_i$  found is retained (unless it is larger than one) and this determines the penetration depth of the limiting substrate;

4. Some reaction(s) may be switched “off” and others “on” by this absence of substrate in the deeper layers of the biofilm;
5. Unless all reactions are “off” or the smallest  $\beta_i$  is larger than one, go to 2.

### 4.3.2 Step 2: overall model for the bulk liquid in contact with a biofilm

#### 4.3.2.1 Concept for describing bulk liquid - biofilm interaction

The procedure outlined above is only the first step for deriving a mathematical description of the biokinetic processes within the biofilm and of the mass exchange between bulk liquid and biofilm compartment. The result of the analysis with respect to diffusion limitation is a quantification of the active mass of each species present in the whole biofilm with respect to the processes. In addition, the dynamic changes in the bulk liquid need to be considered and the mass transfer between those two phases.

The system is seen in the following as two connected ideally mixed tank reactors where one is representing the bulk liquid and the other the biofilm (Figure 4.6).

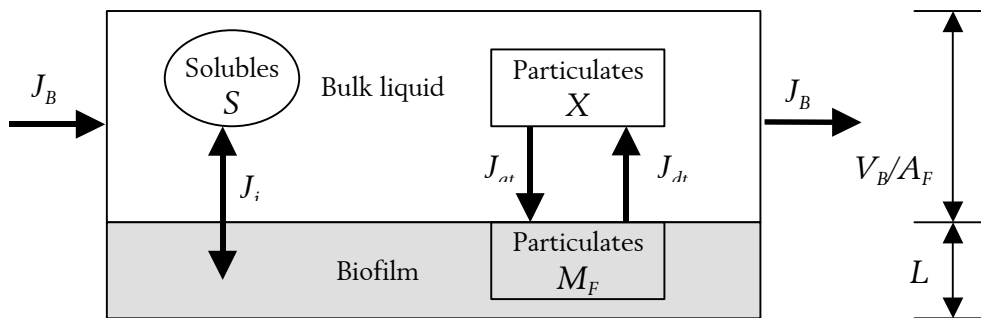


Figure 4.6: Interaction between biofilm and bulk liquid components due to mass fluxes  $J$ .

The components in both tanks are expressed differently, in the bulk liquid in terms of concentrations [ML<sup>-3</sup>], as usual, and in the biofilm as mass  $M_F$  [M]. The reason is that the thickness of the biofilm compartment is changing, which can be taken into account more easily by balancing masses than by concentrations. Neglecting the dynamic changes in biofilm density, the thickness of the biofilm can be computed at any time instant from:

$$L = \frac{\sum M_{Fj}}{\rho_m A_F} \quad (4.20)$$

The different dimensions of the particulate components in both reactors (concentrations in the bulk liquid and mass in the biofilm) do not allow a direct interaction of components in both compartments. Traditionally, the formulation of the mass transfer between the phases has to account for that. Alternatively, one can express the reactions in the biofilm as a volumetric reaction rate  $r_{Bi}$  with respect to the substrate concentration in the bulk liquid. This volumetric reaction rate is derived from equation 4.13, that is from the areal flux  $J_i$  of a substrate  $S_i$  through the surface of the biofilm:

$$r_{Bi} = \frac{J_i}{\frac{V_B}{A_F}} = \frac{A_F}{V_B} \sum_j -\mu_j X_j v_{ij} \phi_j L \quad (4.21)$$

Rewriting this equation gives:

$$r_{Bi} = \sum_j -\mu_j v_{ij} \phi_j L \frac{M_{Fj}}{A_F L} \frac{A_F}{V_B} = \sum_j -\mu_j v_{ij} \phi_j \frac{M_{Fj}}{V_B} = \sum_j -\mu_j v_{ij} \phi_j X_{Bj} \quad (4.22)$$

where  $A_F$  is the surface of the biofilm,  $V_B$  is the volume of the bulk liquid compartment and  $X_{Bj} = M_{Fj}/V_B$  is the concentration of particulate matter  $j$  in the biofilm per unit of volume of the bulk liquid compartment. Hence, the problem of the different dimensions of the particulate components in both phases is taken care of directly and the explicit description of the mass transfer between bulk liquid and biofilm must no longer be considered in the overall model.

#### 4.3.2.2 Physical interaction between biofilm and bulk liquid

Attachment (flux  $J_{at}$ ) is addressing a number of physical processes where suspended matter is transported from the water phase to the biofilm compartment. The most important phenomena are processes such as sedimentation, inclusion or attachment, which are generally described as a first order process with respect to the concentration of the particulate matter in the water phase. The reverse process of displacement is addressed as detachment (flux  $J_{dt}$ ). Detachment describes the material loss from the biofilm matrix and is frequently categorised into the phenomena erosion, sloughing and abrasion. In this model description no such distinction is made and all three phenomena are modelled as one. Following Horn and Hempel (1997a) the rate of biomass detachment  $k_d$  is formulated here as being dependent on the velocity  $u_f$  by which the biofilm surface moves relative to the substratum:

$$\begin{array}{llll} \text{if} & u_f \leq 0 & \text{then} & k_d = 0 \\ \text{if} & u_f > 0 & \text{then} & k_d = k_{dt} u_f \end{array} \quad (4.23)$$

where  $k_d$  is the detachment rate,  $u_f$  the velocity by which the surface of the biofilm moves perpendicular to the substratum and  $k_{dt}$  the detachment coefficient.

## 4.4 Description of biokinetic processes in the biofilm - Process matrix: an example

The biokinetic process description is straightforward once the fractions of the active biomass have been computed as previously outlined. Expressing the components in the biofilm as above in terms of concentrations with respect to the volume of the bulk liquid compartment ( $X_{Bj}$ ) does not violate mass conservation principles. In the following illustrative example aerobic and anoxic growth of heterotrophs and aerobic growth of autotrophs is simulated, as well as hydrolysis and decay. It is important that the process description for biomass growth used here (Table 4.2) is consistent with the one used earlier for determining the active fractions (Table 4.1).

We follow as closely as possible the concepts formulated in the activated sludge model No 1 (Henze *et al.*, 1987) for the description of the biokinetic processes in the biofilm (Table 4.2). The main difference to other biofilm models (e.g. Wanner and Gujer, 1986; Wanner and Reichert, 1996; Horn and Hempel, 1997a, b) is the consistent application of the death-regeneration principle (Dold *et al.*, 1980) together with the introduction of slowly biodegradable organic matter ( $X_S$ ), which is considered as a particulate component of the biofilm. The reasoning for choosing this approach is to allow both a consistent process description and wastewater characterisation for direct linkage of models of the various compartments in aquatic systems (e.g. Rauch *et al.*, 1998). However, the choice of this concept is not mandatory for using the presented simplified biofilm model and it can be easily replaced.

**Table 4.2. Process matrix for biokinetic processes in the biofilm and corresponding effect to the concentration of soluble components in the bulk liquid.**

Process	Bulk liquid				Biofilm				Process rate $ML^{-3}T^{-1}$
	$S_O$ $ML^{-3}$	$S_S$ $ML^{-3}$	$S_{NO}$ $ML^{-3}$	$S_{NH}$ $ML^{-3}$	$X_{BH}$ $ML^{-3}$	$X_{BA}$ $ML^{-3}$	$X_{BS}$ $ML^{-3}$	$X_{BI}$ $ML^{-3}$	
aer. het. growth	$(Y_H-1)/Y_H$	$-1/Y_H$		$-i_x$	1				$\mu_H \cdot X_{FBH} \cdot \phi_H$
an. het. growth		$-1/Y_H$	$-\frac{(1-Y_H)}{2.86 \cdot Y_H}$	$-i_x$	1				$\mu_H^* \cdot X_{FBH} \cdot \phi_H^*$
aer. aut. growth	$\frac{(Y_A - 4.57)}{Y_A}$		$1/Y_A$	$-1/Y_A \cdot i_x$		1			$\mu_A \cdot X_{FBA} \cdot \phi_A$
decay het.					-1		$1-f_p$	$f_p$	$b_H \cdot X_{BH}$
decay aut.						-1	$1-f_p$	$f_p$	$b_A \cdot X_{BA}$
hydrolysis		1		$i_x$			-1		$k_h \cdot X_{BS}$

Still, with respect to the activated sludge model No 1 (ASM1) some simplifications had to be implemented as a result of the active fraction concept. First of all, bacterial growth is not expressed as a Monod-type reaction as done in ASM1 but instead as a first order process with respect to the active fraction of the bacterial mass alone. This is due to the requirements for zero-order in substrate kinetics and diffusion limitation. In ASM1 also the limitation of reactions with respect to oxygen and ammonium is expressed by Monod-type switching functions. These functions can be dropped conveniently as all limitations are already considered in the active fraction concept.

In Table 4.2 it is postulated that hydrolysis is a first-order process with respect to the concentration of slowly biodegradable organic matter. This hypothesis is supported by experimental results from Janning *et al.* (1997). According to the assumptions underlying the model concept (assumption No 5) readily biodegradable organic matter from hydrolysis is modelled as being instantaneously transferred into the bulk liquid.

## 4.5 Proposed parameter set

Based on parameter values proposed in literature, a parameter set is proposed that will serve as a starting point for model calibrations and applications in the next chapters (Table 4.3). The basis for

this parameter set are the kinetic and stoichiometric parameter values proposed in the Activated Sludge Model No. 1 (Henze *et al.*, 1987). Parameters specific to biofilm systems were derived from reviews by Henze *et al.* (1995) and Horn and Hempel (1995). For the biofilm density, a typical value of 40 g/l was taken which was found in Melcer *et al.* (1995).

Note that the value proposed for the decay coefficient  $b_H$  may seem quite high compared to parameter values proposed in other biofilm models. It should however be stressed that in this model the death-regeneration principle has been applied (Dold *et al.*, 1980), whereas the coefficients used in other biofilm models and in the more recent Activated Sludge Model No. 3 (Gujer *et al.*, 1999) are the more traditional decay coefficients obtained from measuring endogenous respiration. The decay coefficient used in the death-regeneration cycle can be calculated from the traditional decay coefficient  $b'_H$ , for which a value of 0.2 d<sup>-1</sup> is proposed in ASM3 at 20 °C, by

$$b_H = \frac{b'_H}{1 - Y_H(1 - f_p)} \quad (4.24)$$

**Table 4.3. Proposed parameter set**

<i>Parameter</i>	<i>Value</i>
$\mu_H$ (1/d)	4
$Y_H$ (gCOD/gCOD)	0.6
$b_H$ (1/d)	0.4
$\mu_A$ (1/d)	0.15
$Y_A$ (gCOD/gN)	0.1
$b_A$ (1/d)	0.05
$k_h$ (1/d)	3
$k_a$ (1/d)	0.05
$i_X$ (gN/gCOD)	0.08
$f_p$ (-)	0.08
$D_{f,So}$ (cm <sup>2</sup> /d)	2.1
$D_{f,Ss}$ (cm <sup>2</sup> /d)	0.58
$D_{f,Snh}$ (cm <sup>2</sup> /d)	1.8
$D_{f,Sno}$ (cm <sup>2</sup> /d)	1
$\rho_m$ (kg/m <sup>3</sup> )	40

## 4.6 Extended model description

### 4.6.1 Introduction

For several reasons, explained in the next chapters, the model described above was adapted and completed. As described above, the original model description relies upon several assumptions. One of the assumptions - No 5 - states that soluble components that emerge from conversion processes inside the film are assumed to be subject to immediate out-diffusion at the surface of the biofilm. This assumption neglects the possible effect of the accumulation of soluble species inside the biofilm.

Another assumption - No 6 - states that an instantaneous steady-state profile is assumed. Together, these assumptions are in principle violating the mass balances during dynamic simulation.

Assumption No 5 is for example of importance when nitrate is formed during the nitrification process. In the original model description the possible accumulation of nitrate in the biofilm is not accounted for and thus the penetration depth of nitrate needed for the denitrification process might be underestimated. The first addition to the model that is described below, does account for this accumulation and thus guarantees a correct determination of the penetration depths. This extension starts with the use of total masses in the mass balances rather than only the concentrations in the bulk liquid. This way, the component present in the biofilm itself is also integrated in the calculation and a violation of the mass balance, even if it would only be small, is avoided.

Next, the introduction of an external diffusional resistance is studied. As stated in the original model, the improvement of the model description by including this resistance is highly dependent on the biofilm loading and the fluid velocity. Christiansen *et al.* (1995) conducted experiments in a fixed bed reactor using different superficial velocities. The liquid film diffusion had no significant influence on the modelled reaction rate. However, Hem *et al.* (1994) found that in the case of a moving bed biofilm reactor, the nitrification kinetics as a function of oxygen were very close to first order. This indicates a great influence of the liquid film diffusion on the biofilm kinetics in this specific reactor set-up. Rusten *et al.* (1994) postulated that the reason for this behaviour is the fact that the major part of the biomass is growing on the protected surface within the carrier elements. This biomass is not subject to high fluid velocities and this might be the reason for the big influence of the diffusional resistance of the liquid film.

#### 4.6.2 *Correcting the mass balances: use of total masses*

As mentioned before, the original model description expresses all the components present in the biofilm relative to the bulk liquid volume. The adapted model description developed in this section on the other hand, will only describe the components in the biofilm and in the liquid phase in terms of their total mass. Starting from the knowledge of the mass of a component in the system, the concentration profile and the component's concentration in the bulk liquid volume can then be calculated. This makes the calculation of the active fractions and the conversion processes possible just like in the original model description. The bulk liquid concentration calculated is also used to calculate the advective exchange of the component under study to and from adjacent biofilm modules.

A side effect of the use of total masses is that the component balances can be respected at each time step during the simulation. High concentration peaks coming into the biofilm module can no longer give rise to even more of the component being "generated" in the biofilm. Indeed, when the bulk liquid concentration suddenly increases, higher concentrations in the biofilm are calculated in the next time step (Figure 4.7). This way, mass is created in the biofilm that was not present before. This is a possibility in the original model, because of the assumption of an instantaneous steady-state profile. However, since the time constants of biofilm diffusion and reaction differ about one order of magnitude, this effect will be hardly noticeable in any of the simulated case studies (see also Wik, 1999).

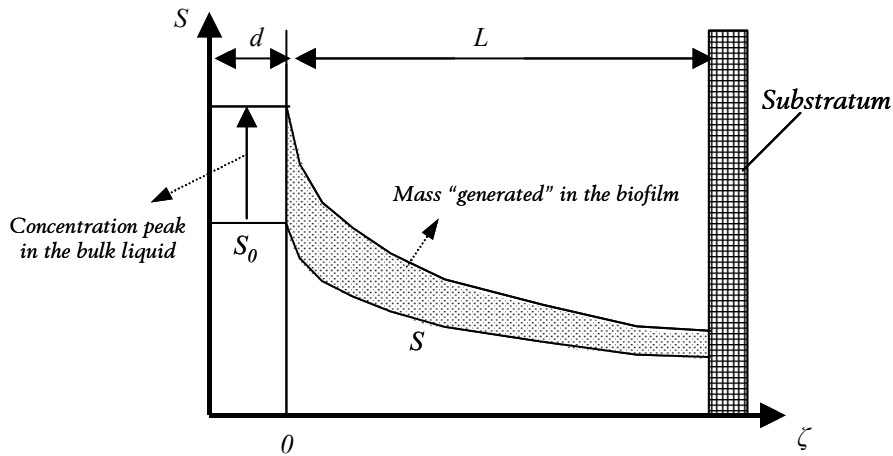


**Figure 4.7:** Possible “generation” of extra mass of a component in the biofilm following a concentration peak in the bulk liquid

For the analytical calculation of the penetration depth using total masses instead of concentrations, the starting point is the same. The central equation for calculating diffusion-limited biofilm reactions assuming an idealised geometry and instantaneous steady-state is:

$$\frac{\partial^2 S}{\partial \zeta^2} = \frac{r}{D_f} \quad (4.25)$$

If calculations are done using the total mass of each component, the penetration depths of the substrates calculated by the model give rise to six different concentration profiles.

#### 4.6.2.1 Case 1: fully penetrated biofilm

In case a substrate penetrates the biofilm completely, a concentration profile is found as drawn in Figure 4.8. The substrate diffuses from the bulk liquid layer into the biofilm and is at the same time consumed by the micro-organisms in the biofilm. Also, production over the complete thickness of the biofilm is possible, *e.g.* in the case of nitrate from nitrification.

To solve equation 4.25, a number of boundary conditions is necessary. These conditions are the same as the ones that have been used to calculate the penetration depth of the substrates in the original model. For reasons of clarity, these conditions are repeated here.

Denoting the substrate concentration at the biofilm surface as  $S_0$ , the following boundary conditions are important:

$$(S)_{\zeta=0} = S_0 \quad (4.26)$$

$$\left( \frac{dS}{d\zeta} \right)_{\zeta=L} = 0 \quad (4.27)$$

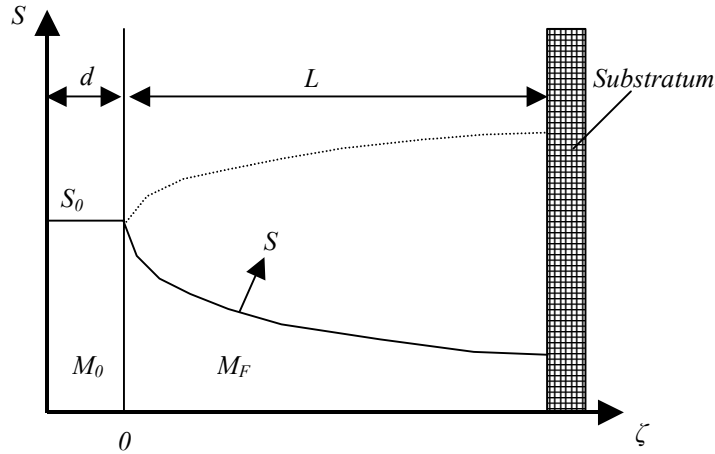


**Figure 4.8: Concentration profile for a fully penetrated biofilm**

Integration of equation 4.25 then yields the concentration gradient in the biofilm as function of the distance to the biofilm surface.

$$S = \frac{r}{2D_f} \zeta^2 + \frac{rL}{D_f} \zeta + S_0 \quad (4.28)$$

However, the state variables in the new model description are the masses of the components and no longer the concentrations. The total mass of a component in a biofilm compartment which is made up of a liquid layer with thickness  $d$ , e.g. as on a tilted plate or in a trickling filter with a cross-flow packing, and the biofilm itself is given as:

$$M = M_0 + M_F \quad (4.29)$$

The mass in the bulk liquid  $M_0$  is dependent on the thickness of the water layer or the total water volume that is taken into account. In case of a liquid layer of thickness  $d$ , this mass is given as  $S_0Ad$ . The total mass can then be rewritten as:

$$M = S_0Ad + \int_0^L ASd\zeta = S_0Ad + A \cdot \left( \frac{r}{6D_f} L^3 - \frac{r}{2D_f} L^3 + S_0L \right) \quad (4.30)$$

or

$$S_0 = \frac{1}{d+L} \left( \frac{M}{A} + \frac{rL^3}{3D_f} \right) \quad (4.31)$$

This way, starting from the total mass  $M$ , the biofilm thickness  $L$ , the zero-order reaction rate  $r$ , the biofilm surface area  $A$ , the diffusion coefficient  $D$  and the thickness of the bulk water layer  $d$ , the

substrate concentration in the bulk liquid can be calculated. This concentration is then used to calculate the advective transport to and from the biofilm compartment.

#### 4.6.2.2 Case 2: a single limiting substrate

The concentration profile most commonly encountered is the profile depicted in Figure 4.9. Using similar boundary conditions as in the previous case, the substrate concentration gradient in the biofilm can be calculated. It can then be used for the calculation of the total mass in the biofilm compartment.

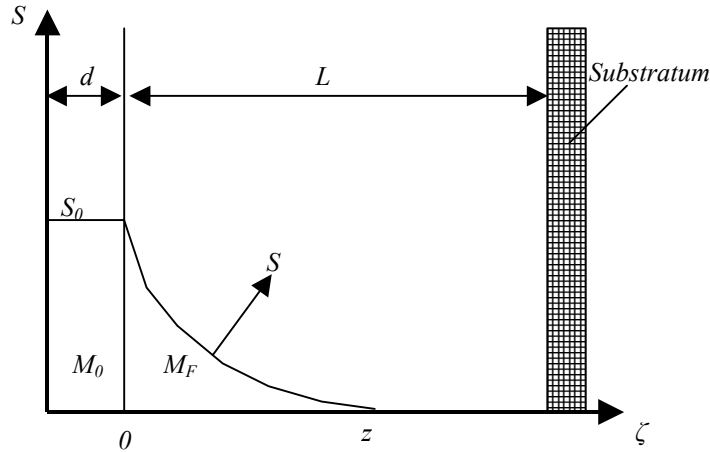


Figure 4.9: Concentration profile for a diffusion-limited reaction in a biofilm

$$M = AS_0d + AS_0 \frac{z}{3} \quad (4.32)$$

and since  $z = \sqrt{\frac{2D_f S_0}{r}}$

$$S_0^3 - \frac{3rd^2}{2D_f} S_0^2 + \frac{9rMd}{AD_f} S_0 - \frac{9rM^2}{2D_f A^2} = 0 \quad (4.33)$$

This is a third-order equation of the form  $x^3 + a_1x^2 + a_2x + a_3 = 0$ , which in general has three roots of which at least one is real. An analytical method to find these roots can be found in standard mathematics textbooks. Let

$$Q = \frac{3a_2 - a_1^2}{9}, \quad R = \frac{9a_1a_2 - 27a_3 - 2a_1^3}{54} \quad (4.34)$$

$$S = \sqrt[3]{R + \sqrt{Q^3 + R^3}}, \quad T = \sqrt[3]{R - \sqrt{Q^3 + R^3}}$$

Then, the solutions can be found as:

$$\begin{cases} x_1 = S + T - \frac{1}{3}a_1 \\ x_2 = -\frac{1}{2}(S + T) - \frac{1}{3}a_1 + \frac{1}{2}i\sqrt{3}(S - T) \\ x_3 = -\frac{1}{2}(S + T) - \frac{1}{3}a_1 - \frac{1}{2}i\sqrt{3}(S - T) \end{cases} \quad (4.35)$$

To find out which of the three roots is the correct one, all positive real roots are used to recalculate the total mass of the component under study. This calculated mass is compared to the actual mass in the system. The real positive root yielding the correct component mass is considered to be the correct one. The total component mass is known, since it is the starting point of the procedure to calculate the penetration depth and the concentration profile.

#### 4.6.2.3 Case 3: sequential diffusion limitation of a limiting substrate

The next concentration profile to be studied is the profile containing sequential diffusion limitation (Figure 4.10).

Here again, the concentration profile in the biofilm is described by differential equation 4.25. In this equation, a zero-order reaction rate  $r_{ua}$  is used in the biofilm above  $z_b$  and a reaction rate  $r_{la}$  is used below  $z_b$ . At  $z_b$ , the following extra boundary conditions are needed to solve the set of differential equations:

$$\left( \frac{dS_{ua}}{d\zeta} \right)_{\zeta=z_b} = \left( \frac{dS_{la}}{d\zeta} \right)_{\zeta=z_b}, \quad (S_{ua})_{\zeta=z_b} = (S_{la})_{\zeta=z_b} \quad (4.36)$$

After integration, the concentration gradients in the biofilm above and below  $z_b$  can be calculated.

$$\begin{aligned} S_{ua} &= \frac{r_{ua}}{2D_f} \zeta^2 + \left( \frac{r_{la}z_b - r_{la}z_a - r_{ua}z_b}{D_f} \right) \zeta + S_{0a} \\ S_{la} &= \frac{r_{la}}{2D_f} \zeta^2 - \frac{r_{la}z_a}{D_f} \zeta + \frac{r_{la}z_a^2}{2D_f} \end{aligned} \quad (4.38)$$

The total mass in the biofilm compartment  $M$  can be found after integration over the depth of the biofilm.

$$M_a = M_{0a} + \int_0^{z_b} AS_{ua} d\zeta + \int_{z_b}^{z_a} AS_{la} d\zeta = A \left( S_{0a}d + \frac{z_b^3}{6D_f} (r_{ua} - r_{la}) + \frac{r_{la}z_a^3}{6D_f} \right) \quad (4.39)$$



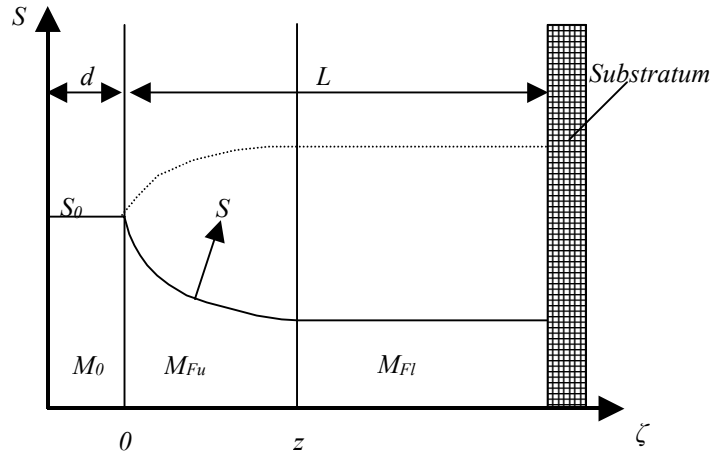


Figure 4.11: Concentration profile for a non-limiting component with production or consumption up to  $z$

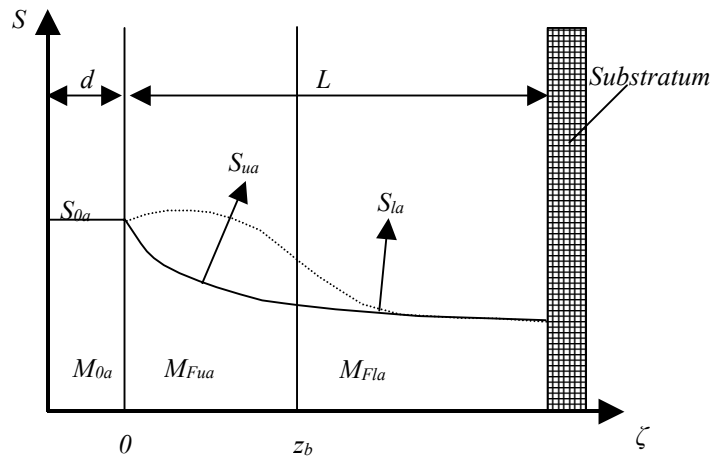
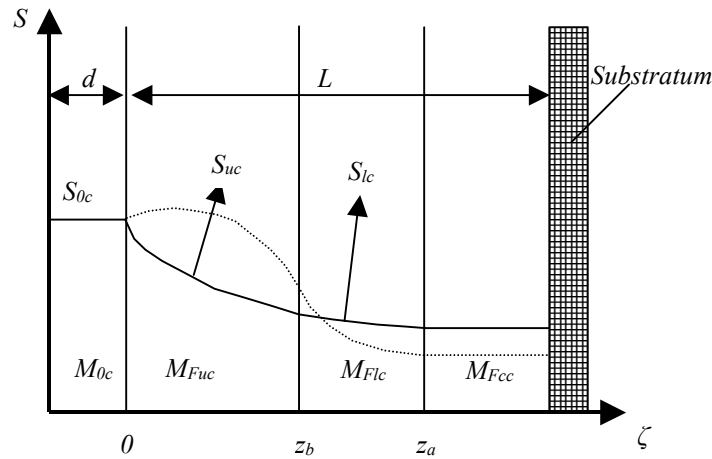


Figure 4.12: Concentration profile for a non-limiting component with two rates of production/consumption

In case with two rates of consumption/production of a non-limiting component  $a$ ,  $S_{0a}$  can be found from:

$$S_{0a} = \frac{\frac{M}{A} + \frac{z_b^3}{6D_f}(r_{ua} - r_{la}) - \frac{z_b^2 L}{2D_f}(r_{la} - r_{ua}) + \frac{L^3 r_{la}}{3D_f}}{(d + L)} \quad (4.42)$$

where  $z_b$  is known from the rate limiting substrate  $b$ .



**Figure 4.13: Concentration profile for a non-limiting component with two levels of production/consumption and limitation of the conversion by two other components**

Finally, when a non-limiting component is produced and/or consumed in the biofilm at two separate rates, and two other components  $a$  and  $b$  are limiting the conversion process,  $S_{0c}$  is to be calculated from the following formula:

$$S_{0c} = \frac{\frac{M}{A} - \frac{z_b^3}{6D_f}(r_{uc} - r_{lc}) - \frac{z_a^3 r_{lc}}{6D_f} + \frac{z_b^2 L}{2D_f}(r_{lc} - r_{uc}) + \frac{z_a^2 L r_{lc}}{2D_f}}{(d + L)} \quad (4.43)$$

The application of the modified model is similar to the application of the original model description. In the stoichiometry matrix, all negative stoichiometric values should be indicated. For the species for which the processes are "on" in the current conditions (e.g. anoxic growth is not operational as long as oxygen is "on", assimilation of nitrate as nitrogen source is "off" as long as ammonium is "on", etc.) the penetration depth and the liquid film concentration should be calculated. The smallest  $\beta$  is retained. If all  $\beta$ -values are above 1, then a concentration profile alike the one in Figure 4.8 is to be used.

In case one of the  $\beta$ -values is smaller than 1, this component has a concentration profile as described in Figure 4.9. If this component is for example  $S_{NH}$ , then all other processes are limited because of the absence of ammonium. All other components then have a profile described by Figure 4.11.

In case of sequential limitations, several possibilities exist. If the calculated penetration depth of the second limiting component is larger than the biofilm thickness, profiles similar to Figure 4.12 are to be expected. If not, then the profiles in Figure 4.10 and Figure 4.13 are important.

### 4.6.3 Incorporation of a stagnant liquid layer

The set of equations developed below is a common way to include liquid film diffusion in a biofilm diffusion-reaction model (Figure 4.14). It expresses the fact that liquid film diffusion is the resistance for a substrate to be transferred from the bulk liquid to the liquid-biofilm interface. Several models have been developed for this liquid film diffusion. However, for soluble components, this process is most commonly approximated by molecular diffusion through a stagnant liquid layer (Harremoës,

1978; Rittmann and McCarty, 1980b; Wanner and Gujer, 1986; Hem *et al.*, 1994). The thickness of this layer is dependent on the mixing conditions, and thus on the Reynolds number in the reactor under study. It approaches zero for increasing values of the Reynolds number (Harremoës, 1978). Depending on the conditions in which the biofilm is grown, liquid film diffusion may thus be varying from insignificant to being the major factor limiting the overall reaction. The mass transfer coefficient can either be measured or estimated experimentally, but it can also be correlated to other factors describing the flow regime in the set-up under study, like Sherwood and Schmidt numbers. The flux of a component into the biofilm  $N_{\text{int}}$  is given by:

$$N_{\text{int}} = h(S_0 - S^*) = -D_f \left( \frac{dS}{d\zeta} \right)_{\zeta=0} \quad (4.44)$$

In this equation,  $h$  is the mass transfer coefficient ( $\text{m}\cdot\text{d}^{-1}$ ).  $S$  is the concentration of the substrate in the biofilm, while  $S_0$  is its concentration in the bulk liquid. The substrate concentration at the biofilm interface is denoted as  $S^*$ .

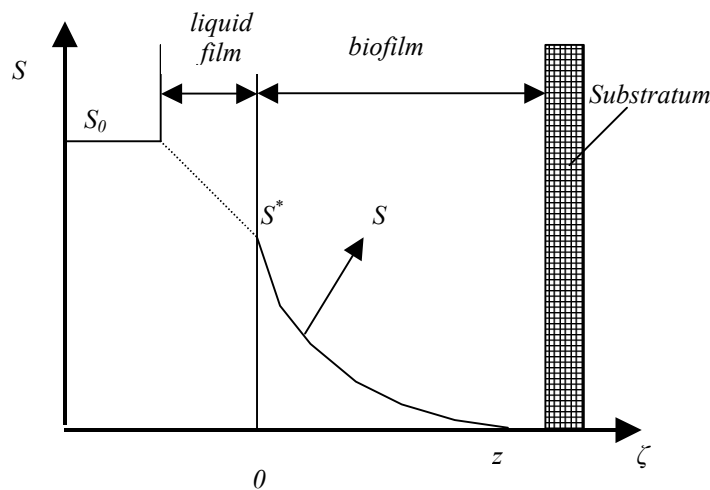


**Figure 4.14: Concentration gradient due to liquid film diffusion and biofilm diffusion-reaction in a substrate-limited biofilm**

In the biofilm itself, the following equation still holds:

$$\frac{d^2S}{d\zeta^2} = \frac{r}{D_f} \quad (4.45)$$

Integration yields the following second-order differential equation for the substrate concentration in the biofilm:

$$S = \frac{1}{2} \frac{r}{D_f} \zeta^2 + K_1 \zeta + K_2 \quad (4.46)$$

Boundary conditions at the biofilm surface and at the penetration depth  $z$  are:

$$\left. \begin{array}{l} (S = S^*)_{\zeta=0} \\ \left( \frac{dS}{d\zeta} \right)_{\zeta=z} = 0 \end{array} \right\} \Rightarrow K_2 = S^*, \quad K_1 = -\frac{r}{D_f} z \quad (4.47)$$

At the biofilm interface the flux continuity equation yields:

$$-D_f \left( \frac{dS}{d\zeta} \right)_{\zeta=0} = h(S_0 - S^*) \Rightarrow \frac{r}{D_f} z = \frac{h}{D_f} (S^* - S_0) \Rightarrow S^* = S_0 - \frac{r}{h} z \quad (4.48)$$

or with  $z = \sqrt{\frac{2D_f S^*}{r}}$

$$z^2 = \frac{2D_f \left( S_0 - \frac{r}{h} z \right)}{r} \Rightarrow z = \frac{-\frac{r}{h} \pm \sqrt{\left( \frac{r}{h} \right)^2 + 2\frac{r}{D_f} S_0}}{r/D_f} = -\frac{D_f}{h} \pm \sqrt{\left( \frac{D_f}{h} \right)^2 + \frac{2D_f S_0}{r}} \quad (4.49)$$

Since only the positive root is a valid penetration depth, the penetration depth of the substrate  $S$  with bulk liquid concentration  $S_0$  can be calculated as:

$$z_1 = -\frac{D_f}{h} + \sqrt{\left( \frac{D_f}{h} \right)^2 + \frac{2D_f S_0}{r}} \quad (4.51)$$

Note that, compared to equation 4.14, the effect of the liquid layer is directly noticeable in the penetration depth and leads to smaller penetration depth in model applications.

In the case of sequential substrate limitation, the following set of second-order differential equations can be found:

$$\begin{cases} S_{ua} = \frac{1}{2} \frac{r_{ua}}{D_f} \zeta^2 + K_1 \zeta + K_2 \\ S_{la} = \frac{1}{2} \frac{r_{la}}{D_f} \zeta^2 + K_3 \zeta + K_4 \end{cases} \quad (4.52)$$

where  $S_{ua}$  is the concentration of substrate  $S_a$  in the upper part of the biofilm.  $S_{la}$  is the concentration in the lower part. The zero-order conversion rates are  $r_{ua}$  and  $r_{la}$  for the upper and the lower part of the biofilm respectively. The integration constants can be found from the boundary conditions (note that  $z_b$  is determined by the first limiting substrate):

$$\left. \begin{aligned} (S_{ua} = S_a^*)_{\zeta=0} \\ \left( \frac{dS_{ua}}{d\zeta} \right)_{\zeta=z_b} = \left( \frac{dS_{la}}{d\zeta} \right)_{\zeta=z_b} \\ \left( \frac{dS_{la}}{d\zeta} \right)_{\zeta=z_a} = 0 \\ (S_{la})_{\zeta=z_a} = 0 \end{aligned} \right\} \Rightarrow \begin{cases} K_1 = \frac{r_{la}z_b - r_{la}z_a - r_{ua}z_b}{D_f} \\ K_2 = S_a^* \\ K_3 = -\frac{r_{la}}{D_f}z_a \\ K_4 = \frac{r_{la}}{2D_f}z_a^2 \end{cases} \quad (4.53)$$

A fifth boundary condition can be used to determine the penetration depth of the substrate  $S$  dependent on the substrate concentration  $S_a^*$  at the biofilm interface.

$$(S_{la})_{z=z_b} = (S_{ua})_{z=z_b} \Rightarrow z_a = \sqrt{z_b^2 \left( 1 - \frac{r_{ua}}{r_{la}} \right) + \frac{2D_f S_a^*}{r_{la}}} \quad (4.54)$$

Again, at the biofilm interface the flux continuity equation yields:

$$\begin{aligned} -D_f \left( \frac{dS_a}{d\zeta} \right)_{\zeta=0} = h(S_{0a} - S_a^*) &\Rightarrow \frac{r_{la}z_b - r_{la}z_a - r_{ua}z_b}{D_f} = \frac{h}{D_f}(S_a^* - S_{0a}) \\ \Rightarrow S_a^* = S_{0a} + \frac{r_{la}z_b - r_{la}z_a - r_{ua}z_b}{h} \end{aligned} \quad (4.55)$$

or

$$z_a^2 + \frac{2D_f}{h}z_a - z_b \left( 1 - \frac{r_{ua}}{r_{la}} \right) \left( z_b + \frac{2D_f}{h} \right) - \frac{2D_f S_{0a}}{r_{la}} = 0 \quad (4.56)$$

This equation can easily be solved, using the discriminant for this second-order algebraic equation. Again, only the positive value for the penetration depth is a valid solution for this problem.

$$Discr = \frac{4D_f^2}{h^2} + 4 \left( z_b \left( 1 - \frac{r_{ua}}{r_{la}} \right) \left( z_b + \frac{2D_f}{h} \right) + \frac{2D_f S_{0a}}{r_{la}} \right) \quad (4.57)$$

$$z_a = -\frac{D_f}{h} \pm \frac{\sqrt{Discr}}{2} = -\frac{D_f}{h} + \frac{\sqrt{Discr}}{2} \quad (4.58)$$

It should be noted that the only difference between the implementation of the original model and this adapted model description is a different set of equations for the calculation of the penetration depth and an extra parameter  $h$ . The rest of the procedure to solve the model remains identical.

## 4.7 Conclusions

A simplified mixed-culture biofilm model was presented. The basic idea of the proposed model is to decrease model complexity in order to allow fast but sufficiently accurate simulation of biofilm dynamics. This is achieved by decoupling the calculation of substrate diffusion into the biofilm from the computation of the conversion processes in the biofilm. The first step of the procedure assumes a pseudo steady-state situation with respect to the diffusion which allows to solve the problem analytically. The result of this first step is an estimate on the fraction of each biomass species that is active in the present situation. In the second step of the procedure all conversion processes within the biofilm are computed dynamically. The bacterial species are assumed to be homogeneously distributed as in an ideally mixed tank reactor but with only a certain fraction of each species active.

The critical assumption made in the model is the homogeneous distribution of the bacterial species. However, the avoidance of partial differential equations for computation of the biofilm dynamics by using the two-step procedure instead results in a significant reduction of the model structure complexity as compared to state-of-the-art mixed-culture biofilm models. This feature allows a direct implementation of standard biokinetic conversion models as used in activated sludge modelling. This means that the simplified mixed-culture biofilm model is an attractive tool when emphasis is put more on fast predictions of system behaviour than on detailed understanding.

In addition, two extended model descriptions were presented that can easily be implemented along with the original one. One of the assumptions of the original model - No 5 - states that soluble components that emerge from conversion processes inside the film are assumed to be subject of immediate out-diffusion at the surface of the biofilm. This assumption neglects the possible effect of the accumulation of soluble species inside the biofilm. Another assumption - No 6 - states that an instantaneous steady-state profile is assumed. Together, these assumptions are in principle violating the mass balances during dynamic simulation. The first extension of the model accounts for this accumulation and thus guarantees a correct determination of the penetration depths. Also, the introduction of an external diffusional resistance was studied. In some cases this resistance may be of big importance for the correctness of the model predictions. The implementation of the diffusional resistance does not substantially complicate the model as only the calculation of the penetration depths needs to be adapted.



# 5 Development and characterisation of a pilot-scale trickling filter

---

## 5.1 Introduction

In this chapter the construction of a pilot-scale trickling filter is presented in which non-invasive measurement techniques were evaluated for use in calibration of models for process optimisation. The pilot-scale trickling filter has been constructed to be able to collect experimental data on a fully characterised biofilm system for the selection, development, calibration and corroboration of mathematical models which describe such a system's dynamic behaviour. The design of the unit was made such that it would allow a full characterisation of the relevant model parameters, and an easy monitoring of the system's performance only using measurements of inflow and outflow. Among other measurements, the off-gas is continuously monitored for CO<sub>2</sub> and O<sub>2</sub>. Also, the results of the monitoring of the weight of the filter by means of an electronic balance are presented as well as a hydraulic characterisation of the filter with two tracer tests.

## 5.2 Design and development

As the pilot-scale trickling filter unit was to be used for several purposes, besides the work described in this thesis, its design was focused on practical feasibility and on the possibility to easily quantify and control all relevant operating parameters and conditions.

### 5.2.1 Dimensioning

In Table 5.1, a number of general design criteria for trickling filter waste water treatment plants is given. No consensus exists for the terminology 'high rate', 'low rate', etc. In this text, the nomenclature of Metcalf & Eddy (1991) was used.

The filter unit's dimensions were chosen to represent a cylindrical core taken from a full-scale unit. In contrast to completely mixed pilot or bench scale activated sludge units, the reactor's depth can not be scaled down without fundamentally affecting the system's behaviour. Practical considerations limited the depth to 1.8 m, which is within the range given in Metcalf & Eddy (1991) for both intermediate rate [1.8 m - 2.4 m] and high rate [0.9 m - 1.8 m] filters. Contrary to the depth, it is possible to downscale the diameter, provided wall effects (hydraulic shortcuts) remain negligible. Based on the availability of standard PVC sewer pipe components, an internal diameter of 0.388 m was chosen. Hence, the filter's cross-sectional area was 0.118 m<sup>2</sup>, and its volume was 0.213 m<sup>3</sup>.

For the settler design calculations, it was assumed that the entire flow through the trickling filter (1.3 l/min) also passes through the settler ('worst-case' hydraulics). For practical and cost reasons, the settler diameter was fixed at 0.25 m, hence its surface area was 0.049 m<sup>2</sup>. The corresponding overflow velocity (at maximal flow) is 1.5 m/h, which is within the safety range for poor settling

sludge (SVI = 200 ml/g) (Metcalf & Eddy, 1991). Based on Grijspeerdt *et al.* (1996), the downscaled settler's height was fixed at 0.75 m.

**Table 5.1. Typical trickling filter design criteria**

	Carrier medium	$B_A$  ( $m^3/m^2 \cdot d$ ) { $m/h$ }	$B_V$  ( $kgBOD/m^3 \cdot d$ )	$R$  (-)	$h_{ff}$  ( $m$ )
<i>Metcalf &amp; Eddy (1991)</i>					
Low Rate	rock	1.2 - 3.5 {0.05 - 0.15}	0.08 - 0.4	none	1.8 - 2.4
Intermediate Rate	rock	3.5 - 9.4 {0.15 - 0.40}	0.24 - 0.48	0 - 1	1.8 - 2.4
High Rate	rock	9.4 - 37.5 {0.40 - 1.60}	0.48 - 0.96	1 - 2	0.9 - 1.8
Super High Rate	plastic	12 - 70 {0.50 - 2.9}	0.48 - 1.6	1 - 2	3 - 12
Roughing	plastic (or redwood)	47 - 188 {1.96 - 7.8}	1.6 - 8	1 - 4	4.6 - 12
<i>Henze et al. (1995)</i>					
Low Rate		4.8 {0.2}	0.2		
Moderate Rate		9.6 - 19.2 {0.4 - 0.8}	0.2 - 0.45	*	
Normal Rate		14.4 - 28.8 {0.6 - 1.2}	0.45 - 0.75		
High Rate		> 28.8 {> 1.2}	> 0.75		
<i>ATV (1989)</i>					
No nitrification	rock	11.8 - 23.5 {0.5 - 1.0}	0.4	$\leq 1$	2.8 - 4.2
	plastic	18.8 - 42.3 {0.8 - 1.8}	0.4 - 0.8	$\leq 1$	2.8 - 4.2
With Nitrification	rock	9.4 - 18.8 {0.4 - 0.8}	0.2	$\leq 1$	2.8 - 4.2
	plastic	23.5 - 35.3 {1.0 - 1.5}	0.2 - 0.4	$\leq 1$	2.8 - 4.2

\* on the one hand it is recommended in this book to use  $R < 1$ ; on the other hand a recycle ratio of  $> 8$  was calculated for a high rate example

### 5.2.2 Carrier material

To ensure uniform conditions throughout the filter, to allow quantification of specific surface area and biofilm parameters, and to ensure a low weight, a plastic carrier medium was used. The selected medium was obtained from the company Filtermat (Temse, Belgium) (Figure 5.1). Its specific surface area was  $220 m^2/m^3$ , its density  $61 kg/m^3$ , and it had 96% voids. The surface area of a carrier material unit ( $0.0225 m^2/carrier$ ) was calculated based on its actual geometry.

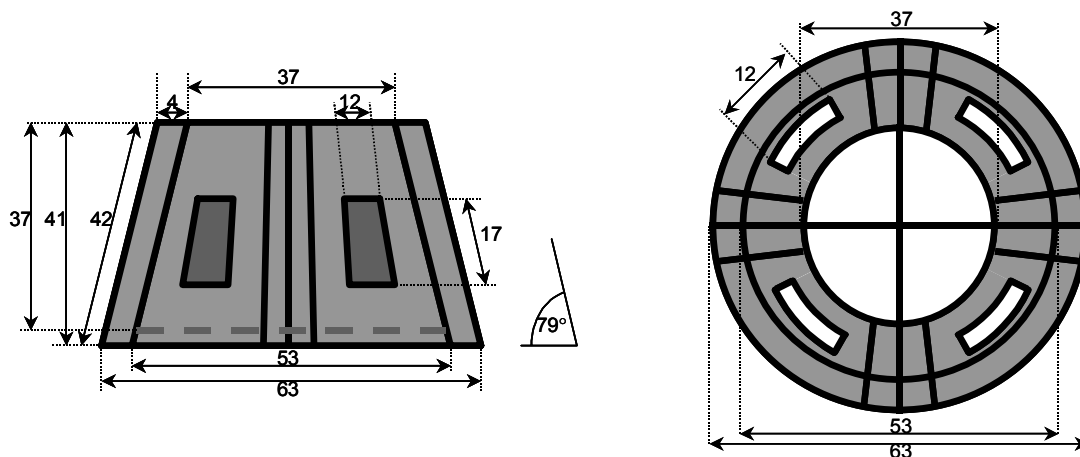


**Figure 5.1: Carrier material (lengths in mm)**

### 5.2.3 Loading and flows

Metcalf & Eddy (1991) advise to apply a high rate loading with a plastic filter medium. A volumetric loading rate  $B_V = 0.6 \text{ kg BOD/m}^3 \cdot \text{d}$  was selected. The hydraulic surface loading rate  $B_A$  was set at  $15 \text{ m}^3/\text{m}^2 \cdot \text{d}$  ( $= 0.625 \text{ m/h}$ ). These values are within the range for high and super high rate trickling filters (Metcalf & Eddy, 1991), or for normal rate filters as mentioned by Henze *et al.* (1995). A  $B_V$  of  $0.2 \text{ kg BOD/m}^3 \cdot \text{d}$  is recommended for nitrifying filters by ATV (1989), hence a large degree of nitrification is not expected in this case. The total flow through the filter (influent + recycle flow) is equal to  $B_A$  multiplied by the surface area  $= 1.3 \text{ l/min}$ . Assuming an influent BOD level of  $300 \text{ mg/l}$  (typical for domestic sewage, Metcalf & Eddy (1991)), the influent flow ( $=$  the product of  $B_V$  and volume divided by BOD) is  $0.29 \text{ l/min}$ .

From the total and the influent flow, it can be derived that the recycle ratio has to be 3.5. This is higher than mentioned in Metcalf & Eddy (1991) for super high rate filters, but within the range for roughing filters. It is also higher than recommended in Henze *et al.* (1995) for typical cases, but on the other hand much lower than the factor 8 from their calculation example. It was decided to retain this relatively high recycle ratio (and wetting rate) as a default for the experiments, to ensure proper wetting of the filter material and a uniform spatial distribution of the influent over the filter's surface. The recycle rate was assumed to have no effect on sloughing, as this is generally quite unpredictable and often related to atmospheric conditions.

In many trickling filters, air flow is induced by natural ventilation (chimney effect), and is generally poorly quantified. No design criteria were found for this parameter. Based on an example of a pilot-scale TF plant (Melcer *et al.*, 1995), an upward air flow through the filter of  $15 \text{ l/min}$  was chosen (upward air flow velocity of  $7.5 \text{ m/h}$ ).

### 5.2.4 Construction

The influent is pumped into the pumping reservoir of the treatment plant, where it is mixed with the recycle water. This mixture is pumped up into the filter unit itself. The water trickles down the filter and is then split into two fractions: the short recycle which flows directly to the pumping reservoir, and the long recycle which flows into the settler. Of the latter, one part (equal in flow rate to the influent) is the plant's effluent; the other part - the long recycle - flows to the pumping reservoir. An overview is given in Figure 5.2.

#### 5.2.4.1 Filter unit

The filter was constructed using a PVC tube (ext. diameter  $= 0.4 \text{ m}$ , wall thickness  $= 6.2 \text{ mm}$ ). The filter length is  $1.8 \text{ m}$ ; the total length of the tube is  $2.1 \text{ m}$ . Five sampling ports were provided. To counteract hydraulic wall effects (short circuiting), four horizontal rings (width of  $5 \text{ cm}$ ) were placed in the filter. At the bottom of the filter, a perforated disc was used to support the carrier material. At the top of the filter unit, the inflow coming from the pumping reservoir by means of a Watson Marlow 605Di pump, is split into 16 subflows, and each subflow tube is attached to a horizontal perforated disc to ensure a uniform partitioning over the filter's surface. The top of the filter was closed by a polyethylene funnel, which is connected to an air pump (KNF-Verder). At the bottom of the filter

body, a polyethylene funnel was used to direct the filter's outflow to a small collection vessel, from which it is pumped to a timer-controlled three-way pinch valve (Sirai S307-01, silicone tubing of 4.8/7.9 mm int./ext. diameter) allowing to switch between the short and the long recycle (by means of an aquarium pump: Rena C40 Turbo, max. capacity 1000 l/h). A schematic overview of the filter unit is shown in Figure 5.3.

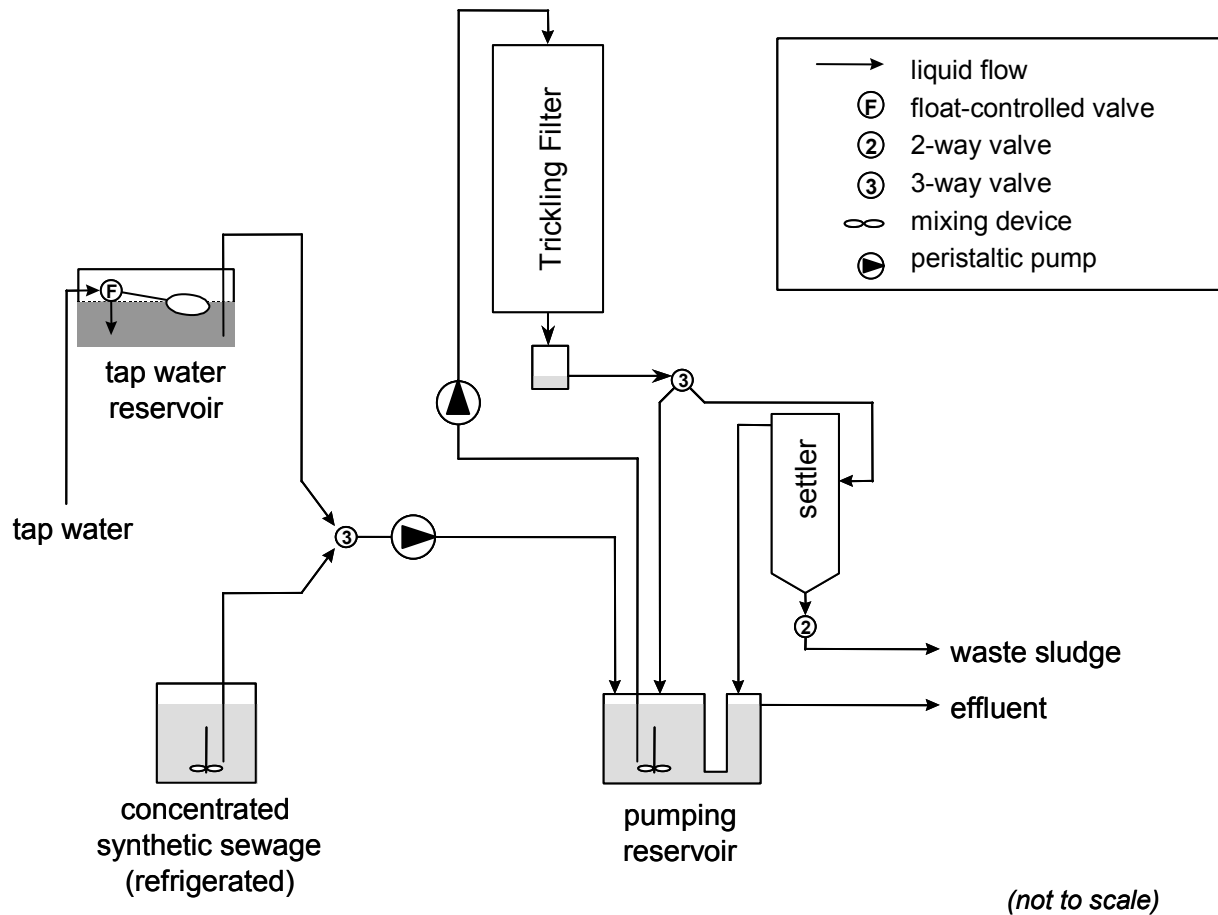


Figure 5.2. Overview of trickling filter hydraulics

#### 5.2.4.2 Settler

The settler was constructed from transparent plexi-glass. The settler is located below the filter unit, but hydraulic headlosses in the tubing made gravitational flow unreliable. Hence, a small pump was required (see higher). The waste sludge flow is periodically switched on by means of a timer-controlled two-way pinch valve (Sirai S106-03, with silicone tubing of 6.4/9.5 mm internal/external diameter).

#### 5.2.4.3 Pumping reservoir

The influent and the short recycle flows are mixed in the pumping reservoir. Through hydraulic contact with the effluent reservoir (which received the settler's outflow), the long recycle flow can also enter the pumping reservoir. To avoid settling of solids, the pumping reservoir is continuously mixed by means of a small aquarium pump (Rena C10, max. capacity 240 l/h).

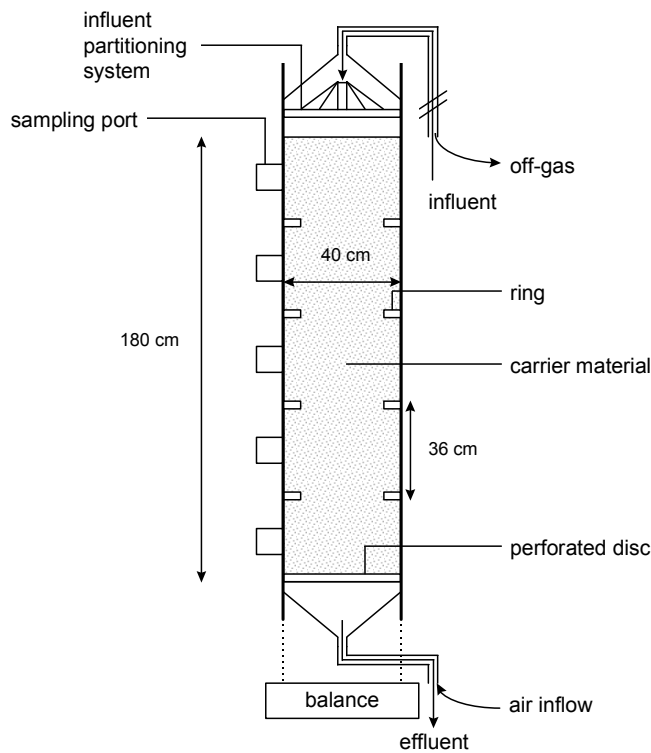


Figure 5.3: Scheme and picture of filter body

#### 5.2.4.4 Influent

As influent to the trickling filter plant, a synthetic sewage is used which mimics real domestic wastewater. A synthetic medium was preferred over actual sewage, because (1) its composition is constant, (2) its composition is well-characterized, (3) its composition can be controlled and (4) for practical reasons: a synthetic sewage can be prepared as a concentrate which is only to be diluted when it enters the plant. The composition of the sewage was based on the *Syntho* medium (Boeije *et al.*, 1998). For cost reduction, this medium was slightly simplified: urea: 55,  $\text{NH}_4\text{Cl}$ : 13, Na-acetate.3 $\text{H}_2\text{O}$ : 148, peptone: 17,  $\text{MgHPO}_4 \cdot 3\text{H}_2\text{O}$ : 29,  $\text{K}_3\text{PO}_4$ : 20,  $\text{CaCl}_2$ : 2.3,  $\text{FeSO}_4 \cdot 7\text{H}_2\text{O}$ : 5.8,  $\text{NaHCO}_3$ : 29, starch: 122, milk powder: 116, yeast: 52, soy oil: 29, Na-LAS paste (60%): 14, Alkyl Ethoxylate (Neodol) (100%): 9,  $\text{Cr}(\text{NO}_3)_3 \cdot 9\text{H}_2\text{O}$ : 0.770,  $\text{CuCl}_2 \cdot 2\text{H}_2\text{O}$ : 0.536,  $\text{MnSO}_4 \cdot \text{H}_2\text{O}$ : 0.108,  $\text{NiSO}_4 \cdot 6\text{H}_2\text{O}$ : 0.336,  $\text{PbCl}_2$ : 0.100,  $\text{ZnCl}_2$ : 0.208 (in mg/l). The calculated COD:N:P ratio of the synthetic sewage is 462:43:9 or 100:9.3:2. The theoretical BOD (assuming a COD to BOD conversion factor of 0.65) is 300 mg/l.

In practice, the influent is prepared as a concentrated liquid (20x or 30x), and is diluted with tap water when it is pumped into the filter set-up. One pump is used for this purpose (Watson Marlow 505U), which alternates between concentrate and tap water by means of a timer-controlled three-way pinch valve (Sirai S307-01, with silicone tubing of 4.8/7.9 mm internal/external diameter). A constant supply of tap water is provided in a reservoir which is continuously filled by means of a float-controlled valve. To keep its quality constant, the concentrated sewage is stored in a refrigerator, and is continuously stirred by a mixer (IKA RW 28 W).

## 5.3 On-line sensors

### 5.3.1 Balance

By means of an electronic balance (a modified Mettler-Toledo Spider 1S-150), the weight of the filter unit is continuously monitored with an accuracy of 10 g. Information about the filter's weight (both at steady-state and under dynamic conditions) can be used to determine biofilm and hydraulic characteristics.

### 5.3.2 Off-gas analysis

The off-gas of the filter is continuously monitored for CO<sub>2</sub> and O<sub>2</sub> (Maihak Multor 610). These measurements allow to establish closed carbon and COD mass balances for the filter unit.

The O<sub>2</sub> measurement is based on the paramagnetic characteristic of oxygen. The measuring cell contains a diamagnetic part, suspended in a permanent magnetic field in such a way that it can rotate out of the magnetic field. However, an opto-electrical compensation circuit is provided to keep the dumbbell in a defined resting position. The paramagnetic characteristic of the O<sub>2</sub> in the sample gas will change the magnetic field. This effects an adaptation of the opto-electrical compensation. This compensation difference is used to calculate the O<sub>2</sub> concentration.

CO<sub>2</sub> is measured with the NDIR (non-dispersive infrared) method. The sample gas is pumped through one compartment (the measuring side) of a measuring cuvette. The other compartment (the reference side) is filled with a reference gas. A turning modulation wheel directs the radiation to one side of the cuvette at a time. Behind this cuvette, the rest of the infrared radiation is absorbed in a detector. This detector consists of two optical absorption layers in series, pneumatically separated by a window and is also filled with a certain amount of the component of interest (CO<sub>2</sub> in this case). Due to the unequal absorption of infrared radiation at each side in the measuring cuvette, a time-fluctuating amount of infrared radiation is still to be absorbed in the detector. This fluctuation induces pressure pulses of the window that separates the two compartments in the detector, due to unequal heating in both compartments. The amplitude of this fluctuation is used as a measure of the CO<sub>2</sub> concentration in the sample gas.

An automatic calibration of these sensors is done once a day. Gas pre-treatment consists of cooling and removing condense water with a Peltier cooling element followed by a silicagel filter. The response time of the instrument is in the order of 30 seconds. Extra delay of a few seconds is introduced only by the transport of the sample gas to the instrument by a built-in gas pump at a flow rate of 0.5 l/min.

## 5.4 Biofilm and suspended solids characterization

### 5.4.1 Biofilm density

Biofilm density was determined by measuring the dry weight (24 hours at 100 °C) of a known volume (2 ml) of biofilm, which was scraped off the trickling filter's carriers. Three replicates were performed, for which the biofilm was sampled from three different carriers, taken from different

locations in the filter. The biofilm density was found to be  $38.8 \pm 0.8$  g/l. This corresponds well with the typical value of 40 g/l which is *e.g.* mentioned in Melcer *et al.* (1995).

#### 5.4.2 Biofilm thickness

Total biofilm thickness was determined using two different methods: (1) based on the wet and dry biofilm mass attached to individual carriers, and (2) based on the mass of the entire filter unit.

##### 5.4.2.1 Based on mass of individual carriers

The wet biofilm mass attached to one carrier was calculated as the difference of the wet (but leaked out) mass of a carrier taken out of the filter, and the dry mass of a 'clean' carrier. The associated dry biofilm mass is obtained as the difference of the dried mass (24 hours at 100 °C) of the carrier, and the dry mass of a 'clean' carrier. The wet biofilm volume was derived from its wet mass by assuming a density of 1 kg/l. The dry biofilm mass was calculated back to wet biofilm volume by means of the measured biofilm density of 38.8 g/l (see above). Biofilm thickness was obtained by dividing the wet biofilm volume by the surface area of one carrier material (Table 5.2).

**Table 5.2. Total biofilm thickness based on mass of individual carriers**

	May 18	June 11
Based on wet biofilm mass	$430 \pm 64 \mu\text{m}$	$526 \pm 205 \mu\text{m}$
Based on dry biofilm mass	$428 \pm 86 \mu\text{m}$	$687 \pm 354 \mu\text{m}$
Number of measurements	4	3

##### 5.4.2.2 Based on the entire filter unit mass

###### *Method and measurements*

The dry mass of the filter was determined prior to the experiments: 62.93 kg. Several experiments were performed before any biofilm had developed. The total mass of water present in the filter was determined at a filter inflow rate (= influent + recycle flow) of 1.3 l/min (normal operating conditions). This was calculated as the difference between the total mass and the dry mass of the filter: 6.66 kg. The mass of the filter was then measured when the influent flow had been stopped. This way, it was possible to quantify the 'dynamic' amount of water which was present in the filter, *i.e.* the water which leaks out when the influent flow is stopped: 1.45 kg.

The 'static' amount of water, *i.e.* the water which remains in the filter even if there is no influent flow, could be determined by subtracting the dynamic water mass from the total mass of water present in the filter. Note that this 'static' water layer was assumed to be independent of the flow rate: 5.21 kg.

Later on, in the presence of biofilm, the experiment was repeated. This allowed to measure the 'dynamic' water layer's mass when biofilm was present. Note that this value was relatively stable during the whole period of operation:  $3.12 \pm 0.23$  kg over a total of 14 measurements. Assuming that the 'static' water mass was not affected by the presence of biofilm, the total water mass in the filter in the presence of biofilm was 8.33 kg. Also, the mass of wet biofilm in the filter could be determined by subtracting the 'dynamic' and the 'static' water mass and the dry filter mass from the total measured

mass. During the experiment, which was conducted approximately one month after inoculation of the filter, the biofilm mass was calculated to be 4.91 kg.

The wet biofilm mass can be converted to volume by assuming a density of 1 kg/l. If this volume is divided by the total surface area within the filter (46.86 m<sup>2</sup>), an average biofilm thickness is obtained: 105  $\mu\text{m}$ .

During the first month of operation, the calculated biofilm thickness evolved from 50 to 100  $\mu\text{m}$ . The next month it quickly evolved to more than 900  $\mu\text{m}$ . Because of the balance's limited capacity, it was necessary to reduce the filter's mass by feeding with only tap water for 1 week. This reduced the biofilm thickness, which varied between 500 and 750  $\mu\text{m}$  during the next 2 months. The average calculated biofilm thickness over the entire period was 410 ( $\pm 260$ )  $\mu\text{m}$  (Figure 5.4).

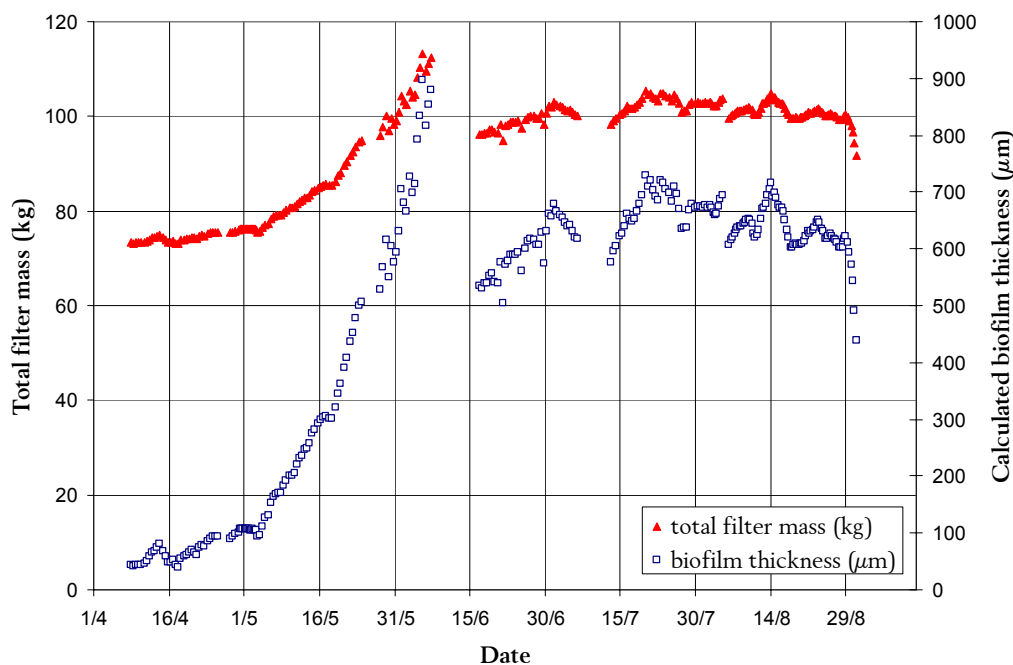


**Figure 5.4. Filter mass and calculated total biofilm thickness**

### *Interpretation*

The order of magnitude of average biofilm thickness measurements obtained by the different methods presented is the same, which shows the reliability of the results. The individual carriers were taken from the middle of the filter bed. The amount of biomass as well as the biofilm thickness is however bigger at the top of the filter. This is confirmed by visual inspection and by the tracer test results (see further in this chapter). The total biofilm mass is thus a more reliable method to represent the evolution of biomass build-up in the filter.

### **5.4.3 Suspended Solids**

Suspended solids were determined in the influent, the pumping reservoir, the filter outflow, and the final effluent. Duplicate measurements were made at four different dates, resulting in the following values: influent:  $124 \pm 51$  mg/l, pumping reservoir:  $22 \pm 14$  mg/l, filter outflow:  $33 \pm 31$  mg/l, effluent:  $15 \pm 8$  mg/l. The variability was especially high for the filter outflow. This is most probably

due to the irregularity of the biomass sloughing process. Based on the SS measurements in the filter outflow and in the final effluent, a solids removal efficiency in the settler of  $(36.5 \pm 7.5)\%$  could be calculated.

## 5.5 Hydraulic characterization

### 5.5.1 Tracer test without biofilm

#### 5.5.1.1 Method

Two tracer tests at different flow rates were conducted on the filter without biofilm (*i.e.*, before the start-up of the biological experiments). Salt ( $NaCl$ ) was used as a tracer. A known amount of  $NaCl$  was injected into the filter as a pulse (20 g). The  $NaCl$  in the effluent of the filter was detected using continuous conductivity measurements (Yokogawa sensor). The filter was operated in ‘single-pass’ mode (hence, no effluent recycle was applied) for ease of interpretation. After the injection of the tracer, tap water was pumped over the filter. The test was conducted at two flow rates (1.66 and 0.81 l/min).

#### 5.5.1.2 Results

The results are presented in Figure 5.5. Note that the raw conductivity data (in mS/cm) were transformed to E-curves (for which the surface under the curve = 1).

Based on the tracer response curve, the mean, median and mode hydraulic residence times were obtained. The mode is taken from the peak of the curve. The median is derived from the cumulative tracer response curve (F-curve). The mean is calculated as:

$$HRT_{mean} = \frac{\sum E(t) \cdot t \cdot \Delta t}{\sum E(t) \cdot \Delta t} \quad (5.1)$$

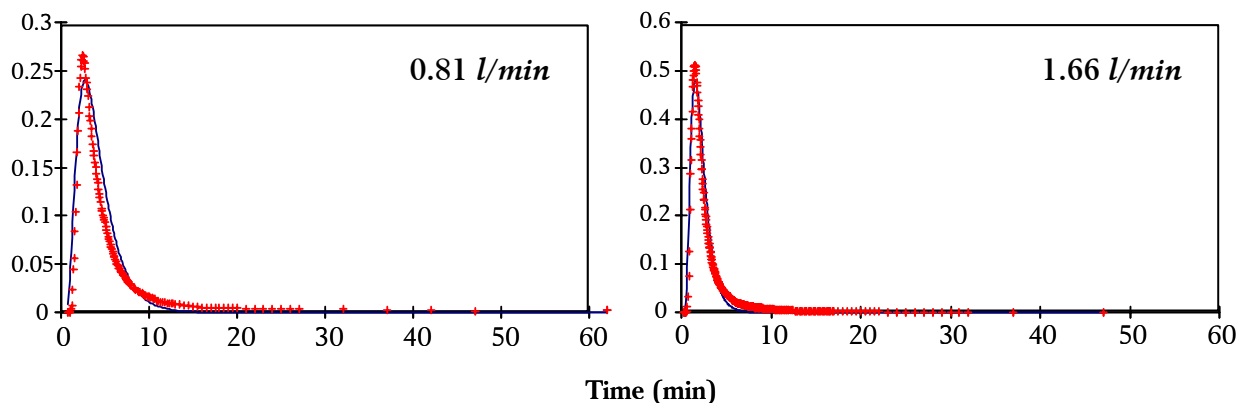


Figure 5.5. Tracer test results (E-curves) - no biofilm (- : Model, + : Data)

For the tracer test in the trickling filter, in absence of biofilm, the HRT's are given in Table 5.3.

**Table 5.3. Tracer test results - no biofilm**

		0.81 l/min	1.66 l/min
mean HRT	(min)	8.75	3.28
median HRT	(min)	3.92	2.04
mode HRT	(min)	2.42	1.50

An open vessel advection-dispersion model (Levenspiel, 1972) was fitted to the experimental tracer data ( $u$  and  $D$  fitted,  $L$  fixed at 1.8 m):

$$E_t = \frac{u}{\sqrt{4\pi Dt}} \exp\left[-\frac{(L-ut)^2}{4Dt}\right] \quad (5.2)$$

where  $u$  denotes the superficial liquid velocity (m/s),  $D$  is the dispersion coefficient (m<sup>2</sup>/s),  $t$  is the time in seconds and  $L$  denotes the length of the plug flow pipe (m).

The best fit was found with the parameter values given in Table 5.4 (SSE minimisation, SPSS software, version 7.5, SPSS Inc.). The determination coefficient  $R^2$  indicates the quality of the fit was acceptable but not perfect. The measured tracer response data were heavier in the right tail region compared to the model, while the model underpredicted the importance of the mode.

**Table 5.4. Tracer test results - no biofilm**

		0.81 l/min	1.66 l/min
$u$	(m/s)	0.009491	0.017159
$D$	(m <sup>2</sup> /s)	0.002533	0.003685
$R^2$	(-)	0.9075	0.9676

## 5.5.2 Tracer test with biofilm

### 5.5.2.1 Method

Three tracer tests were conducted on the filter when biofilm was present (*i.e.*, during the biological experiments). The fluorescent agent *Thioflavine-S* was used as a tracer, since a high *NaCl* may disrupt biological activity. A fixed amount of tracer was injected into the filter as a pulse. *Thioflavine-S* was detected in the effluent of the filter using continuous fluorescence measurements (Ingold Fluoresensor) (excitation wavelength: 360 nm, measurement wavelength: 450 nm). Again, the filter was operated in 'single-pass' mode (hence, no effluent recycle was applied). After the injection of the tracer, tap water was pumped over the filter. The test was conducted at 3 flow rates (0.42, 0.83 and 1.3 l/min).

### 5.5.2.2 Results

The results are presented in Figure 5.6. Note that also the raw fluorescence data were transformed to E-curves.

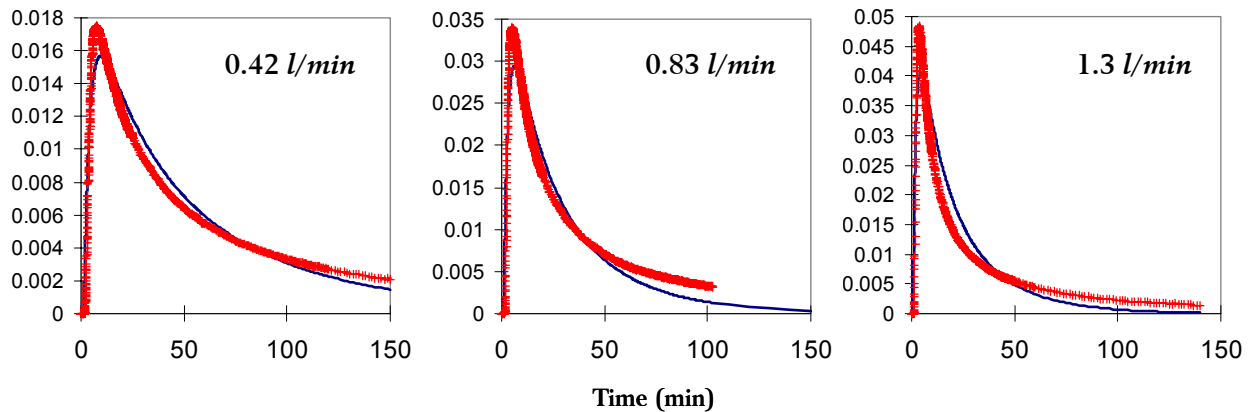


**Figure 5.6. Tracer test results (E-curves) - with biofilm (- : Model, + : Data)**

In the tracer experiment with biofilm present, the response curves' tails were especially heavy. Because of this, the tracer experiments were not conducted until the complete disappearance of tracer from the effluent. To complete the E-curves, an exponential tail extrapolation was performed. The HRT's calculated that way are given in Table 5.5.

**Table 5.5. Tracer test results - with biofilm**

		0.42 l/min	0.83 l/min	1.3 l/min
Mean HRT	(min)	84.0	40.0	38.6
Median HRT	(min)	54.2	27.7	21.4
Mode HRT	(min)	7.8	5.1	3.7

Again, the advection-dispersion model was fitted to the experimental data (SSE minimisation, SPSS software, version 7.5, SPSS Inc.). The quality of the fit was similar to that in the 'no biofilm' case. As for the tracer test without biofilm, the measured tracer response data were heavier in the tail region compared to the model, and the model also underpredicted the importance of the mode HRT (Figure 5.6). However, the large discrepancy between the modelled and real tracer tail is not fully reflected in the  $R^2$  values, as the measurements used to fit the model were not continued until complete disappearance of the tracer. Hence, it is expected that the presented coefficients of determination are too optimistic

**Table 5.6. Tracer test results - with biofilm**

		0.42 l/min	0.83 l/min	1.3 l/min
$u$	(m/s)	0.001312	0.002288	0.003207
$D$	(m <sup>2</sup> /s)	0.002319	0.003179	0.004682
$R$	(-)	0.94287	0.93943	0.91104

It can be seen from the results that there is a very large difference in hydraulic retention time compared to the case without biofilm. Therefore it is assumed that a major part of the tail section of the E-curves should be attributed to diffusion of the tracer into the biofilm. In order to link the hydraulic model developed here to a model of the biodegradation in the biofilm, the tracer test data were also interpreted via the "continuously stirred biofilm reactor" approach (Wik, 1999). Here, the biofilter is described as a series of completely stirred tank reactors (CSTR). Each CSTR is connected

to a biofilm compartment by a diffusive link permitting diffusion of components in and out of the biofilm compartment. The parameters of the model are (1) the number of CSTR's (2) the volume of the CSTR's, (3) the volumes of the biofilm compartments and (4) the mass transfer coefficients. These can be varied to fit the modelled response curve to the experimental tracer test data.

At first, model parameter estimations (WEST, Hemmis, Kortrijk) were done with equal volumes for the CSTR's and the biofilm compartments. It showed not to be possible to obtain a reasonable fit with such a model. Letting all volumes vary independently, however, would make the model overparametrised. Hence, an exponential function for the volume decrease along the depth of the filter was chosen, minimising the number of parameters to be estimated (equation 5.3).

$$V_i^w = V_\alpha \cdot e^{-i\alpha} \text{ and } V_i^{\text{biofilm}} = V_\beta \cdot e^{-i\beta} \quad (5.3)$$

The best fit was found with 7 CSTR's in series, each linked to a biofilm compartment. As an example, the model fit for a flow rate of 1.3 l/min through the filter – the design flow rate – is given on Figure 5.7. A determination coefficient ( $R^2$ ) of 0.997 was found in this example. The parameters found were  $V_\alpha = 1.59$ ,  $\alpha = 0.165$ ,  $V_\beta = 84.3$  and  $\beta = 1.136$ .

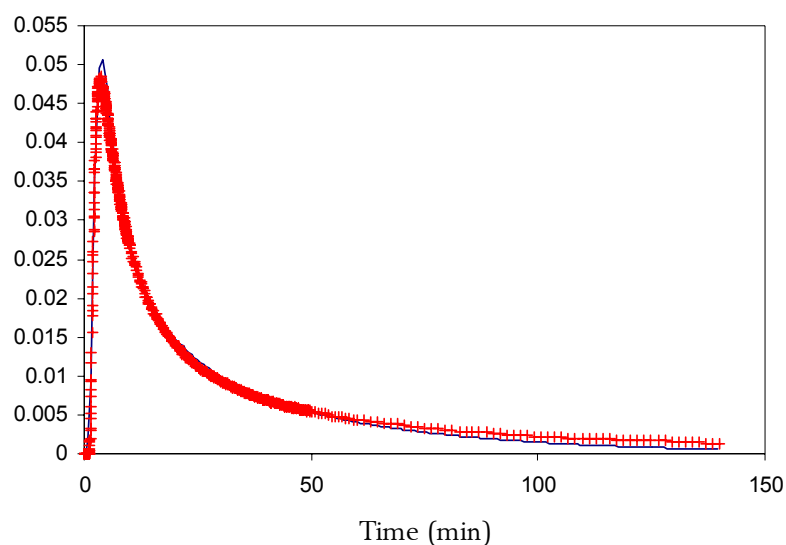


**Figure 5.7. Tracer test results - with biofilm - 1.3 l/min (- : Model, + : Data)**

The volumes of the tanks found by this approach can be found in Table 5.7. Both total volumes are in very good agreement with the findings of the experiments conducted to estimate the biofilm thickness with a balance. The total volume of the CSTR's can be correlated to the mass of water in the filter, which is estimated to be 8.27 l ('dynamic' + 'static' water layer). Note that all the water in the CSTR's is considered to be 'dynamic'. In order to model the transfer resistance from the liquid phase to the biofilm, a transfer coefficient was implemented, which has an estimated value of  $0.019 \text{ s}^{-1}$ .

Furthermore, the volume of the biofilm compartments is very close to the measured value with the balance. The filter weight at the time of the tracer experiment was 104.70 kg. When the dry weight of the filter, the weight of the water in the CSTR's and the weight of the biofilm – assuming wet biofilm

to have a density of 1 kg/l – are added, a value of 109.83 kg is found. This indicates that the total volume of the biofilm compartments is a reasonable guess of the biofilm volume in the trickling filter.

**Table 5.7. Tracer test results - with biofilm**  
**Completely stirred biofilm reactor model volumes**

	<i>Volume of CSTR's (l)</i>	<i>Volume of biofilm compartments (l)</i>
Level 1	1.35	28.07
Level 2	1.14	8.75
Level 3	0.97	2.73
Level 4	0.82	0.85
Level 5	0.70	0.30
Level 6	0.59	0.10
Level 7	0.50	0.03
Total	6.07	40.83

## 5.6 Preliminary COD removal experiments

Four different experimental series were conducted. In series (A) and (B), only the short recycle (i.e., bypassing the settler) was used. In series (A), the operating conditions were typically high-rate, while in series (B), conditions were closer to low-rate as the recycle flow was much lower. Series (C) and (D) were conducted to determine the influence of the long recycle (i.e., over the settler). Except for the recycle regime, they were identical to series (A). The experimental conditions in the different series are given in Table 5.8 below. COD concentrations were measured at four locations: (1) influent (total); (2) pumping reservoir (total); (3) filter outflow (total); (4) final effluent (total + dissolved). The average total biofilm thickness is also given in Table 5.8. COD was determined by means of Dr. Lange test kits (Dr. Bruno Lange GmbH) (Table 5.9). Dissolved effluent samples were obtained after filtration using an Schleicher & Schuell filter (S&S 597½).

**Table 5.8. Experimental conditions**

		<i>Series A</i>	<i>Series B</i>	<i>Series C</i>	<i>Series D</i>
Date (from - to)		28-Apr 28-May	28-May 4-Jun	11-Jun 2-Jul	2-Jul 3-Aug
Influent flow rate	(ml/min)	290	290	290	290
Recycle ratio	(-)	3.5	0.5	3.5	3.5
- Short recycle ratio	(-)	3.5	0.5	1.75	0
- Long recycle ratio	(-)	0	0	1.75	3.5
Total biofilm thickness	( $\mu\text{m}$ )	100 - 500	500 - 700	500 - 700	550 - 750

The average COD removal efficiency which was measured in the trickling filter was  $85 \pm 6\%$ , with no significant difference between the different experimental series (Tukey test,  $\alpha = 0.05$ ). For COD, the average removal over the settler was  $(16 \pm 21)\%$ . This high variability can be explained by the poor settling properties of the filter's sludge, and by the very irregular sloughing behaviour.

**Table 5.9. Chemical oxygen demand**

Sampling Location	CODt (mg/l)	CODs (mg/l)
(1) Influent	352 ± 34	284 ± 67
(2) Pumping reservoir	182 ± 69	96 ± 31
(3) Filter outflow	61 ± 24	47 ± 16
(4) Final Effluent	50 ± 20	43 ± 14

The COD removal experiments showed that the trickling filter had a normal treatment efficiency. The measured COD removal of  $85 \pm 6\%$  corresponds well with ATV (1985), whose rule of thumb predicts a treatment efficiency of  $(93 - 17 \cdot B_V)\% = 82.8\%$  in this case. There was no significant effect of the different experimental operating conditions on COD elimination.

## 5.7 Off-gas measurement results

The result of the influent concentration step change from normal influent to tap water can be seen on Figure 5.8. During the first 20 hours of the test, the concentration change of both  $O_2$  and  $CO_2$  looks normal, with a decrease of  $CO_2$  and an increase of  $O_2$  due to lowered oxidation rates. However, after this period, a sudden decrease of the  $O_2$  concentration can be observed without concomitant increase in  $CO_2$  evolution. This can be explained as follows. Under normal operating conditions, no significant nitrification is expected. There is, however, some autotrophic biomass present in the filter leading to a small nitrification activity. During the test, more oxygen becomes available for nitrification. As a result, the autotrophic biomass can start to nitrify more intensively. This hypothesis was checked using the nitrogen and COD measurements. An unexpected change of the measured RQ (respiration coefficient) in Figure 5.8 points in this direction too. The RQ is the ratio between  $CO_2$  production and oxygen consumption, and is near 1 for heterotrophic growth (Hellinga *et al.*, 1996). It will drop in case significant nitrification occurs.

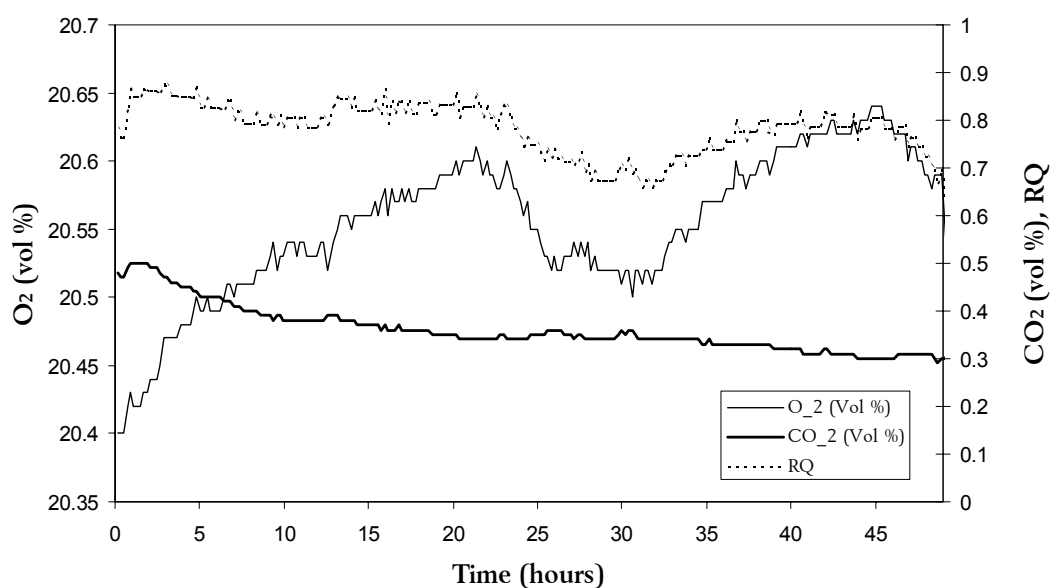


**Figure 5.8. Results of the step change in influent concentration**

## 5.8 Conclusions

In this chapter, the construction and start-up of a pilot-scale trickling filter was studied. The filter was constructed to allow the collection of experimental data on a fully characterised biofilm system. The design of the unit allowed for the full characterisation of operational parameters and on-line monitoring of the system was possible by means of an electronic balance and off-gas analysis measurement equipment.

To characterise the filter's hydrodynamic behaviour, two tracer tests were conducted without and with biofilm. The hydraulic behaviour of the filter without biofilm could be described using an advection-dispersion model. If a biofilm was present however, a CSBR (continuously stirred biofilm reactor) approach was found necessary to yield an optimal description of the hydraulics.

Preliminary COD removal experiments showed that – although a high variability was noticed – the COD removal efficiency corresponded well with what could be expected for a filter with these dimensions and loading. Off-gas measurements showed that monitoring of the degree of nitrification in the filter is possible at lower influent loading rate.



# 6

## Monitoring off-gas $O_2$ and $CO_2$ concentrations and their use in the model description of a pilot-scale trickling filter

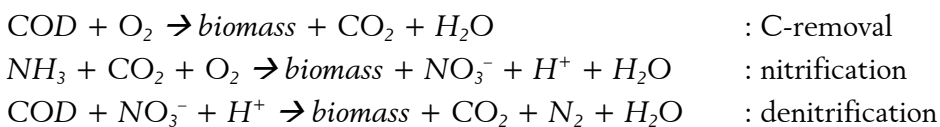
### 6.1 Introduction

The pilot-scale trickling filter described in the previous chapter was used for a series of experiments. First of all, a load shift experiment was conducted in which the influent load to the trickling filter system was suddenly decreased. As described before, it seemed to be possible to increase the nitrification rate in the filter system by lowering the load of organic material to the filter. In this chapter, the load shift experiment is described, next to the modelling results obtained with the simplified mixed-culture biofilm model. Therefore, this model was extended with a part describing the production and consumption of  $CO_2$  and  $O_2$  in the off-gas of a biofilm wastewater treatment plant.

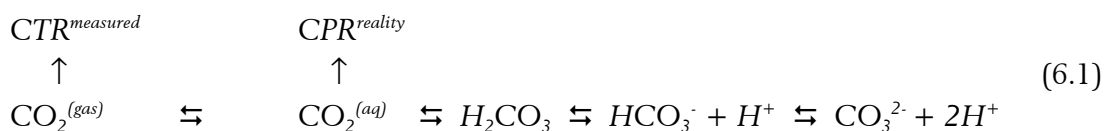
### 6.2 The use of off-gas analysis in wastewater treatment

#### 6.2.1 Off-gas composition in wastewater treatment

The composition of the off-gasses of biological wastewater treatment systems, in terms of oxygen and carbon dioxide, is the result of complex interactions between the biodegradation activity of the biomass and the distribution of these substances over the liquid and the gas phase in the reactor. The oxygen uptake rate (OUR) and the carbon dioxide production rate (CPR) can be derived theoretically from the reactions that describe carbon removal, nitrification and denitrification. These reactions can be written as (Hellinga *et al.*, 1996):



This shows us that the OUR, the CPR and the evolution of the  $pH$  in the system incorporate a lot of information about the biological processes occurring in the system. The CPR is, however, not directly measurable. The dynamic equilibria in which  $CO_2$  plays a role result in a distribution of  $CO_2$  over the liquid and the gas phase so that not the CPR but rather a CTR ( $CO_2$  transfer rate) is measured as represented in this figure (Noorman *et al.*, 1992; Govind *et al.*, 1997).



The measurement of OUR is less subject to these phenomena because oxygen can not accumulate in the water phase to the same extent as inorganic carbon.

For the measurement of O<sub>2</sub> and CO<sub>2</sub> in the gas phase, paramagnetic and infrared measurement techniques are used. These methods are robust, accurate, relatively cheap and widespread in the fermentation industry. The use of these sensors for on-line monitoring of wastewater treatment plants is relatively new. However, it is known that measurements of the oxygen concentration in the off-gasses of activated sludge plants can be used for the calculation of the oxygen transfer rate and for the control of the aeration and thus indirectly of the concentration of dissolved oxygen in the system (Tanuma *et al.*, 1981).

Off-gas analysis, however, has some advantages over measurements in the liquid phase (Hellings *et al.*, 1996). The measurement equipment is clean, robust and accurate. They also do not require any chemicals and are taken from a well mixed gas flow, reflecting the state of the reactor as a whole rather than on a specific point (which is the case for liquid measurements). The investment costs are in the same order of magnitude as for the analyses of components in the liquid phase. As in the future a lot of treatment plants will be covered – which is already the case for most biofilm systems – in order to avoid odour nuisance, the implementation of gas measurements will be easier than it is at this moment.

### 6.2.2 The oxygen measurement and its interpretation

Oxygen related measurements are, however, almost always performed in the liquid phase with DO-sensors or respirometers. The application of these measurements, however, is limited to systems where the liquid phase is readily accessible. On top of that, the measurement does not provide an overview of all processes going on in the reactor, only one point in space is monitored.

To interpret the gas phase oxygen measurement, a combined gas and liquid phase mass balance must be solved to find a value for the actual oxygen uptake rate (Spanjers *et al.*, 1996). For example, in an ideally mixed system, the gas phase mass balance can be written as:

$$\frac{d}{dt}(V_G C_G) = Q_{G,in} C_{G,in} - Q_{G,out} C_{G,out} - V_L K_L a (C_L^{sat} - C_L) \quad (6.2)$$

where  $V_G$  is the volume of the gas phase,  $V_L$  denotes the volume of the liquid phase,  $C_{G(in,out)}$  are the concentrations in the gas phase (in- and outlet),  $Q_{G(in,out)}$  is the gas flow rate and  $C_L^{sat}$  denotes the (saturation) concentration in the liquid phase. The final term on the right hand side, including the mass transfer coefficient  $K_L a$ , describes the mass transfer between the gas and the liquid phase.

The liquid phase balance is:

$$\frac{d}{dt}(V_L C_L) = Q_{L,in} C_{L,in} - Q_{L,out} C_{L,out} + V_L K_L a (C_L^{sat} - C_L) - V_L r \quad (6.3)$$

where  $r$  represents the respiration rate (or oxygen uptake rate) and  $Q_{L(in,out)}$  is the liquid flow rate.

To solve this mass balances, obviously measurements in both the gas and the liquid leaving the reactor are needed. If, however, the mass transfer is fast enough, so that the concentration in both phases are in equilibrium, one can write (De heyder *et al.*, 1997):

$$C_G = H_{O_2} \cdot C_L \quad \text{and} \quad \frac{dC_G}{dt} = H_{O_2} \cdot \frac{dC_L}{dt} \quad (6.4)$$

where  $H_{O_2}$  is Henry's law constant for oxygen ( $\text{atm}^{-1}\text{M}$ ). This assumption should however be used with care, since it is not evident that the transfer resistance, expressed as  $K_L a$ , can be neglected.

### 6.2.3 *The carbon dioxide measurement and its interpretation*

In microbial fermentation technology, the value of the  $\text{CO}_2$  measurement has been appreciated for a long time. The  $\text{CO}_2$  production rate is often used to estimate the cell growth and to calculate mass balances (Bonarius *et al.*, 1995). Contrary to  $\text{O}_2$ ,  $\text{CO}_2$  can accumulate in the liquid phase to quite high concentrations. When estimating the CPR from the measured CTR, a value for the volumetric transfer coefficient  $(K_L a)_{\text{CO}_2}$  is needed (Yegneswaran *et al.*, 1990; Royce, 1992; Hellinga *et al.*, 1996). It can be estimated assuming that the  $K_L a$  values of oxygen and  $\text{CO}_2$  can be related by their respective diffusion coefficients (Noorman *et al.*, 1992; De heyder *et al.*, 1997).

$$(K_L a)_{\text{O}_2} = \sqrt{\frac{D_{\text{O}_2}}{D_{\text{CO}_2}}} (K_L a)_{\text{CO}_2} \quad (6.5)$$

where  $D_{\text{O}_2/\text{CO}_2}$  are the liquid diffusion coefficients of  $\text{O}_2$  resp.  $\text{CO}_2$ .

On the other hand, practical applications of the use of  $\text{CO}_2$ -monitoring in wastewater treatment are very scarce (Hellinga *et al.*, 1996). This has a lot to do with the problem addressed above. A lot of  $\text{CO}_2$  may leave the reactor in the form of dissolved  $\text{CO}_2$  or bicarbonate, which means that there is a difference between the measured and the actual  $\text{CO}_2$  production rate when only the off-gas measurements are available. Measurements of bicarbonate or alkalinity in the liquid phase can be used to remedy this problem, but they complicate the interpretation of the data and, obviously, make a measurement in the water necessary, hereby undoing some of the inherent benefits of off-gas measurements. The different microbiological processes that can use or produce  $\text{O}_2$  and/or  $\text{CO}_2$  add another level of complexity to the problem.

### 6.2.4 *Application of off-gas measurements*

The question can be asked whether combined  $\text{O}_2$  and  $\text{CO}_2$  measurements can be used for the evaluation of the processes taking place in a wastewater treatment plant. In theoretical evaluations it was possible to find a link between the measured RQ (the ratio between the CPR and the OUR) and the COD/TOC ratio of the substrate used (Hellinga *et al.*, 1996). It, however, proved to be very difficult – in a combined carbon removing and nitrifying plant – to separate the processes going on in the reactor based on the off-gas measurements. Measurements of alkalinity are a possible solution to

this problem in combination with a modelling of the inorganic carbon equilibrium. These findings, in combination with extra measurements like  $pH$ , Total Organic Carbon (TOC) and bicarbonate, indicate the potential of off-gas measurements.

### 6.2.5 Measurement of dissolved inorganic carbon using titration

A single measurement of the  $CO_2$  concentration in the off-gasses of the filter is not sufficient for a complete description of the inorganic carbon (IC) equilibrium. For that reason, additional measurements of the dissolved inorganic carbon concentration and the  $pH$  are needed in the liquid phase inside the reactor. This can be done using the titration technique developed by Van Vooren *et al.* (1999). Titration curves are monitored adding a 0.1 N  $HCl$  solution from the actual  $pH$  of the sample, down to  $pH$  2.5.

Software developed in C++ is used for the calculation of the buffer capacity profiles from the titration curves. Such a profile is the inverse of the first derivative of the titration profile (Figure 6.1). The calculation of the derivative is performed using a parabolic regression in a moving window of 5 experimental data points of the titration curve.

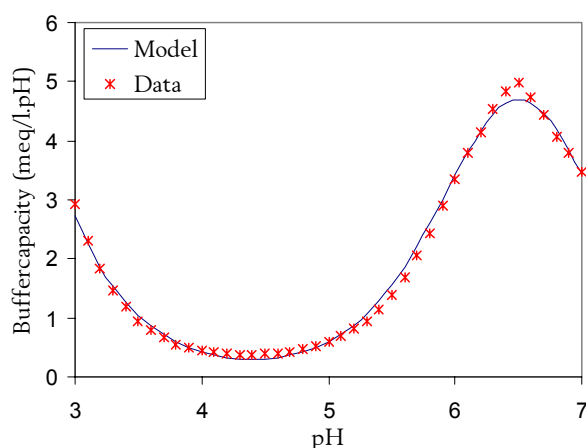


**Figure 6.1: Measurement and modelling of a buffer capacity profile for tap water.**

For the interpretation of the titration curves, a simulation interval between  $pH$  4 and  $pH$  7.3 is optimal (Figure 6.1). Even if the initial  $pH$  of the sample is higher than 7.3, it was found not to be worthwhile to extend the simulation interval and, for instance, incorporate ortho-phosphate or ammonium in the model, because the magnitude of the  $CO_2$  buffer interferes with the other smaller buffer systems. Furthermore, once the total concentration  $C_{CO_2}$  is determined, the partitioning of the 3 forms  $CO_3^{2-}$ ,  $HCO_3^-$  and  $CO_{2,aq}$  can be determined using a partitioning model in function of the actual  $pH$  of the sample. This can be done using the following equations (for more detail, the reader is referred to Van Vooren *et al.*, 1999):

$$\begin{aligned}
 [\text{CO}_{2,aq}] &= \frac{10^{-2pH}}{10^{-2pH} + 10^{-(pH+pK_1)} + 10^{-(pK_1+pK_2)}} C_{\text{CO}_2} \\
 [\text{HCO}_3^-] &= \left( 1 - \frac{10^{-2pH} + 10^{-(pK_1+pK_2)}}{10^{-2pH} + 10^{-(pH+pK_1)} + 10^{-(pK_1+pK_2)}} \right) C_{\text{CO}_2} \\
 [\text{CO}_3^{2-}] &= \left( 1 - \frac{10^{-2pH} + 10^{-(pH+pK_1)}}{10^{-2pH} + 10^{-(pH+pK_1)} + 10^{-(pK_1+pK_2)}} \right) C_{\text{CO}_2}
 \end{aligned} \tag{6.6}$$

### 6.3 Model extension for off-gas measurements

The model described earlier in this thesis has been extended with a model for the description of the production and exchange of carbon dioxide in a biofilm reactor based on the model developed by Spérandio and Paul (1997). The amount of  $\text{CO}_2$  produced/used by the biomass can be written as the sum of the carbon dioxide produced during oxic and anoxic heterotrophic growth and the  $\text{CO}_2$  used during nitrification:

$$r_{\text{CO}_2} = r_{H,\text{CO}_2} - r_{A,\text{CO}_2} \quad \left[ \frac{\text{g CO}_2}{\text{m}^3 \text{d}} \right] \tag{6.7}$$

During heterotrophic growth, it is assumed that all organic carbon that is converted by the biomass is converted into either  $\text{CO}_2$  or new cells. If the turnover of readily biodegradable COD is written as  $r_{S_s}$  the production rate of biomass as  $r_{X_H}$  and the relation between the organic carbon and the COD in these species is denoted as  $i_C$ , we can write:

$$r_{H,C} = [r_{S_s} \cdot i_{C,S_s}] - [r_{X_H} \cdot i_{C,X_H}] \quad \left[ \frac{\text{g TOC}}{\text{m}^3 \text{d}} \right] \tag{6.8}$$

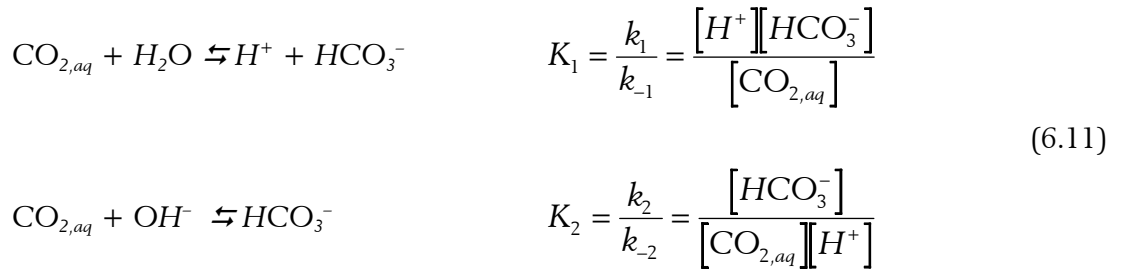
and for the production of carbon dioxide:

$$r_{H,\text{CO}_2} = r_{H,\text{TOC}} \cdot \frac{44}{12} \quad \left[ \frac{\text{g CO}_2}{\text{m}^3 \text{d}} \right] \tag{6.9}$$

On the other hand, the  $\text{CO}_2$  uptake of the nitrifying biomass is proportional to the growth of autotrophic biomass.

$$r_{A,\text{CO}_2} = [r_{X_A} \cdot i_{C,X_A}] \cdot \frac{44}{12} \quad \left[ \frac{\text{g CO}_2}{\text{m}^3 \text{d}} \right] \tag{6.10}$$

Excess  $\text{CO}_2$  is released to the liquid phase or  $\text{CO}_2$  is taken up from the liquid phase in case of net consumption. In the liquid phase, the following equilibrium reactions with their corresponding dissociation constants  $K_1$  and  $K_2$  play an important role.



Note that the concentrations of the different components are expressed here in molar units. The production rate of bicarbonate can thus be written as

$$r_{\text{HCO}_3^-} = 44 \cdot \left( k_1[\text{CO}_{2,aq}] - k_{-1}[\text{HCO}_3^-][\text{H}^+] + k_2[\text{CO}_{2,aq}][\text{OH}^-] + k_{-2}[\text{HCO}_3^-] \right) \left[ \frac{\text{g CO}_2}{\text{m}^3 \text{d}} \right] \tag{6.12}$$

The production of  $\text{CO}_2$ , combined with the equilibria described above, gives rise to the following mass balance equations:

$$\begin{aligned}
V_L \frac{d[\text{CO}_{2,aq}]}{dt} &= \frac{r_{\text{CO}_2}}{44} V_L - \frac{r_{\text{HCO}_3^-}}{44} V_L - \phi_{\text{CO}_2}^{L \rightarrow G} + \phi_{\text{CO}_2}^L \\
V_L \frac{d[\text{HCO}_3^-]}{dt} &= \frac{r_{\text{HCO}_3^-}}{44} V_L + \phi_{\text{HCO}_3^-}^L
\end{aligned} \tag{6.13}$$

whereby  $V_L$  is the volume of the liquid phase,  $\phi_{\text{CO}_2}^L$  and  $\phi_{\text{HCO}_3^-}^L$  are the transport terms of  $\text{CO}_2$  and  $\text{HCO}_3^-$  in the liquid phase.

The mass transfer between gas and liquid phase for carbon dioxide is expressed as

$$\phi_{\text{CO}_2}^{L \rightarrow G} = \text{CTR} = K_L a^{\text{CO}_2} \cdot \left( [\text{CO}_{2,aq}] - [\text{CO}_{2,aq}]^{\text{sat}} \right) \cdot V_L \tag{6.14}$$

with

$$[\text{CO}_{2,aq}]^{\text{sat}} = \frac{P_{\text{CO}_2}}{H_{\text{CO}_2}} \tag{6.15}$$

where  $H_{\text{CO}_2}$  is the Henry constant for  $\text{CO}_2$  ( $\text{atm}^{-1}\text{M}$ ), typically about  $28.6 \text{ atm}^{-1}\text{M}$  at 273 K (Sander, 1996).

## 6.4 Experiment set-up

The load shift experiment that was modelled, was performed during the time period between January 17 and April 14, 2000. On February 22<sup>nd</sup> the loading to the filter was lowered. At the same time, after a new air pump came into use, the air flow rate through the filter was increased from 11 to 15 l/min. In general, two sets of samples were taken a day, including measurements in the influent, the effluent and the water in the pumping reservoir. Because of the poor settling properties of the trickling filter sludge and therefore the difficulty to calculate sludge balances and because of the large water hold-up in the clarifier, it was removed from the set-up.

The samples were tested for total COD (COD<sub>t</sub>), soluble COD (COD<sub>s</sub>), ammonium, nitrate, nitrite, total nitrogen and total inorganic carbon (TIC). All analysis, except the TIC were done using Dr. Lange test kits (Dr. Bruno Lange GmbH). To measure the soluble COD, samples were filtered through a 0.45  $\mu\text{m}$  filter. The TIC concentration was measured using the titration technique developed by Van Vooren *et al.* (1999) as described earlier.

## 6.5 Results

### 6.5.1 Influent characterisation

#### 6.5.1.1 COD and nitrogen measurements

As mentioned before, the influent composition was measured twice a day. Note that some nitrate nitrogen was measured in the influent since the concentrated influent solution was mixed with tap water before being fed to the trickling filter. The results of these measurements were quite unreliable, especially for COD, despite the fact that a constant influent composition was used, the influent was stored in the fridge and was continuously mixed (Table 6.1). Measurements of the off-gas concentrations of both oxygen and carbon dioxide were however rather stable, showing that the load to the filter was constant. The reasons for these poor measurement results should be sought in the difficulty to take representative samples of the filter influent. Due to the dilution mechanism, a large volume was needed to obtain a well mixed sample of the filter influent. On the other hand, the use of a large sample size disrupts the filter's operation quite drastically. Moreover, the mixing of the samples is very critical since the sample size used in the Dr. Lange test kits is only 2 ml for COD analyses.

**Table 6.1. Measured influent concentrations at high and low loading conditions (mg/l)**

	Total N	NO <sub>3</sub> <sup>-</sup> -N	NO <sub>2</sub> <sup>-</sup> -N	NH <sub>4</sub> <sup>+</sup> -N	COD <sub>t</sub>	COD <sub>s</sub>	SS
High load	37.4±11.9	4.9±1.3	0.31±0.29	30.2±4.9	268±125	81±45	176±55
Low load	20.5±4.7	4.2±0.9	0.21±0.27	10.8±2.9	96±43	27±11	92±46

For this reason, an extra set of measurements was performed to produce an influent file for the simulations. For this reason, samples were taken from a carefully mixed concentrated influent batch. Dilution was done manually and measurements were performed on a well mixed sample of this diluted influent. A set of 10 independent measurements was carried out this way (Table 6.2).

**Table 6.2. Influent COD concentrations at high and low loading conditions (mg/l)**

	COD <sub>t</sub>	COD <sub>s</sub>
High load	506±21	117±17
Low load	168±14	57±12

These measurements clearly show that the initially measured COD concentrations were quite low compared to the set of independent test measurements. This indicates the importance of a well mixed and homogenised sample for COD measurements with a small test volume.

### 6.5.1.2 Influent fractionation

The model description of the trickling filter contains four COD-components:  $S_s$  (readily biodegradable substrate),  $S_I$  (soluble inert organic matter),  $X_s$  (slowly biodegradable substrate) and  $X_I$  (particulate inert organic matter). This means the influent to the filter also has to be divided into these fractions to be able to use the measurements as an information source for the simulation. The subdivision of the total COD over the four model components (the biomass concentration in the influent is assumed to be 0), is given in Table 6.3. The fractions of the soluble and particulate inerts are deliberately kept low, because the influent composition is known and does not contain considerable amounts of non biodegradable substances. As can be seen, the soluble part in the simulator influent does not agree with the COD<sub>t</sub>/COD<sub>s</sub> relationship that was measured. After some initial simulations using the measured COD<sub>t</sub>/COD<sub>s</sub> relationship, the fraction of readily biodegradable substrate was drastically increased to the detriment of the slowly biodegradable substrate. As confirmed by respirometric tests of the substrate (Boeije, 1999), part of the particulate (or colloidal) COD is most certainly rapidly hydrolysed in the filter's bulk liquid phase and in the pumping reservoir. Also for other reasons, stated further in this chapter, the relative increase of the readily biodegradable substrate fractions was needed.

**Table 6.3. Influent COD concentrations at high and low load (mg/l)**

	$S_I$	$S_s$	$X_I$	$X_s$
High load	10	396	10	90
Low load	3	132	3	30

Modelling the influent requires four nitrogen components to be specified:  $S_{NO}$  (nitrate and nitrite nitrogen),  $S_{NH}$  (ammonium nitrogen),  $S_{ND}$  (soluble biodegradable organic nitrogen) and  $X_{ND}$  (particulate biodegradable organic nitrogen). Since – except for  $X_{ND}$  – these components are dissolved and the measurement results were better compared to the COD measurements, the daily measurements for the nitrogen components could be used directly. Organic nitrogen was calculated by subtracting the ammonium and nitrate concentration from the measured total nitrogen concentration. The organic nitrogen  $S_{ND}$  and  $X_{ND}$  was subdivided using a simple 1-to-1 proportion (Table 6.4).

**Table 6.4. Averaged measurement values and influent compositions of nitrogen compounds at high and low loading conditions (mg/l)**

<i>High load</i>			
<i>Averaged measurement values</i>		<i>Influent composition</i>	
$\text{NO}_3^-$ -N	4.9	$S_{\text{NO}}$	4.9
$\text{NH}_4^+$ -N	30.2	$S_{\text{NH}}$	30.2
$N_{\text{tot}}$	37.4	$S_{\text{ND}}$	3.6
		$X_{\text{ND}}$	3.6

<i>Low load</i>			
<i>Averaged measurement values</i>		<i>Influent composition</i>	
$\text{NO}_3^-$ -N	4.2	$S_{\text{NO}}$	4.2
$\text{NH}_4^+$ -N	10.8	$S_{\text{NH}}$	10.8
$N_{\text{tot}}$	20.5	$S_{\text{ND}}$	2.8
		$X_{\text{ND}}$	2.8

### 6.5.1.3 Influent TIC measurements

As mentioned before, measurements of the TIC concentrations were performed. These measurements were needed so as to correctly use the off-gas concentration measurements of  $\text{CO}_2$  and  $\text{HCO}_3^-$ . The TIC concentration of the influent was determined using the titration technique (Van Vooren *et al.*, 1999). After this, the  $\text{CO}_{2,\text{aq}}$  and  $\text{HCO}_3^-$  concentrations were calculated using the chemical equilibria. Table 6.5 shows the average measured values of these compounds. The equilibrium reactions of the TIC are strongly dependent on the *pH* in the sample. Therefore, influent *pH* was measured during the experiments. The average influent *pH* during the course of the experiments was 7.66.

**Table 6.5. Influent TIC concentrations at high and low load ( $\text{mol/m}^3$ )**

	$\text{CO}_{2,\text{aq}}$	$\text{HCO}_3^-$
High load	$0.34 \pm 0.06$	$7.47 \pm 1.30$
Low load	$0.27 \pm 0.04$	$5.96 \pm 0.81$

## 6.5.2 Effluent characterisation

### 6.5.2.1 COD and nitrogen measurements

In the effluent, daily measurements were performed for COD and nitrogen compounds. The results of these measurements can be seen in Table 6.6. From this table, the increase of the nitrate concentration after the load shift experiment is clear. This indicates an increased nitrification in the filter. Indeed, more oxygen becomes available for this process once the organic loading to the filter is lowered.

**Table 6.6. Measured effluent concentrations at high and low loading conditions (mg/l)**

	Total N	$\text{NO}_3^-$ -N	$\text{NO}_2^-$ -N	$\text{NH}_4^+$ -N	COD <sub>t</sub>	COD <sub>s</sub>	SS
High load	$26.5 \pm 8.2$	$7.4 \pm 2.1$	$0.74 \pm 0.32$	N.A.	$72 \pm 25$	$23 \pm 12$	$64 \pm 45$
Low load	$16.0 \pm 4.6$	$11.4 \pm 3.0$	$0.55 \pm 0.31$	$2.2 \pm 1.8$	$44 \pm 26$	$7 \pm 3$	$36 \pm 46$

When the start-up period of nitrification (from February 22<sup>nd</sup> to March 2<sup>nd</sup>) is not included, the average effluent nitrate concentration at low loading conditions was 13.0 mg/L. In this case, the average ammonium concentration was 1.76 mg/l.

### 6.5.2.2 Off-gas and effluent TIC measurements

Concentrations of CO<sub>2</sub> and O<sub>2</sub> were registered on-line by the off-gas measurement equipment (Figure 6.2). It is clear that the off-gas O<sub>2</sub> concentration increases and the CO<sub>2</sub> concentration drops after the load shift. The drop of the O<sub>2</sub> concentration is clearly caused by a decreased activity of the heterotrophic biomass, possibly slightly compensated by an increased activity of the autotrophic biomass using CO<sub>2</sub> as a carbon source.

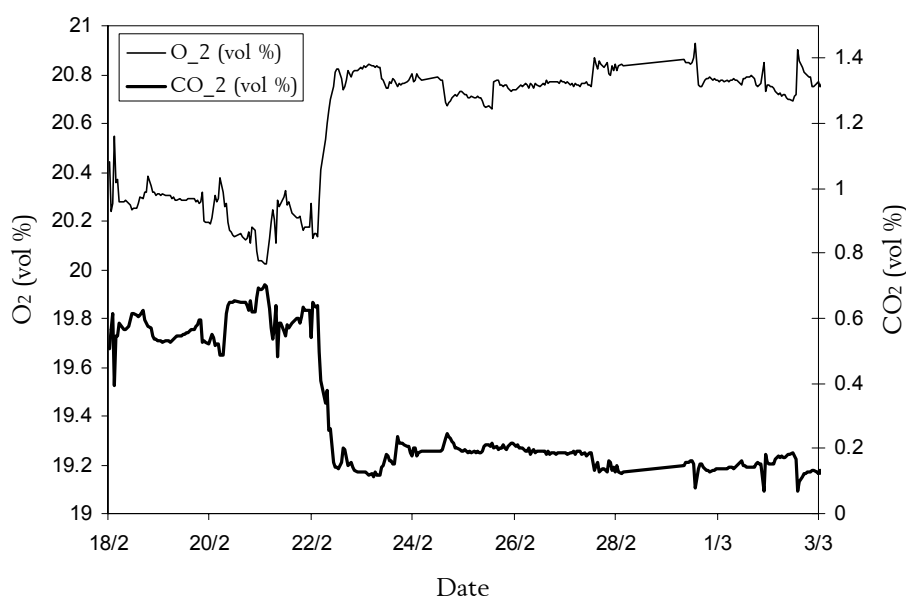


Figure 6.2: On-line measurement results of the O<sub>2</sub> and CO<sub>2</sub> concentrations in the filter's off-gas

Table 6.7 shows the average off-gas CO<sub>2</sub> and O<sub>2</sub> concentrations before and after the load shift experiment. Also, measurements of the TIC concentration of the effluent were done. The effluent CO<sub>2, aq</sub> concentration was 0.34 mol/m<sup>3</sup> before and 0.22 mol/m<sup>3</sup> after the load shift experiment. For HCO<sub>3</sub><sup>-</sup> this was 7.35 and 5.83 mol/m<sup>3</sup> respectively.

Table 6.7. Averaged off-gas concentrations at high and low loading conditions (vol%)

	CO <sub>2</sub>	O <sub>2</sub>
High load	0.56	20.27
Low load	0.15	20.77

## 6.6 Model development in WEST

Figure 6.3 shows the layout of the filter in the WEST simulator. The number of tanks and their respective volumes were determined using the tracer test described in the previous chapter.

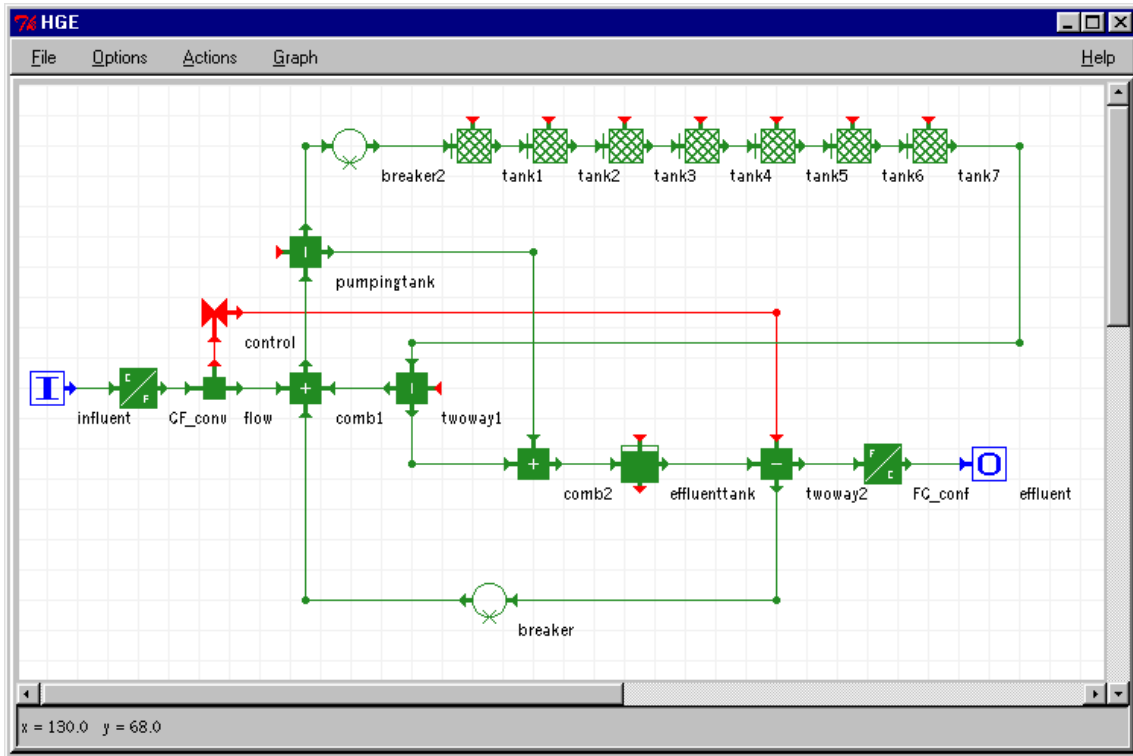


Figure 6.3. Filter layout in the simulator WEST (Hemmis NV, Kortrijk, Belgium)

For the modelling of the biochemical conversions in the filter, the simplified mixed-culture biofilm model was used. In order to respect the mass balances, the model based on the total masses of soluble components in the system was implemented (paragraph 4.6.2). To describe the off-gas measurements in the model, a gas phase compartment had to be included. The gas phase is modelled as one single mixed tank. This gas phase is linked to each biofilm compartment as shown in Figure 6.4. The volume of the gas phase could be calculated from the internal volume of the filter column and the approximate void volume of the carrier material. Theoretically, a gas volume of 200 l should be implemented. However, biomass growth and water hold-up could have a considerable influence on this volume.

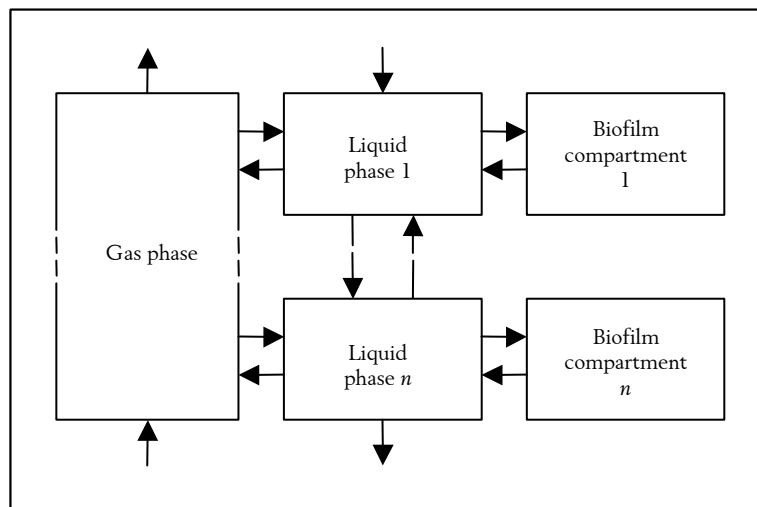


Figure 6.4: Introduction of the gas phase compartment in the trickling filter model

Therefore, the actual gas volume was checked using the gas phase measurements after a change of the air flow rate in the filter. The air flow in the filter was stopped for several hours and then started up again. The actual gas phase volume could be checked by fitting a simple gas phase mass balance to the measured off-gas concentrations.

$$\frac{d}{dt}(V_G C_G) = Q_{G,in} C_{G,in} - Q_{G,out} C_{G,out} - V_L K_L a (C_L^{sat} - C_L) \quad (6.16)$$

Assuming a perfect mixing of the gas phase in the filter at a reasonably high flow rate, the gas phase concentration of both O<sub>2</sub> and CO<sub>2</sub> could be assumed homogeneous. Assuming that the  $K_L a$  at a given air flow rate is constant, this equation can in a steady state case be simplified to:

$$\frac{1}{V_G} (Q_{G,in} C_{G,in} - Q_{G,out} C_{G,out}^{steady-state}) = \frac{V_L}{V_G} K_L a (C_L^{sat} - C_L) \quad (6.17)$$

Introducing this into equation 6.16 and integrating gives:

$$C_{G,out}(t) = C_{G,out}^{steady-state} + (C_{G,out}(0) - C_{G,out}^{steady-state}) \exp\left(-\frac{Q_{G,out} t}{V_G}\right) \quad (6.18)$$

Both O<sub>2</sub> and CO<sub>2</sub> profiles were used to fit the above formulae. As an example, the optimal fit to the CO<sub>2</sub>-profile is given in Figure 6.5. With a coefficient of determination  $R^2$  of 0.98, an estimated gas phase volume of 168 l was found. This agrees very well with the estimated gas phase volume. At the time of the experiment the weight of the filter was about 97 kg. Subtracting the dry weight of the filter leads to about 34 kg (or 34 l assuming a density of 1 kg/l) of biomass and water is present in the filter, giving an estimated volume of 166 l.

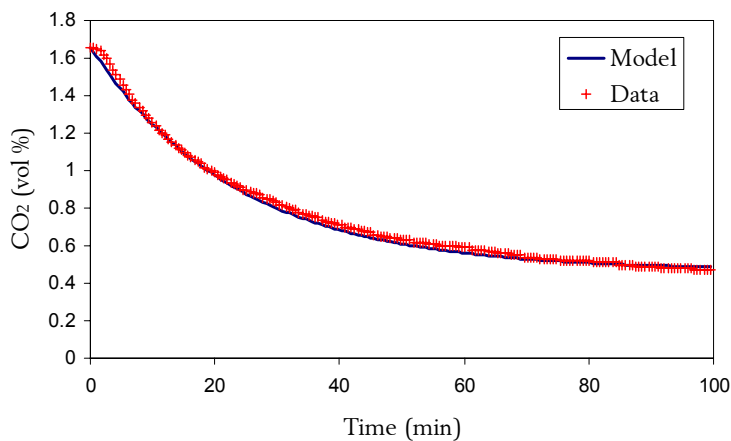


Figure 6.5: Optimal fit of the gas phase mass balance model to the CO<sub>2</sub> concentration profile

## 6.7 Model description of the filter before the load shift

As a start, a steady-state simulation was carried out so as to model the measured effluent concentrations and the off-gas measurements as accurately as possible.

### 6.7.1 Initial choice of the parameters

When carrier material units were removed from the filter for reasons of batch experiments, it became clear that far from the complete surface of the carriers was covered by a biofilm. It should be noted that this is not unusual in trickling filter systems using this type of carrier material. Furthermore, on the inner wall of the filter, four horizontal rings (with a width of 5 cm) were placed to avoid short circuit flows in the filter. This construction may have led to a bad wetting of some of the carrier material at the outside of the filter column. Next, the specific surface area of the carrier material is measured based on a large bulk volume of carrier material units. This might not be a good representation of the actual specific volume in the filter due to the small volume and the wall effect. For these reasons, an initial estimation of the specific surface area in the filter available for biomass growth was done from the oxygen uptake measurements rather than from the filter's volume.

Before the load shift, the oxygen uptake in the filter was 0.68 vol%, at an air flow rate of 11 l/min. This indicates an oxygen consumption of 143.4 g/d. As the oxygen uptake of biofilms in trickling filter systems is on average 10 g O<sub>2</sub>/m<sup>2</sup>.d (Logan, 1993; Hinton and Stensel, 1994), the available surface area for biomass growth was initially estimated to be 14.3 m<sup>2</sup> instead of the estimated total carrier area of 46.86 m<sup>2</sup>. This surface area was subdivided equally among the 7 tanks of the filter.

Other kinetic and stoichiometric parameters were taken from the Activated Sludge Model No 1 (Henze *et al.*, 1987).

Parameters specific to biofilm systems were estimated using reviews by Henze *et al.* (1995) and Horn and Hempel (1995) (Table 6.8). For the biofilm density, the measured density of 38.8 kg/m<sup>3</sup> was used.

**Table 6.8. Overview of the diffusion constant values in the model (cm<sup>2</sup>/d)**

Name	Description	Initial Value
$D_{f,S_o}$	Diffusion constant for $S_O$	2.1
$D_{f,S_s}$	Diffusion constant for $S_S$	0.58
$D_{f,S_{no}}$	Diffusion constant for $S_{NO}$	1
$D_{f,S_{nh}}$	Diffusion constant for $S_{NH}$	1.8

### 6.7.2 Model calibration

From the initial simulation using the compiled parameter set and the COD<sub>t</sub>/COD<sub>s</sub> relationship that was found using the COD measurements, it became clear that the model predicted substrate limitation in the entire filter. This result was not expected, since a respirometric assay on the effluent of the filter, following the procedure published in Spanjers and Vanrolleghem (1995), showed that some, although very limited, readily biodegradable substrate was leaving the reactor at these loading conditions. However, as mentioned before, only the soluble COD (COD<sub>s</sub>) was used in these simulation runs to estimate the readily biodegradable COD of the influent. From respiration tests with the synthetic wastewater from which the influent composition of the pilot-scale trickling filter was derived, it was estimated that more than 50% of the total COD of the medium can be considered readily biodegradable (Boeije, 1999). Moreover, it is clear that quite some material with a colloidal or

particulate nature is readily hydrolysed in wastewater treatment. Also in biofilm wastewater treatment, the biomass releases extracellular enzymes to hydrolyse substances with a molecular weight that is too high to diffuse into the biofilm directly (*e.g.* starch) (Henze *et al.*, 1995). Especially because of the quite high recirculation ratio used in the pilot-scale trickling filter plant, this bulk liquid hydrolysis process is a major influence in the biodegradation. Instead of integrating the release of extracellular enzymes in the model description – for which insufficient data was available – or incorporating an extra substrate in the model, the  $S_y/\text{COD}_t$  ratio was increased in the influent partitioning (see section 6.5.1.2).

Furthermore, the oxygen transfer from the liquid phase to the biofilm had to be adjusted so as to provide the biomass with enough oxygen to degrade the substrate. A  $K_L a$  value of  $2700 \text{ d}^{-1}$  was incorporated for  $\text{O}_2$ . Since it can be shown that  $(K_L a)_{\text{CO}_2} \cong 0.9 \cdot (K_L a)_{\text{O}_2}$  (Spérandio and Paul, 1997), the  $K_L a$  for  $\text{CO}_2$  was set to 2430. The results from the above manipulations were that an oxygen limited regime was established in the upper five tanks of the filter. The simulated off-gas  $\text{O}_2$  concentration was 20.28 vol%, the  $\text{CO}_2$  concentration in the simulations was 0.54 vol%. These values agree very well with the measurement results (Table 6.7).

Next, the simulated outflow total COD concentration was fitted to the measurement results. It was very difficult to simulate the actual fluctuation of the effluent COD<sub>t</sub> and SS measurements. Indeed, to avoid biofilm growth in the pumping reservoir, this reservoir was cleaned every day. During this cleaning process, the suspended solids in the pumping tanks were removed which caused a discontinuous removal of suspended solids from the bulk liquid in the filter system. Instead of modelling this discontinuous process, the effluent COD<sub>t</sub> was modelled using a pointsettler with a fixed removal of suspended solids. This way the effluent COD<sub>t</sub> could easily be fitted to the average measurement value of 72 mg/l. The simulated result was 71.3 mg/l.

In Table 6.9, a comparison is made between the measured and simulated effluent concentrations and fluxes before the load shift experiment. In addition, the carbon fluxes leaving the trickling filter systems are calculated. Note that the carbon fluxes leaving the filter in the gas phase and in the liquid phase are in the same order of magnitude. Fluxes are calculated using the measured output air flow rate in the trickling filter systems: 11 l/min or  $15.84 \text{ m}^3/\text{d}$ . The influent and effluent liquid flow rate were  $0.418 \text{ m}^3/\text{d}$ .

**Table 6.9. Comparison between measured and simulated outflow concentrations and fluxes**

Compound	Measured		Simulated	
	Concentration	C-Flux (g C/d)	Concentration	C-Flux (g C/d)
COD <sub>t</sub> (mg/l)	72		71.3	
Total N (mg/l)	26.5		14.17	
$\text{O}_2$ (vol%)	20.27		20.28	
$\text{CO}_2$ (vol%)	0.56	44.28	0.54	42.69
$\text{CO}_{2,\text{aq}}$ (mol/m <sup>3</sup> )	0.34	1.70	0.31	1.55
$\text{HCO}_3^-$ (mol/m <sup>3</sup> )	7.35	36.83	6.98	34.98

## 6.8 Model description of the filter after the load shift

Using the low load influent characterisation given in Table 6.3 to Table 6.5, the load shift experiment was simulated. Quickly after the start of the simulated period, it became clear that the conversions in the filter were completely ammonium limited, which made that the measured COD-removal could not be simulated. To remedy this problem, the ammonification constant ( $k_a$ ) in the model was increased from 0.05 to 0.1  $\text{m}^3/(\text{g COD}\cdot\text{d})$ . This way, more organic nitrogen is converted to ammonium that becomes available for the biomass. A further increase would have meant that all soluble organic nitrogen ( $S_{ND}$ ) would have been converted to  $S_{NH}$ , which is unrealistic because of the organic nitrogen found in the filter effluent (Table 6.11). However, still the  $S_{NH}$  concentration is underestimated in the filter effluent.

A possible explanation is ammonium storage in the filter system. Excess ammonium that has been adsorbed onto the biomass during high loading periods could be released when the influent loading is low. This could result in relatively slow ammonium effluent concentration changes following step changes in the influent load. Nielsen (1996) showed that ammonium adsorption to activated sludge flocs is possible. Wik (1999) was not able to repeat such adsorption measurements in biofilm systems, but only a model including ammonium adsorption into the biofilm was able to simulate the relatively slow ammonium effluent concentration changes after step changes in the ammonium influent concentration. Also a cyclic re-use of nitrogen compounds seems to be possible. It is known that several compounds can be used and re-used in a biofilm without a corresponding high concentration in the influent. Lens *et al.* (1995) were able to show a sulphur cycle in the biofilm, where sulphide formed in the biofilm is oxidised in situ to sulphate so that sulphate reducing bacteria in the biofilm can survive without correspondingly high sulphate concentrations in the influent to the biofilm system. Is it possible that organic nitrogen released during biomass decay or hydrolysis of particulates in the biofilm is ammonified in situ and is used directly again for biomass growth in the biofilm. This means that the net ammonium consumption of the biomass in the biofilm is lower compared to what is expected in the model. This situation could be mimicked in the simulations by lowering the nitrogen content  $i_x$  of the biomass in the biofilm, so indeed the net nitrogen consumption would decrease.

To be considered too is the assumption that no mass transfer resistance between the bulk liquid and the biofilm is present. If this resistance would be integrated in the model, then the ammonium concentration in the bulk liquid would need to be higher for ammonium to diffuse to an equal depth in the biofilm. In a later stage of the research, this model became available. It was successfully used to describe liquid film mass transfer resistance in chapter 10.

An overview of the final parameter set used during the modelling of the load shift experiment is given in Table 6.10, while Table 6.11 gives a comparison between measurements and simulation results using this parameter set.

The increase of the air flow rate from 15.84  $\text{m}^3/\text{d}$  to 21.6  $\text{m}^3/\text{d}$  was incorporated in the calculations of the C-fluxes in Table 6.11. The simulated effluent values are relatively close to the measured effluent variables. However, especially in the off-gas concentrations, a quite high discrepancy can be seen. The following paragraphs focus especially on this discrepancy.

**Table 6.10. Parameters used in the simulations**

<i>Parameter</i>	<i>Value</i>	<i>Changed</i>
$\mu_H$ (1/d)	4	
$Y_H$ (gCOD/gCOD)	0.6	
$b_H$ (1/d)	0.4	
$\mu_A$ (1/d)	0.15	
$Y_A$ (gCOD/gN)	0.1	
$b_A$ (1/d)	0.01	*
$k_h$ (1/d)	6	*
$k_a$ (1/d)	0.1	*
$i_X$ (gN/gCOD)	0.08	
$f_p$ (-)	0.08	
$k_{at}$ (-)	4	*
$k_{dt}$ (-)	0.05	*
$\rho_m$ (kg/m <sup>3</sup> )	38.8	*

**Table 6.11. Comparison between measured and simulated outflow concentrations and fluxes**

<i>Compound</i>	<i>Measured</i>		<i>Simulated</i>	
	<i>Concentration</i>	<i>C-Flux (g C/d)</i>	<i>Concentration</i>	<i>C-Flux (g C/d)</i>
CODt (mg/l)	44		35	
Total N (mg/l)	16.0		16.2	
$NO_3^-$ (mg N/l)	11.4		13.4	
$NH_4^+$ (mg N/l)	1.2		0.002	
$O_2$ gas (vol%)	20.77		20.67	
$CO_2$ gas (vol%)	0.15	16.20	0.27	29.11
$CO_{2,aq}$ (mol/m <sup>3</sup> )	0.22	1.10	0.17	0.85
$HCO_3^-$ (mol/m <sup>3</sup> )	4.83	24.20	4.41	22.09

### 6.8.1 Carbon balance of the trickling filter system at low loading conditions

At high loading conditions, a difference of only 0.12 mol/m<sup>3</sup> of total inorganic carbon in the liquid phase was measured between influent and effluent of the trickling filter system. At low loading conditions, as much as 1.18 mol/m<sup>3</sup> TIC (51 mg CO<sub>2</sub>/l) is removed from the water phase in the filter system. As the flow rate is 0.418 m<sup>3</sup>/d, the net C-flux removed from the water phase is 5.91 g C/d. The gas phase concentration of CO<sub>2</sub> is increased with 0.1 vol% during the passage through the filter. Using the measured air flow rate of 21.6 m<sup>3</sup>/d and the ideal gas law at 20°C, this means a net C-flux of 10.81 g C/d leaves the filter through the gas phase. Subtracting the 5.91 g C/d that is removed from the water phase from the 10.81 g C/d that enters the gas phase, leaves 4.9 g C/d to be produced by the biomass in the filter. In the simulations however, the net carbon production by the biomass is estimated to be 15.5 g C/d, including the 1.5 g C/d that is consumed by the autotrophic organisms for growth. Obviously, using these measurements, the mass balance of the measurements after the load shift is not correct (Figure 6.6).

A possible explanation for this discrepancy is the replacement of the gas pump at the same time the load shift experiment started. After investigating this problem, it was concluded that during the second part of the experiment (after lowering the load to the system), the connection between the air pump and the filter was not completely air tight. This way, fresh air could come into the off-gas tubing and dilute the filter's off-gas. The simulation results which give a quite good fit for all the compounds except for the off-gas concentrations, confirm these findings. Therefore a new series of measurements was performed at low loading.

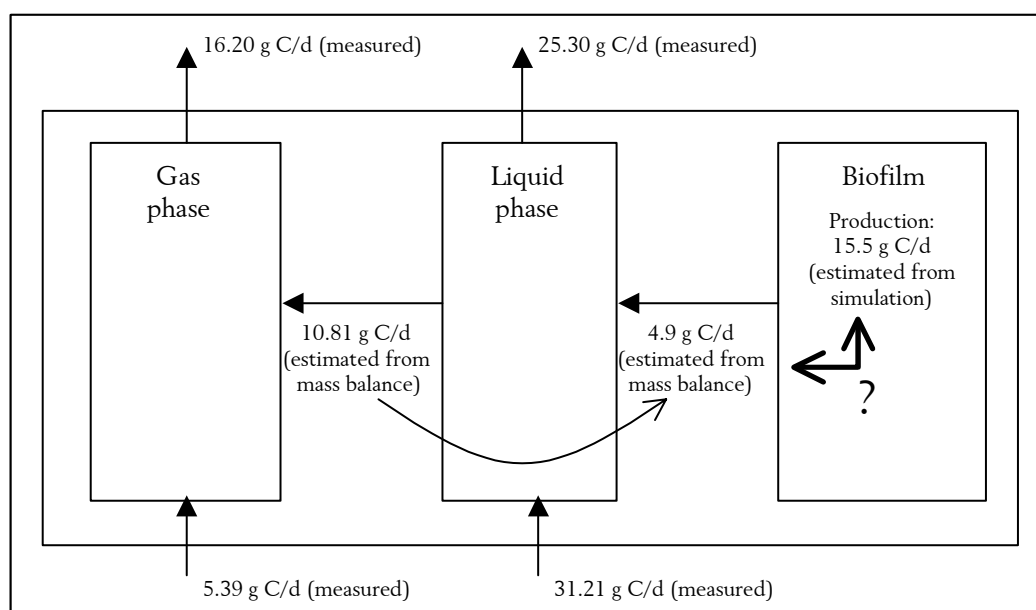


Figure 6.6: Carbon balance of the trickling filter system after the load shift (low loading)

### 6.8.2 Repeated off-gas measurements at low loading

After the data analysis and the model description of the load shift, the possibility of the existence of a leak in the off-gas collection system was investigated. A leak was found which was indeed caused by the installation of a new gas pump in the experimental set-up. The situation was fixed and a new period with a low influent load to the trickling filter systems was studied. The off-gas concentrations recorded during that period, using the same air flow rate as was used during the low load period in the initial experiment, are shown in Table 6.12. For reasons of availability of the measurement equipment, it was not possible to repeat the TIC measurements during this measurement period. There is, however, no reason to assume the results would have deviated significantly from the first measurement period results. When these off-gas measurement results are included in the carbon balance computed in Figure 6.6, it is possible to close the balance. This supports the quality of the conversion rates computed using the simplified mixed culture biofilm model.

Table 6.12. Averaged measured off-gas concentrations at low loading conditions (vol%)

	CO <sub>2</sub>	O <sub>2</sub>
High load	0.25±0.03	20.68±0.04

### 6.8.3 Nitrification and denitrification in the trickling filter after the load shift

As shown in the effluent characterisation after the load shift, a start-up of the nitrification activity could be seen in the filter at low load. A decrease of the ammonium concentration and an increase of the nitrate concentration was noticed. However, in the simulation, this nitrification start-up was not reproduced. The simulated concentration of nitrifying biomass in the filter was very low after a relatively elongated period of high loading conditions. In reality, the high loading rate was maintained in the filter for a period of 7 weeks after it had been working at relatively low loading rate for several months before. After these 7 weeks, there was obviously still some nitrifying biomass present in the filter that could immediately start to nitrify when the conditions became favourable. Thus, some niches in the biofilm system were present where nitrifying biomass could survive high loading conditions even for prolonged periods. Wik (1999) also noticed that nitrifying biomass stayed present in the system for longer periods than expected from the loading conditions. He concluded the nitrifying biomass was in a “dormant” state instead of dying off completely.

To remedy this modelling problem, the decay coefficient of the autotrophic biomass ( $b_a$ ) was decreased from 0.05 down to  $0.01 \text{ d}^{-1}$ . This ensured that the autotrophic bacteria did not completely die off during the high loading period and a reasonable amount of autotrophs remained in the system to start up the nitrification after the load shift. The start-up of the nitrification activity can be followed on Figure 6.7 and Figure 6.8. In Figure 6.7, a temporary increase of the ammonium concentration after the load shift was observed, the reason for which is not clear. It was not attempted to describe this by the simulations.

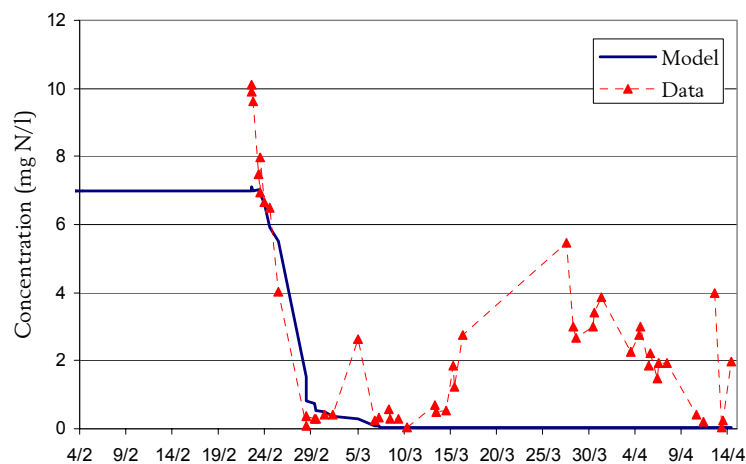
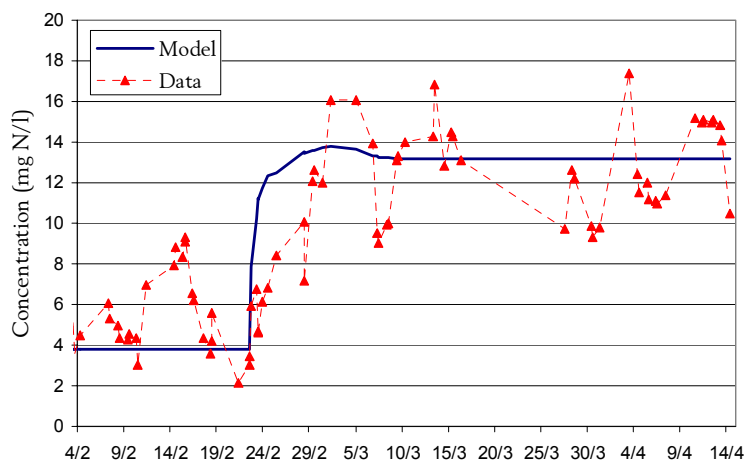


Figure 6.7: Measured and simulated ammonium concentration after the load shift experiment



**Figure 6.8: Measured and simulated nitrate concentration after the load shift**

To check the hypothesis of a slow decay of autotrophic biomass at high COD loading rate, several batch test experiments were conducted parallel to the load shift (Tremblay, 2000). In these experiments, carriers from different sites in the pilot-scale filter (top, middle and bottom) were removed from the filter and placed in an aerated beaker of 0.5 l. Before putting the carriers in the beaker, they were gently washed with demineralised water to remove loosely adhering biomass. The aeration of the water in the beakers was regulated so that an oxygen concentration of 5 mg/l was sustained. The water in which the carriers were submerged was tap water. This was needed to supply alkalinity to the biomass and provide for enough buffering capacity to keep the *pH*-fluctuations during the experiments rather small, since no *pH* control was implemented. Note that the tap water used contains some nitrate. The beakers with the carriers were allowed to stabilise overnight, so as to remove as much of the readily biodegradable COD in the samples as possible. Indeed, some biodegradable COD is generated from hydrolysis of particulate matter in the biofilm and may be used for aerobic metabolism or even denitrification. The results show that denitrification took place in the carriers that were submerged in the aerated medium. It is obvious from the results that the denitrification was more pronounced at the top and in the middle of the filter. There, the biofilm was clearly thicker than at the filter bottom, so anoxic and anaerobic zones were more likely to be present. Also more of the particulate hydrolysable material is retained at the top of the filter, so more readily biodegradable substrate (and ammonium) from hydrolysis was available there (Figure 6.9, figure shown is for carriers taken during low loading conditions).

After the stabilisation period a pulse of ammonium was added to the liquid phase, so that a bulk liquid concentration of about 5 mg/l of  $NH_4^+-N$  was attained (Figure 6.10). The nitrate and ammonium concentration was then followed over the next hours to obtain information about the nitrification capacity of the biomass on the carriers. The batch test experiments were performed after the filter had been allowed to stabilise for five weeks at high and low loading conditions. Estimated nitrogen conversion rates during the batch experiments can be found in Table 6.13 and Table 6.14.

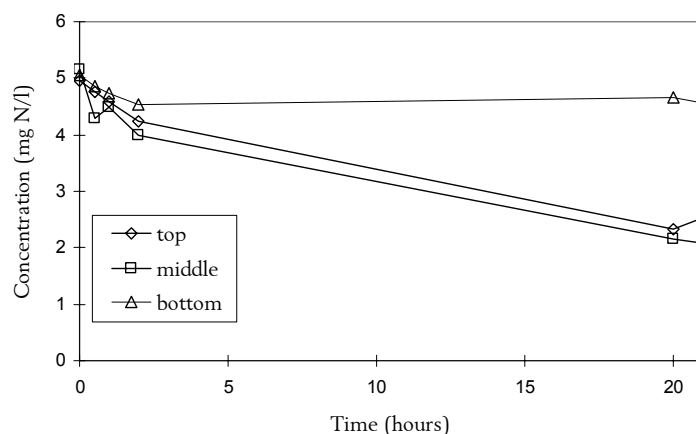


**Figure 6.9:** Evolution of the nitrate nitrogen concentration in the batch test during the overnight stabilisation period (low loading situation)

**Table 6.13.** Estimated nitrogen production and consumption rates during high loading conditions (mg N/h) (averages from 2 batch tests)

	<i>Top</i>	<i>Middle</i>	<i>Bottom</i>	<i>Average</i>
$NO_3^-$ production rate	0.4329	0.4813	0.4447	0.4530
$NH_4^+$ consumption rate	0.6833	0.7304	0.7116	0.7084

**Table 6.14.** Estimated nitrogen production and consumption rates during low loading conditions (mg N/h) (averages from 2 batch tests)

	<i>Top</i>	<i>Middle</i>	<i>Bottom</i>	<i>Average</i>
$NO_3^-$ production rate	0.5459	0.6465	0.6948	0.6291
$NH_4^+$ consumption rate	0.7158	0.7222	0.7695	0.7258

It can be seen that the  $NH_4^+$  consumption rate was not significantly different at high compared to low loading conditions (Tukey test,  $\alpha = 0.05$ ). However, the  $NO_3^-$  production rates were significantly different. Within the experiments at high and low loading, no significant differences could be found between the top, middle and bottom part of the filter. It could thus be concluded that nitrification activity decreased at high loading conditions, but that the rate of inactivation of the autotrophic biomass was relatively slow in the biofilm. This observation supports the choice of a lower decay coefficient in the model description of the filter. It is interesting to note that, although most of the particulate material was probably retained at the top of the filter, no significant difference could be found between the nitrification activity at the top and at the bottom of the filter.

Note also that the  $NH_4^+$  conversion rate was the same in the batch experiments conducted during the high and low loading period. Since the nitrifying activity was different, this indicates that certainly some degree of aerobic and/or anoxic heterotrophic activity was present during the batch tests that incorporated some ammonium into biomass. This is especially pronounced during the high loading period. The extra hydrolysis present in this situation probably enhanced heterotrophic activity once ammonium was added to the samples.

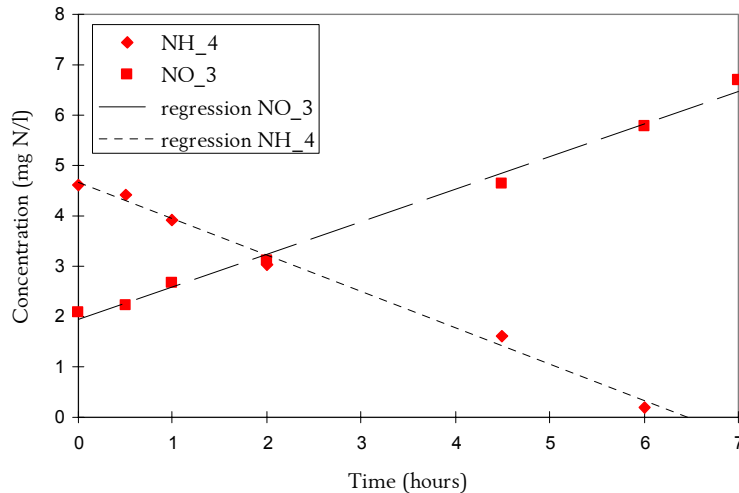


**Figure 6.10: Nitrate and ammonium evolution during a batch test experiment at low loading conditions with a carrier taken in the middle of the filter**

From the simulations of the load shift, it also became clear that before the load shift, a limited amount of denitrification was present in the filter. Basically, the nitrate denitrified was the nitrate in the tap water used for the dilution of the concentrated influent. The simulated nitrate conversion was 5.25 g  $\text{NO}_3^-$ -N/d. No further measurement data were available at this point to verify this simulation data. After the load shift no readily biodegradable organic matter was available in the filter to sustain denitrification. In chapter 7, the denitrification activity in the filter was triggered and investigated by adding additional nitrate to a highly loaded filter system.

## 6.9 Conclusions

A pilot-scale trickling filter was used to investigate the dynamic model description of such a filter's behaviour. Therefore, the filter was subjected to a load shift experiment during a measurement campaign. During this campaign, analysis for the COD and nitrogen content of the water phase at different locations in the filter set-up was measured. Also the off-gas composition for oxygen and carbon dioxide was measured. To be able to use the measurements, extra analyses of the inorganic carbon content of the liquid phase were needed as well as measurements of the *pH* in the filter. A simplified mixed-culture biofilm model was used to model the load shift experiment. This model was extended with a part describing the production and consumption of gaseous components in the filter.

It could be concluded following a drop in the loading of the filter system that the nitrification capacity increased due to a higher availability of oxygen for this process. The start-up of nitrification could be followed using the model provided the decay coefficient for autotrophic biomass was sufficiently low to assure a certain amount of autotrophs to stay in the system at high loading conditions. The hypothesis that nitrifying biomass could survive prolonged periods with high loading in a trickling filter was confirmed with batch tests performed on carrier elements taken out of the filter.

After the load shift, the model underestimated the ammonium concentration in the filter effluent. Ammonium adsorption to the biofilm could result in relatively slow concentration changes following a load shift. Also, a cyclic re-use of nitrogen compounds is possible. In such cycle, organic nitrogen

released during biomass decay or hydrolysis of particulates in the biofilm is ammonified in situ and is used directly again for biomass growth in the biofilm. This means that the net ammonium consumption of the biomass in the biofilm would be lower compared to what was expected in the model.

The off-gas analysis measurements supplied extra information to calibrate the gas-liquid mass transfer coefficient. On top of that, the combined interpretation of the carbon dioxide and the inorganic carbon measurements together with the model calculations made it possible to find a leak in the off-gas collection system. After repairing this leak, it became clear that the model predictions were indeed an accurate description of the filter's behaviour after the load shift.

# 7 Induction of denitrification in a pilot-scale trickling filter by adding nitrate at high loading rate

---

## 7.1 Introduction

Aerobic degradation in a trickling filter, or more generally in all biofilm systems, is mainly limited by the amount of oxygen that can be transferred from the bulk liquid phase to the biofilm. In literature, it has frequently been stated that the oxygen uptake of biofilms in trickling filter systems is on average  $10 \text{ g O}_2/(\text{m}^2\text{d})$  (see among others: Logan, 1993; Hinton and Stensel, 1994). This oxygen can be used for aerobic degradation of organic matter, and, if any oxygen is left after this (fast) conversion process is finished, nitrification can proceed. This basically entails that nitrifying activity in trickling filters only takes place in case the organic loading to the filter is sufficiently low to allow for the growth and activity of autotrophic biomass in the biofilm.

Next to aerobic degradation, a second pathway for the removal of organic matter is denitrification in anoxic zones of the biofilm. At high organic loading rates, and whenever the oxygen supply to the biofilm is insufficient to obtain good treatment capacity, denitrification could be induced by providing the biofilm with an extra portion of electron acceptor besides oxygen. This possibility was tested in the pilot-scale trickling filter by adding a pulse of nitrate to a highly loaded trickling filter. The response was monitored using measurements in the liquid phase and in the off-gas of the filter system. The measured response was also modelled using the simplified mixed culture biofilm model, since this is a particularly good test for the ability of the model to describe degradation in different layers of the biofilm.

Before the test was carried out, the influent composition to the trickling filter was changed. To avoid problems with the identification of the readily biodegradable soluble substrate in the influent as in chapter 6, ethanol was used as a single carbon source for a limited time period. Also, *pH* control of the influent was implemented to facilitate the interpretation of the inorganic carbon measurements in the filters influent and effluent. This is explained below.

## 7.2 Incorporation of *pH* control in the filter set-up

In the previous chapter, the modelling of a load shift experiment was described. During this modelling exercise, the usefulness of carbon balances was illustrated. For instance, the carbon balance made it possible to identify a problem with the off-gas collection system after the incorporation of a new air pump. During the calculation of this carbon balance, it was noticed that the in- and outfluxes of inorganic carbon via the liquid phase are in the same order of magnitude as the carbon fluxes in the off-gas. These high in- and outfluxes make it especially difficult to accurately measure the net flux of

inorganic carbon in the liquid phase, since two relatively large numbers need to be subtracted to obtain these.

Therefore, a method was devised to dramatically decrease the inorganic carbon content of the incoming liquid. This was done by dosing a solution of  $HCl$  (1M) in the tap water reservoir (Watson Marlow 101U, Figure 7.1). The flow rate of the acid was 5 ml/min. In this way, the  $pH$  in this reservoir was decreased to a value of about 4.5. At this  $pH$ , the majority of the inorganic carbon can be stripped out of the reservoir in the form of  $CO_2$ . This was achieved by aerating this vessel with compressed air.

Of course, the low  $pH$  of the influent should be compensated by adding a base solution ( $NaOH$  0.1M) to the set-up. A  $pH$  as low as 4.5 would hamper biological activity in the filter. This adjustment was done in the pumping reservoir (Figure 7.1). Here, a  $pH$  control system adjusted the  $pH$  to a value of 7.0. The control system was made up of a glass electrode (Metrohm, Switzerland) connected to a  $pH$  controller which in turn regulated the opening of a three-way valve, permitting the addition of the  $NaOH$  solution in case the  $pH$  dropped below 7.0.

The constant  $pH$  in the recirculating liquid had the extra advantage of largely eliminating the effect of a fluctuating  $pH$  to the carbon dioxide exchange between the liquid and the gas phase in the pilot-scale trickling filter. As a consequence, the modelling exercise became easier.

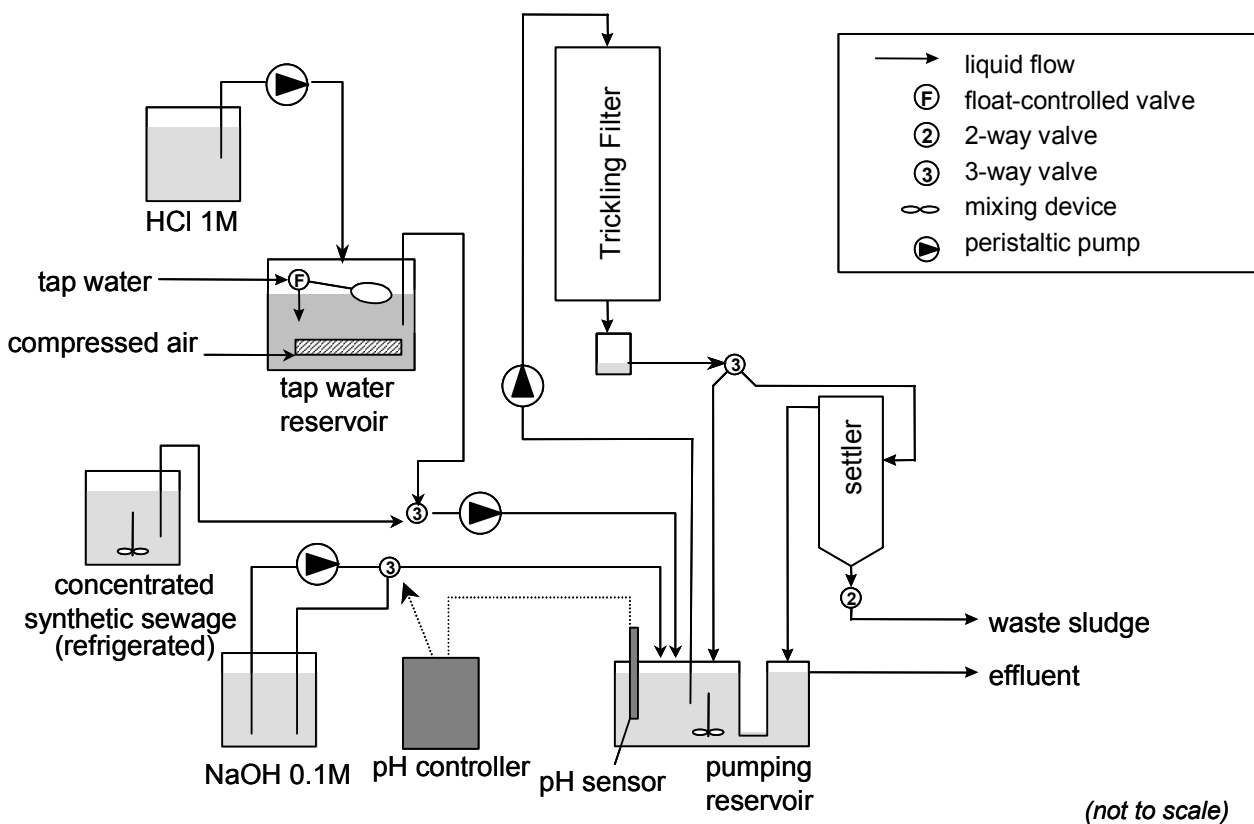


Figure 7.1: Layout of the  $pH$  controlled pilot-scale trickling filter

Figure 7.2 shows part of the results obtained by implementing the  $pH$  control system. In this figure, two buffer capacity profiles (obtained as described in paragraph 6.2.5) are shown that are typical for

the situation before and after the implementation. As can be seen and will be shown in the measurements further on in this chapter, the majority of the inorganic carbon is removed from the influent, which makes the interpretation of the carbon fluxes easier and more reliable.

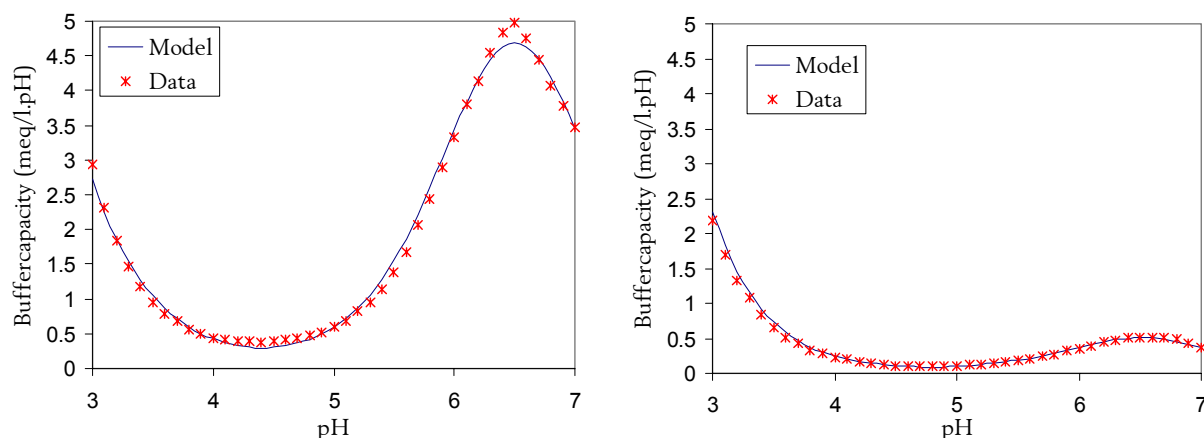


Figure 7.2: Influent buffer capacity profile before (left) and after (right) implementing TIC removal and  $pH$  control

### 7.3 Set-up of the nitrate addition test

As mentioned above, the filter's influent was changed from the synthetic sewage used during normal operation to a solution of ethanol, ammonium and orthophosphate. This way, the difficulty of estimating the readily biodegradable fraction of the influent COD was overcome. To make sure the biofilm had adapted to the ethanol, some 50 mg/l ethanol had been mixed in the normal synthetic sewage influent in the weeks before the experiment. During the experiment, an air flow rate of 15 l/min was applied through the filter column. Alike during the load shift experiment, the influent flow rate was 0.418 m<sup>3</sup>/d. The different phases in the nitrate addition test are summarised in Table 7.1.

Table 7.1. Overview of the trickling filter operation during the nitrate addition test. The first column denotes the event numbers used to identify the events in the graphs

Phase	Starting time	Plant operation
1	September 26, 16:30	Start of low loading with ethanol as influent
2	September 27, 9:30	Pump calibration and cleaning of tubing, calibration of off-gas equipment
3	September 27, 10:55	Start of high loading with ethanol as influent
4	September 27, 16:08	Start of nitrate addition to the pilot-scale trickling filter
5	September 28, 9:00	Pump calibration and cleaning of tubing
6	September 28, 12:00	Stop of nitrate addition
7	September 28, 14:30	Start of low loading with ethanol as influent

The test started with a period of low loading. The influent composition during this period is denoted in Table 7.2. After a small disturbance of the measurement system due to calibration of the pumps and the off-gas analysis equipment, the COD loading to the system was increased significantly while the nitrogen loading remained equal (Table 7.2). Measurements in Table 7.2 are averages over 4 measurements except for the nitrate concentration at high loading, for which only one measurement was available.

**Table 7.2. Influent composition at low and high loading**

<i>Compound</i>	<i>Low loading</i>	<i>High loading</i>
CODt (mg/l)	134.5 ± 2.1	653.6 ± 28.4
NH <sub>4</sub> <sup>-</sup> (mg N/l)	18.5 ± 0.42	15.45 ± 0.49
NO <sub>3</sub> <sup>+</sup> (mg N/l)	4.29 ± 0.06	4.68

After about five hours, during which the system was allowed to stabilise in the high loading operation mode, the dosing of extra nitrate to the influent was started. The influent nitrate concentration used was 83.5 ± 0.5 mg N/l. The dosing of nitrate was continued for about 20 hours. 3 hours before the end of this dosing, the pumps were calibrated, introducing a disturbance on the signal. Mainly the CO<sub>2</sub> off-gas signal suffered from this disturbance, since the calibration includes the introduction of some fresh water into the set-up (Figure 7.3). This water did not necessarily have the same IC-concentration as the bulk liquid in the filter at that moment and can have had an effect on the *pH* in the trickling filter. Unfortunately, measurements of the *pH* in the pumping tank and in the filter's effluent were not stored during this period and this hypothesis can thus not be checked.

At the start of the nitrate dosing, a clear effect on the CO<sub>2</sub> signal could be noticed (Figure 7.3). An extra degradation of organic matter by denitrification was expected. This obviously did not cause a change of the oxygen uptake in the filter, but it had an effect on the carbon dioxide production. This carbon dioxide was formed in the deeper, anoxic, layers of the biofilm.

It is important to note that a constant *pH* of 7.0 could be guaranteed by the *pH* control system during the complete period before the nitrate dosing experiment. *pH* values higher than 7.0 in the filter set-up were however possible because acid addition to the pumping reservoir was not foreseen since this was not necessary during normal operation. During the nitrate dosing period, a considerable amount of alkalinity was produced by the denitrification process. This caused the *pH* to gradually increase up to a value of 7.29 in the effluent of the trickling filter. This makes clear that the amount of inorganic carbon stripped from the influent was high enough to seriously compromise the buffering capacity of the bulk liquid in the filter. Unlike the higher *pH* in the trickling filter effluent, the *pH* in the pumping tank was at most 7.15 due to the dosing of the low *pH* influent.

These measurement results were incorporated in the modelling of the nitrate dosing test. It should however be clear that the *pH* value is not an output of the modelling, but is considered as an input. This simplification has been made since *pH* electrodes are widespread in wastewater treatment and are known to be robust sensors. Complete modelling of the *pH* and the equilibria associated with it would substantially complicate the model and make it more vulnerable to numerical problems.

When the dosing of nitrate to the filter was stopped, the  $pH$  almost instantaneously decreased to its normal working value of 7.0. However, due to the high  $pH$ , quite some IC accumulated in the bulk liquid of the filter in the form of  $HCO_3^-$ . When the  $pH$  dropped after stopping the nitrate addition, this extra IC was transferred to  $CO_{2,aq}$  and was partly transferred to the gas phase. This gave rise to a clear “bump” in the  $CO_2$  off-gas signal (Figure 7.3).

After about 3 hours, the loading was lowered again, and a drop of the  $O_2$  consumption and the  $CO_2$  production could be seen.

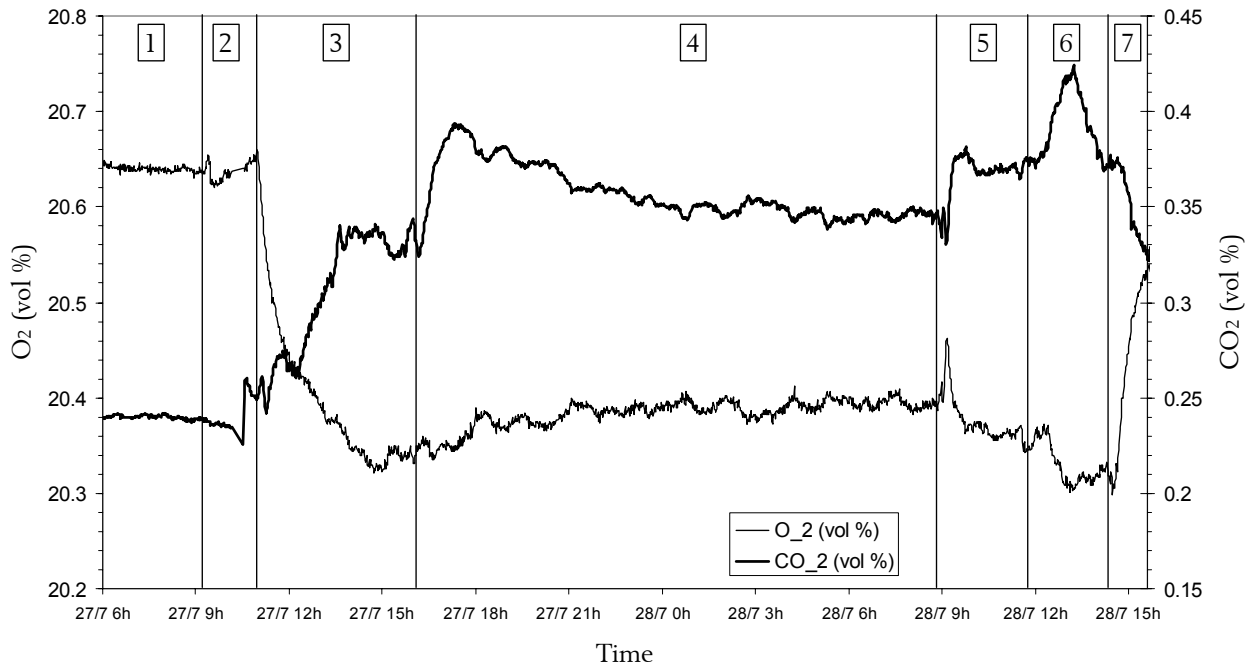


Figure 7.3: On-line measurement results of the  $O_2$  and  $CO_2$  concentrations in the filter's off-gas during the nitrate addition experiment (numbers indicate phases given in Table 7.1)

## 7.4 Modelling of the nitrate addition test

For the modelling of the load shift experiment, the model of the pilot-scale trickling filter developed for the description of the load shift experiment was used. Large parameter adaptations were not needed to achieve a good fit. In Table 6.10 the parameter set used for the description of the experiment can be seen.

For the correct description of the off-gas measurement results, the actual value of the TOC/COD ratio of ethanol was implemented. This is 0.25 g TOC/g COD.

Two other changes compared to the parameter set used during the modelling of the load shift experiment can be noted. First of all, the growth rate of the autotrophic biomass had to be lowered. This was done because it was found that the nitrification activity in the filter at low load dropped significantly after implementing the  $pH$  control and using ethanol as an influent. This decrease was not observed when the normal synthetic sewage was used, even with the  $pH$  control system activated. The influent ammonium concentration of  $18.5 \pm 0.42$  mg N/l resulted in an outflow concentration of 12.5 mg  $NH_4^+$ -N/l, whereas at a comparable COD loading in the load shift experiment, a much lower

effluent ammonium concentration was obtained. The reason for this drop of the nitrifying activity remains unclear. Maybe the process to remove the alkalinity from the tap water that was used for the dilution of the influent had an influence on the nitrification. A TIC concentration of only  $0.78 \pm 0.02$  mol/m<sup>3</sup> was measured in the effluent (Figure 7.4). Compared to the measurements during the load shift experiment, this is a very low value. The effluent CO<sub>2, aq</sub> concentration then was 0.34 mol/m<sup>3</sup> at high load and 0.22 mol/m<sup>3</sup> at low load. The HCO<sub>3</sub><sup>-</sup> concentration was 7.35 and 5.83 mol/m<sup>3</sup> respectively. Another possible explanation is the inhibition of nitrification by the ethanol used in the influent. Lab tests have shown methanol to inhibit nitrification starting from concentrations between 20 and 40 mg/l. Possibly ethanol too, that was used with a concentration starting from 134.5 mg COD/l in the low loading phase, is somewhat inhibiting towards nitrification in this concentration range.

**Table 7.3. Parameters used in the modelling experiments**

<i>Parameter</i>	<i>Value</i>	<i>Changed</i>
$D_{f,So}$ (cm <sup>2</sup> /d)	2.1	
$D_{f,Ss}$ (cm <sup>2</sup> /d)	0.28	*
$D_{f,Sno}$ (cm <sup>2</sup> /d)	1	
$D_{f,Sh}$ (cm <sup>2</sup> /d)	1.8	
$\mu_H$ (1/d)	4	
$Y_H$ (gCOD/gCOD)	0.6	
$b_H$ (1/d)	0.4	
$\mu_A$ (1/d)	0.05	*
$Y_A$ (gCOD/gN)	0.1	
$b_A$ (1/d)	0.01	
$k_h$ (1/d)	5	
$k_a$ (1/d)	0.1	
$i_X$ (gN/gCOD)	0.08	
$f_p$ (-)	0.08	
$k_{at}$ (-)	4	
$k_{dt}$ (-)	0.05	
$\rho_m$ (kg/m <sup>3</sup> )	38.8	

Next, the diffusion constant for readily biodegradable substrate was about halved. First of all, it is noteworthy to mention that during the modelling of the load shift experiment, this diffusion constant did not play a major role. At high loading rate, the filter was modelled as being oxygen limited. Even at low loading, and mainly due to the gradual release of readily biodegradable substrate from hydrolysis, the first three tanks of the 7-tank filter model showed oxygen limitation. Even in the substrate limited lower part of the filter, reducing the diffusion constant for readily biodegradables would only lead to a shift of biodegradation activity to lower areas of the filter. Indeed, quite some extra capacity was available for degradation, since at low load the conversion activity in the lowest two tanks in the model was found negligible. Consequently, a change of this diffusion coefficient would not have changed the overall result of the modelling exercise or in other words, this parameter was not identifiable from the measurement data at that point. Therefore, during the modelling of the load shift, it was chosen to keep the default value for this diffusion constant.

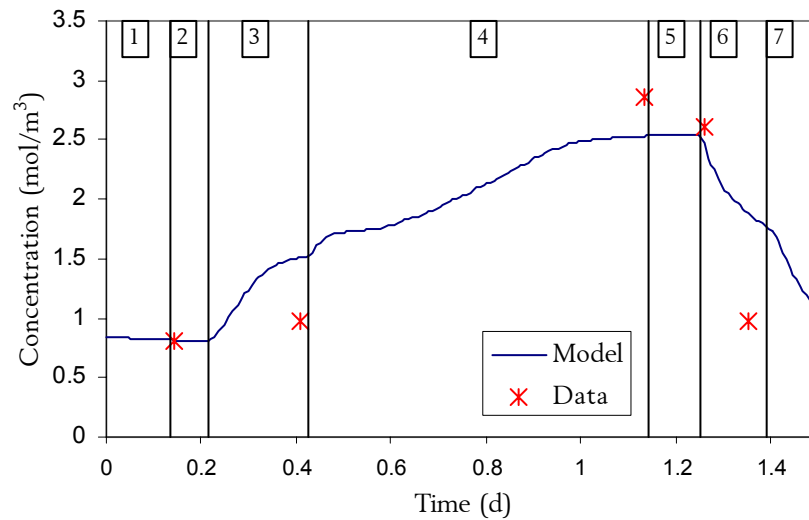


**Figure 7.4: Measured and simulated inorganic carbon concentration during the nitrate addition test ( $D_{f,SS} = 0.28 \text{ cm}^2/\text{d}$ ) (numbers indicate phases given in Table 7.1)**

In this experiment however, the diffusion coefficient for readily biodegradable substrate appears to govern the amount of denitrification that proceeds after the nitrate addition. In Figure 7.5, it is clear that the start of the addition of nitrate had a clear influence on the predictions of  $\text{O}_2$  in the off-gas. In this figure, a diffusion coefficient of  $0.58 \text{ cm}^2/\text{d}$  was used, which is the default value. The discrepancy between the measured and predicted  $\text{O}_2$  concentration during the nitrate addition is the result of a very high denitrification activity at the top of the filter. There, the readily biodegradable ethanol diffused relatively deep into the biofilm. This makes that the readily biodegradable substrate in the simulation was depleted at the bottom of the filter, and there oxygen limitation started to prevail. It is very unlikely that this happened to this extent in reality, not only because of the smaller effect in the  $\text{O}_2$  observation, but also because the effluent concentration of soluble COD was measured to be over  $30 \text{ mg/l}$  during the nitrate addition. Moreover, the nitrate consumption was overestimated. An effluent concentration as high as  $40 \text{ mg NO}_3^- \text{-N/l}$  was measured during the addition period (Figure 7.6). Although the number of off-line measurements during the test was rather limited, the trend is clear in these figures.

Based on the above findings, the diffusion coefficient for the readily biodegradable substrate  $S_S$  was changed and by manual tuning via trial and error a value of  $0.28 \text{ cm}^2/\text{d}$  was selected. The result can be seen on Figure 7.7. It is clear that the increase of the oxygen concentration due to substrate limitation is very small with this diffusion coefficient. Also, the agreement with the off-line measurements is good (Figure 7.6), although the effluent substrate concentration at high loading rate without nitrate addition is somewhat underestimated.

In Figure 7.8 a typical graph of the dimensionless penetration depths of the substrates in the biofilm is depicted. At low loading, substrate was limiting all conversion processes. At high loading, oxygen took over this role. Only a very limited amount of denitrification was present. When nitrate was added, oxygen still limited aerobic metabolism, but more substrate could be degraded via denitrification. This situation was reversed again when the nitrate dosing was stopped and further when the loading was lowered.

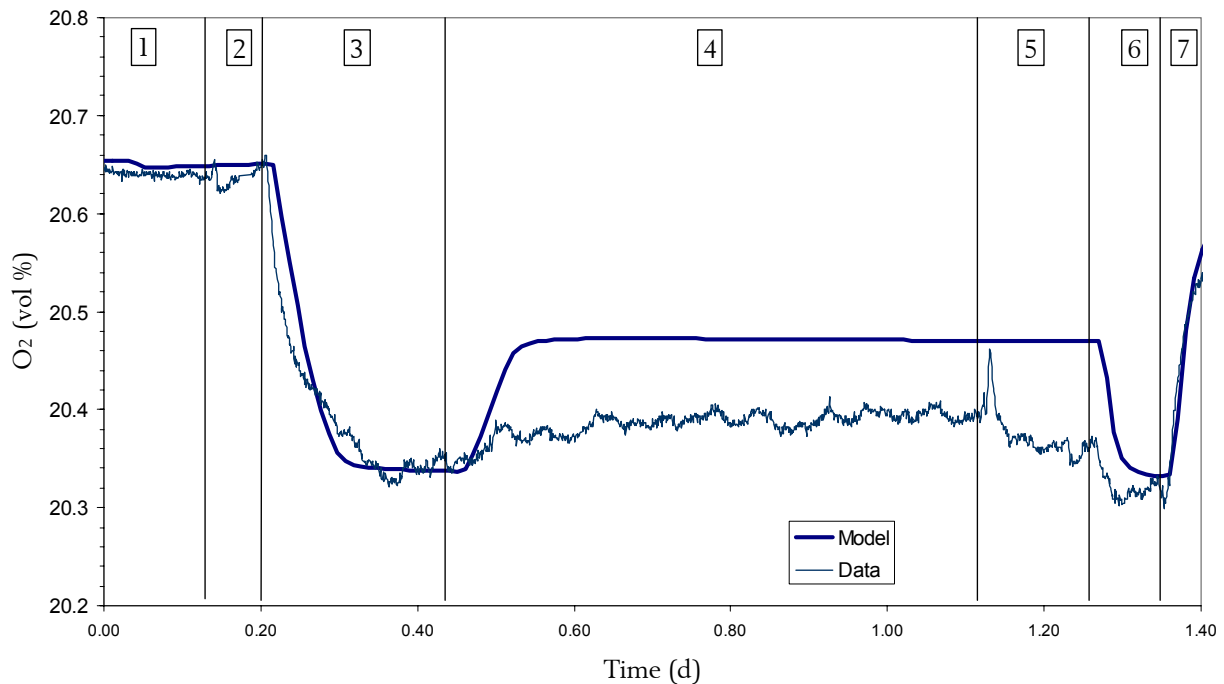


**Figure 7.5:** On-line measurement and modelling results of the  $O_2$  concentration in the filter's off-gas during the nitrate addition experiment ( $D_{f,ss} = 0.58 \text{ cm}^2/\text{d}$ ) (numbers indicate phases given in Table 7.1)

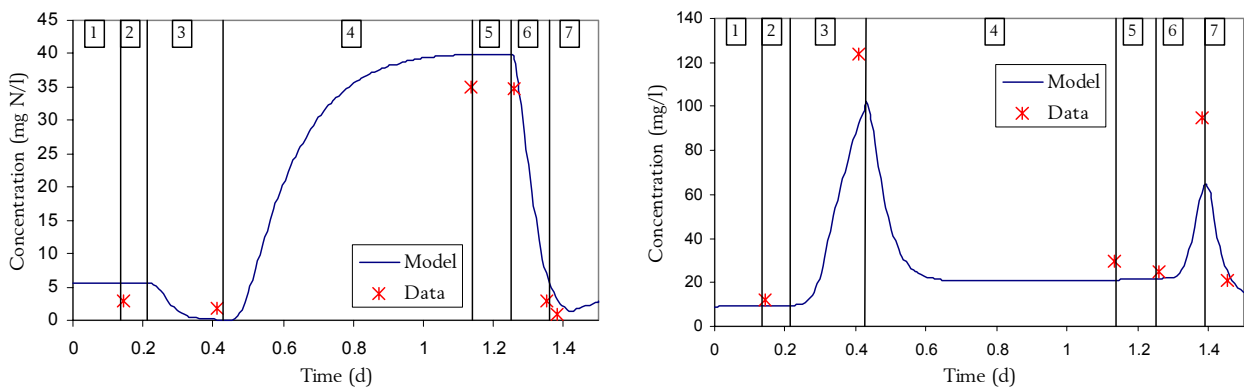


**Figure 7.6:** Measured and simulated nitrate-nitrogen (left) and readily biodegradable COD (right) concentration during the nitrate addition test ( $D_{f,ss} = 0.28 \text{ cm}^2/\text{d}$ ) (numbers indicate phases given in Table 7.1)

In Figure 7.9, the result of the  $\text{CO}_2$  concentration modelling can be seen. It is obvious that the model description of the experiment is very good. During the phases 1 until 3, a constant  $pH$  value of 7.05 was used in the simulations. At the start of period 4, when the addition of nitrate to the highly loaded system was started, an increase of the off-gas  $\text{CO}_2$  concentration (induced by the nitrate addition that stimulated denitrification) is noticed. During this phase, the  $pH$  gradually increased up to 7.26 in the filter's effluent. This was caused by the absence of acidifying  $pH$ -control. This increase decreased the  $\text{CO}_2$  transfer to the gas phase somewhat. This explains the declining  $\text{CO}_2$  concentration in the gas phase along phase 4. To obtain a smooth curve, a linear interpolation between the available  $pH$  data was used. It was not attempted to describe the increased  $\text{CO}_2$  concentration in phase 5, following the calibration of the pumps. Here,  $pH$  data were not available that could have explained the sudden

increase of  $\text{CO}_2$  transfer to the gas phase. In phase 6, after stopping the nitrate addition to the filter, the extra IC accumulated in the liquid phase was stripped to the gas phase because of the quite sudden drop of the  $pH$  in the filter system down to 6.83.

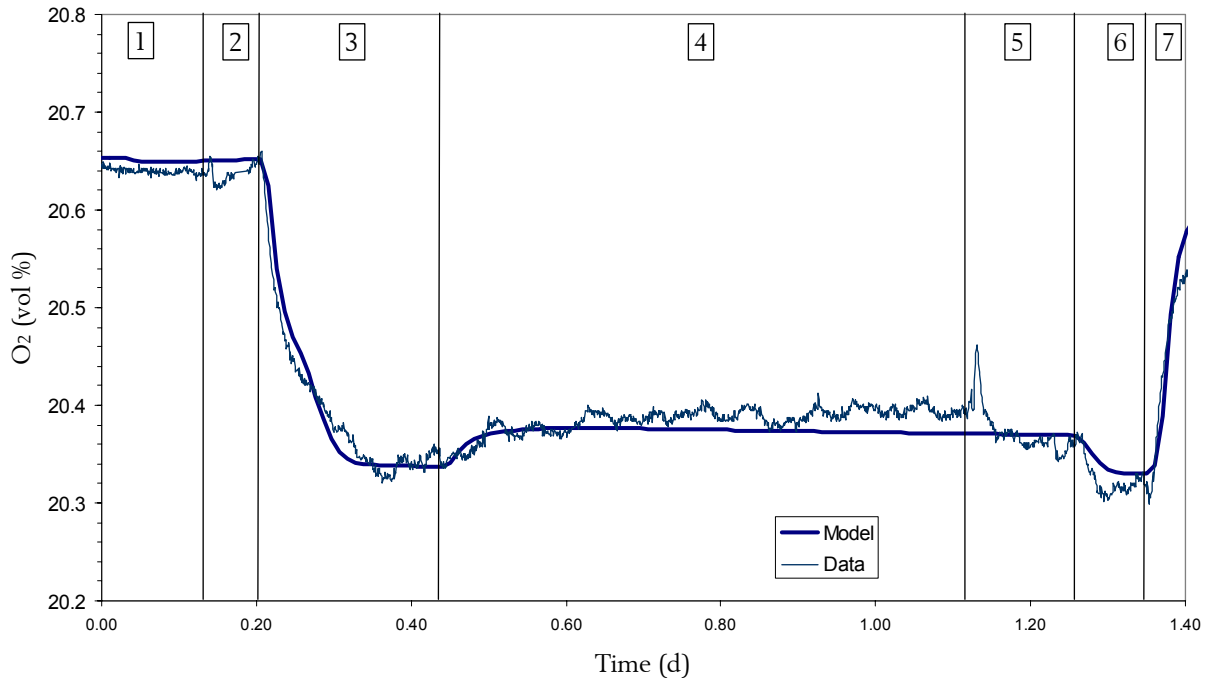


Figure 7.7: On-line measurement and modelling results of the  $\text{O}_2$  concentration in the filter's off-gas during the nitrate addition experiment ( $D_{f,ss} = 0.28 \text{ cm}^2/\text{d}$ ) (numbers indicate phases given in Table 7.1)

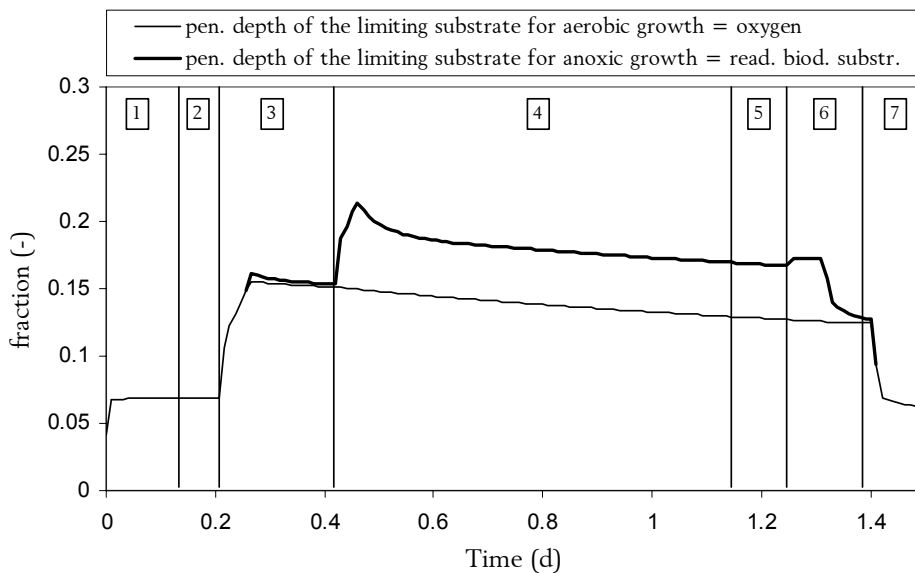


Figure 7.8: Dimensionless penetration depths of the substrates limiting to aerobic and anoxic growth in tank 4 (*i.e.* the middle tank in the model of the filter set-up) (numbers indicate phases given in Table 7.1)

## 7.5 Increased conversion capacity

As described in the introduction to this chapter, the use of denitrification could be interesting to overcome periods where the treatment capacity of a biofilm system is insufficient. At high organic

loading rates, and whenever the oxygen supply to the biofilm is insufficient to obtain good treatment capacity, denitrification could be induced by providing the biofilm with an extra portion of electron acceptor besides oxygen. As can be seen on Figure 7.6, the effluent COD concentration increased quite drastically after increasing the influent load to the filter. However, the filter didn't have the time to stabilise completely before the nitrate addition was started. It is therefore difficult to assess the extra treatment capacity obtained by denitrification.

Using the model, estimates of the extra capacity of the filter were made. It turns out that 54.3 g COD/d were removed using the denitrification pathway on top of the 206.1 g COD/d removed via aerobic degradation. For this extra COD removal capacity, 22.0 g  $\text{NO}_3^-$ -N g/d was used. Using the effluent quality calculation proposed in the simulation benchmark introduced further in this thesis (chapter 10) and the cost multiplication factors proposed by Vanrolleghem and Gillot (2001), the effluent fine for COD is estimated to be 0.137 €/kg COD. The cost for the industrial application of nitrate-nitrogen is estimated to be about 0.7 €/kg  $\text{NO}_3^-$ -N. Consequently, at first sight, the addition of nitrate is not an economically feasible solution. However, the effluent fines for COD are highly country-specific and are subject to rise in the future. Moreover, no extra penalty for the violation of effluent constraints is included in these numbers. On the other hand, in many industries, cheap nitrate sources are available as a waste product. This nitrate could be used to perform denitrification as proposed here.

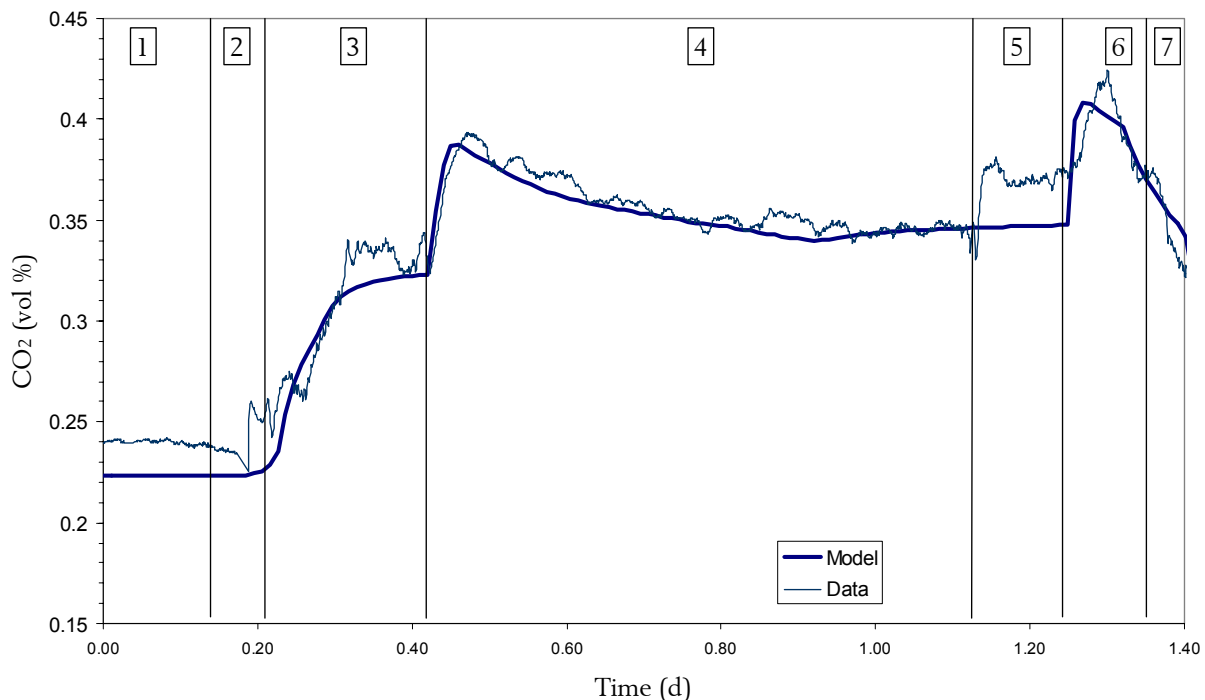


Figure 7.9: On-line measurement and modelling results of the  $\text{CO}_2$  concentrations in the filter's off-gas during the nitrate addition experiment ( $D_{f,ss} = 0.28 \text{ cm}^2/\text{d}$ ) (numbers indicate phases given in Table 7.1)

## 7.6 Conclusions

The pilot-scale trickling filter was used to investigate and model the result of the addition of nitrate at high organic loading rate. At these loading conditions, oxygen supply can be insufficient to obtain good treatment capacity. The addition of nitrate was used to provide the biomass with an extra amount of

electron acceptor next to oxygen. In the deeper anoxic layers of the biofilm, denitrification can then proceed.

To facilitate the interpretation of the test results, ethanol was used as the sole carbon source in the influent, a majority of inorganic carbon in the influent was stripped and *pH* control was implemented. The test showed that denitrification can indeed be induced by adding nitrate at high loading conditions and that this way a considerably increased substrate removal capacity can be obtained. The production of CO<sub>2</sub> from bioconversion processes increased, while no decrease of the O<sub>2</sub> consumption was noticed. The production of alkalinity from denitrification had an effect on the *pH*, since only base addition *pH* control was implemented. Due to the higher *pH*, a larger amount of inorganic carbon was stored in the liquid phase. This IC was released into the gas phase when the *pH* dropped back again after the denitrification has ended.

The simplified mixed-culture biofilm model extended for the description of off-gas measurements was able to describe the results of the experiment very well. Only the effective diffusion constant of the biodegradable substrate in the biofilm had to be adjusted. It should however be noted that this parameter was not identifiable from previous experiments. This value should thus be considered to be more correct than the one initially used to describe the load-shift in chapter 6.

Economic evaluation of the simulation results revealed that, at first sight, the addition of nitrate is not an economically feasible solution. However, this situation is subject to change. The effluent fines for COD are highly country-specific and will most probably rise in the future. Moreover, no extra penalty for the violation of effluent constraints was included. On the other hand, in many industries, cheap nitrate sources are available as a waste product. This nitrate could be used to perform denitrification as proposed in this chapter.



# 8

## Measurement and modelling of COD removal in a full-scale industrial trickling filter system

---

### 8.1 Introduction

In Flanders more and more industries are confronted with the fact that discharge of treated wastewater into the municipal sewer system becomes more difficult because of legislation. This disconnection forces these industries to produce an effluent that meets the surface water standards. In many cases, efforts close to or even exceeding the BATNEEC (Best Available Technology Not Entailing Excessive Costs) principle are needed to achieve this effluent quality. To complicate this, the number of processes that take place in industrial wastewater treatment is increasing which makes it more difficult to manage the overall functioning of the plant.

Therefore, at a particular wastewater treatment plant (WWTP) in Belgium, a project has been performed to demonstrate the application of on-line monitoring, modelling and process control in a industrial wastewater treatment. In this chapter, the modelling of the trickling filter process at this plant is described. The plant under study has an average influent flow of 2700 m<sup>3</sup>/d. One of the main characteristics of the plant is the high influent COD concentration (in the range of 6000 mg/l with peaks up to 10000 mg/l and more). Moreover, this concentration can vary dramatically over time because of the batch-wise production of different products in the industrial plant. The nitrogen in the influent can be split up in different parts. The average Kjeldahl nitrogen concentration is 250 mg/l of which only 10% is ammonium nitrogen. The influent total phosphorous concentration range is between 0 and 2 mg/l (90% of the measurements), so a lack of phosphorus in the biological treatment steps is to be expected.



Figure 8.1: Picture of the wastewater treatment plant under study, with the trickling filters in the background

The main reason to start the project was the plan to significantly increase the production at the industrial facility. An extra 35% load to the wastewater treatment was expected. Therefore, it was necessary to optimise the current plant. This project investigated the possibilities perform to this optimisation using only minor process changes but, on the other hand, including on-line monitoring and process control (De Clercq *et al.*, 1999a; De Clercq *et al.*, 1999b; Devisscher *et al.*, 2000; Debusscher *et al.*, 2001; Demey *et al.*, 2001). Each of the unit processes was analysed individually to determine potential methods of optimisation. Based on real-time data and dynamic models, control strategies for the different unit processes were established.

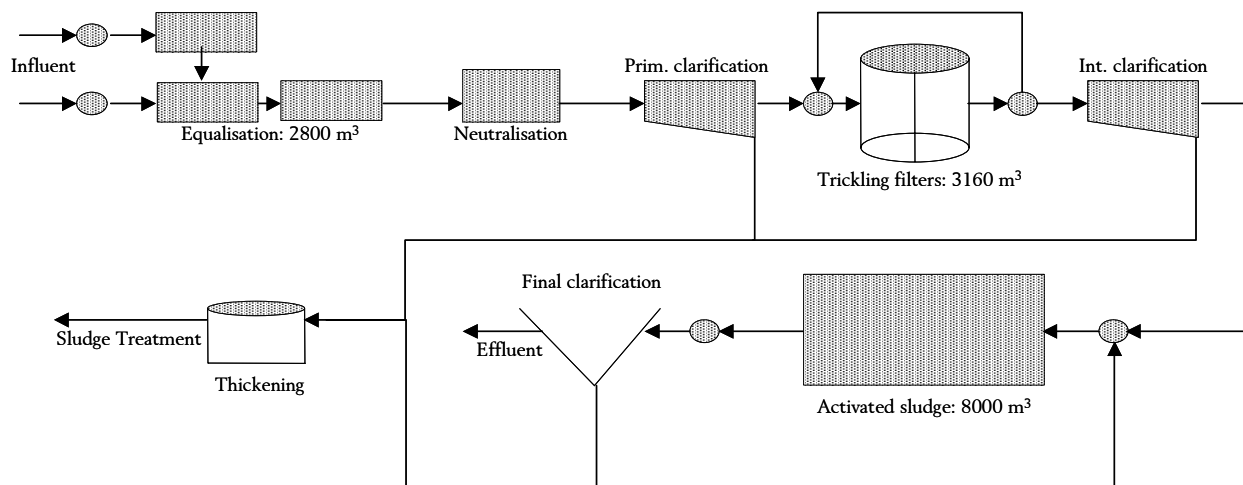


**Figure 8.2: Schematic representation of the wastewater treatment plant under study**

In the framework of the project on-line sensors were installed at the plant. A TOC-sensor (ISCO UV 3500, Applitek, Belgium), was used to monitor the organic load at the outlet of the equalisation system. Respirometry (using a RODTOX biosensor, Kelma, Belgium) was used to measure the  $COD_{st}$  (short term or readily biodegradable COD) and possible toxicity. The respirometer could be operated in a multiplexed way, so as to alternately characterise the influent and the effluent of the trickling filter. In a later stage of the project, on-line ammonium, phosphate and turbidity sensors were installed at the effluent of the activated sludge plant.

As mentioned before, this chapter focuses on the trickling filter process. Its process characteristics were quantified by means of a 5 day intensive measurement campaign with the use of the on-line respirometer mentioned above complemented with on-line off-gas analysis. This measurement campaign had to allow for a model based evaluation and optimisation of the trickling filter process.  $COD_{st}$  measurements were conducted at the inflow and the outflow of the filters and the off-gas sensor was used to monitor the  $O_2$  and  $CO_2$  content of the off-gasses. Off-gas analysis together with measurements or estimates of the sludge production allow to close the carbon balance and can in this way support the modelling of organic matter biodegradation in the filters. It can also give information about their behaviour under changing process conditions (*e.g.* changing air flow rates). To model the biodegradation in the filters, the simplified mixed-culture biofilm model introduced in chapter 4 was used. As already described in chapter 6, the model was extended with equations for the production and the  $pH$ -dependent liquid-phase equilibrium for inorganic carbon (IC).

## 8.2 Description of the trickling filter plant under study

A scheme of the trickling filter plant under study is depicted in Figure 8.3. It consists of two trickling filters (TF01 and TF02) working in parallel. Each filter has a height of 6 m and a diameter of 18.5 m. The total reactor volume is 3160 m<sup>3</sup>. This volume is filled with a PVC carrier material of the cross-flow type with a specific surface area of 100 m<sup>2</sup>/m<sup>3</sup> and a porosity of about 95%. There are several recycle loops, which ensure that each filter receives a constant recycle flow of 300 m<sup>3</sup>/h. Two “short” loops recycle the effluent of each filter to its pumping tank. A “long” recycle loop takes the water through an intermediate clarifier. Part of this flow serves as the influent to the subsequent activated sludge system, the rest is distributed again over both trickling filters. Both pumping tanks have a volume of 128 m<sup>3</sup>. To provide the biomass in the filters with oxygen, two ventilators suck air through the bed volume with a flow rate of approximately 7800 m<sup>3</sup>/h for TF01 and 9500 m<sup>3</sup>/h for TF02. Both ventilators also have a “low position”, providing a flow of 4300 m<sup>3</sup>/h for TF01 and 6600 m<sup>3</sup>/h for TF02. These flow rates have been measured using a pitot tube. The average total influent flow rate was 110 m<sup>3</sup>/h of which part is coming from a ground water pump. This ground water is partly used for cleaning of vessels. The organic load of the plant equals 15000 kg COD/d.

The measurements conducted were used to monitor and model the biodegradation of components in the filters and their behaviour under changing process conditions. To investigate the response of the system to a changing air flow rate through the filters, the air flow was halved halfway through the measurement campaign.

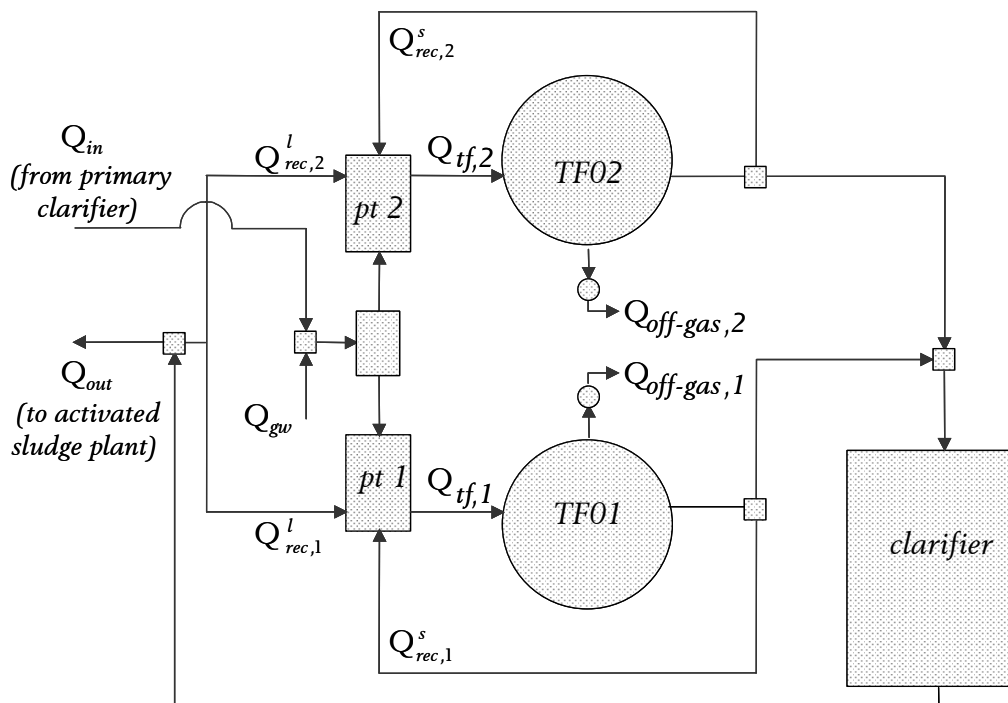


Figure 8.3: Schematic representation and picture of the hydraulic layout of the trickling filter system (pt = pumping tank, gw = ground water)

### 8.3 Design of the measurement campaign

Liquid samples were taken by automatic refrigerated samplers. This was done on two locations on a time-proportional basis during 5 consecutive days. The location of the samplers is indicated on Figure 8.4. In this figure, the two trickling filters are represented to be a single system to limit the complexity of the scheme. The sampling time of the sampler at the effluent was only six hours whereas the influent sampler had a sampling time of three hours.

Influent samples were taken before the addition of the ground water and thus before the influent was subdivided to feed the two filters. Sampling after the addition of ground water was not possible because of the mixing tank construction. Daily average flow rates of the ground water addition were available. Actual values of the ground water flow could also be monitored on-site. This flow is fluctuating during working hours due to the cleaning of vessels (the ground water used for this purpose is discharged in the equalisation system). The liquid samples were collected and analysed for COD,  $\text{NH}_4^+ \text{-N}$ ,  $\text{NO}_3^- \text{-N}$ , Total N,  $\text{PO}_4^{3-} \text{-P}$  and SS. Mass balances could be calculated using the effluent flow rate which was collected every 15 minutes.

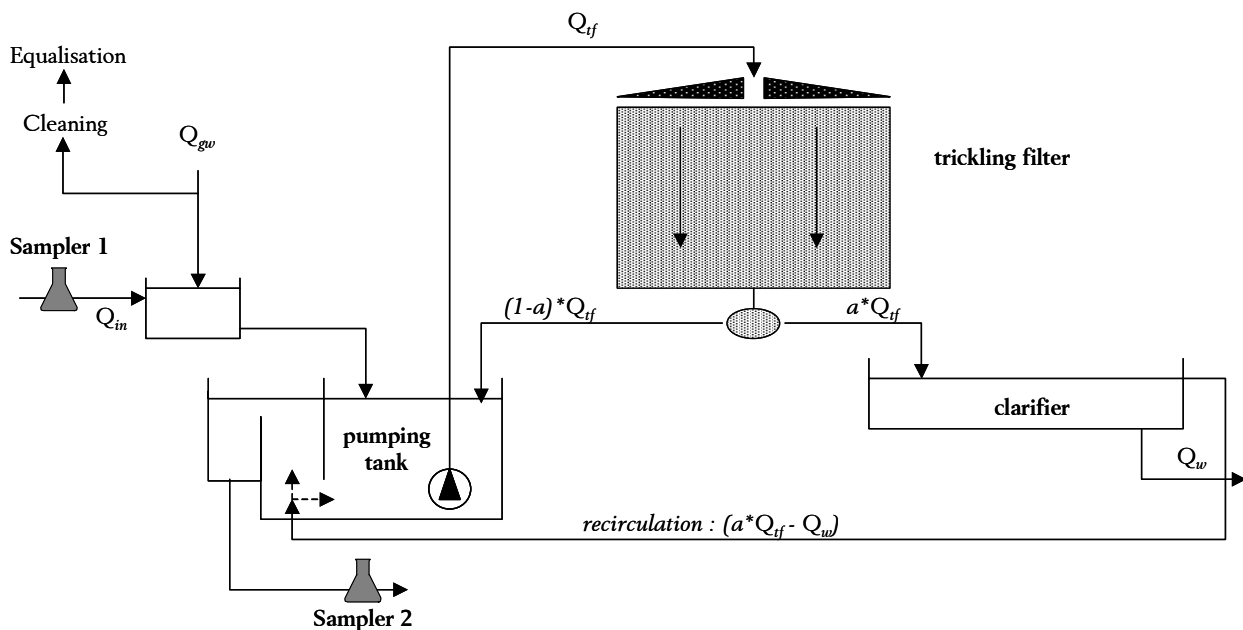


Figure 8.4: Simplified layout of the trickling filters and sampling locations

The same measurement locations were used for  $\text{COD}_{\text{st}}$  measurements with the RODTOX bio-sensor (Kelma bvba, Niel, Belgium) available on-site (Vanrolleghem *et al.*, 1994). Measurements of  $\text{COD}_{\text{st}}$  were conducted in the influent as well as in the effluent of the filters by sensor multiplexing. Two “fast loops” were implemented. The RODTOX took samples from each fast loop during 90 minutes before switching to the other loop. To determine the  $\text{COD}_{\text{st}}$  of these samples, the RODTOX performs batch experiments, in which the wastewater sample is added to a continuously stirred and aerated reactor filled with activated sludge. From the oxygen uptake rate (OUR) curve that is monitored, the  $\text{BOD}_{\text{st}}$  is determined. This  $\text{BOD}_{\text{st}}$  is defined as the amount of oxygen that is used for the degradation of readily biodegradable substrates during the batch experiment. Dividing the  $\text{BOD}_{\text{st}}$  by  $(1-Y)$ , gives the estimated  $\text{COD}_{\text{st}}$ . For this case study, lab experiments have shown that the well-

accepted yield (Henze *et al.*, 1987) of 0.67 is too high and that a value of 0.5 is more appropriate (Petersen, 1999).

Apart from this, daily BOD<sub>5</sub> measurements were done on grab samples of influent and effluent. All other parameters were also measured on these grab samples.

Here too, comparable to the measurements on the pilot-scale trickling filter set-up described earlier, the O<sub>2</sub> content of the off-gas was measured on the basis of the paramagnetic characteristic of oxygen gas and CO<sub>2</sub> was measured with the NDIR (non-dispersive infrared) method.

A single measurement of the CO<sub>2</sub> concentration in the off-gases of the filter is not sufficient to describe the inorganic carbon (IC) equilibrium. Quite some microbially produced CO<sub>2</sub> can leave the system with the water and not with the gas phase. For that reason, extra measurements of the IC concentration and the *pH* were needed. This was done using the titration technique developed by Van Vooren *et al.* (1999). Titration curves are collected while adding a 0.1 M HCl solution to lower the *pH* from the actual *pH* of the sample, down to *pH* 2.5. Software developed in C++ calculates the buffer capacity profiles from the titration curves and estimates the IC concentration from them. Once the total IC is determined, the partitioning among the forms HCO<sub>3</sub><sup>-</sup> and CO<sub>2,(aq)</sub> can be performed using a partitioning model that is a function of the actual *pH* of the sample. This can be done using the following equations:

$$\begin{aligned}
 [\text{CO}_{2,aq}] &= \frac{10^{-2pH}}{10^{-2pH} + 10^{-(pH+pK_1)} + 10^{-(pK_1+pK_2)}} C_{\text{CO}_2} \\
 [\text{HCO}_3^-] &= \left( 1 - \frac{10^{-2pH} + 10^{-(pK_1+pK_2)}}{10^{-2pH} + 10^{-(pH+pK_1)} + 10^{-(pK_1+pK_2)}} \right) C_{\text{CO}_2} \\
 [\text{CO}_3^{2-}] &= \left( 1 - \frac{10^{-2pH} + 10^{-(pH+pK_1)}}{10^{-2pH} + 10^{-(pH+pK_1)} + 10^{-(pK_1+pK_2)}} \right) C_{\text{CO}_2}
 \end{aligned} \tag{8.1}$$

Note that CO<sub>3</sub><sup>2-</sup> is only present in very small concentrations at the *pH* values usually encountered in wastewater treatment systems.

## 8.4 Measurement campaign results

### 8.4.1 Measurements in influent and effluent

#### 8.4.1.1 Flow rate

The evolution of the flow rate during the measurement campaign can be followed on Figure 8.5. The increase of the flow rate during the week was obvious.

### 8.4.1.2 COD concentration and load

The influent COD concentrations can be seen on Figure 8.6. Several very high peaks are noticed in the influent concentrations. This demonstrates the sub-optimal behaviour of the upstream equalisation system. Adequate control of the equalisation system should allow to reduce these peaks. Advanced control was investigated and implemented in a later stage of the project mentioned above (Harmand *et al.*, 1999; Devisscher *et al.*, 2000).

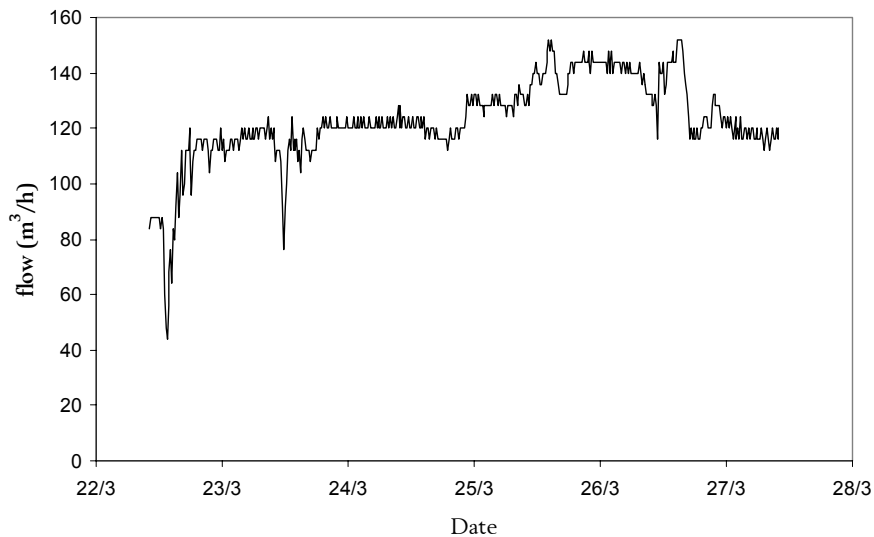


Figure 8.5: Evolution of the flow rate during the measurement campaign

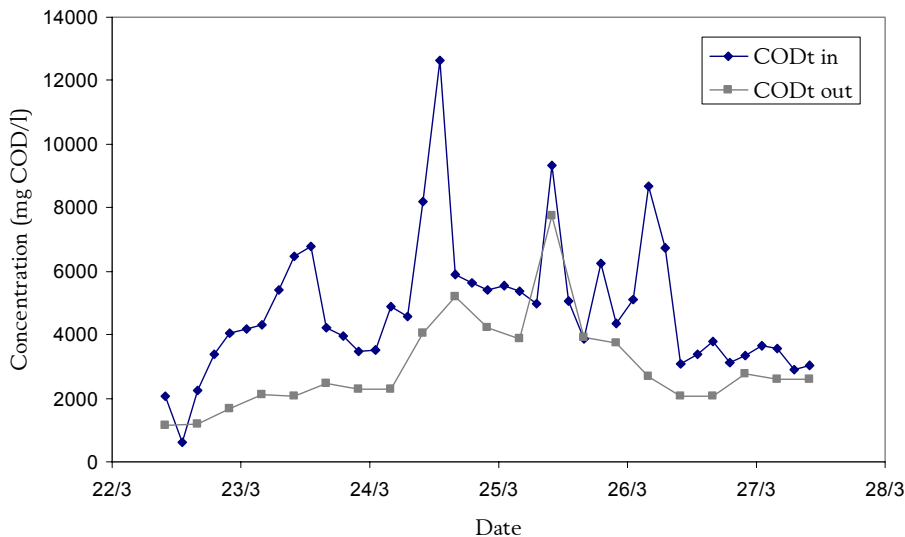


Figure 8.6: Evolution of the total COD concentration during the measurement campaign

In Figure 8.7, the COD load of the influent and effluent are plotted. It is rather dangerous to use these data to directly calculate a removal efficiency over the complete trickling filter system. On the one hand, the dynamics are very fast, on the other hand, the hydraulic retention time over the complete system (including the pumping tanks) is only about three hours. The fact that there are more measurements in the influent than in the effluent (only every 6 hours = 2 times the retention time) makes the calculation even more complicated. As will be seen further-on, the off-gas

measurements were able to cope with these dynamics and were thus more suitable to calculate removal efficiencies. A mean COD removal efficiency over the trickling filter system can still be calculated and was only 37.6%. This low removal efficiency does indicate a possible effect of phosphorus limitations in the system.

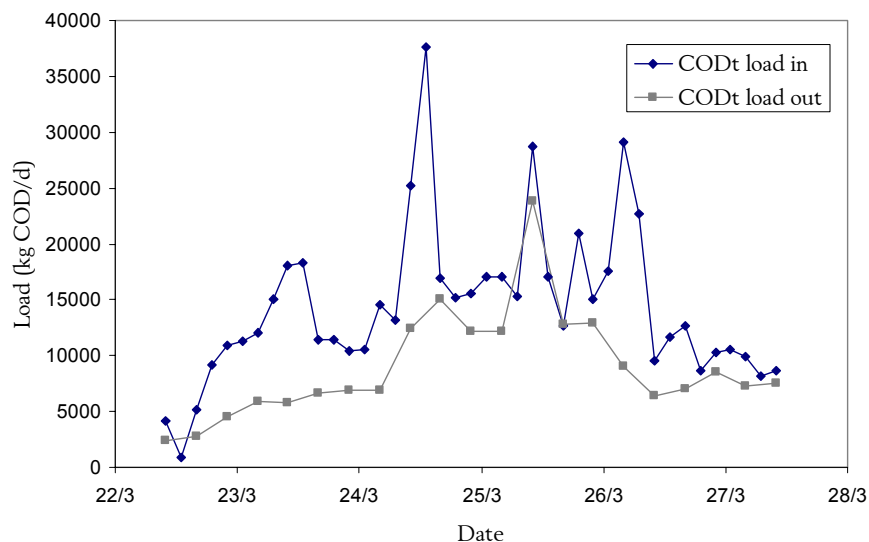


Figure 8.7: Evolution of the total COD load during the measurement campaign

#### 8.4.1.3 $COD_{st}$ concentration and load

$COD_{st}$  concentrations and loads collected with the RODTOX biosensor can be seen in Figure 8.8 and Figure 8.9. Investigation of the  $COD_{st}$  load shows that most probably there was a hydrolysis process going on in the trickling filters. As calculated above, about 37.6% of the total COD was removed in the trickling filter system. The  $COD_{st}$  loads however do not reflect this removal efficiency. This means that part of the COD in the influent that was not readily biodegradable (the difference between the total COD and the  $COD_{st}$ ) was hydrolysed in the filters to readily biodegradable components. This conversion to  $COD_{st}$  can have a considerable effect on the efficiency of the subsequent activated sludge system.

The total COD concentrations are compared with the  $COD_{st}$  concentrations in Figure 8.10. The  $COD_{st}$  measurements seem to lag a bit behind the COD measurements. This has two reasons: (1) the COD measurements were three-hour averages while the  $COD_{st}$ 's were point measurements and (2) there was a dead volume in the valve system between the fast loops and the RODTOX itself. This time lag was less clear in the effluent measurements partly because there were less effluent  $COD_{st}$  measurements available.

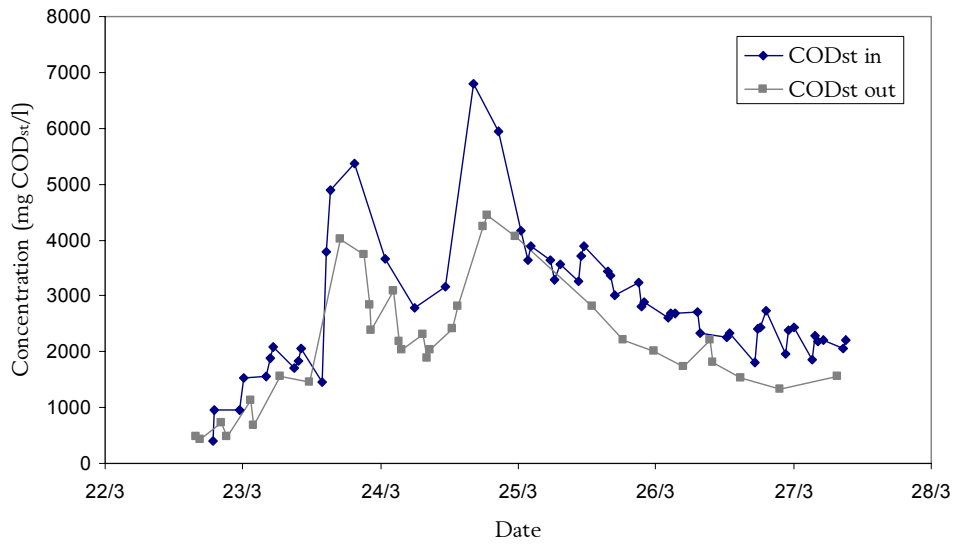


Figure 8.8: Evolution of the  $COD_{st}$  concentration during the measurement campaign

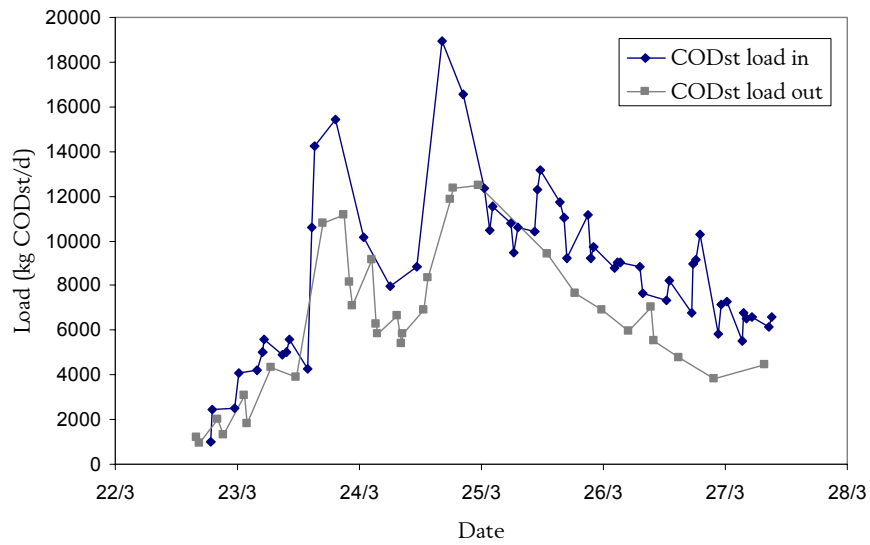


Figure 8.9: Evolution of the  $COD_{st}$  load during the measurement campaign

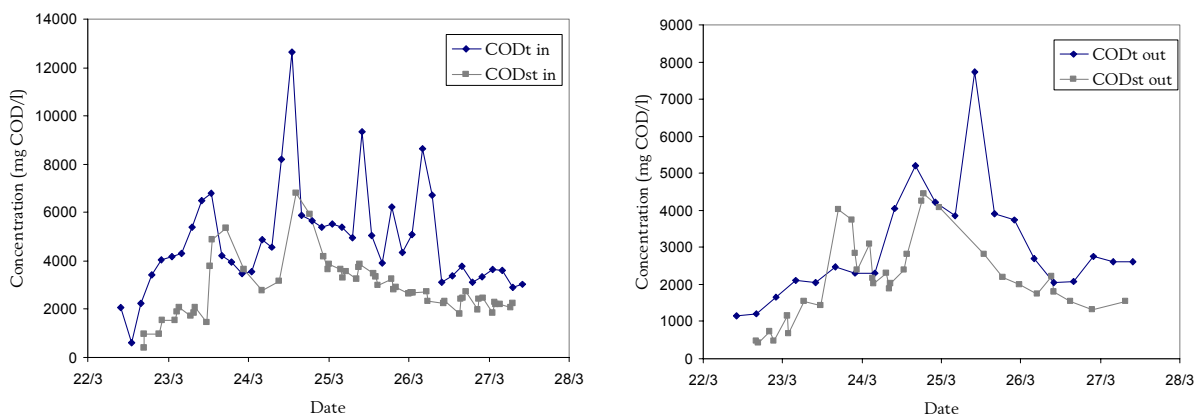


Figure 8.10: Comparison between the total COD and the  $COD_{st}$  in the influent and the effluent

#### 8.4.1.4 $\text{NH}_4^+ - \text{N}$ and total nitrogen concentration and load

Figure 8.11 and Figure 8.12 display the ammonium and total nitrogen concentrations in the influent and effluent of the trickling filter process. The influent measurements show more dynamics than the effluent measurements, which is logical because the measurement interval of the latter was larger and the trickling filter system itself had a mixing effect. These figures show that the major part of the influent nitrogen concentration was organic nitrogen. There were no clear signs of ammonification during the process. With this nitrogen load, no ammonium limitation was to be expected in the trickling filters. In the subsequent activated sludge system, however, ammonium limitation is a possibility if ammonification does not proceed. Obviously, in that case, nitrification is impossible. These findings show the importance of the ammonification process in industrial wastewater treatment. This conversion process should therefore explicitly be considered when modelling such processes.

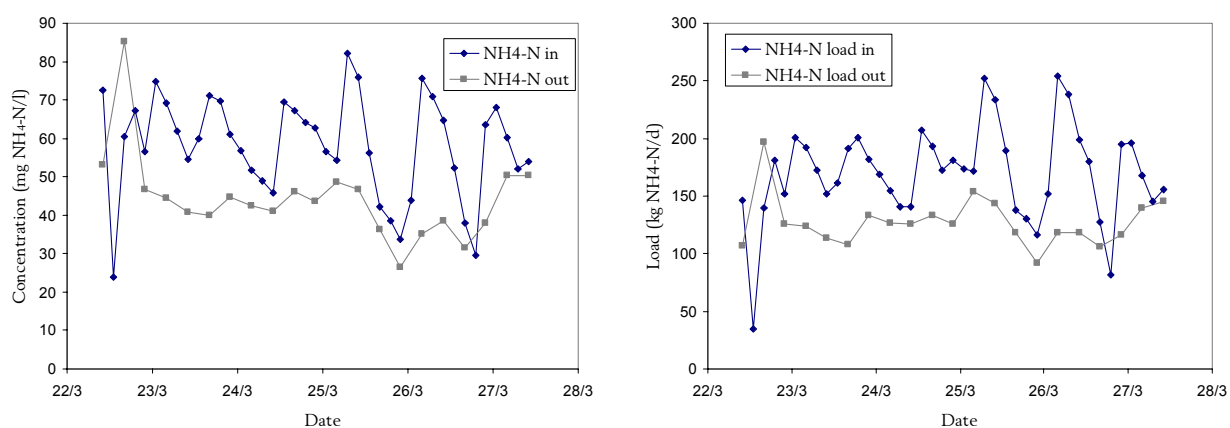


Figure 8.11: Evolution of the  $\text{NH}_4^+ - \text{N}$  concentration and load during the measurement campaign

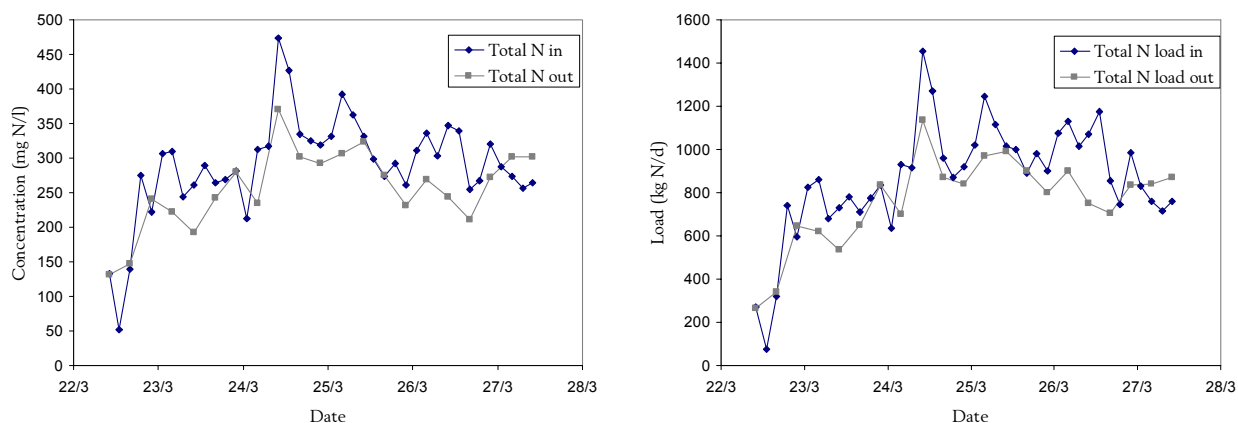


Figure 8.12: Evolution of the Total N concentration and load during the measurement campaign

#### 8.4.1.5 Phosphorus components

No phosphorus (measured as total phosphorus) was detected at any sampling location at any time during the measurement campaign. This was confirmed by on-site measurements on grab samples during the campaign. The low phosphorus content of the biomass in the activated sludge system also revealed the P-limitation in the system (Janssen *et al.*, 2000). Obviously, an adequate phosphorus dosing strategy should be developed.



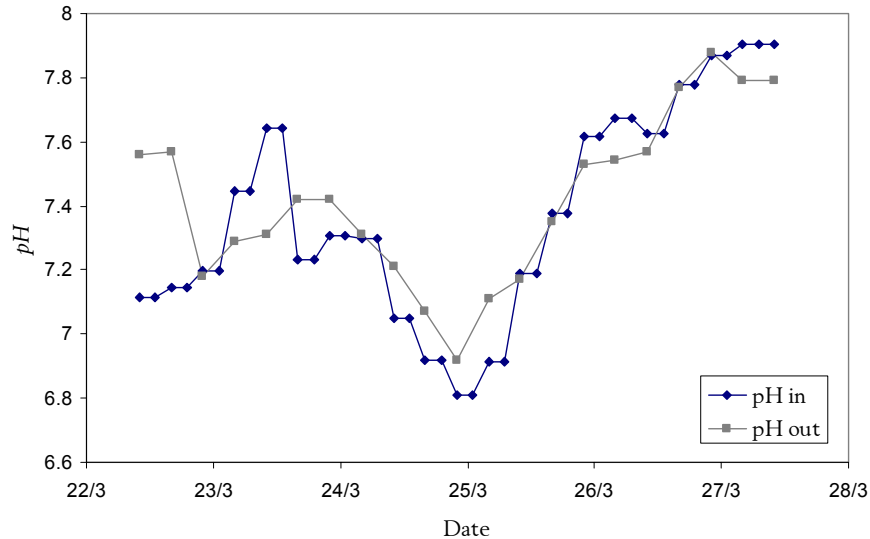


Figure 8.14: pH measurements during the measuring campaign

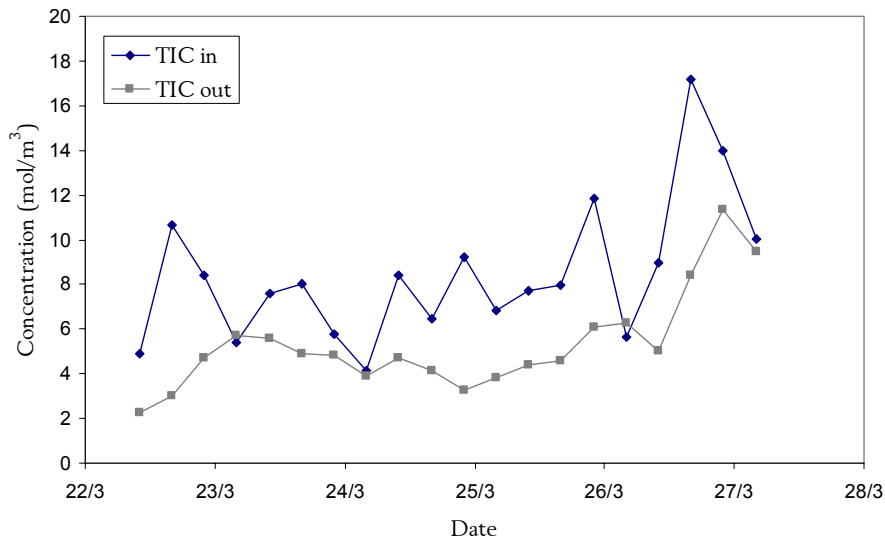


Figure 8.15: TIC measurements during the measuring campaign

On March 24<sup>th</sup> at 15:30 the air flow rate through both filters was changed from high flow to low flow. The effect of this change is visible in Figure 8.16, but it becomes even more clear in Figure 8.17. This Figure zooms in around the time the air flow rate was changed. After about three hours, the total amount of carbon leaving the system via the gas phase returned to the same value of about 450 kg/d as compared to the period before the change. This means that the CER (carbon dioxide evolution rate) remained constant during the test. The drop of the C production after the air flow change revealed the transient behaviour of the CO<sub>2</sub> concentration in the gas phase before reaching a new steady state. As no accumulation of inorganic carbon in the liquid was noticed during the measurements, also the CPR (carbon dioxide production rate) was constant too. This shows that on a short term basis, there was no effect of the air flow rate on the total CO<sub>2</sub> production. It can be concluded that the change of air flow and air retention time apparently has no effect on the oxygen and carbon dioxide mass transfer to and from the water and the biofilm. Also, the very small drop of the driving force for gas-liquid mass transfer does not have a considerable effect.

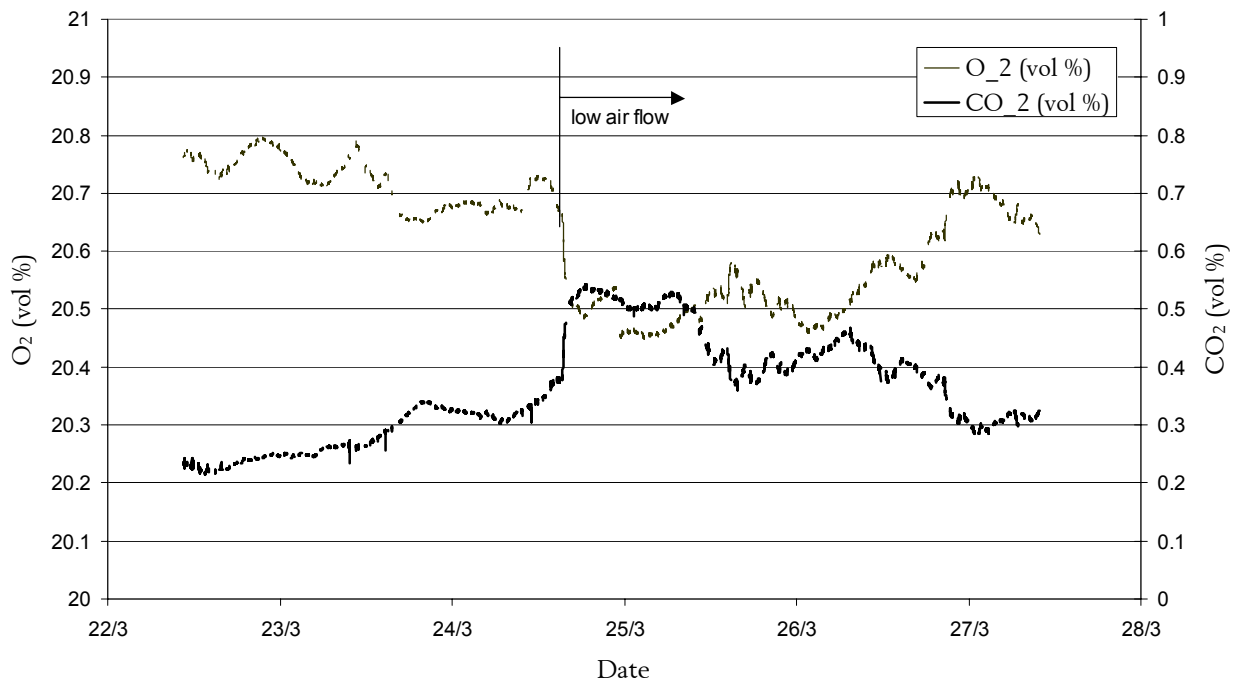


Figure 8.16: Concentrations of  $O_2$  and  $CO_2$  in the off-gas of Trickling Filter TF02

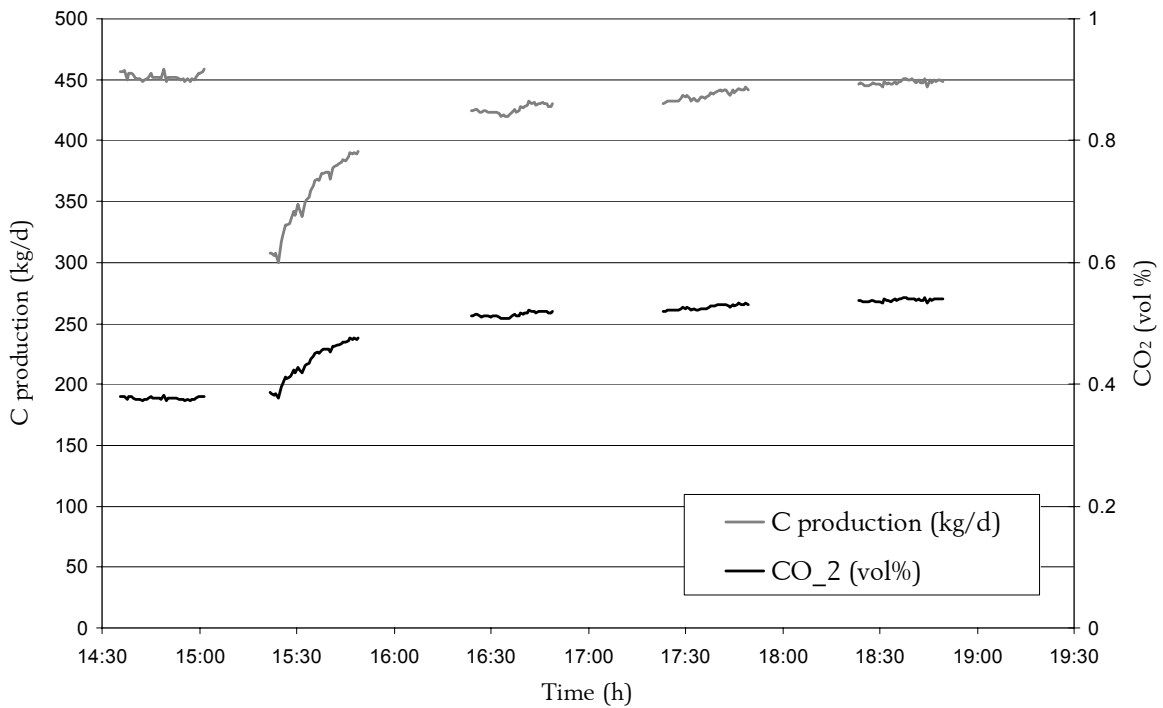


Figure 8.17: C production and  $CO_2$  concentration in the off-gas of TF02 before and after the change in air flow rate.

## 8.5 Dynamic biodegradation modelling

### 8.5.1 Introduction

Using the set of measurements described above, a dynamic model for the trickling filter process was built. A slightly adapted version of the simplified mixed culture biofilm model introduced in chapter 4 was used to describe the bioconversions in the trickling filter. This model was extended for the description of the off-gas analysis measurements as already described in chapter 6. However, to obtain a good description of the overall performance of the system, this bioconversion model was implemented in a framework that describes the mixing and flow propagation of the water and the air phase in the filters. To this end, a tracer test was performed using *LiCl*. Using the results of this test, a hydrodynamic model of the water phase could be built. With the results of the off-gas measurements described earlier, the gas mixing in the filters could be described. The next step in the model development was the adaptation of the bioconversion model to the specific wastewater characteristics of this industrial plant. This adapted model was then implemented and calibrated.

### 8.5.2 Model implementation

#### 8.5.2.1 A simple model for mixing and flow propagation in the trickling filters

The hydraulic behaviour of the trickling filter system could be modelled with the tanks-in-series principle (Levenspiel, 1972). Calibration of this simple mixing model was done using a tracer test with Lithium (De Clercq *et al.*, 1999a).

As already shown on Figure 8.4, the filter has a complicated flow path. It is linked to a pumping tank with a considerable volume and two recycle loops, *i.e.* a “short” recycle and a “long” recycle over the clarifier. The long recycle complicates the flow path considerably, as there is only one clarifier to which the two trickling filters are connected. As a result, the dynamics of both filters are not independent. Hence, the possibility to temporarily disconnect the clarifier was taken advantage of. Also, the sampling points were chosen carefully to allow the identification of a tanks-in-series model of both the pumping tank and the filter (Figure 8.18).

The tracer, 5 kg of *LiCl*, was injected as a pulse in the pumping tank. The measurement of the concentration was performed in the short recycle flow and in the effluent of the pumping tank. The former makes it possible to determine the hydraulics of the trickling filter. The effluent measurement is necessary to distinguish between the hydraulics of the pumping tank and the trickling filter.

The hydraulics of the pumping tank could adequately be described by two tanks-in-series. Physically, it can be assumed that they correspond with the volumes before and after the baffle in the tank. Next to this, a considerable dead volume was found. Before the baffle only 58% of the volume contributes to the advective flow. Behind the baffle merely 15% of the total volume appears to be active (Table 8.1). This could be the result of a thick sludge layer and the absence of mixing devices in the tank.

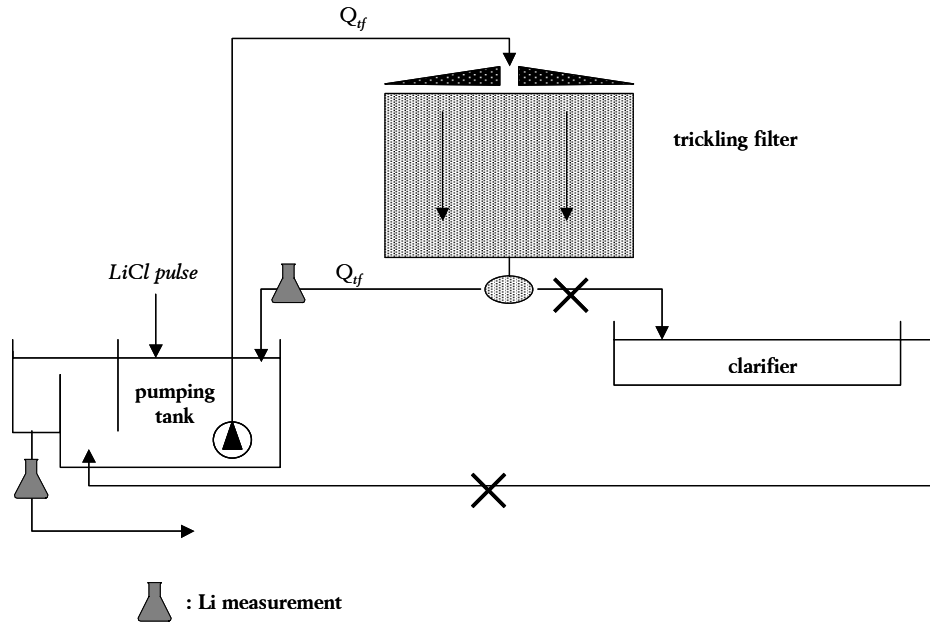


Figure 8.18: Schematic representation of the tracer test set-up

Table 8.1. Simulation results of the hydraulics in the pumping tank

compartment	total volume (m <sup>3</sup> )	active volume (m <sup>3</sup> )	dead volume (m <sup>3</sup> )
before baffle	128	74	54
behind baffle	34	5	29

Once the concentration profile in the pumping tank could be simulated (serving as the influent for the filter), it was possible to study the hydraulic behaviour of the trickling filter itself. For this, it is important to consider the influence of the film structure of the filter. This structure in theory consists of a biofilm, a stagnant and a free flowing liquid film. In such system, diffusion has to be taken into account. Diffusion can be modelled by placing tanks in a parallel configuration, linked to the series of CSTR's describing the free flowing liquid (Rozzi and Massone, 1995; Wik, 1999). It was found that the free flowing liquid in the filter could be described as a two tanks-in-series system with two tanks of 15 m<sup>3</sup> (Figure 8.19, note the “bumps”, *e.g.* around 1 hour, resulting from the recycled tracer). A parallel configuration of tanks was not necessary in the model to describe the lithium dynamics. Apparently, diffusion is sufficiently fast not to influence the residence time distribution.

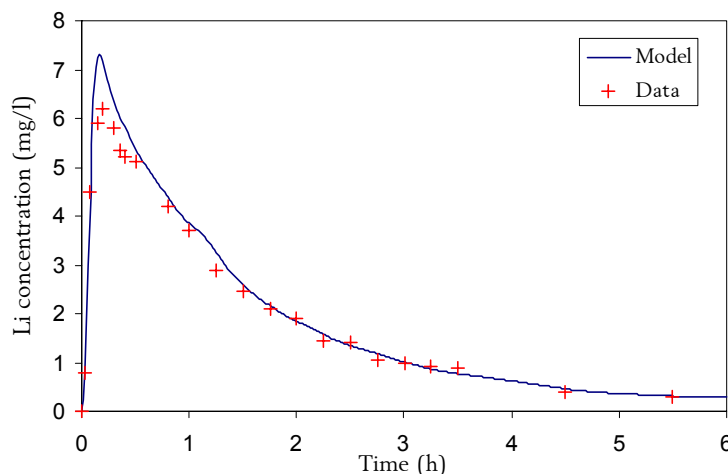


Figure 8.19: Tracer test results and modelling

### 8.5.2.2 Gas mixing in the trickling filters

To investigate the gas mixing in the trickling filter system, the data obtained by switching the ventilators from “high” to “low” position were used. The short term response provided information on the mixing properties of the gas phase inside the reactor. The CO<sub>2</sub> and O<sub>2</sub> data were used to determine the hydrodynamic behaviour of the gas phase in the trickling filters. The measured values of the air flow rate were implemented, together with a fixed production rate of CO<sub>2</sub> and a fixed consumption rate of O<sub>2</sub>. As was shown in paragraph 8.4.2, this assumption could be made because the wastewater composition did not change significantly during the short period around the step change in air flow rate (this was followed with COD measurements) and because the biodegradation was not affected by the air flow rate (at least not within the ranges of air flows used in this study). The results show that the gas phase could be modelled as a single ideally mixed tank. The volume of the single perfectly mixed tank was 2000 m<sup>3</sup>. This volume is larger than the actual volume of the filter bed, but the head space above the bed must be considered too. The result of the simulations – no calibration was needed – can be seen on Figure 8.20. As an example, the measured and simulated CO<sub>2</sub> concentrations are depicted. An equally good result was obtained with the O<sub>2</sub> measurements.

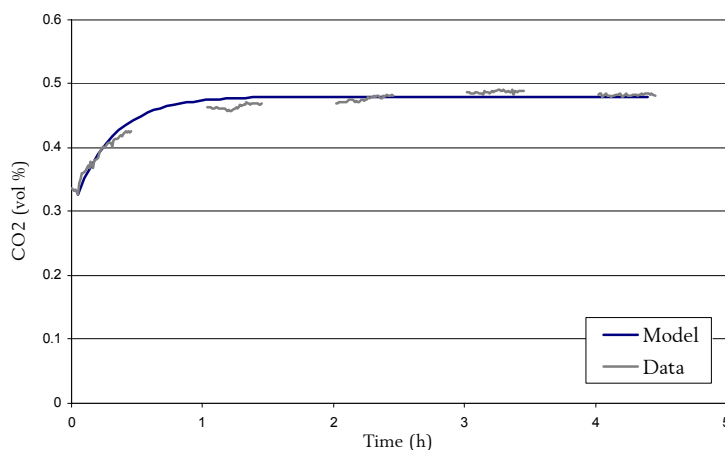


Figure 8.20: Evaluation of the gas phase hydrodynamics, modelled as a single mixed tank of 2000 m<sup>3</sup>

### 8.5.2.3 WEST implementation

Figure 8.21 shows the layout of the filter in the WEST simulator. The number of tanks and their respective volumes were determined using the tracer tests described in paragraphs 8.5.2.1 and 8.5.2.2. For the modelling of the biochemical conversions in the filter, the simplified mixed-culture biofilm model was used. The dynamic model along with the extension for off-gas analysis measurements as described in chapter 6 was implemented in the WEST simulator.

### 8.5.3 Model adaptation and wastewater composition

The simplified mixed-culture biofilm model was slightly adapted to describe the specific wastewater characteristics at the WWTP under study. A new influent component was introduced, named  $S_R$ . This was needed to make the mass balance of soluble COD fit. Some soluble COD was not biodegraded fast enough and could therefore not be measured using the RODTOX biosensor. Hydrolysis of  $S_R$  was described by a simple first-order equation and is producing  $S_S$ .

The fraction of readily biodegradable substrate  $S_S$  was estimated from the available on-line RODTOX data, after a conversion to COD values. At the plant under study, it was the experience from short term RODTOX experiments that the yield with acetate is in the range 0.7-0.85, whereas the yield for wastewater lies a bit lower, around 0.5 (Petersen, 1999).

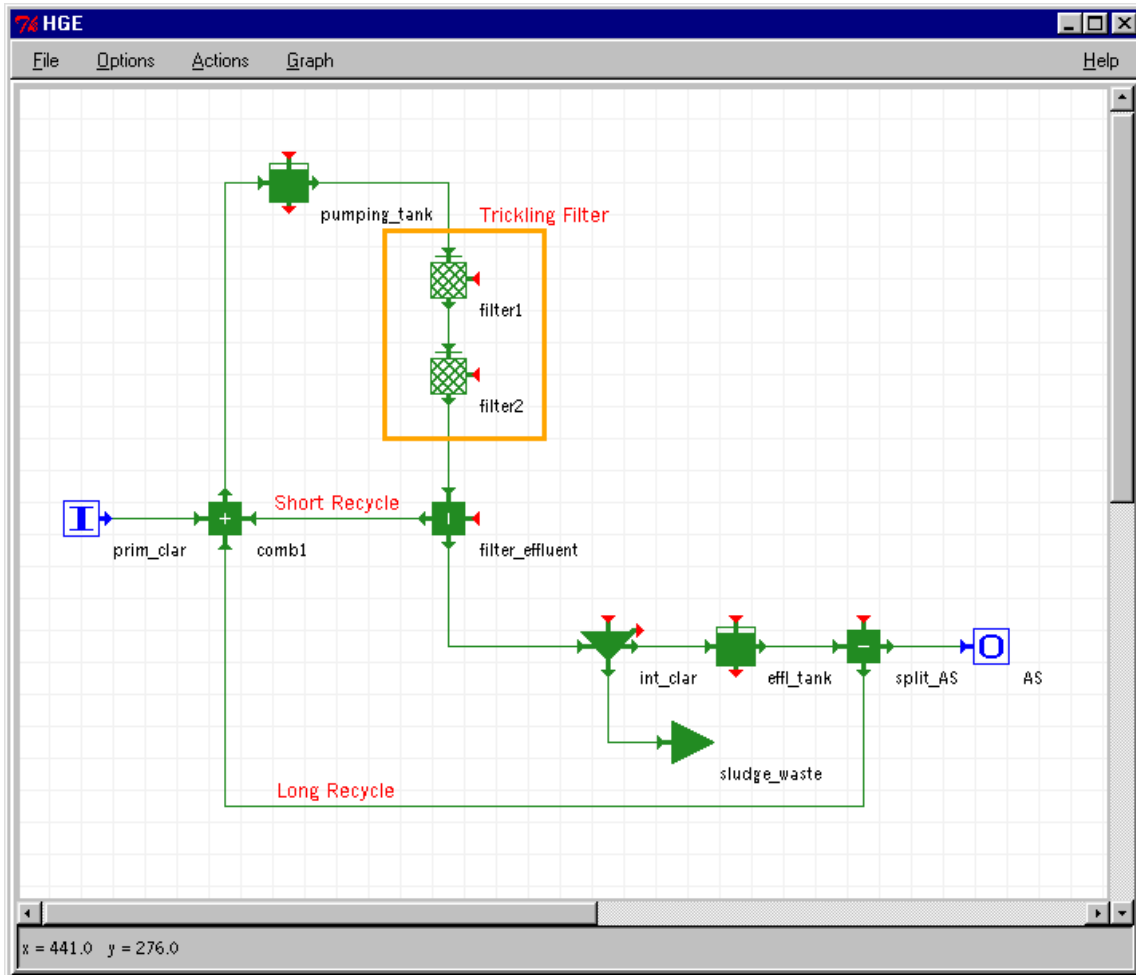


Figure 8.21: Layout of the trickling filter system in the simulator WEST

The soluble, inert non-biodegradable substrate is typically determined by a mass balance with data of the final effluent. The  $S_S$  content of the effluent was estimated from the available  $BOD_5$  measurements converted to COD. An estimate of the particulate fraction was obtained from the available SS measurements. Consequently, the soluble inert could be estimated from the mass balance:

$$COD = S_I + S_S + S_R + X_{BH} + X_I \quad (8.2)$$

The soluble hydrolysable substrate  $S_R$  could be determined by a mass-balance of soluble COD.

$$COD_S = S_I + S_R + S_S \quad (8.3)$$

The amount of particulate COD in the wastewater was rather insignificant. It was estimated as the difference between the measured total and soluble COD. However, this value was very small

compared to the suspended solids measurements in the influent. This indicates that a considerable part of this suspended solids was inorganic. For this reason, the amount of  $X_f$  in the influent was adapted in view of these high SS measurements. However, this inorganic fraction of the SS has in reality no COD. It is however important to consider it in order to be able to calibrate the sludge balance in the trickling filter system.

Nitrogen was measured as Total Nitrogen and ammonium. As particulate nitrogen in the influent was considered insignificant, the mass balance for nitrogen became straightforward. During the measurement campaign, the influent ammonium concentration was rather high, so no limitations were expected. Therefore, no special attention was given to the definition of an inert nitrogen fraction.

### 8.5.4 Model Calibration

In the calibration of the model, the model parameters were adapted to fulfil :

1. The sludge balance: It is important that the sludge balance of the model matches. However, good data about the sludge production of the plant were not available. Only suspended solids of the intermediate clarifier influent and effluent were measured. It was chosen to change the attachment and detachment model coefficients to approximate the suspended solids measurements. To have an extra check on the sludge balance, the removal of nitrogen from the system was monitored (Figure 8.27). Since neither nitrification nor denitrification were occurring, these processes were removed from the model. Nitrogen removal is then only via assimilation and, thus, due to sludge removal from the intermediate clarifier.
2. The effluent concentrations: A major aim of the model is that it describes the concentrations of the biodegradable substrates and the nitrogen components. The parameters to which the model is most sensitive in this respect are the specific growth rate  $\mu_{max}$ , the decay rate  $b_H$  and the yield coefficient  $Y_H$ . For this case study, lab experiments have shown that the well-accepted yield (Henze *et al.*, 1987) of 0.67 is too high and that a value of 0.5 is more appropriate (Petersen, 1999). Typically, for biofilm models the diffusion coefficients of substrates in the biofilm ( $D_f$ ) have to be calibrated. In the measured data, it is clear that a load-peak in the influent is followed by a peak in the  $O_2$  uptake and the  $CO_2$  production in the filters (Figure 8.22 and Figure 8.23). Initially, it was assumed that the system would be oxygen limited. Under this limitation, these peaks would not occur. The system observations could thus not be modelled by an oxygen limited system. As an alternative, the diffusion constant for the readily biodegradable substrate  $S_S$  was adjusted. A very low value was necessary to reach a good fit.
3. The off-gas concentrations: The model parameters were adapted to make the predictions follow the measured off-gas concentrations. For the inorganic carbon components, it is also important to model the liquid phase inorganic carbon concentrations,  $CO_{2,(aq)}$  and  $HCO_3^-$ . Particularly, the knowledge of  $IC$  in both the liquid and the gas phase can be used to obtain good estimates of the  $K_L a$  for  $CO_2$  and thus also for  $O_2$ . Indeed, it can be shown that  $(K_L a)^{CO_2} \approx 0.9(K_L a)^{O_2}$  (Spérandio and Paul, 1997).

The calibration results are given in Figure 8.22 to Figure 8.27. The parameters used are shown in Table 8.2. A TOC/COD ratio of 0.33 was selected using the results of a measuring campaign with a TOC sensor at the influent of the plant.

**Table 8.2. Biodegradation model parameters**

$\text{CO}_2 / \text{HCO}_3^-$ equilibrium and mass transfer parameters			Biofilm characteristics		
$k_1$	0.018 [a]	$\text{s}^{-1}$	$\mu_H$ [growth rate heterotrophs]	2.5	$\text{d}^{-1}$
$K_1$	$4.065 \cdot 10^{-7}$ [a]	$\text{mol.l}^{-1}$	$Y_H$ [heterotrophic yield]	0.5	$\text{g COD/ g COD}$
$k_2$	4600 [a]	$\text{l. (mol/s)}^{-1}$	$b_H$ [heterotrophic decay]	0.25	$\text{d}^{-1}$
$K_2$	$4.065 \cdot 10^{+7}$ [a]	$\text{l.mol}^{-1}$	$k_r$ [hydrolysis of $S_R$ ]	50	$\text{d}^{-1}$
$K_{La}(\text{O}_2)$	5000	$\text{d}^{-1}$	$k_h$ [hydrolysis of $X_s$ ]	2	$\text{d}^{-1}$
$K_{La}(\text{CO}_2)$	4500	$\text{d}^{-1}$	$k_a$ [ammonification of $S_{ND}$ ]	0.005	$\text{m}^3.(\text{g COD.d})^{-1}$
$D_f(S_{\text{O}})$	$2.10 \cdot 10^{-5}$ [b]	$\text{cm}^2/\text{s}$	$k_{at}$ [attachment coefficient]	20	$\text{d}^{-1}$
$D_f(S_{\text{S}})$	$6.10 \cdot 10^{-7}$	$\text{cm}^2/\text{s}$	$k_{dt}$ [detachment coefficient]	0.05	$\text{d}^{-1}$

[a] Spérandio and Paul, 1997 [b] Bird *et al.*, 1960

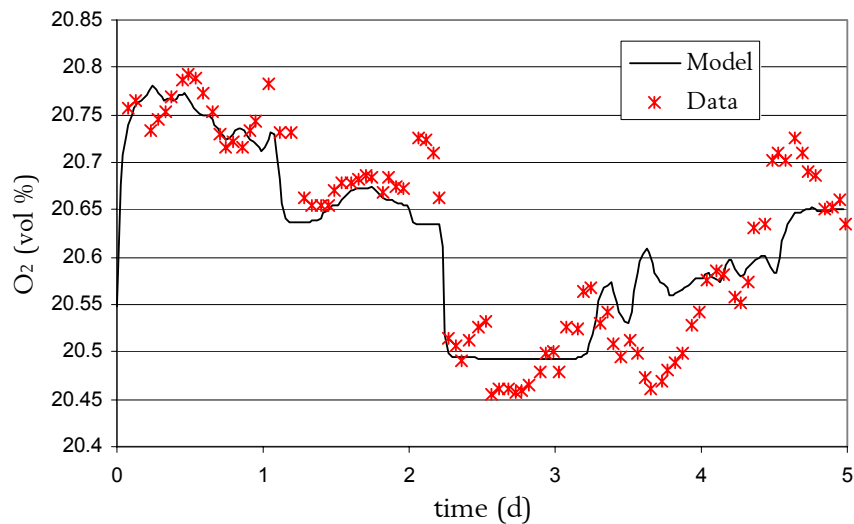


**Figure 8.22: Measured and simulated off-gas  $\text{O}_2$  concentration**

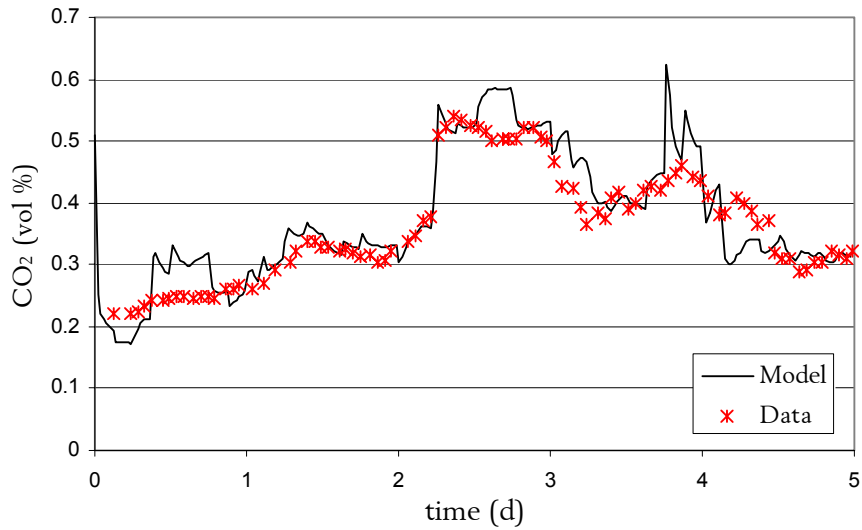


Figure 8.23: Measured and simulated off-gas  $CO_2$  concentration

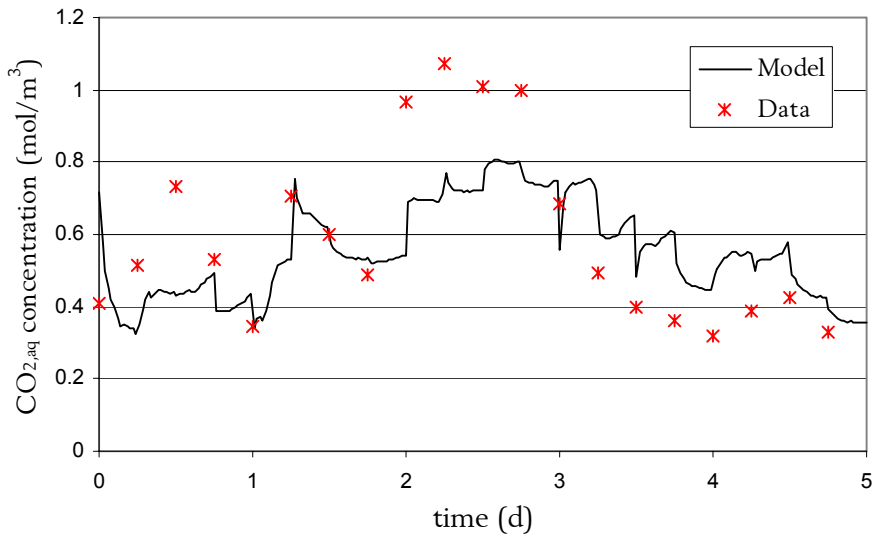


Figure 8.24: Measured and simulated effluent concentration of  $CO_{2,aq}$

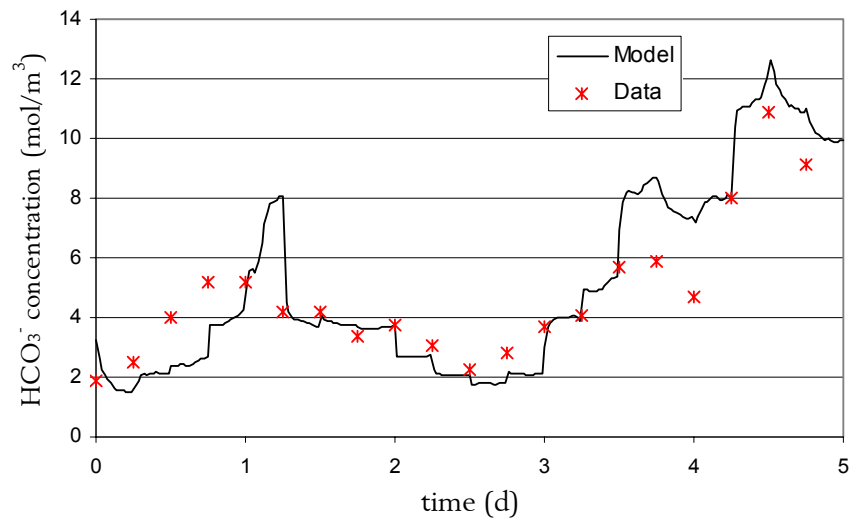


Figure 8.25: Measured and simulated effluent concentration of  $HCO_3^-$

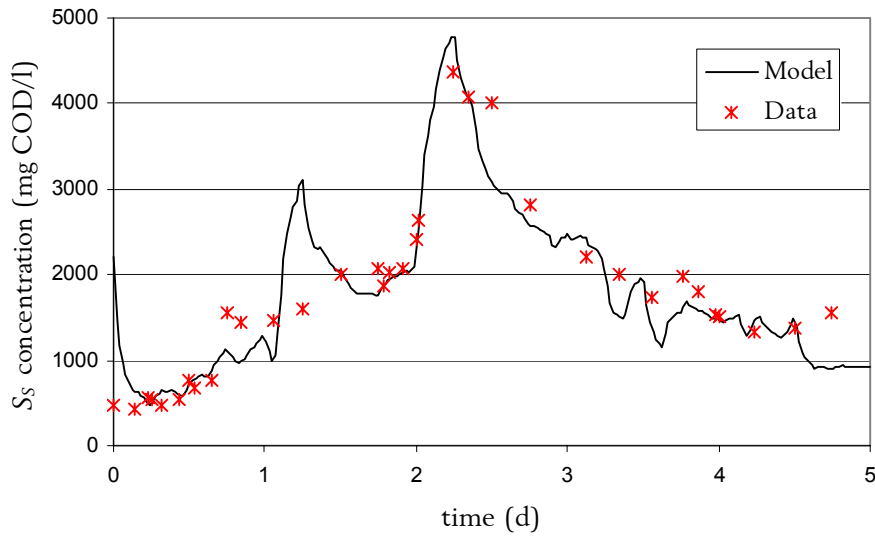


Figure 8.26: Measured and simulated effluent concentration of readily biodegradable substrate

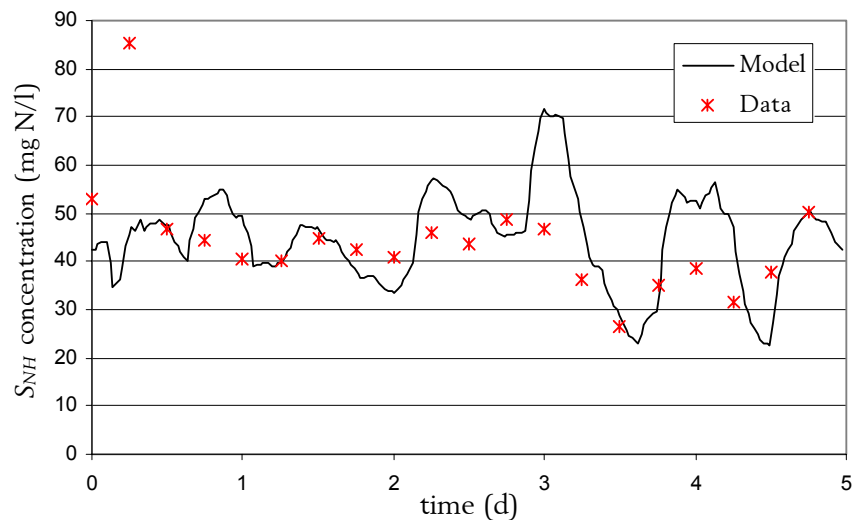


Figure 8.27: Measured and simulated effluent concentration of ammonium nitrogen

### 8.5.5 Bulk liquid biodegradation and anaerobic biofilm activity

Because the necessary diffusion coefficient for  $S_S$  was so low, there was still some doubt about the validity of the model regarding the substrate limitation in the biofilm. For that reason, the possibility was studied that significant biodegradation could occur in the liquid phase outside the biofilm and in the pumping tank and remove enough substrate so that the biofilm would become oxygen limited. To this end, a model describing biodegradation was added to the model description of the pumping tank and of the liquid phase of the trickling filters. To obtain the parameters needed to describe the biodegradation in the liquid phase in the filters, a respiration test was performed with the effluent of the trickling filters. A maximal respiration rate of  $0.218 \pm 0.012$  mg  $O_2$ /l.min was measured. In the pumping tank, a Monod-type dependency of substrate utilisation to oxygen concentration was implemented. The Monod saturation constant needed, was obtained from the calibrated model of the subsequent activated sludge plant (Petersen, 1999). Since the pumping tanks are not aerated nor mixed, no oxygen supply to the pumping tank was modelled. In the simulations, only 2% of the total biodegradation was due to degradation in the liquid and not in the biofilm.

Finally, the possibility of substrate removal via anaerobic metabolism in the deeper layers of the biofilm was studied. Measurements of the CH<sub>4</sub> concentration in the off-gas were performed using gas chromatography. A concentration of only 50 ppm CH<sub>4</sub> was found in the off-gas of trickling filter TF02. The air flow in the filter at the time of the measurement was 6600 m<sup>3</sup>/h. This means 7.92 kg CH<sub>4</sub> is produced every day, which is equivalent to 31.7 kg COD/d. Obviously some anaerobic metabolism is present in the deeper layers of the biofilm, but methanogenesis is not present to such a degree as to cause a significant removal of organic matter.

## 8.6 Phosphorus dosing

### 8.6.1 Introduction

During the measurement campaign, no phosphorus could be detected in any of the influent samples. It therefore seems obvious that a good phosphorus dosing strategy should be implemented so as to avoid major nutrient limitation of the biomass in the trickling filters. To investigate the effect of the dosing of phosphorus to the biomass, a second measurement campaign was carried out during which phosphorus was dosed to the trickling filter system. The phosphorus addition was chosen such that an excess amount of phosphorus was added. This meant that in the effluent of the trickling filters an orthophosphate concentration of 5 to 6 mg/l was measured. This excess of phosphorus was then consumed in the subsequent activated sludge system. The frequency of the off-line measurements was lower as compared to the first measurement campaign. Only two COD samples were examined per day in the influent and the effluent of the filter system. However, an extra on-line measurement was included. Next to the off-gas analysis sensor and the RODTOX biosensor for the estimation of readily biodegradable substrate, an on-line TOC sensor was included. Since the RODTOX sensor produced an estimate of the effluent quality, the TOC sensor was placed at the influent line of the filter. The TOC sensor was chosen because the measurement apparatus was available on-site during the tests of an advanced control strategy for equalisation of the influent composition to the plant (Harmand *et al.*, 1999; Devisscher *et al.*, 2000).

### 8.6.2 Measurement results

The results of the measurement campaign are depicted in Figure 8.28 to Figure 8.31. In these figures, the flow rate, the influent TOC concentration, the effluent COD<sub>st</sub> concentration and the off-gas concentrations can be followed. As can be seen on Figure 8.28, the peaks in the influent composition are not as high as the ones observed during the first measurement campaign. Also, the concentration peak on March 29<sup>th</sup> was compensated by a lower influent flow rate, so the influent load remained rather constant during the measurement campaign (Figure 8.29).

The dosing of phosphorus was started at 10:00 on March 28<sup>th</sup>. This was exactly at the time a high COD<sub>st</sub> load was measured in the effluent. Because of the hydraulic retention time in the system, the dosing of phosphorus can not have had an effect on the highest effluent load measured at 10:05 (Figure 8.30). It is not known what caused the worsening treatment efficiency at that point. There is only limited evidence of an increasing influent load before 10:00 on March 28<sup>th</sup> (Figure 8.28 and Figure 8.29). Apart from this peak, there was no noticeable difference between the treatment

efficiency before and after the addition of phosphorus. It should be noted that it is hard to define the treatment efficiency using the available data.

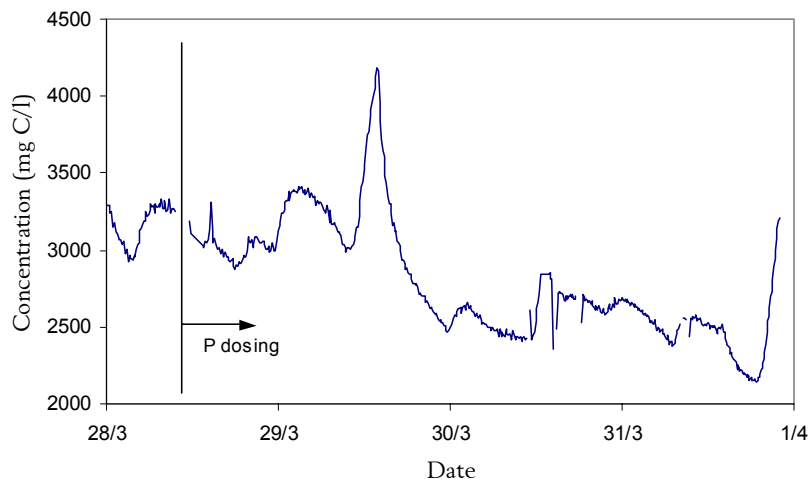


Figure 8.28: Evolution of the influent TOC concentration during the second measurement campaign

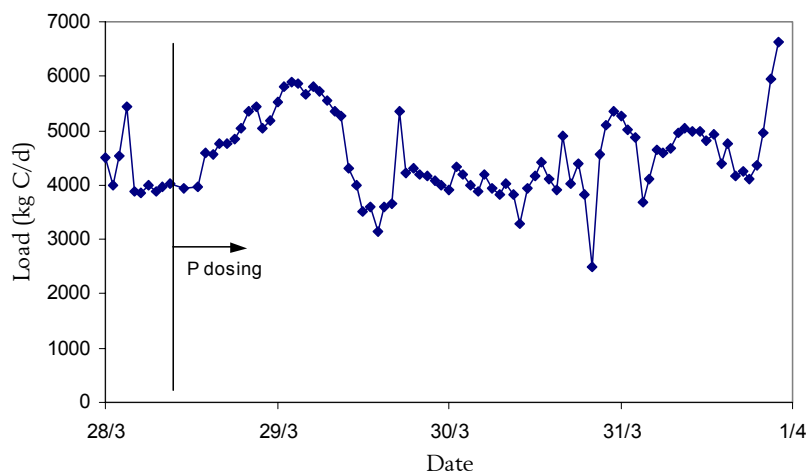


Figure 8.29: Evolution of the influent TOC load during the second measurement campaign

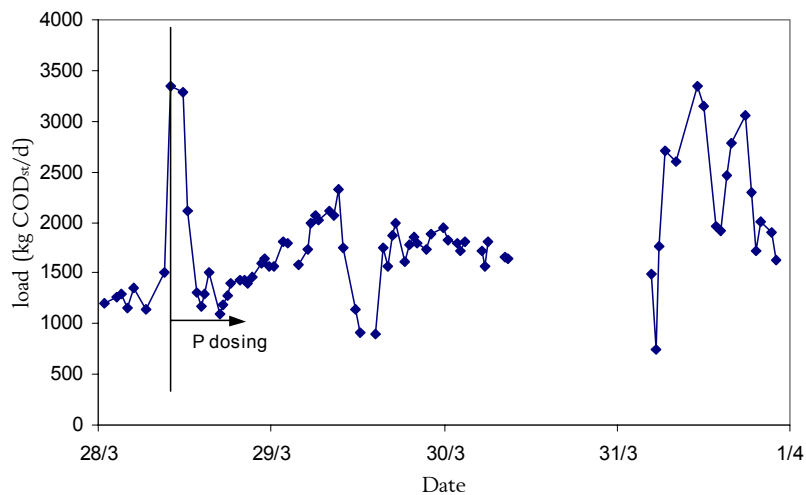


Figure 8.30: Evolution of the effluent COD<sub>st</sub> load during the second measurement campaign

In contrast with the unclear effects on the treatment efficiency, there was a clear effect of the phosphorus dosing on the off-gas measurement results (Figure 8.31). There was a decrease of the oxygen consumption and a decrease of the carbon dioxide production. This was somewhat unexpected, because it had been anticipated that a higher amount of phosphorus available would have increased the treatment capacity and the oxygen consumption and carbon dioxide production with it. As mentioned before, an increased treatment capacity was apparently not available. A possible reason for the effects on the off-gas measurements is an increase of the sludge yield. Part of the substrate consumed is used to for biomass growth, the rest is used as electron donor to yield energy for growth. In this last part, oxygen is consumed that is reduced to carbon dioxide. A change of this equilibrium toward more cell growth lowers the oxygen demand and the carbon dioxide production. This could explain the temporary effect seen on Figure 8.31. It was not possible to isolate data on the sludge production of the trickling filter plant alone, since the sludge is treated together with the sludge coming from the subsequent activated sludge treatment plant. However, after consulting the plant operators, it could be concluded that the sludge yield had increased. This was confirmed by visual inspection of the intermediate clarifier where a relatively large sludge wash-out was noticed. Biofilm pieces coming from these high rate trickling filters are rather small compared to activated sludge flocs and are therefore poorly settleable. An increase in the sludge production can therefore immediately be noticed in the intermediate clarifier effluent.

### 8.6.3 Modelling

It was attempted to use the model developed in paragraph 8.5 to model the effect of the phosphorus dosing. The influent TOC data were converted to COD based on the COD/TOC ratio of  $2.85 \pm 0.37$  g/g measured on the samples collected twice a day during the measurement campaign. A rough estimation of the readily biodegradable fraction of this COD was done based on the average fraction of biodegradable COD during the first measurement campaign. This is however not of very big importance since even with the increasing oxygen concentration, the upper half of the filter was still modelled as being oxygen limited over the complete period of the measurement campaign. Indeed, the influent COD concentration is continuously relatively high during the second measurement campaign. The effluent total COD was estimated based on a COD/COD<sub>st</sub> ratio of  $2.9 \pm 1.3$  g/g. Because of the large standard deviation, this can only be used as a very rough estimation of the effluent concentration.

Most important, however, was the modelling of the off-gas measurement results. This can be seen in Figure 8.32. The X-axis displays the time elapsed after the start of the phosphorus dosing. Because of the observed increase of the sludge production, it was chosen to use the yield parameter  $Y_H$  to fit the model to the measured data. This parameter is the only parameter that has the ability to change the oxygen consumption without a considerable impact on the modelled treatment efficiency. With any other combination of model parameters (for example growth or decay rate) it is not possible to change the oxygen consumption and carbon dioxide production to this extent without drastically changing the treatment efficiency of the overall system. Therefore it was decided to change the yield coefficient to a value of 0.8 g/g immediately after the phosphate dosing.

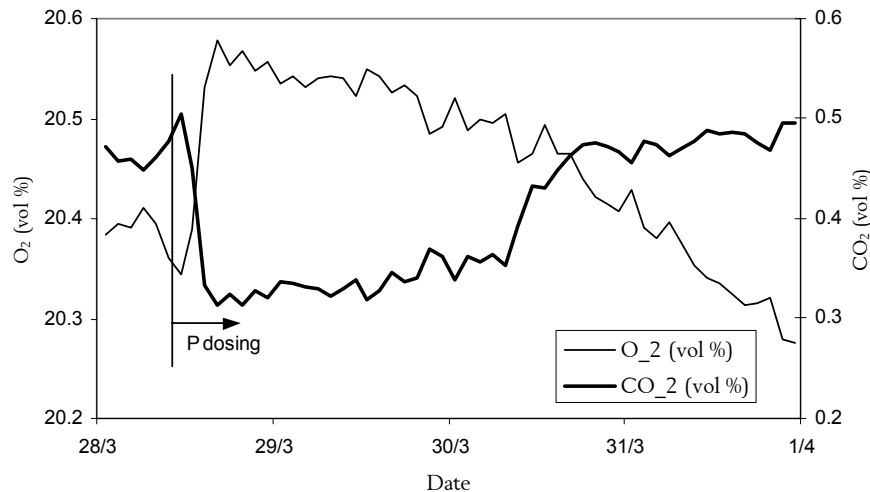


**Figure 8.31: Concentrations of  $O_2$  and  $CO_2$  in the off-gas of Trickling Filter TF02**

It is remarkable that the effect of the dosing of phosphate attenuates during the days that follow the start of the dosing. To model this behaviour, the yield coefficient was gradually returned to its normal working value of 0.5 g/g after 3 days, using an exponential decrease (Figure 8.32). This could possibly be explained by a storage phenomenon where the biomass is saturated with phosphate after a while and returns to normal activity. However, this hypothesis should be stated with care, since the duration of the intensive measurement campaign was not long enough for a long-term evaluation. The phosphate dosing was stopped after 7 days, because the increased sludge production caused a considerable sludge wash-out from the intermediate clarifier.

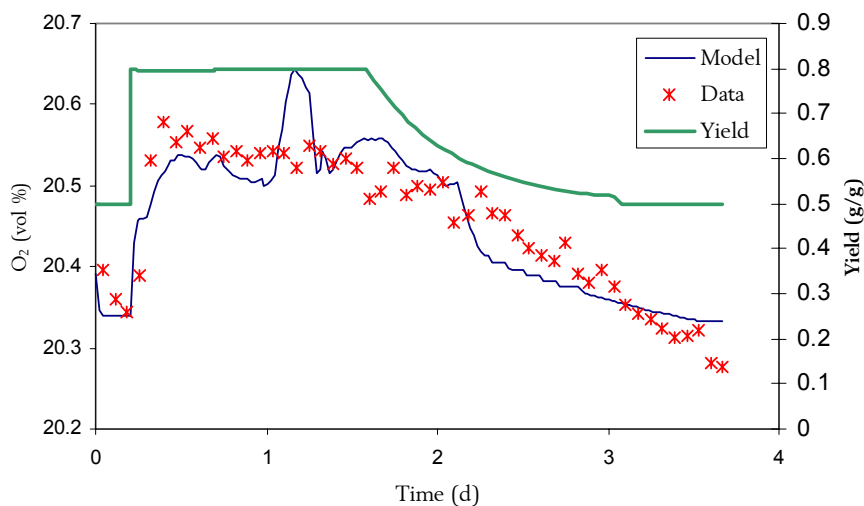


**Figure 8.32: Monitored and modelled  $O_2$  concentration in the off-gas of Trickling Filter TF02**

## 8.7 Conclusions

A model was built and calibrated to describe the biodegradation in an industrial scale trickling filter. The calibration was based on the results of a 5 day intensive measurement campaign with the use of on-line respirometry and off-gas analysis. Respirometry was used to measure the readily biodegradable COD in the influent and the effluent of the plant. Off-gas analysis was used to monitor the  $O_2$  and

CO<sub>2</sub> content of the off-gasses. The model was extended with a section describing the production and transport of CO<sub>2</sub> and inorganic carbon (IC). The measured effluent and off-gas concentrations could be followed very closely by the calibrated model. O<sub>2</sub> and CO<sub>2</sub> measurements revealed that the system was not always oxygen limited. In the model calibration the use of a very low value of the diffusion constant for readily biodegradable substrate was found to be the best means for describing the observed data. Alternative modelling approaches such as liquid film biodegradation and anaerobic degradation within the biofilm were investigated, but these could not account for sufficient COD removal to change the conclusions above.

As only a very limited amount of phosphate is available in the influent, the effect of the dosing of phosphate on the trickling filter system was studied. Apparently, the net phosphate take-up by the biofilm is very limited under normal operating conditions, since the phosphate dosing did not bring along higher treatment efficiency. Apparently phosphate can be recycled inside a full-grown biofilm, so the net phosphate demand is rather small. However, shortly after the start of the dosing, a clear effect on the off-gas measurement results and the sludge production was noticed. This effect damped out in some days time and could only be modelled by temporarily increasing the yield coefficient for heterotrophic growth making the oxygen consumption decrease and the sludge production increase.



# 9

## Modelling VOC stripping in a trickling filter

---

### 9.1 Introduction

Industrial wastewater treatment plants have to cope with heavily loaded wastewaters. Often, a considerable part of the chemicals in the wastewater is highly volatile (*e.g.* solvents). As aeration is a basic process in aerobic biological treatment, there is a big risk for stripping off these volatile organic contaminants (VOC's) together with the air used for aeration (Melcer *et al.*, 1995). The environmental impact of VOC's is high because some of them are toxic, while others contribute to ground-level ozone generation. Most of the studies concerning stripping of VOC's have focused on activated sludge systems. Less is known about their fate in trickling filter systems or other fixed film wastewater treatment plants. Also, stripping is likely to be the most important removal mechanism of volatile components in such systems, as VOC biodegradation is known to be low in systems with short retention times (Dobbs *et al.*, 1989).

In this study, the VOC removal in an industrial wastewater treatment plant was monitored and modelled. The plant under study has a very highly loaded influent carrying a considerable amount of volatile components. The plant consists of a downflow trickling filter system with forced countercurrent aeration, followed by an activated sludge system. Environmental legislation enforces the construction of an off-gas treatment facility for the trickling filter system. The capital and operating cost and the efficiency of this facility are dependent on the air flow to be treated and the concentration of VOC's. In the trickling filter process, a high removal efficiency of the VOC's – next to biodegradation of non-volatile components – is desired, to prevent volatile compounds in the wastewater to wash out to the activated sludge system where they could strip into the open air or hamper the biomass activity.

Two models describing the stripping of volatile organic contaminants (VOC's) in this industrial trickling filter system are developed. The aim of the models is to investigate the effect of different operating conditions (VOC loads and air flow rates) on the efficiency of VOC stripping and the resulting concentrations in the gas and liquid phases. The first model uses the same principles as the steady-state non-equilibrium activated sludge model *SimpleTreat*, in combination with an existing biofilm model. The second model is a simple mass balance based model only incorporating air and liquid phases and thus neglecting biofilm effects.

In a first approach, the *SimpleTreat*-like model was incorporated in a five-layer hydrodynamic model of the trickling filter, using the carrier material design data for porosity, water hold-up and specific surface area. A tracer test with lithium was used to validate this approach, and the gas mixing in the filters was studied using continuous CO<sub>2</sub> and O<sub>2</sub> measurements. With the tracer test results, the biodegradation model was adapted. On the basis of the results obtained with this adapted model, a simple dynamic mass balance model was built and used to perform scenario analysis so as to optimise the design of the off-gas treatment facility.

## 9.2 Non-equilibrium steady-state modelling

The first model used, is a model for the fate of individual chemicals that was built based on the *SimpleBox* approach (van der Meent, 1993) combined with the existing steady-state biofilm diffusion/biodegradation model of Melcer *et al.* (1995). In *SimpleBox*, chemical fate is calculated under non-equilibrium steady-state conditions, using a mass balance between several completely mixed boxes. Previously, this method was applied in the activated sludge chemical fate model *SimpleTreat*, which is used as a standard model for activated sludge systems in EU environmental risk assessment (Struijs, 1996; Boeije, 1999; Verbrugge, 1999). This new approach for chemical fate modelling in trickling filters was published in Boeije *et al.* (2000), where it was tested using experimental results for the surfactant LAS (Linear Alkylbenzene Sulfonate), obtained in the pilot-scale trickling filter described earlier in this thesis (chapter 5). Here, the capability of the model to describe the fate of VOC's in trickling filters is tested using data from the full-scale industrial trickling filter described in chapter 8.

### 9.2.1 Processes occurring in a trickling filter system

An overview of biological and chemical processes occurring in a trickling filter is given in Figure 9.1. Chemicals are present in the dissolved phase and sorbed to suspended solids; the interchange between these phases goes via ad-/desorption. The dissolved chemical can diffuse into the biofilm. Suspended solids with sorbed chemicals may be filtered out of the water; chemicals associated with biofilm solids may be released in the sloughing process. (Bio)degradation may take place inside the biofilm and in the water. Finally, the dissolved chemical may be subject to volatilisation and may thus be removed with ventilation air.

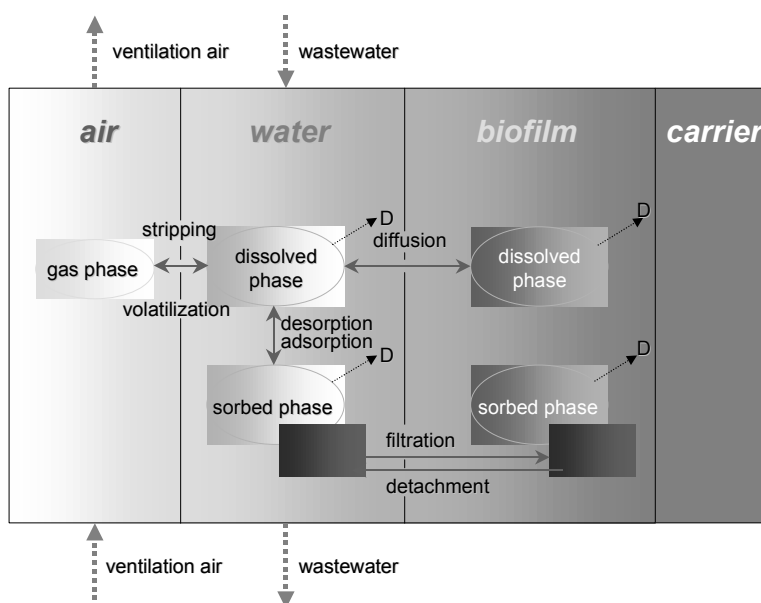


Figure 9.1: Overview of the biological and chemical processes in a trickling filter (D = degradation)

### 9.2.2 Segmentation of the filter system

The trickling filter system was subdivided into a number of completely mixed boxes. The first segmentation was between the air above the plant, the filter unit and the settler. The settler was divided further into a dissolved and a sorbed phase. The filter itself was split up into five horizontal

layers to mimic the plug flow behaviour of such a plant. Each of these layers was subdivided into three compartments: air, pore water (dissolved phase) and pore water (sorbed phase). Downward transport of (dissolved and sorbed) chemicals through the filter unit occurs between the pore water of the different layers. By ventilation, air is transported upward between the layers. Within a layer, exchange processes take place between air and water (volatilisation) and between the sorbed and dissolved phases. To simplify the model, it was assumed that filtration and release (by sloughing) of the sorbed chemical balance each other (resulting in a zero net effect), and chemical sorption equilibria within the biofilm were not considered.

Biodegradation mainly occurs in the biofilm. Continuous chemical diffusion from the pore water into the biofilm is sustained by a concentration gradient due to biodegradation in the biofilm. These coupled processes are dealt with by the steady-state biofilm model of Melcer *et al.* (1995). In this model, the calculated chemical diffusion flux from the pore water into the biofilm is expressed as chemical removal out of the water phase. Hence, the biofilm compartment need not be represented as an extra box.

Next to the between-layer transport, there is also transport of air from the top layer of the filter to the air above the plant, and volatilisation from the settler surface. Air flows counter-current through the filter unit (in this case by forced aeration). There is water and solids transport by means of the effluent recycles to the top filter layer. Influent enters the plant into the top filter layer, and effluent, as well as waste sludge, leave the plant via the settler.

As the number of layers used to describe the filter unit is not necessarily fixed, the following flexible box numbering approach was introduced by Boeije (1999) (Figure 9.2). The 'outside world' is box 0; the air compartment above the WWTP is box 1. Each horizontal layer  $i$  has the box number  $L_i+1$  until  $L_i+3$  (dissolved, sorbed, air), with  $L_i=1+3*(i-1)$ . The settler has box numbers  $S+1$  and  $S+2$  (dissolved, sorbed), with  $S=1+3*n$ .

### 9.2.3 Model equations

Non trickling filter specific equations were taken as such from *SimpleTreat* version 3.0 (Struijs, 1996). More details on the exact model equations can be found in Boeije (1999). For the calculation of diffusive exchanges, the fugacity approach was applied. Expressions for fugacities, diffusion coefficients and kinetics were taken directly from *SimpleTreat*, after Mackay and Paterson (1982). Box volumes in the filter unit were calculated from the number of horizontal layers, the total filter volume and the carrier material's porosity. Volatilisation was modelled using the two-layer approach (Trybal, 1980). Surface volatilisation in the filter unit occurs at the interface between air and water.

Biodegradation in the dissolved phase of the water compartment is expressed as the sum of two first-order rates: biodegradation by suspended biomass and disappearance of the chemical into the biofilm. In the sorbed phase, only the suspended biomass activity is taken into account. For suspended biodegradation, "double" first-order kinetics (both in active biomass and in chemical concentration) are used. Melcer *et al.* (1995) developed a biofilm model which predicts the mass flux of a chemical from the bulk water into the biofilm per unit of interfacial area and an analytical solution for the chemical mass flux into the biofilm is given. This was converted to a first-order elimination rate

coefficient for combined diffusion and biodegradation in one horizontal layer of the trickling filter. In the presented model, the biofilm/water interfacial area has to be known.

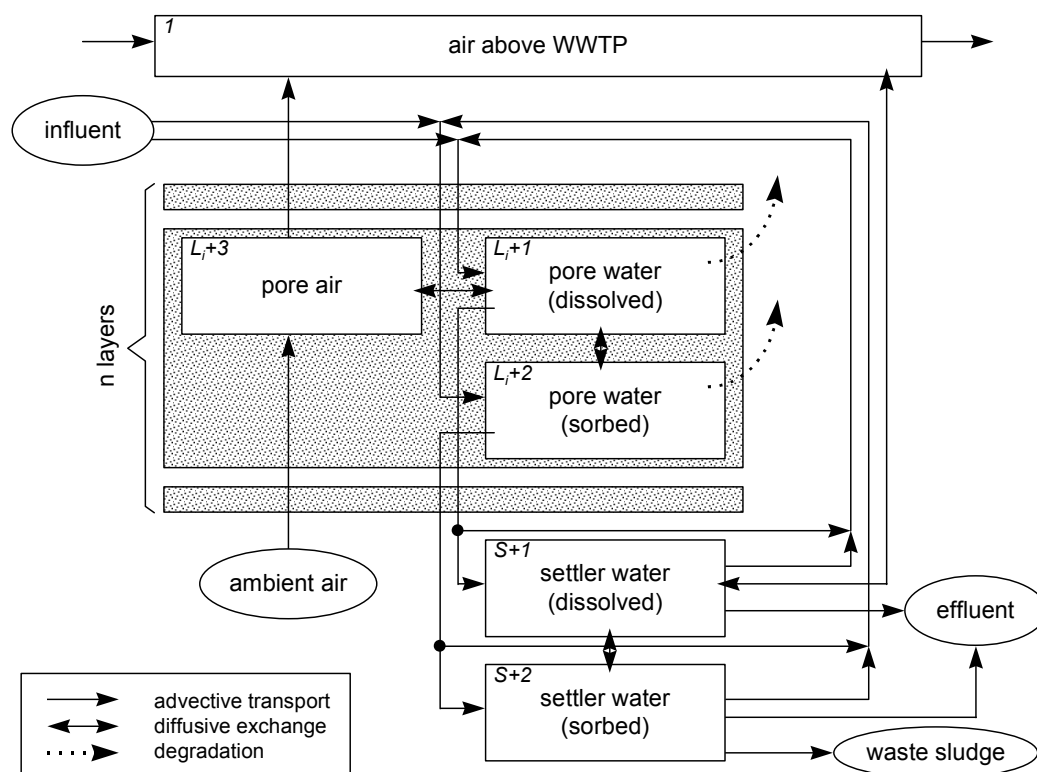


Figure 9.2: Model scheme of the trickling filter plant (Boeije, 1999)

#### 9.2.4 Parameter selection and validation of the model

Most of the parameters needed by the model were taken from various literature sources. For the modelling of processes at the biofilm-bulk liquid interface, diffusion coefficients and "double" first-order biodegradation parameters were taken from Melcer *et al.* (1995). Selected parameter values are listed in Table 9.1 and Table 9.2. It has to be noted that water diffusion coefficients of low water soluble components are difficult to measure and therefore are very rarely stated in literature. Approximation formulas are found in literature e.g. relating the diffusion coefficient to the inverse of the molecular weight of the component (Perry and Chilton, 1974).

Table 9.1. VOC-specific model parameters ( $H$ : Henry's law coefficient,  $K_{ow}$ : octanol-water partitioning constant,  $K_b$ : double 1<sup>st</sup> order biodegradation rate constant,  $D_l$ : water diffusion coefficient)

VOC	$H_{VOC}^{25^\circ C}$ ( $m^3/m^3_g$ )	$\log K_{ow}$ (-)	$K_b$ ( $m^3/kg.h$ )	$D$ ( $10^{-5} m^2/d$ )
Dichloromethane	0.087 [b]	1.25 [c]	0.77 [d]	8.0 [d]
Chloroform	0.146 [b]	1.97 [c]	0.43 [d]	9.2 [d]
Toluene	0.273 [a]	2.69 [c]	1.74 [d]	7.8 [d]
Chlorobenzene	0.157 [a]	2.84 [c]	0.77 [d]	8.0 [d]

The parameters still to be determined were the gas phase and liquid phase mass transfer coefficients for the different VOC's. According to the two resistance theory (Trybal, 1980),  $K_L a$  can be defined as:

$$\frac{1}{K_L a} = \left( \frac{1}{H_{VOC} \cdot k_g} + \frac{1}{k_l} \right) \cdot \frac{1}{a} \quad (9.1)$$

where  $k_{gl}$  is the mass transfer coefficient for the gas and liquid interface and  $a$  is the gas-liquid interface surface per unit volume liquid ( $m^2 \cdot m^{-3}$ )

If the liquid film is in turbulent motion, it can be assumed that (De heyder *et al.*, 1997).

$$k_l \propto \sqrt{D} \quad (9.2)$$

Mainly because of the poor knowledge of the liquid diffusion coefficient of the VOC's under study, it was decided to use the same value for the mass transfer coefficients for all four components. These values were  $86.4 \text{ m} \cdot \text{d}^{-3}$  for  $k_g$  and  $0.0864 \text{ m} \cdot \text{d}^{-3}$  for  $k_l$ . These values were based on estimations by Parker *et al.* (1996). This resulted in an almost constant value for the total mass transfer coefficient  $K_L$  of  $0.085 \text{ m} \cdot \text{d}^{-1}$  ( $K_L a = 8.5 \text{ d}^{-1}$ ), where the very small changes are only due to the different Henry-constant for the four VOC's.

**Table 9.2. Plant-specific model parameters**

Plant dimensions			Biofilm and carrier		
$A_{TF02}$ [TF02 filter area]	269	$m^2$	$(1-f_c)$ [filter porosity]	0.95	-
$V_{TF02}$ [TF02 filter volume]	1613	$m^3$	$f_g$ [fraction of filter pores filled with air]	0.05	-
$A_{sec}$ [clarifier area]	52	$m^2$	$f_l$ [fraction of filter pores filled with water]	0.05	-
$V_{sec}$ [clarifier volume]	122.5	$m^3$	$\delta_{bl}$ [stagnant water film thickness]	$10^{-4}$	$m$
Flow rates and recycle ratios			$L$ [biofilm thickness]	$2 \cdot 10^{-4}$	$m$
$Q_{L,2}$ [TF02 influent flow rate]	$52.7^{[a]} / 72.0^{[b]}$	$m^3/h$	$X_F$ [biofilm density]	$40 \cdot 10^3$	$g/m^3$
$f_{rec,2}^s$ [TF02 short loop recycle ratio]	$4.70^{[a]} / 3.16^{[b]}$	-	$a_{substr}$ [specific substratum interfacial area]	100	$m^2/m^3$
$f_{rec,2}^l$ [TF02 long loop recycle ratio]	0	-			
$Q_{G,2}$ [TF02 air flow rate]	$9720^{[a]} / 6660^{[b]}$	$m^3/h$			

[a] low loading - high air flow [b] high loading - low air flow

To test the model, six measurements for VOC's in the liquid and the gas phase of filter TF02 were done under high air flow rate conditions, complemented with four measurements under low air flow rate conditions. The results were averaged to minimise the effect of measurement errors. It is noteworthy that the VOC loading was quite different before compared to after the air flow change. After the lowering of the air flow rate, the load (influent flow as well as influent concentration) increased considerably.

The validation results were very good as far as the concentrations in the off-gas are concerned. The model predictions deviated only  $5.0 (\pm 3.0)\%$  from the measured data for the different individual VOC's. The simulated effluent concentrations, on the other hand were less accurate. In the low loading - high air flow case, the deviation was  $37.3 (\pm 36.3)\%$ , in the high loading - low air flow case, the deviation amounted  $89.2 (\pm 58.1)\%$ . These high deviations are however acceptable because in all cases, more than 90% of the volatile contaminant is stripped (Table 9.3). This means that the effluent concentrations were very low compared to the influent VOC-concentrations, so small measurement

errors have a considerable effect. Indeed, comparing liquid phase and gas phase VOC-concentrations should be done with care, due to the different sampling and measurement methods.

**Table 9.3. Influent concentration and removal of chloroform as modelled with the five-layer steady-state model**

	water influent conc. (mg/l)	% removed via	
		stripping	biodegr.
low loading - high air flow	62.1	97.1	0.3
high loading - low air flow	148.5	90.1	0.7

### 9.2.5 Hydrodynamics of the filter system and model reduction

As shown in the previous chapter, two tanks in series were enough to model the hydraulic behaviour of the trickling filter. The number of layers in the original model could thus be reduced to two. Also, in the original model, the total water volume in the filter was estimated to be 80 m<sup>3</sup> per filter, based on the carrier material characteristics. However, the tracer test showed this volume was only 30 m<sup>3</sup>. After the adaptation of the steady-state model, a calibration needed to be performed, and a  $K_La$  of 50 d<sup>-1</sup> was suited to obtain similar good simulation results. The deviation between modelled and simulated off-gas concentrations was now 5.8 ( $\pm$  4.8)%. The average deviation from the measured effluent concentrations for both high and low air flow was still relatively high at 28 ( $\pm$  28.5)%. Note that, as can be seen on Figure 9.3, the result was good for high as well as for low flow. As mentioned above, the same mass transfer coefficient  $K_La$  was used for high and low flow. Apparently, the mass transfer coefficient was independent of the applied air flow rate. In literature it is shown that the interfacial area is the most sensitive parameter for the mass transfer in trickle flow reactors (Iliuta *et al.*, 1998). In the range of air flows applied, a change of the interfacial area between liquid and gas phase is not to be expected, so a change of the mass transfer coefficient was unlikely.

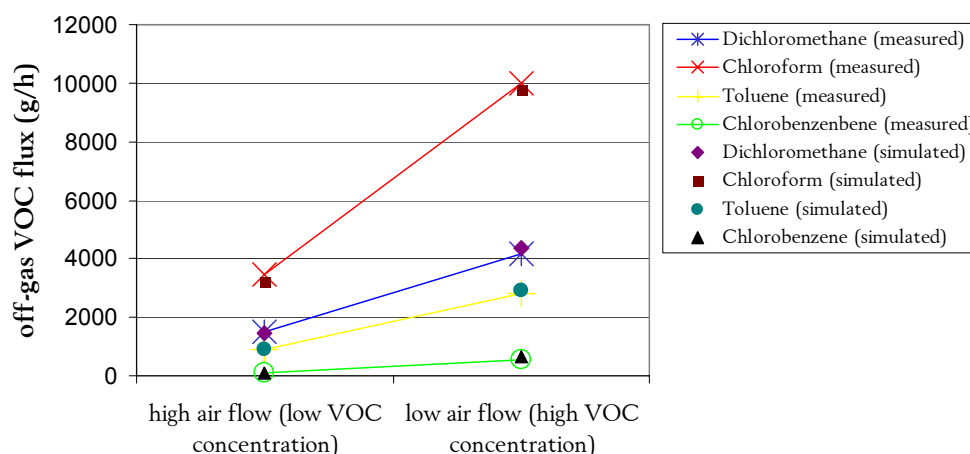


**Figure 9.3: Result of the calibration of the off-gas VOC flux with a  $K_La$  of 50 d<sup>-1</sup>**

From Table 9.3 it becomes clear that the model predicted only very little biodegradation for these very volatile components. It could thus be anticipated that the model could further be simplified by neglecting the biodegradation term in the model formulation. Also, the amount of VOC's adsorbed to suspended biomass was negligible. Neglecting these terms in the model formulation in fact simplified

the model to a simple mass balance model that can be reformulated as a dynamical model very easily. This dynamical model was then used for scenario analysis.

Here again, the gas phase in filter TF02 was modelled as a single ideally mixed tank of 2000 m<sup>3</sup>, while the water phase inside the filter was modelled as two ideally mixed tanks (tank *a* and *b*) in series of 15 m<sup>3</sup> each. A mass balance over the gas phase yields:

$$\frac{dS_{off-gas}}{dt} = \frac{Q_{off-gas}}{V_{gas-phase}} \cdot (S_{ambient-air} - S_{off-gas}) + N_{s,a} + N_{s,b} \quad (9.3)$$

where  $N_{s,a/b}$  is the flux of VOC due to stripping from the liquid phase to the gas phase (g/m<sup>3</sup>.d). The liquid phase mass balances are:

$$\begin{cases} \frac{dS_{liquid,a}}{dt} = \frac{Q_{tf}}{V_{liquid-phase,a}} \cdot (S_{liquid,pt} - S_{liquid,a}) - N_{s,a} \\ \frac{dS_{liquid,b}}{dt} = \frac{Q_{tf}}{V_{liquid-phase,b}} \cdot (S_{liquid,a} - S_{liquid,b}) - N_{s,b} \end{cases} \quad (9.4)$$

The flux from liquid to gas phase was modelled as follows (for both tanks 1 and 2):

$$N_{s,a/b} = K_L a \cdot \left( S_{liquid,a/b} - \frac{S_{off-gas}}{H_{VOC}} \right) \quad (9.5)$$

## 9.2.6 Scenario Analysis

### 9.2.6.1 Scenario 1: high loading - high air flow rate

As mentioned in the introduction, environmental legislation enforces the construction of an off-gas treatment facility for the trickling filter system. The dimensions of this facility and the construction material needed are dependent on the air flow to be treated and the concentration of VOC's. Therefore, a worst-case scenario was investigated. After the above model reduction and calibration for high loading - low air flow and low loading - high air flow conditions, simulations were done to predict the effect of a third situation, namely a high loading of VOC's in the influent together with a high air flow rate. This situation was compared with the high loading – low air flow case. The question to be answered was whether the stripping efficiency would be higher with a high flow and what effect this would have on the VOC concentrations in the off-gas and the effluent.

The simulation results are shown in Table 9.4. A small increase of the VOC stripping efficiency was noticed when the high air flow case was compared to the low air flow case. A high air flow rate resulted in a larger driving force for stripping because of the higher concentration gradient at the gas-liquid interface. On the other hand, a high flow rate also means a lower gas residence time. The combination of these two effects diminished the effect to only a few percentages in removal efficiency. The air flow rate can thus be lowered without incurring a considerable effect on the stripping efficiency, but it will obviously result in higher concentrations in the air to be treated by the

off-gas treatment facility. Since the size of the off-gas treatment facility is proportional to the air flow rate to be treated and the efficiency increases with increasing VOC concentrations, the investment and operating costs of the facility could be reduced significantly.

**Table 9.4. Effect of two different air flow rates on the VOC removal efficiency in the off-gas at high VOC loading**

VOC	Removal efficiency (%) (low flow rate – high load)	Removal efficiency (%) (high flow rate – high load)
Dichloromethane	87.19	90.46
Chloroform	91.41	93.63
Toluene	92.59	93.93
Chlorobenzene	91.97	94.34

### 9.2.6.2 Scenario 2: fluctuating air flow rate in the trickling filters

At the industrial wastewater treatment plant under study, an overall waste gas management strategy is to be implemented over the next year. Waste gasses are coming from the equalisation system, the trickling filters and the sludge treatment. The waste gas flow rate coming from the sludge treatment (filter presses) is not constant because of batch-wise ventilation during day-time. Four times a day, the presses have to be opened during 30 minutes for cleaning. During these periods, the air flow coming from the presses hall increases from 2.200 m<sup>3</sup>/h to 7.600 m<sup>3</sup>/h. The VOC loading of these off-gasses can be neglected. However, to keep the flow rate in the off-gas treatment facility constant (which is necessary for its operation), the flow over the two trickling filters could be temporarily lowered during these periods. It is therefore important to know what effect these gas flow rate changes will have on the concentration and the total load of the VOC's in the off-gas treatment facility.

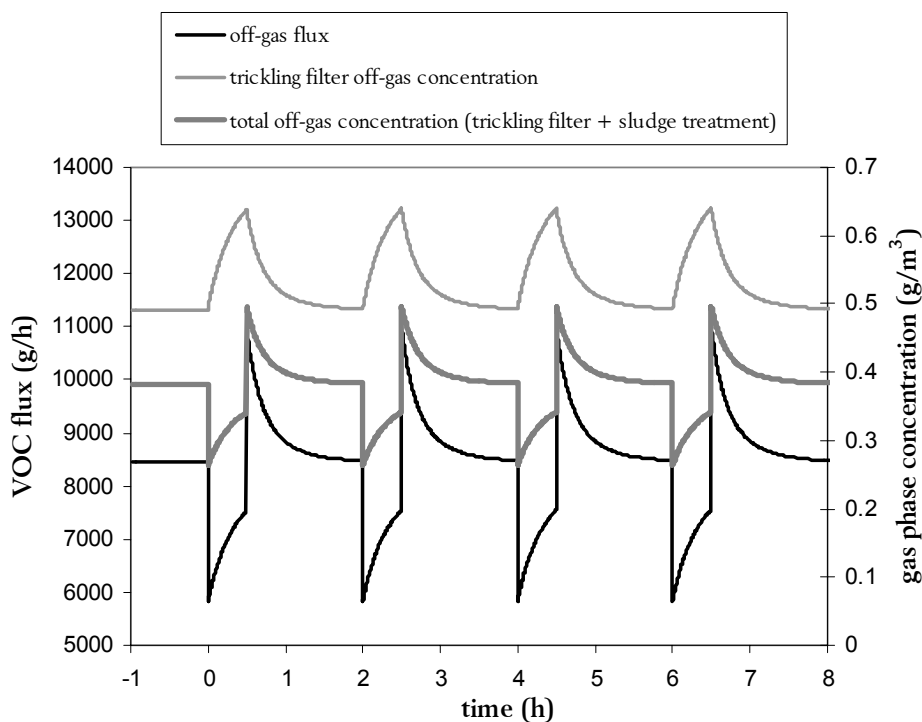


**Figure 9.4: Effect of air flow rate changes (low to high air flow and vice versa) with a constant wastewater composition on the flux and the off-gas concentration of chloroform at the trickling filters and the VOC treatment facility**

Dynamic simulations were performed to predict the flux and concentration profiles immediately after an air flow change. The results of these simulations are shown in Figure 9.4. As an example, only chloroform is shown. At time 0, the air flow through the filters is decreased during 30 minutes to allow the waste gas treatment to cope with the high air flow coming from the sludge treatment. In this period, the concentration in the trickling filters off-gas increases as seen above. The increase of the flow rate after this 30 minutes period, therefore results in a quite high flux-peak of chloroform to the VOC treatment facility. The chloroform concentration in the trickling filter off-gas immediately starts to drop during high flow periods. These are factors certainly to be taken care of when designing the off-gas treatment facility.

Using the findings of this research, the air flow through the trickling filters was lowered. On the one hand, as investigated during the COD modelling, the oxygen concentration in the off-gas was not significantly lower as compared to the high-flow case. An effect on the biodegradation was thus not to be expected. On the other hand, higher VOC concentrations and a lower off-gas flow rate were beneficial for the investment cost and the efficiency of the off-gas treatment facility. To avoid fluctuating off-gas flow rates, relatively clean off-gas from the sludge treatment is now first fed into the trickling filters so that a constant air flow and a relatively constant VOC concentration can be obtained.

### 9.3 Conclusions

Two mathematical models describing the stripping of VOC's in an industrial wastewater treatment plant were developed. The first model was based on the non-equilibrium steady-state model *SimpleTreat* combined with a biofilm degradation model of Melcer *et al.* (1995). The second model was a simple dynamic mass balance model, built on the basis of the results of simulations with the biodegradation model and of a tracer test. Simulations with the non-equilibrium steady-state model showed that biodegradation as well as adsorption to suspended solids could be neglected for the volatile organics under study. Furthermore, based on the results of a tracer test with *LiCl*, the hydrodynamic description of the original model (five layers in the trickling filter), could be simplified down to a two-layer model. Scenario analyses with the simplified dynamic model built on the basis of these findings showed that stripping was virtually independent of the applied air flow rate. At high air flow, the total stripping efficiency only increased with a few percentages, resulting in a lower gas phase VOC concentration. Dynamic simulations, however, revealed that immediately after changes in air flow rate, quite high flux and concentration peaks are to be expected. These peaks were of importance for the design of an off-gas treatment facility.



# 10 Performance evaluation of nitrogen removal suspended-carrier biofilm systems using dynamic simulation

---

## 10.1 Introduction

We are witnessing an enormous growth in biological nitrogen removal from wastewater. Nitrogen removal presents specific challenges beyond traditional COD (carbon) removal. The optimisation of biological nitrogen removal processes has attracted a lot of research in the past few years. Considerable achievements in not only optimised process operation and control but also improved process design have resulted.

Compared to the traditional COD removal activated sludge process, biological nitrogen removal systems have the following fundamental differences (Yuan *et al.*, 2001):

- Autotrophs grow slowly and therefore require a long sludge retention time (SRT). This causes over-growth of heterotrophs and over-accumulation of inert solids, incurring large capital cost. This capital cost is mainly due to the large volume that is needed to accommodate the high amount of MLSS produced during the long retention time. When the dependency of the MLSS concentration on the SRT in a nitrogen removal plant is calculated, it is seen that the amount of MLSS increases almost linearly with the SRT (Figure 10.1). The declining fraction of active biomass in MLSS indicates that the increase is mainly due to inert solids.
- The traditional nitrogen removal process requires two types of bacteria: autotrophs and heterotrophs. Autotrophs function aerobically, denitrifiers function anoxically. A nitrogen removal plant has to be operated such that both aerobic and anoxic conditions are present. Since in a single sludge system, each type of solids goes through all of the existing conditions in the plant, at any moment only a fraction of nitrifiers and denitrifiers is functional. In terms of SRT design, this implies an even longer SRT than required by a fully aerobic nitrification plant.
- An inherent problem with biological nitrogen removal is that denitrification should be preceded by nitrification that produces the nitrate, while the latter is always accompanied by aerobic COD oxidation. A fraction of the influent COD is carried over to the aerobic zone and is therefore not available for denitrification. This leakage is happening in three ways, particulate COD which is adhered to sludge flocs, cell COD and soluble COD.

The above complexities make the operation of a biological nitrogen removal plant difficult. However, they have also offered greater possibilities for performance improvement by means of optimised process design and on-line monitoring and control.

One possibility for optimised process design is the use of biomass-supporting media, either fixed or as suspended carriers. These systems have been developed as high-rate COD removal processes or as an economic means for upgrading COD removal plants to nutrient removal. The attached growth processes (AGP) are analysed here in terms of their volume requirement, treatment capacity, influent COD utilisation efficiency for nitrate reduction as well as other properties. An important feature of the system is that autotrophs and heterotrophs can be physically separated by adding carriers to different zones in the treatment plant. Autotrophs cannot grow in anoxic conditions and are outcompeted by heterotrophs in an alternating oxic/anoxic zone following the anoxic zone. In the fully oxic zone, heterotrophs can hardly grow due to lack of COD. Qualitative steady-state analysis of this system already showed its interesting features (Yuan *et al.*, 2001):

- More bacteria are maintained in the system, at high solids densities in the biofilm. The system thus can be accommodated in a smaller space and needs a smaller settler since the suspended biomass concentration is lower which entails that the solids loading rate to the settler is reduced.
- The treatment capacity of this kind of systems was found to be significantly higher than that of a conventional activated sludge system. Both nitrifiers and denitrifiers are only present in the zones of the reactor where they are needed. This means the full capacity of the plant in nitrification and denitrification can be used.
- In an AGP, most of the COD is kept in the biofilm. The COD leakage in the form of sludge flocs and cell COD is decreased dramatically. This leads to a better availability of influent COD to the denitrifiers.

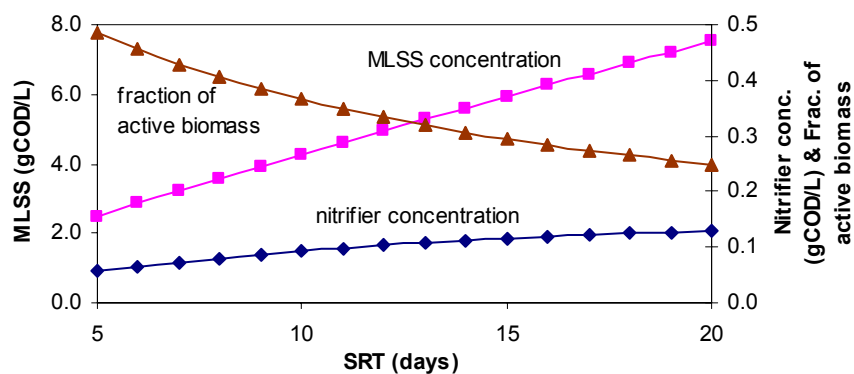


**Figure 10.1: Autotrophic biomass and MLSS concentrations and the fraction of active biomass in MLSS, as a function of SRT of a single-sludge system (Yuan *et al.*, 2001).**

The main drawback of attached growth systems has been identified as its high aeration cost (among others, Welander *et al.*, 1998). The reason for this is that a high bulk DO concentration is needed to drive the diffusion of oxygen into the biofilm. It has been reported that a bulk DO concentration below 3-4 mg/l starts limiting the nitrification rate. However, the added aeration cost due to the increased bulk DO concentration might be partially compensated by a lower oxygen uptake rate in the aerobic zone due to the lack of or at least reduced heterotrophic activity. The bulk DO concentration should be controlled at the minimum level achieving complete nitrification.

In this chapter, the attached growth system described above is evaluated using dynamic simulations. The advantages of the system that were qualitatively described elsewhere (Yuan *et al.*, 2001), are

validated quantitatively based on a simulation benchmark for activated sludge treatment systems (Spanjers *et al.*, 1998; Copp, 2001). This simulation benchmark is extended with the biofilm model developed in chapter 4 of this thesis that allows for fast and accurate simulation of the microbial conversion of different substrates in a biofilm. Not only the achievable volume reduction by introducing suspended biofilm carriers is evaluated, but also the higher efficiency of COD utilisation in the anoxic zone of the treatment plant and the increased nitrification efficiency of the attached growth system compared to classical activated sludge nitrogen removal. The economic feasibility of this system is evaluated using the data generated with the benchmark simulation (Gillot *et al.*, 1999). Capital savings due to volume reduction and reduced sludge production are weighed out against increased aeration costs (and the investment costs for carriers and grids). Also, effluent quality and the possible use of external carbon sources are integrated in this evaluation.

## 10.2 The benchmark, an objective performance evaluation procedure

### 10.2.1 Introduction

Many operating and control strategies for the activated sludge process have been proposed in literature. It is however difficult to find a clear basis for the comparison of these strategies. Indeed, a number of influences has an impact on the activated sludge process. Many of these influences are easily recognised. For instance, physical characteristics of the process can have an impact on process performance, which makes the comparison of strategies applied to different reactor layouts difficult. Also, the lack of standard evaluation criteria complicates the evaluation. Effluent requirements and treatment costs are often specific to the country where the treatment is located. This makes it difficult to judge the influence of a strategy on a reported performance increase. Furthermore, the objective of reported strategies is not always consistent which may result in the omission of data necessary to make fair and unbiased comparisons (Spanjers *et al.*, 1998)

From a practical point of view, it is not reasonable to experimentally test and verify the effectiveness of all reported strategies. Alternatively, given a standardised procedure, it is possible to efficiently evaluate numerous strategies through realistic dynamic computer simulations. Simulations provide a cost-effective means for the evaluation of operating and control strategies, but the unlimited possibilities to run simulations makes the need for a standardised protocol very important if different strategies (and different simulation results) are to be compared. Each strategy must be simulated under the same conditions to ensure unbiased comparisons. Validation of the computer simulations is difficult without supporting experimental or full-scale data, but the value of the work is enhanced through the use of accepted activated sludge models (Spanjers *et al.*, 1998).

This approach has numerous advantages, but still there is a need for a standardised procedure. To this end, there has been a recent effort to develop a standardised simulation protocol - a '*simulation benchmark*'. The idea to produce a standardised '*simulation benchmark*' was first developed by the first *IWA Task Group on Respirometry-Based Control of the Activated Sludge Process* (Vanhooren and Nguyen, 1996; Spanjers *et al.*, 1998). This original benchmark was subsequently modified by the European Co-operation in the field of Scientific and Technical Research (COST) 682/624 Actions in co-operation with the second *IWA Respirometry Task Group* (Alex *et al.*, 1999; Copp, 2001). In an

attempt to standardise the simulation procedure and the evaluation of all types of control strategies, the two groups have jointly developed a consistent simulation protocol. In this instance, the COST 'simulation benchmark' is a comprehensive description of a standardised simulation and evaluation procedure including plant layout, simulation models and model parameters, a detailed description of disturbances to be applied during testing and evaluation criteria for testing the relative effectiveness of simulated strategies.

### 10.2.2 Process model

The 'simulation benchmark' plant design is comprised of five reactors in series with a 10-layer secondary settling tank. To increase the acceptability of the results, two internationally accepted process models were chosen. The IWA Activated Sludge Model No 1 (ASM1) was chosen as the biological process model (Henze *et al.*, 1987) and the double-exponential settling velocity function of Takács *et al.* (1991) was chosen as a fair representation of the settling process.

### 10.2.3 Parameter values

To ensure the consistent application of these models in benchmarking studies, all of the model parameters have been defined in the 'simulation benchmark' description (Table 10.1).

### 10.2.4 Influent model

For an unbiased and complete evaluation, it is important that a series of disturbances is defined and that each strategy is subjected to all the disturbances. Only then can a fair comparison be made. To this end, several influent file disturbances have been defined in the 'simulation benchmark' description (Vanhooren and Nguyen, 1996; Spanjers *et al.*, 1998). The flow-averaged values of the influent file disturbance for dry weather are given in Table 10.2. Note that nitrate ( $S_{NO}$ ) and oxygen ( $S_O$ ), alike autotrophic bacteria ( $X_{BA}$ ) are assumed not to be present in the influent.

In total, three influent trajectories have been defined and each is meant to be representative of a different weather condition. The data files are available for download from various sources including the COST 624 web site (<http://www.ensic.u-nancy.fr/COSTWWTP>). Each of the files contains 14 days of influent data at 15-minute intervals. Expected trends in weekly data have been incorporated. That is, much lower peak flows are depicted in the 'weekend' data, which is consistent with normal load behaviour at a municipal treatment facility. The files are representative of three conditions: *dry weather*, a *storm event* and a *rain event*.

### 10.2.5 Plant configuration

The layout is fully defined. The benchmark plant is composed out of 5 biological tanks-in-series with a secondary settler (Figure 10.2). The total biological tank volume is about 6000 m<sup>3</sup> (tanks 1 and 2 each 1000 m<sup>3</sup> and tanks 3, 4 and 5 each 1333 m<sup>3</sup>). Tanks 1 and 2 are unaerated, but fully mixed. The aeration of tanks 3, 4 and 5 is achieved using a *maximum*  $K_La$  of 10 h<sup>-1</sup>. The default  $K_La$  is 10 h<sup>-1</sup> in tanks 3 and 4 and 3.5 h<sup>-1</sup> in tank 5, the dissolved oxygen saturation level is of mg O<sub>2</sub>/l. A non-reactive secondary settler is implemented with a volume of 6000 m<sup>3</sup> (area of 1500 m<sup>2</sup> and a depth of 4 m) subdivided into 10 layers. The feed point to the settler is chosen at 2.2 m from the bottom (*i.e.* feed

enters the settler in the middle of the sixth layer). Waste sludge is pumped continuously from the secondary settler underflow at a default rate of 385 m<sup>3</sup>/d.

**Table 10.1. Parameter values proposed for the simulation benchmark (Spanjers *et al.*, 1998)**

	<i>Parameters</i>	<i>Units</i>	<i>Value</i>
<i>Heterotrophs</i>	$\mu_H$	d <sup>-1</sup>	4
	$K_s$	mg/l	10
	$b_H$	d <sup>-1</sup>	0.3
	$\eta_h$	-	0.5
	$\eta_g$	-	0.8
<i>Hydrolysis</i>	$k_h$	d <sup>-1</sup>	3.0
	$K_x$	-	0.1
<i>Ammonification</i>	$k_a$	m <sup>3</sup> /(g COD.d)	0.05
<i>Autotrophs</i>	$\mu_A$	d <sup>-1</sup>	0.5
	$K_{NH}$	mg/l	1.0
	$b_A$	d <sup>-1</sup>	0.05
<i>Switching Functions</i>	$K_{OH}$	mg/l	0.2
	$K_{OA}$	mg/l	0.4
	$K_{NO}$	mg/l	0.5
<i>Stoichiometry</i>	gCOD/gVSS	-	1.48
	gVSS/gSS	-	0.9
	gCOD/gSS	-	1.33
	$Y_H$	gCOD/gCOD	0.67
	$Y_A$	gCOD/gN	0.24
	$i_{XB}$	gN/gCOD	0.08
	$i_{XP}$	gN/gCOD	0.06
	$f_p$	-	0.08
<i>Settler Model</i>	$v_0$	m/d	250
	$v'_0$	m/d	474.4
	$r_h$	m <sup>3</sup> /g SS	0.000576
	$r_p$	m <sup>3</sup> /g SS	0.00286
	$f_{ns}$	-	0.00228
	$X_t$	g SS/m <sup>3</sup>	3000

**Table 10.2. Flow-weighted average influent composition for dry weather**

Variable	Value	Unit
$Q$	18 446	$\text{m}^3/\text{d}$
$S_S$	69.50	$\text{g COD}/\text{m}^3$
$S_I$	30	$\text{g COD}/\text{m}^3$
$X_S$	202.32	$\text{g COD}/\text{m}^3$
$X_{BH}$	28.17	$\text{g COD}/\text{m}^3$
$X_I$	51.20	$\text{g COD}/\text{m}^3$
$S_{NH}$	31.56	$\text{g N}/\text{m}^3$
$S_{ND}$	6.95	$\text{g N}/\text{m}^3$
$X_{ND}$	10.59	$\text{g N}/\text{m}^3$

There are two internal recycles:

- nitrate internal recycle from the 5<sup>th</sup> to the 1<sup>st</sup> tank at a default flow rate of 55338  $\text{m}^3/\text{d}$ ;
- Return Activated Sludge (RAS) recycle from the underflow of the secondary settler to the front end of the plant at a default flow rate of 18446  $\text{m}^3/\text{d}$  (as there is no biological reaction in the settler, no oxygen is consumed in the settler and therefore the oxygen concentration in the recycle is non-zero).

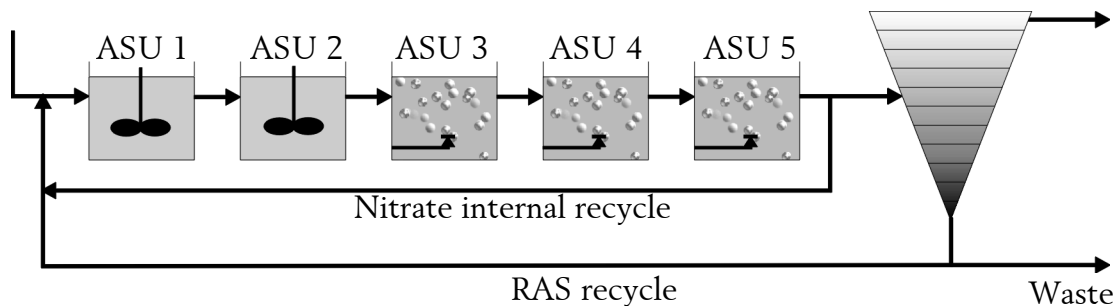


**Figure 10.2 Configuration of the benchmark plant for carbon and nitrogen removal**

### 10.2.6 Simulation procedure

Once the benchmark configuration has been set-up in the simulator of choice, the initial step in the procedure is to simulate the plant to steady-state using an influent of constant flow and composition. The flow-weighted *dry weather* data (Table 10.2) is used for this purpose and steady-state is defined by simulating 100 days using a constant influent (Copp, 2001).

Starting from the steady-state solution, using the *dry weather* influent file as a dynamic input, the system under study should be simulated for 14 days. The resulting state variable values should then be saved for all unit processes. These state variable values represent the starting point for evaluating the dynamic response of the plant to each of the influent disturbance files. From the state achieved above, a further 14 days should be simulated using the *dry weather*, *storm event* and *rain event* influent files in separate simulation studies, but each time starting from the state achieved after the initial 14-day

*dry weather* simulation. The output data generated from the simulations described above is used to examine the dynamic performance of the process.

Because of the extensive amount of raw dynamic output, the dynamic results are summarised using a number of performance indexes. These composite terms include, among others, a general effluent quality measure, energy terms for pumping and aeration, and a measure of sludge production. The equations needed to calculate these terms are outlined below.

### 10.2.6.1 Effluent Quality index

Effluent quality is considered through an effluent quality index (EQ), which is meant to quantify the effluent pollution load to a receiving water body into a single term. Effluent quality (EQ, kg/d) is calculated as follows by integrating through the final 7 days of weather simulations ( $T = 7$  days,  $Q$  in  $\text{m}^3/\text{d}$ ):

$$EQ = \frac{1}{T \cdot 1000} \int_{t_0}^{t_0+7 \text{ days}} [PU_{TSS}(t) + PU_{COD}(t) + PU_{BOD}(t) + PU_{TKN}(t) + PU_{NO}(t)] Q_e(t) dt \quad (10.1)$$

**Table 10.3. Definition of the Pollution Units (PU) used in equation 10.1**

	$\beta$ factors
$PU_{TSS}(t) = \beta_{TSS} TSS_e(t)$	$\beta_{TSS} = 2$
$PU_{COD}(t) = \beta_{COD} COD_e(t)$	$\beta_{COD} = 1$
$PU_{BOD}(t) = \beta_{BOD} BOD_e(t)$	$\beta_{BOD} = 2$
$PU_{TKN}(t) = \beta_{TKN} TKN_e(t)$	$\beta_{TKN} = 20$
$PU_{NO}(t) = \beta_{NO} NO_e(t)$	$\beta_{NO} = 20$

The definition of the composite variables used above is as follows ( $X_S, X_{BH}, X_{BA}, X_P, X_I, S_S, S_I$  in g COD/ $\text{m}^3$ ;  $S_{NH}, S_{ND}, S_{NO}, X_{ND}$  in g N/ $\text{m}^3$ ):

$$\begin{aligned} TSS_e &= 0.75 (X_{S,e} + X_{BH,e} + X_{BA,e} + X_{P,e} + X_{I,e}) \\ COD_e &= S_{S,e} + S_{I,e} + X_{S,e} + X_{BH,e} + X_{BA,e} + X_{P,e} + X_{I,e} \\ BOD_e &= 0.25 (S_{S,e} + X_{S,e} + (1 - f_p) (X_{BH,e} + X_{BA,e})) \\ TKN_e &= S_{NH,e} + S_{ND,e} + X_{ND,e} + i_{XB} (X_{BH,e} + X_{BA,e}) + i_{XP} (X_{P,e} + X_{I,e}) \\ NO_e &= S_{NO,e} \\ N_{tot,e} &= TKN_e + S_{NO,e} \end{aligned}$$

As a check on the EQ calculation, an influent quality index (IQ) can be calculated. To calculate the IQ, the above equations should be applied to the influent files, but the BOD coefficient needs to be changed from 0.25 to 0.65.

### 10.2.6.2 Effluent standard/constraint violations

Also included in the performance evaluation is a measure of effluent standard or constraint violations. Constraints with respect to five effluent components are defined (Table 10.4) and the percentage of time that the constraints are not met is to be reported. The methodology for reporting the number of violations is defined as well.

**Table 10.4. Effluent constraints used for the simulation benchmark**

		<i>Effluent Constraints</i>	<i>Units</i>
Ammonium	$S_{NH,e}$	4	g N/m <sup>3</sup>
Total Nitrogen	$N_{tot,e}$	18	g N/m <sup>3</sup>
BOD <sub>5</sub>	BOD <sub>e</sub>	10	g BOD/m <sup>3</sup>
Total COD	COD <sub>e</sub>	100	g COD/m <sup>3</sup>
Suspended Solids	TSS <sub>e</sub>	30	g SS/m <sup>3</sup>

The effluent violations are reported through two quantities: (i) number of violations and, (ii)% time plant is in violation.

***Number of violations:***

This quantity represents the number of times that the plant is in violation of the effluent constraints (*i.e.* the number of times the plant effluent increases above the effluent constraint). This measure does *not* necessarily reflect the length of time that the plant is in violation.

***% time plant in violation:***

This quantity is a measure of the percentage of the time that the plant is in violation of the effluent constraints.

### 10.2.6.3 Operational Variables

Operational issues are considered through three items: sludge production, pumping energy and aeration energy (integrations performed on the final 7 days of weather simulations (*i.e.* from day 22 to day 28 of weather file simulations,  $T = 7$  days)).

***Sludge production:***

(i) sludge for disposal (kg/d)

$$P_{sludge} = [\Delta M(TSS_{system}) + M(TSS_w)] / T \quad (10.2)$$

where

$\Delta M(TSS_{system})$  = change in system sludge mass from the end of day 21 to the end of day 28

or  $\Delta M(TSS_{system}) = M(TSS_{system})_{end\ of\ day\ 28} - M(TSS_{system})_{end\ of\ day\ 21}$

$M(TSS_{system}) = M(TSS_{reactors}) + M(TSS_{settler})$

and

$$M(TSS_w) = 0.75 \int_{t_0}^{t_0+7\ days} [X_{S,w}(t) + X_{BH,w}(t) + X_{BA,w}(t) + X_{P,w}(t) + X_{I,w}(t)] Q_w(t) dt \quad (10.3)$$

$Q_w(t)$  = waste sludge flow rate at time  $t$  (m<sup>3</sup>/d)

(ii) total sludge production, including effluent suspended solids (kg/d)

$$P_{total\_sludge} = P_{sludge} + M(TSS_e) / T \quad (10.4)$$

where

$$M(TSS_e) = 0.75 \int_{t_0}^{t_{7\text{days}}} [X_{S,e}(t) + X_{BH,e}(t) + X_{BA,e}(t) + X_{P,e}(t) + X_{I,e}(t)] Q_e(t) dt \quad (10.5)$$

$Q_e(t)$  = effluent flow rate at time  $t$  (m<sup>3</sup>/d)

**Pumping energy (kWh/d):**

$$PE = \frac{0.04}{T} \int_{t_0}^{t_{7\text{days}}} [Q_a(t) + Q_r(t) + Q_w(t)] dt \quad (10.6)$$

where  $Q_a(t)$  = internal recycle flow rate at time  $t$  (m<sup>3</sup>/d)  
 $Q_r(t)$  = return sludge recycle flow rate at time  $t$  (m<sup>3</sup>/d)  
 $Q_w(t)$  = waste sludge flow rate at time  $t$  (m<sup>3</sup>/d)

**Aeration energy (kWh/d):**

$$AE = \frac{24}{T} \int_{t_0}^{t_{7\text{days}}} \sum_{i=1}^{i=5} [0.4032 \cdot K_L a_i(t)^2 + 7.8408 \cdot K_L a_i(t)] dt \quad (10.7)$$

where  $K_L a_i(t)$  = the mass transfer coefficient in  $i^{\text{th}}$  aerated reactor at time  $t$  (1/h)

#### 10.2.6.4 Economic analysis

Based on the above calculated operational variables, an economic analysis can be performed. Evidently, the operational variables only provide information to calculate operational costs. Investment costs will only be included as far as the necessary information is available. Also, labour and maintenance costs are left aside. Labour costs are normally estimated as a percentage of the load to the plant and should therefore be considered constant in the benchmark implementation (Gillot *et al.*, 1999), whereas the yearly maintenance cost is regularly estimated based on the investment cost (2.5 to 4% of the investment cost according to Gillot *et al.*, 1999).

An economic analysis is location (typically country-) dependent. Recent work (Haemelinck, 2000) therefore focused on assessing differences with respect to the operational costs associated with sludge treatment, effluent fines and energy, occurring in different countries in Europe, South-East Asia, Australia and North-America. As expected it turned out that the differences can be huge. However, rather than not performing any economic analysis at this point, a set of acceptable “average” weights, proposed by Vanrolleghem and Gillot (2001) is used. In Table 10.5 factors are listed to weigh the different operating costs of the benchmark plant. For instance, to transform the energy consumption for aeration and pumping (expressed as kWh/d in the benchmark criteria) to the associated yearly costs, the criterion value should be multiplied with 25 € per kWh/d. On the basis of a comparison that

was made between the Flemish standards for effluent quality assessment (Vanrolleghem *et al.*, 1996) and the current benchmark EQ-index, Haemelinck (2000) could conclude that the weightings of the different quality indicators (COD, BOD, N, P) are very similar in both criteria. Hence, it could be stated correctly that one Flemish pollution unit corresponds with 0.56 EQs (Haemelinck, 2000). Since, currently, Flemish fines are 30 € per pollution unit, the yearly fine per EQ (expressed in kg/d) was taken as 50 €/EQ, for ease of calculation.

**Table 10.5. Suggested cost multiplication factors to convert benchmark performance criteria into the operational costs (Vanrolleghem and Gillot, 2001)**

Cost factor	Multiplier	Units
Effluent fines	50	(€/EQ) EQ expressed in kg/d
Sludge treatment costs	75	(€/P <sub>sludge</sub> ) P <sub>sludge</sub> expressed in kg TSS/d
Energy costs	25	(€/AE) – (€/PE) AE-PE expressed in kWh/d

Also the following investment cost for an activated sludge tank is of importance for the economic analysis (Gillot *et al.*, 1999): cost (€) = 10304 x (volume (m<sup>3</sup>))<sup>0.477</sup>

## 10.3 Reference benchmark plants

### 10.3.1 Carbon and nitrogen removal without DO control

#### 10.3.1.1 Implementation

To serve as a reference for the implementation of the above mentioned attached growth systems, the standard benchmark configuration described in paragraph 10.2 was implemented in the WEST simulator (Hemmis NV, Kortrijk, Belgium). The graphical set-up in the simulator can be seen in Figure 10.3. The parameters and influent disturbances as described above were applied. After a simulation run of 100 days with the flow-weighted average influent composition, the weather files were applied for dynamic simulation. As described in 10.2.6, only the last 7 days of this *weather* simulation were taken into account for the performance evaluation.

#### 10.3.1.2 Steady state evaluation

The end values of the state variables after 100 days of simulation with the constant influent composition are defined as the steady-state and serve as the initial values for dynamic simulation. From these steady-state values, some operational variables can be calculated:

**Sludge loading:**

$$\begin{aligned}
 B_X &= \frac{Q_{in,mean} \cdot bCOD_{in}}{TSS_{ast} \cdot V_{ast}} \\
 &= \frac{18446 \text{ m}^3/\text{d} \times 294 \text{ g bCOD}/\text{m}^3}{2182 \text{ g MLSS}/\text{m}^3 \times 6000 \text{ m}^3} = 0.28 \text{ kg bCOD}/(\text{kg MLSS} \cdot \text{d})
 \end{aligned}
 \tag{10.8}$$

$$\text{where: } b\text{COD}_{in} = S_{S,in} + X_{S,in} + (1 - f_p)(X_{BH,in} + X_{BA,in})$$

$$TSS_{ast} (\text{g MLSS} / \text{m}^3) = 0.75 \cdot (X_I + X_S + X_{BH} + X_{BA} + X_P)$$

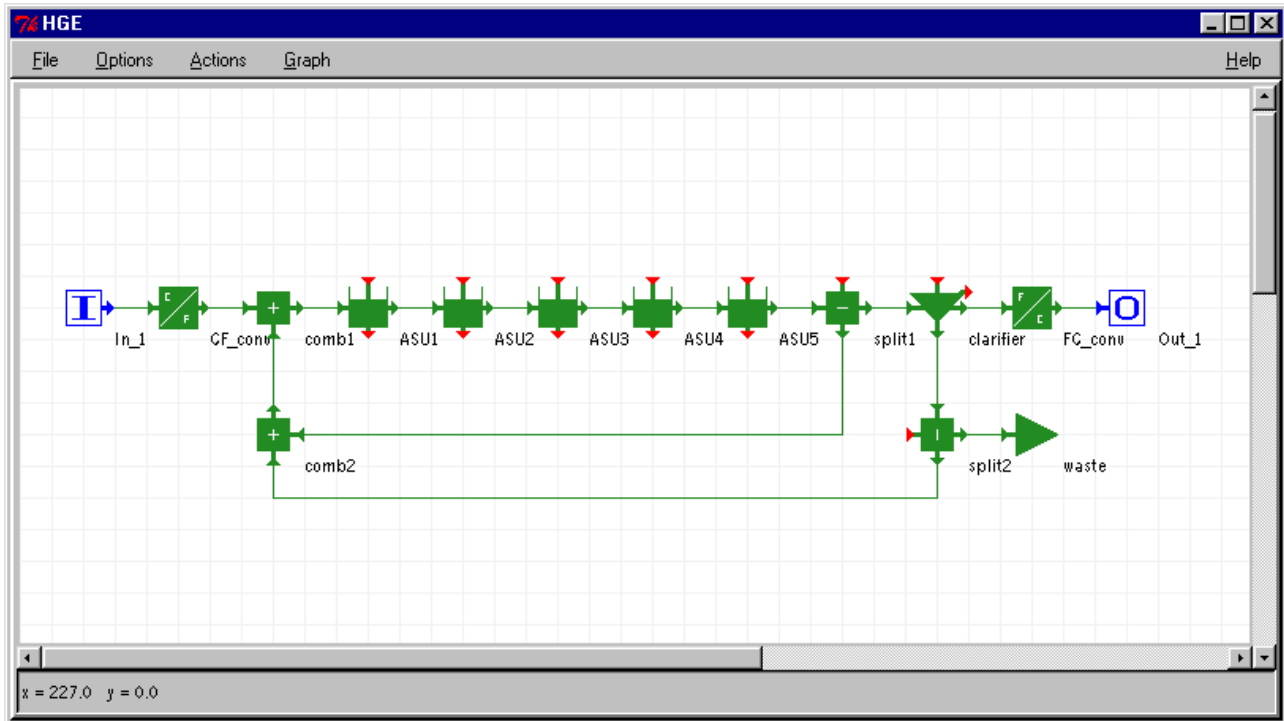


Figure 10.3: Graphical set-up of the benchmark plant in the WEST simulator.

This is a relatively high sludge loading for this type of plant. Henze *et al.* (1995) propose a sludge load up to 0.15 kg BOD/(kg MLSS.d) or about 0.25 kg bCOD/(kg MLSS.d). This relatively high sludge loading has mainly to do with the low sludge concentration compared to what was expected when designing the plant (Vanhooren and Nguyen, 1996).

#### ***Volumetric loading:***

$$B_V = \frac{Q_{in,mean} \cdot b\text{COD}_{in}}{V_{ast}} \quad (10.9)$$

$$= \frac{18446 \text{ m}^3/\text{d} \times 294 \text{ g bCOD}/\text{m}^3}{6000 \text{ m}^3} = 0.9 \text{ kg bCOD}/(\text{m}^3 \cdot \text{d})$$

This volumetric loading is in line with what is proposed by Henze *et al.* (1995).

**Sludge age:**

$$\begin{aligned}\theta_x &= \frac{TSS_{ast} V_{ast} + TSS_{clar} V_{clar}}{TSS_e Q_e + TSS_w Q_w} \\ &= \frac{(4243 \times 6000)g + (824 \times 6000)g}{(17.82 \times 18061)g/d + (8524 \times 385)g/d} \approx 9d\end{aligned}\quad (10.10)$$

This sludge age is relatively short for full nitrogen removal (Henze *et al.*, 1995). Again the relatively low sludge concentration in the system compared to the design is the reason for this.

### 10.3.1.3 Performance evaluation

Simulations were subsequently carried out using the prescribed procedure and the different *weather* files (*dry weather*, *rain event* and *storm event*). The performance was calculated using the indexes in paragraph 10.2.6. The results are summarised in Table 10.6.

Despite the relatively high sludge loading and low sludge age, most of the performance criteria were met by the plant. This was however not the case for the nitrification, since the effluent constraint for ammonium nitrogen was exceeded for more than 50% of the time during dynamic simulation. Also the nitrogen removal was not optimal, since the nitrate effluent concentration was relatively high (8.82 mg/l for dry weather). This sub-optimal denitrification has two causes: (i) the relatively low C/N ratio of the influent and (ii) at low influent load, quite some oxygen from the last aeration tank (tank 5) is recycled to the first anoxic tank. This decreases the denitrification capacity of the plant (Figure 10.4).

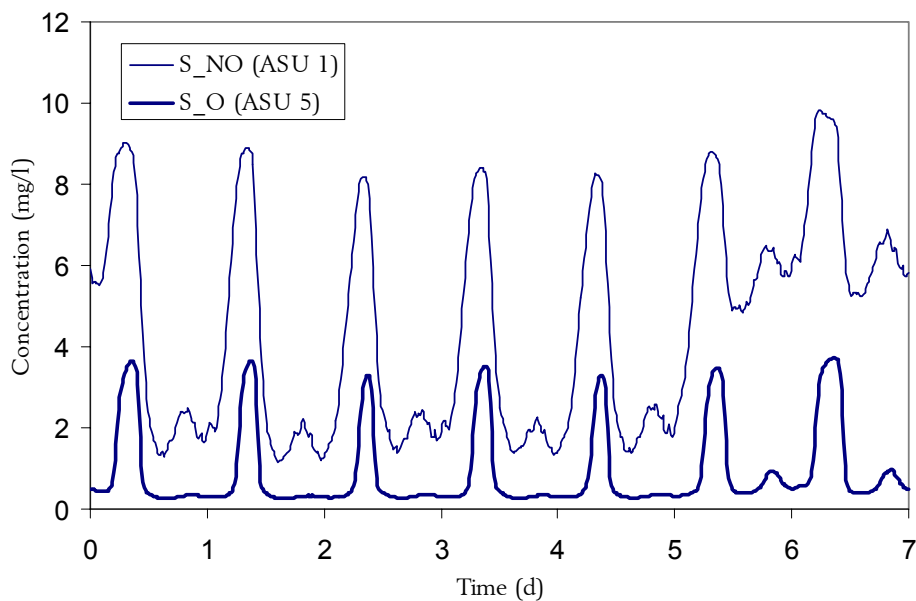


**Figure 10.4:** Nitrate nitrogen concentration in the first anoxic tank compared to the oxygen concentration in the last aerobic tank of the benchmark set-up

**Table 10.6. Performance of the benchmark plant for carbon and nitrogen removal with constant aeration**

	<i>Dry</i> (7d)			<i>Rain</i> (7d)			<i>Storm</i> (7d)		
<i>Indexes</i>									
EQ (PU/d)	7067			8844			7995		
PE (kWh/d)	424			424			424		
AE (kWh/d)	6476			6476			6476		
P <sub>sludge</sub> (kg/d)	2436			2362			2598		
P <sub>total</sub> (kg/d)	2671			2748			2914		
<i>Effluent constraint violations</i>									
	G	#	%T	G	#	%T	G	#	%T
SS <sub>e</sub>	13.00	0	0.0	16.17	0	0.0	15.25	1	0.15
N <sub>tot,e</sub>	15.57	5	8.3	14.33	3	4.5	15.12	4	8.25
S <sub>NH<sub>4</sub>e</sub>	4.77	7	62.3	4.99	7	63.6	5.36	7	64.5
COD <sub>e</sub>	48.30	0	0.0	45.54	0	0.0	47.75	0	0.0
BOD <sub>5,e</sub>	2.78	0	0.0	3.47	0	0.0	3.22	0	0.0

G = flow-weighted average values (in mg/l) over the period under study T; # = number of violations; %T = % time plant in violation.

### 10.3.2 Carbon and nitrogen removal with DO control

#### 10.3.2.1 Implementation and tuning

A first upgrade of the standard benchmark activated sludge plant could be the integration of dissolved oxygen control into the operating strategy. Figure 10.4 clearly shows that the aeration intensity ( $K_L a = 84 \text{ d}^{-1}$ ) is not adequate during daytime and excessive at night. Dissolved oxygen control can reduce the return of oxygen from the aerobic zone to the anoxic zone and optimise denitrification. Especially in the case of AGP, high oxygen concentrations are necessary to overcome oxygen limitations of the nitrifying biomass in the biofilm (Hem *et al.*, 1994; Rusten *et al.*, 1994; Münch *et al.*, 2000; Yuan *et al.*, 2001). This means AGP can more easily be operated cost-effectively when aeration control is implemented. In this study, aeration control was implemented in all cases where suspended carriers were added to activated sludge plants. This brings along the need for a reference benchmark plant where dissolved oxygen or aeration control is implemented.

The purpose of the controllers was to keep the dissolved oxygen concentration in the aerated basins at a constant set point. For ASU 3 and ASU 4, this set point was 2 mg/l. The set point in ASU 5 was set to 1 mg/l to limit the flux of oxygen to the first anoxic tank ASU 1. To this end DO sensors and PI controllers were implemented (Table 10.7). For simplicity, the DO sensor was modelled as an ideal sensor without noise or time delay. The upper limit of the manipulated variable  $K_L a$  of the controllers was set to  $240 \text{ d}^{-1}$  ( $= 10 \text{ h}^{-1}$ ), *i.e.* the upper limit of the blower capacity. The other parameters of the PI controllers were tuned manually so as to obtain an acceptable behaviour of the dissolved oxygen concentration in the aerated activated sludge basins (Figure 10.5). It should be noted that the goal of the tuning was not to keep the oxygen concentration close to its set point at all times. Using the ideal sensor this would certainly have been possible although this was not the goal of this study. However, the behaviour of the oxygen concentration as depicted in Figure 10.5 is more representative for the

concentration fluctuations encountered in practice than a perfectly tuned PI-controller in the simulator would be.

**Table 10.7. Variables of the implemented PI-type DO controllers**

	ASU 3	ASU 4	ASU 5
Controlled variable	$S_{O,ASU3}$	$S_{O,ASU4}$	$S_{O,ASU5}$
Set point	2 mg O <sub>2</sub> /l	2 mg O <sub>2</sub> /l	1 mg O <sub>2</sub> /l
Manipulated variable	$K_L a_{ASU3}$	$K_L a_{ASU4}$	$K_L a_{ASU4}$
$K_c$ (mg O <sub>2</sub> /l.d)		100	
$T_i$ (d)		0.03	
$u_0$ (d <sup>-1</sup> )		100	
$u_{min}$ (d <sup>-1</sup> )		0	
$u_{max}$ (d <sup>-1</sup> )		240	

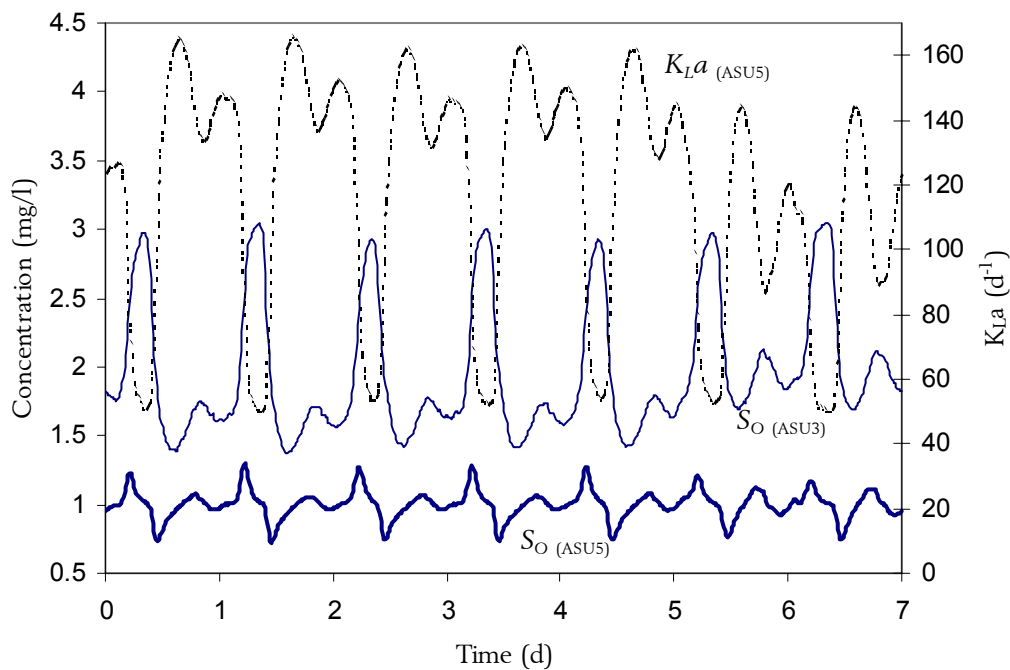


**Figure 10.5: Oxygen concentration in the third and fifth tank of the DO-controlled benchmark plant and  $K_L a$  in the fifth tank**

### 10.3.2.2 Performance evaluation

After obtaining a steady-state, simulations were performed with the *weather* files to calculate the performance (Table 10.8). From this table, it can be seen that the energy consumption for aeration and, together with that, the aeration cost could be reduced by about 7%. There was a clear decrease of the cumulative time the ammonium effluent concentration exceeded the constraint. On the other hand, the situation for total nitrogen had worsened somewhat. The decrease of the ammonium concentration can be explained by the increase of the aeration in the last aerobic tank at high loading rate, thanks to the aeration control. This entailed a more complete nitrification. However, on average more nitrogen left the system. This had to do with the set points of the aeration controllers. The average oxygen concentration in the last tank of the non-controlled plant was about 0.8 mg/l, which was lower than the set point of the DO controller there (1 mg O<sub>2</sub>/l). Optimising this set point could result in a lower reflux of oxygen to the anoxic phase without limiting oxygen supply to the aerobic

degradation in tank 5. Also, dissolved oxygen set points of 2 mg O<sub>2</sub>/l were selected in the first two aerobic tanks. Because of the quite high dissolved oxygen concentrations, less denitrification in these tanks was noticed during high loading periods than in the non-controlled plant. Here, a lower oxygen set point together with a more stringent control tuning might produce better results (Vanrolleghem and Gillot, 2001). This optimisation was however not the aim of this study.

**Table 10.8. Performance of the benchmark plant for carbon and nitrogen removal with controlled aeration**

	Dry (7d)	Rain (7d)	Storm (7d)						
<i>Indexes</i>									
EQ (PU/d)	7099	8810	7932						
PE (kWh/d)	424	424	424						
AE (kWh/d)	6118	5889	6113						
P <sub>sludge</sub> (kg/d)	2399	2316	2565						
P <sub>total</sub> (kg/d)	2630	2697	2875						
<i>Effluent constraint violations</i>									
	G	#	%T	G	#	%T	G	#	%T
SS <sub>e</sub>	13.01	0	0.0	16.21	0	0.0	15.29	1	0.15
N <sub>tot,e</sub>	16.03	7	14.3	14.49	7	12.9	15.30	7	15.1
S <sub>NH<sub>4</sub>e</sub>	3.29	12	32.9	4.08	11	46.7	3.94	12	42.9
COD <sub>e</sub>	48.29	0	0.0	45.46	0	0.0	47.68	0	0.0
BOD <sub>5,e</sub>	2.77	0	0.0	3.48	0	0.0	3.22	0	0.0

G = flow-weighted average values (in mg/l) over the period under study *T*; # = number of violations; %T = % time plant in violation.

## 10.4 Attached growth processes: suspended carriers in the aerobic phase

### 10.4.1 Introduction

A first attached growth process was implemented, where suspended carriers were only present in the aerobic phase of the plant. The general idea behind this implementation is to provide an extra growth platform for the nitrifying biomass and to enhance the nitrogen removal in a plant with a relatively small volume compared to what is normally needed in single sludge nitrogen removal plants. The growth of nitrifying biomass on carriers implies that the nitrifiers are only present in the phase of the plant where they are active and thus that high sludge concentration and sludge ages of the biomass in suspension can be avoided.

### 10.4.2 Implementation and modelling

Münch *et al.* (2000) implemented an attached growth process in a pilot plant at the Oxley Creek WWTP (Brisbane, Australia). This plant was limited by clarifier capacity which only allows a relatively low MLSS concentration (1300 mg/l) and therefore low sludge retention times of only 4 to 5 days. In this plant, carriers were placed in the nitrification zone. This zone was preceded by another aerobic

zone for carbon removal (Figure 10.6). The three zones (corresponding to reactor 1, 2 and 3) were designed equally large.

From Münch *et al.* (2000), the volumetric loading rates were calculated. The volumetric COD load to the plant was 1.3 kg COD/m<sup>3</sup>.d, the total nitrogen loading was 0.18 kg N/m<sup>3</sup>.d. Based on these loadings and the above composition of the benchmark influent, a volume of 4000 m<sup>3</sup> would be required to attain the same COD loading, and about 4700 m<sup>3</sup> would be necessary to treat the nitrogen loading using the same process characteristics. A volume of 4400 m<sup>3</sup> was selected. This volume was spread over the 5 tanks of the benchmark layout. The volumes of the tanks can be seen in Table 10.9. The biofilm reactors were filled with carriers for 50%. An active specific surface area (using the complete reactors volume as a reference) of 200 m<sup>2</sup>/m<sup>3</sup> was used (Münch *et al.*, 2000).

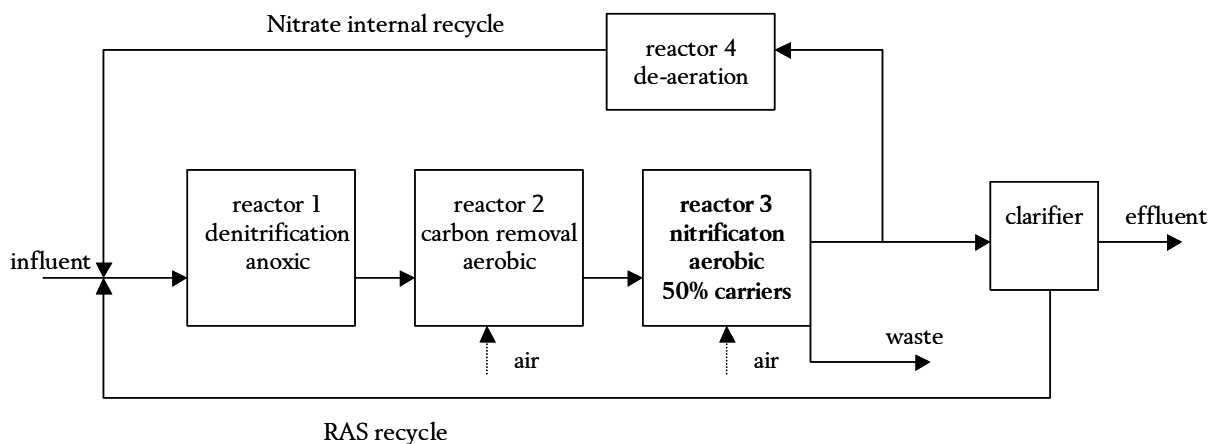


Figure 10.6: Oxley Creek pilot plant flow sheet (Münch *et al.*, 2000)

Table 10.9. Volumes and operating modes of the 5 tanks in the benchmark layout

Tank	Volume (m <sup>3</sup> )	Operating mode
ASU 1	800	anoxic, denitrification
ASU 2	800	anoxic, denitrification
ASU 3	1000	aerobic, carbon removal
ASU 4	900	aerobic, nitrification, 50% carriers (200 m <sup>2</sup> /m <sup>3</sup> )
ASU 5	900	aerobic, nitrification, 50% carriers (200 m <sup>2</sup> /m <sup>3</sup> )

For the description of the biodegradation in the first three tanks, the Activated Sludge Model No 1 model (Henze *et al.*, 1987) was used with an identical parameter set as in the original benchmark description. In the last two tanks, the ASM 1 model was coupled with the simplified mixed culture biofilm model presented in chapter 4. As described in this chapter, the basic idea behind this model implementation is to decouple the calculations of the two major processes occurring in the biofilm, the diffusive transport of soluble substrates and microbial conversion of these substrates. The model is an extension to the well-known half-order reaction concept that combines a zero-order kinetic dependency on substrate concentration with diffusion limitation. Previous studies already indicated that this modelling approach can easily be used in combination with a substrate conversion model for suspended biomass (Rauch and Vanrolleghem, 1998).

However, a limitation of the original model description is that no mass transfer resistance is modelled between the bulk liquid phase and the biofilm. Quite some authors (among others: Hem *et al.*, 1994; Rusten *et al.*, 1994; Aravinthan *et al.*, 1998; Rusten *et al.*, 2000) noticed a very strong oxygen dependency of the nitrification capacity in pilot studies with an attached growth reactor. According to Hem *et al.* (1994), this dependency can not be modelled using a simple half-order reaction concept, since the influence of the liquid film diffusional resistance on the biofilm kinetics is quite large. This apparently has to do with the growth of biomass at the protected inside surface of the carriers, where shear stress and liquid flow is lower than on the outside of the carriers. When the liquid film transport coefficient  $h$  becomes high, the diffusional resistance is of minor importance and a half-order reaction prevails. When  $h$  is low, the diffusional resistance is significant, and the overall reaction rate tends towards first order kinetics. This type of kinetics was noticed during the above-mentioned experiments. Hem *et al.* (1994) measured a transport coefficient  $h$  of 1.2-1.3 m/d, which, according to the authors, resulted in a quite high sensitivity of the nitrification in moving bed biofilm reactors to the oxygen concentration in the bulk liquid.

For the reasons mentioned above, the adapted mixed culture biofilm model including liquid film diffusional resistance (see section 4.6.3) was implemented and used for the simulations. A value of 1.3 m/d for the liquid film transport coefficient of oxygen was chosen. Since the oxygen concentration is so important for the nitrifying activity in the plant, oxygen controllers were implemented in all three aerobic tanks (Figure 10.7). The same PI-controller parameters ( $K_C$  and  $T_i$ ) were used as in Table 10.7. The set point in the first aerobic tank (carbon removal) was set to 1 mg/l to limit the aeration energy requirements and to allow some denitrification in this tank during high loading periods.

For the other parameters, the standard parameter set proposed in the benchmark was used. It is known that parameters in biofilms can deviate from values in activated sludge. For example the yield coefficient in biofilm is frequently modelled quite low (Horn and Telgmann, 1999). However, sufficient information to justify a significant deviation from the standard parameter set could not be gathered. Hence, also for reasons of simplicity, the parameter set was copied unchanged. For the parameters specific to biofilm systems, the values in Table 6.10 were used.

**Table 10.10. Parameters used in the modelling experiments**

Parameter	Value
$D_{f,S_o}$ (cm <sup>2</sup> /d)	2.1
$D_{f,S_s}$ (cm <sup>2</sup> /d)	0.58
$D_{f,S_{no}}$ (cm <sup>2</sup> /d)	1
$D_{f,S_{nh}}$ (cm <sup>2</sup> /d)	1.8
$\rho_m$ (kg/m <sup>3</sup> )	40

### 10.4.3 Steady-state evaluation

#### 10.4.3.1 Dissolved oxygen dependency of nitrification

The oxygen dependency of the nitrification rate in the reactors containing carriers is shown in Figure 10.8 (DO concentrations are equal in both reactors at all times). A linear dependency of the nitrification rate on the dissolved oxygen concentration in the first suspended carrier reactor can be seen. In the second reactor this was not the case. The reason for this is that at high DO concentration,

most of the available ammonium is already nitrified in the first reactor. This made the second reactor ammonium limited at elevated DO concentrations (above 3 mg/l in both reactors).

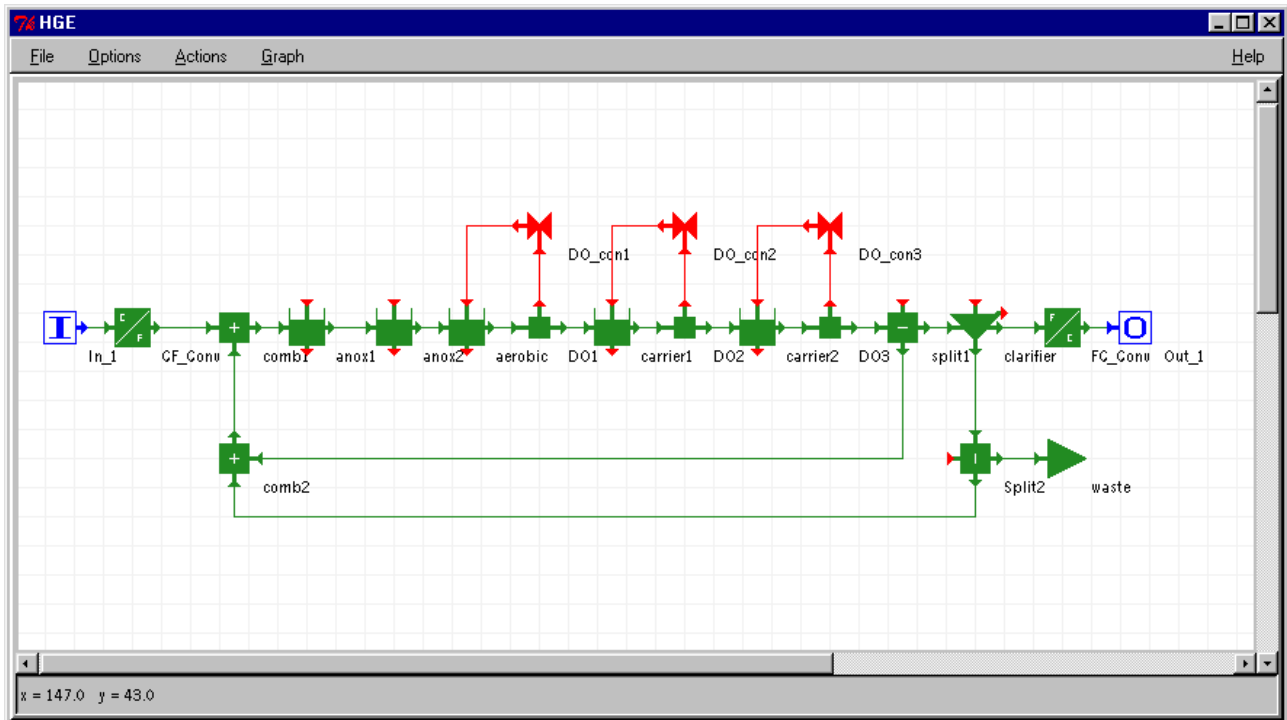


Figure 10.7: Graphical set-up of the suspended carrier plant in the WEST simulator. Carriers are only present in the aerobic phase (*carrier reactors*)

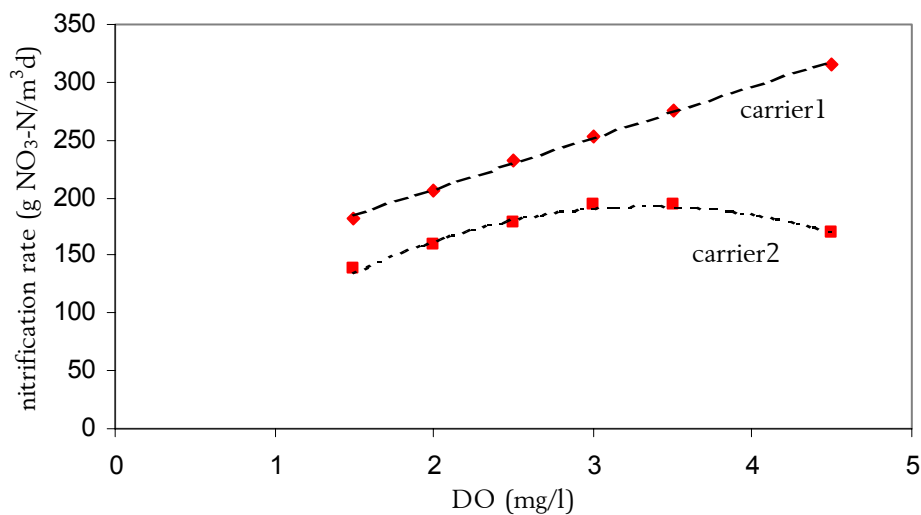


Figure 10.8: Nitrification rate versus imposed DO concentration in the suspended carrier reactors

Concentrating on the linear dependency in the first reactor, it is obvious that the simulated nitrification rates are in line with the values obtained in pilot-scale and full scale investigations (Rusten *et al.*, 1994; Welander *et al.*, 1997). However, the slope of the curve is rather small compared to these and other literature sources (Hem *et al.*, 1994). The slope of the curve changes when the liquid film transport coefficient  $h$  is changed. For the simulations, a value of 1.3 m/d was selected (Hem *et al.*, 1994). When this value is lower, the slope of the curve becomes steeper.

The difference between the simulated slope and the results from studies reported in literature can be the result of different factors. Quite some factors influence the nitrification rate indirectly. For instance, the imposed DO concentration has a major influence on the carbon removal pattern in the system and it therefore also influences the nitrification capacity of the biofilm. Literature data on these effects and on the liquid film transport coefficients of other species than oxygen in suspended carrier reactors were not readily available. Therefore, the value of 1.3 m/d for  $h$  was maintained for the rest of the simulations. It should also be noted that the dependency of the nitrification rate on the DO concentration only deviated from linear behaviour in case the ammonium concentration became limiting to the biofilm at higher DO concentrations.

In order to optimise nitrification, a set point of 4 mg/l in the first suspended carrier tank was selected. Reflux of oxygen to the anoxic phase could then be limited by selecting a set point of 3 mg/l in the second tank.

#### 10.4.3.2 Sludge retention time

When the sludge on the carriers (where most of the autotrophic biomass is situated) is neglected, an estimate of the sludge retention time of the biomass in suspension can be made. In case this is done the following sludge age can be calculated:

$$\begin{aligned}\theta_x &= \frac{TSS_{ast,susp} V_{ast} + TSS_{clar} V_{clar}}{TSS_e Q_e + TSS_w Q_w} \\ &= \frac{(3202 \times 4400)g + (1014 \times 3000)g}{(16.22 \times 18061)g/d + (6232 \times 385)g/d} \approx 6.4d\end{aligned}\quad (10.11)$$

This sludge age of the biomass in suspension is too short to obtain full nitrogen removal. This was confirmed by simulating the benchmark plant using the same volumes but without carriers. Note that the settler was smaller than in the standard benchmark layout (surface area 1000 m<sup>2</sup> and depth 3 m) because, different from what was noticed in the simulations, a lower MLSS concentration had been expected compared to the original benchmark plant.

The sludge concentration in suspension was not significantly lower than the sludge concentration found in the DO controlled benchmark plant. However, since the volume of the plant was smaller, only about 14 tons of sludge (expressed as kg TSS) were present in suspension instead of over 19 tons in the DO controlled benchmark plant. Quite some sludge was also present on the carriers in the suspended carrier plant. Slightly less than 15 tons of the total sludge mass of 28.8 tons was attached to the carriers.

It should be noted that most of the autotrophic biomass in the system was present in the biofilm on the suspended carriers (80.5% of the autotrophic biomass in the system). In Figure 10.9 the subdivision of the biofilm-sludge into its different constituents is depicted. The high percentage of inert biomass can indirectly be derived from this figure, since it makes up the rest of the solids in the biofilm.

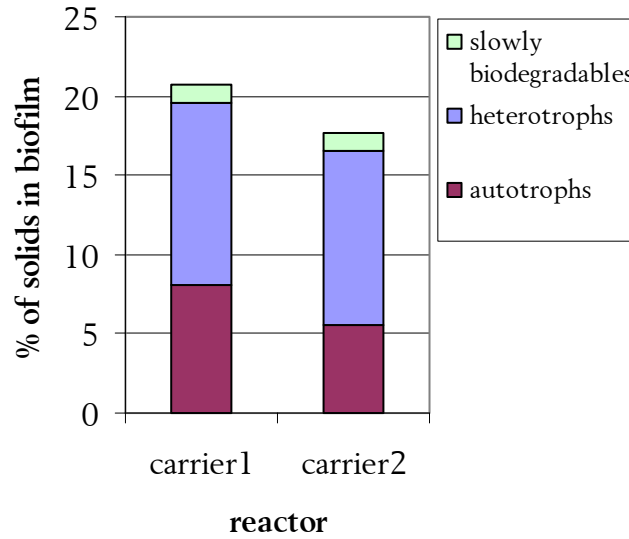


**Figure 10.9: Percentages of the different biofilm-sludge constituents in the suspended carrier reactors**

Since most of the autotrophic biomass is present on the carriers and not in the liquid phase (where an autotrophic sludge concentration of only 79.9 g COD/m<sup>3</sup> or 59.9 g SS/m<sup>3</sup> is found), the sludge age of the autotrophic biomass is significantly longer:

$$\begin{aligned} \theta_{x_{BA}} &= \frac{TSS_{BA,ast} V_{ast} + M(TSS_{BA,biofilm}) + TSS_{clar} V_{clar}}{TSS_{BA,e} Q_e + TSS_{BA,w} Q_w} \\ &= \frac{(59.9 \times 4400)g + 1523400g + (18.96 \times 3000)g}{(0.303 \times 18061)g/d + (116.5 \times 385)g/d} \approx 36d \end{aligned} \quad (10.12)$$

Although only part of the total autotrophic biomass in the biofilm is active at any point in time (due to diffusion limitations in the biofilm), this long sludge age of the autotrophic biomass indicates that the carriers allow for sufficient autotrophic growth to reach full nitrification. This finding supports the hypothesis that the separation of autotrophs and heterotrophs in the zones where they are active is responsible for the increased treatment capacity.

#### 10.4.4 Dynamic performance evaluation

##### 10.4.4.1 Performance indexes

The dynamic performance evaluation was obtained with simulations using the different *weather* files after obtaining a steady-state (Table 10.11). It is very important to realise that the performance indexes obtained in 10.2.6.3 are specific for the standard benchmark implementation. One of the parameters that is specific to the benchmark implementation is the volume of the tanks. Especially for calculation of the aeration energy (based on data by Jacquet, 1999), the volume of the tank is of extreme importance. Therefore, next to the formula stated above that is valid for a volume of 1333 m<sup>3</sup>, extra formulas were derived for other volumes. For 900 and 1000 m<sup>3</sup>, the formulas become respectively (AE in kWh/d):

$$AE(900 \text{ m}^3) = \frac{24}{T} \int_{t_0}^{t_7 \text{ days}} \sum_{i=1}^{i=5} [0.1728 \cdot K_L a_i(t)^2 + 5.328 \cdot K_L a_i(t)] dt \quad (10.13)$$

$$AE(1000 \text{ m}^3) = \frac{24}{T} \int_{t_0}^{t_7 \text{ days}} \sum_{i=1}^{i=5} [0.2304 \cdot K_L a_i(t)^2 + 5.9184 \cdot K_L a_i(t)] dt$$

where  $K_L a_i(t)$  is the mass transfer coefficient in  $i^{\text{th}}$  aerated reactor at time  $t$  ( $\text{h}^{-1}$ )

The indexes in Table 10.11 show a clear decrease of the effluent quality. This decrease has mainly to do with the insufficient degree of nitrification at high ammonium loads and with the high reflux of oxygen to the anoxic zone limiting the denitrification there. At high ammonium loading peaks, the nitrification capacity of the biofilm (mainly limited by the oxygen supply to the biomass) becomes limiting (Figure 10.10). Evidently, a higher oxygen concentration in the aerobic tank (especially in the last aerobic tank) would further increase nitrification capacity. On the other hand, it would limit the denitrification in the anoxic tanks. This denitrification capacity already is a weak point of this set-up, so an increase of the oxygen concentration is not advisable unless a de-aeration tank would be included in the nitrate recycle flow (Münch *et al.*, 2000). The effluent quality is further deteriorated because the use of a smaller settler compared to the standard benchmark layout resulted in a slightly higher effluent suspended solids concentration.

There was no clear decrease of the sludge production. Most of the sludge that was produced resulted from aerobic or anoxic degradation of organic matter. The autotrophic biomass on the carriers had no major influence on this.

There was, however, a considerable increase of the required aeration energy. The energy input increased with a factor of about 2.7, while the volume necessary for treatment only decreased with about 25%.

#### 10.4.4.2 Economic analysis

Table 10.12 shows a comparison between the DO controlled benchmark and the suspended carrier plant. It should be noted that the possible volume decrease of the secondary clarifier was not included here, since there was not enough data available on the settleability of the sludge in this suspended carrier implementation to adjust the parameters of the settler model accordingly. Also the investment cost for the carriers and the grids to keep the carriers inside the tanks was not included in this comparison.

It is obvious that the effluent quality deteriorated quite dramatically. This mainly has to do with the nitrogen removal. Extra biofilm surface for nitrification and high dissolved oxygen concentrations in the aerobic phase should be able to remedy this problem. However, if the DO set point is increased, the aeration cost will increase with it. Also, increasing the biofilm surface area will increase the aeration cost since the oxygen uptake rate will increase. A higher surface area can be obtained by increasing the tank volume or by increasing the specific area of the carriers in the tank. The latter is feasible, since several authors (Hem *et al.*, 1994; Rusten *et al.*, 2000) reported an active specific surface area of more than  $300 \text{ m}^2/\text{m}^3$  in suspended carrier reactors.

**Table 10.11. Performance of the benchmark plant with suspended carriers in the aerobic phase**

	<i>Dry</i> (7d)	<i>Rain</i> (7d)	<i>Storm</i> (7d)						
<i>Indexes</i>									
EQ (PU/d)	8402	10020	9305						
PE (kWh/d)	424	424	424						
AE (kWh/d)	11133	10862	11246						
P <sub>sludge</sub> (kg/d)	2401	2281	2525						
P <sub>total</sub> (kg/d)	2707	2811	2953						
<i>Effluent constraint violations</i>									
	G	#	%T	G	#	%T	G	#	%T
SS <sub>e</sub>	17.25	0	0.0	22.53	11	10.79	20.98	2	5.24
N <sub>tot,e</sub>	18.89	14	49.14	16.26	12	41.50	17.55	13	72.7
S <sub>NH,e</sub>	4.14	13	33.11	3.80	13	33.11	4.13	4	37.01
COD <sub>e</sub>	53.97	0	0.0	53.88	0	0.0	55.27	0	0.0
BOD <sub>5,e</sub>	3.69	0	0.0	4.84	0	0.0	4.41	0	0.0

G = flow-weighted average values (in mg/l) over the period under study *T*; # = number of violations; %T = % time plant in violation.

In case the DO set point is increased, it is of importance to include a de-aeration tank in the set-up since the reflux of oxygen to the anoxic zone hampers denitrification. The de-aeration can also be accomplished by increasing the volume of the anoxic pre-denitrification zone. However, if this is done, the volume saving that is an important incentive to use suspended carriers, is partly eliminated.

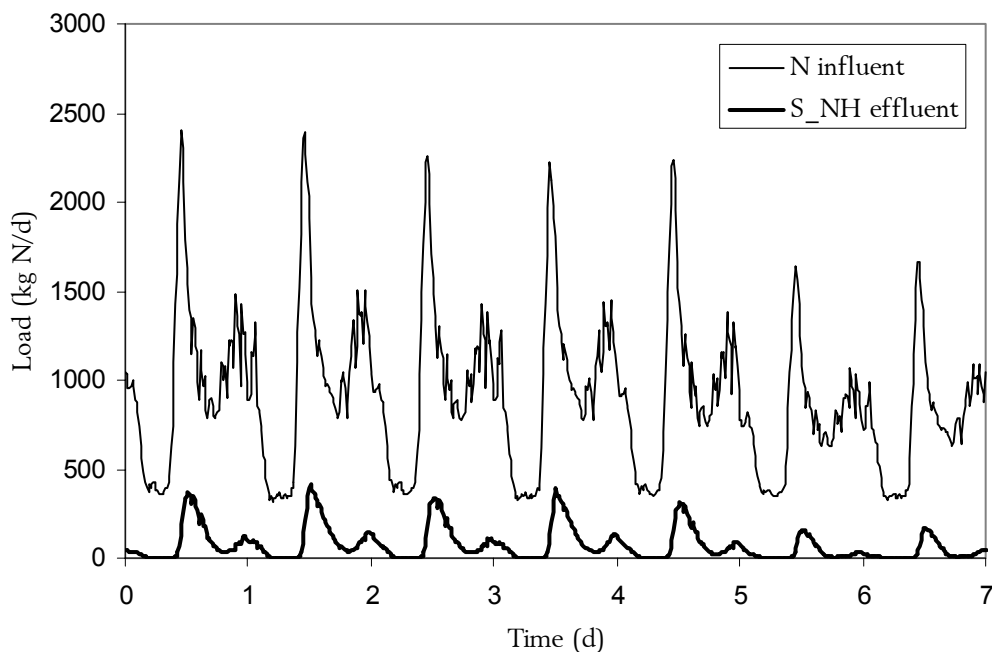


**Figure 10.10: Effluent ammonium nitrogen load compared to the influent total nitrogen loading rate (both in kg N/d)**

**Table 10.12. Economic comparison between the DO-controlled benchmark and the benchmark plant with carriers in the aerobic phase for nitrification (averaged over the different weather conditions)**

	DO-controlled benchmark	Suspended carrier plant	difference
Operational costs (€/year)			
Effluent quality	397 350	462 117	+ 64 767 (+16.3%)
Pumping cost	10 600	10 600	+ 0 (+ 0.0%)
Aeration cost	151 000	277 008	+ 126 008 (+ 83.4%)
Sludge disposal	182 000	181 175	- 825 (- 0.5%)
Investment cost (€)			
Aeration basin	653 407	563 550	- 89 857 (-13.8%)

### 10.4.5 Conclusion

After simulation and performance assessment, it becomes clear that the volume saving that can be accomplished by using suspended carriers in the aerobic phase is rather small. This is certainly the case when a de-aeration tank needs to be incorporated. Also, a quite high cost for extra aeration should be taken into account. Even with a high aeration capacity, the available biofilm surface limits the degree of nitrification that can be accomplished. Optimisation of the design could include aeration control in the aerobic phase on the basis of the ammonium loading in the influent to the plant. This would possibly limit the aeration cost and extend the nitrification capacity in a high loading case.

In short, this technique appears only useful when external factors limit nitrification in an activated sludge plant (*e.g.* if a small settler, that can not be extended, limits the sludge concentration and the sludge age; Rusten *et al.*, 2000).

## 10.5 Attached growth processes: suspended carriers in the complete reactor

### 10.5.1 Introduction

The second implementation of the attached growth process is the one with carriers in all of the tanks. In this case, the biofilm is also used for denitrification. Different plant layouts have been developed over time including pre-denitrification and post-denitrification. Here, only the pre-denitrification example was studied. This means a recycle of nitrate rich mixed liquor was present. However, a settled sludge recycle loop was not present since all settled sludge was wasted.

### 10.5.2 Implementation and modelling

This implementation of the suspended carrier process has mainly been developed as an alternative to submerged biological filters, which have a tendency to clog. This makes regular backwashing necessary. The carriers used in this process are reported to have an active specific surface area (relative to the complete tank volume) of 300 m<sup>2</sup>/m<sup>3</sup> in the tanks at a filling rate of about 70%. However, when mixers are used to maintain the carriers in suspension instead of aeration, an active surface area of 200 m<sup>2</sup>/m<sup>3</sup> is used at a filling of 50% (Hem *et al.*, 1994).

Based on volumetric loading rates published by Rusten (1994) and Rusten *et al.* (1994), the volumes of the different phases in the reactor were calculated. Volumetric COD loading rates of 1.2 to 3 kg

COD/m<sup>3</sup>.d and nitrogen loadings of 222 up to 387 g N/m<sup>3</sup>.d were applied. Based on these loading rates, a volume of 3500 m<sup>3</sup> would have been sufficient. However, after initial simulations with this volume, it was obvious that very high DO concentrations would have been needed in order to obtain sufficient nitrification capacity. For this reason, the tank volume was extended to 4000 m<sup>3</sup> in total. In Rusten (1994), an equal volume was reserved for the anoxic volume as for the aerobic phase in the plant. This can be interpreted as if a de-aeration tank was included at the beginning of the anoxic phase. However, in this de-aeration tank quite some readily biodegradable influent COD will be used in aerobic metabolism that is lost for denitrification in the anoxic tanks. Therefore, it was chosen to implement a de-aeration tank at the end of the aerobic zone instead (Rusten *et al.*, 2000; Figure 10.11). In this tank, with a volume of 600 m<sup>3</sup>, the oxygen set point of the PI controller was lowered to 1 mg/l. This ensures that the oxygen recirculation to the anoxic phase is minimal and that denitrification can proceed in optimal conditions (Rusten *et al.*, 2000). The flow rate of the internal nitrate rich recycle was taken identical to the flow proposed in the benchmark.

For the description of the biodegradation, the Activated Sludge Model No 1 model (Henze *et al.*, 1987) was used. This model was coupled to the simplified mixed-culture biofilm model. For the reasons mentioned in paragraph 10.4.2, the adapted mixed-culture biofilm model that includes liquid film diffusional resistance was implemented and used for the simulations. Again, dissolved oxygen controllers were implemented in all three aerobic tanks (Figure 10.7). The same PI-controller parameters ( $K_C$  and  $T_i$ ) were used as in Table 10.7. The set points in the two first aerobic tank (carbon removal and nitrification) were set to 5 mg/l. The last aerobic tank (de-aeration) had an oxygen set point of 1 mg/l (Figure 10.11).

**Table 10.13. Volumes and operating modes of the 5 tanks in the benchmark layout**

Tank	Volume (m <sup>3</sup> )	Operating mode
ASU 1	900	anoxic, denitrification, 50% carriers (200 m <sup>2</sup> /m <sup>3</sup> )
ASU 2	900	anoxic, denitrification, 50% carriers (200 m <sup>2</sup> /m <sup>3</sup> )
ASU 3	1100	aerobic, nitrification and carbon removal, 70% carriers (300 m <sup>2</sup> /m <sup>3</sup> )
ASU 4	1100	aerobic, nitrification, 70% carriers (300 m <sup>2</sup> /m <sup>3</sup> )
ASU 5	600	aerobic, de-aeration, 70% carriers (300 m <sup>2</sup> /m <sup>3</sup> )

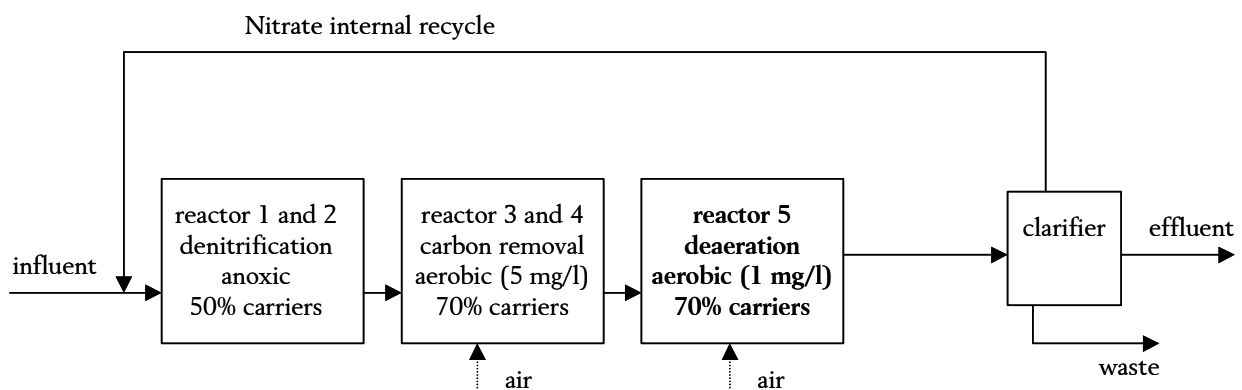


**Figure 10.11: Set-up of the benchmark plant for evaluating suspended carrier systems performance with carriers in all phases**

### 10.5.3 Steady-state evaluation

#### 10.5.3.1 Sludge retention time

When growing on supporting media, bacteria typically have a longer retention time than in conventional activated sludge treatment. This means bacteria are maintained longer in the system, even though no sludge recycle is provided. This fact also means that a smaller settler can suffice to let the limited amount of suspended solids present in the mixed liquor settle. Equations 10.14 and 10.15 show the calculated retention times of the heterotrophic and the autotrophic biomass respectively. These results show not only that the retention time is longer than in the conventional benchmark activated sludge plant, but also that the retention time for the different types of biomass is not identical. This is only possible in case the heterotrophs and autotrophs are separated in space and are only present in the zones where they are active.

$$\begin{aligned}\theta_{x_{BH}} &= \frac{M(TSS_{BH,biofilm}) + M(TSS_{BH,clar})}{TSS_{BH,e} Q_e + TSS_{BH,w} Q_w} \\ &= \frac{14783 \text{ kg} + 481 \text{ kg}}{586 \text{ kg/d} + 45 \text{ kg/d}} \approx 24\text{d}\end{aligned}\quad (10.14)$$

$$\begin{aligned}\theta_{x_{BA}} &= \frac{M(TSS_{BA,biofilm}) + M(TSS_{BA,clar})}{TSS_{BA,e} Q_e + TSS_{BA,w} Q_w} \\ &= \frac{2353 \text{ kg} + 56 \text{ kg}}{68 \text{ kg/d} + 5 \text{ kg/d}} \approx 33\text{d}\end{aligned}\quad (10.15)$$

As an example, Figure 10.12 shows the relative amount of the different solids fractions in the biomass. It is clear that a considerable amount of ammonium oxidisers is only present in the aerobic tanks. It should be noted that even there the concentration is relatively low compared to what is sometimes reported in literature (Zhang *et al.*, 1998). The reason for this is, presumably, heterotrophic activity in the aerobic tanks due to degradation of readily biodegradable substrate resulting from hydrolysis processes in the model.

#### 10.5.3.2 Influent COD utilisation efficiency for nitrate reduction

The sludge retention times calculated in the above equations are also dependent on the attachment and detachment of particulate matter to and from the biofilm. These coefficients were tuned in this case using reported values for the suspended solids concentration in suspended carrier reactors with a similar layout as the model plant (Welander, personal communication). This concentration was about 150 mg SS/l. To reach this value, a detachment coefficient of 0.1 d<sup>-1</sup> and an attachment coefficient of 10 d<sup>-1</sup> needed to be implemented.

These coefficients are also of great importance for the denitrification. Indeed, the attachment/detachment coefficients determined the removal efficiency of suspended solids from the influent in the anoxic nitrate reduction zone. In case the majority of the suspended solids was retained there, the leakage of COD to the aerobic zones was limited and therefore the COD utilisation efficiency for nitrate reduction was optimised. This model description is supported by

several experiments (Rusten *et al.*, 2000). These experiments in batch and pilot-scale set-ups showed that hydrolysis products from particulate COD can be used as a carbon source for denitrification when the available soluble COD is limited.

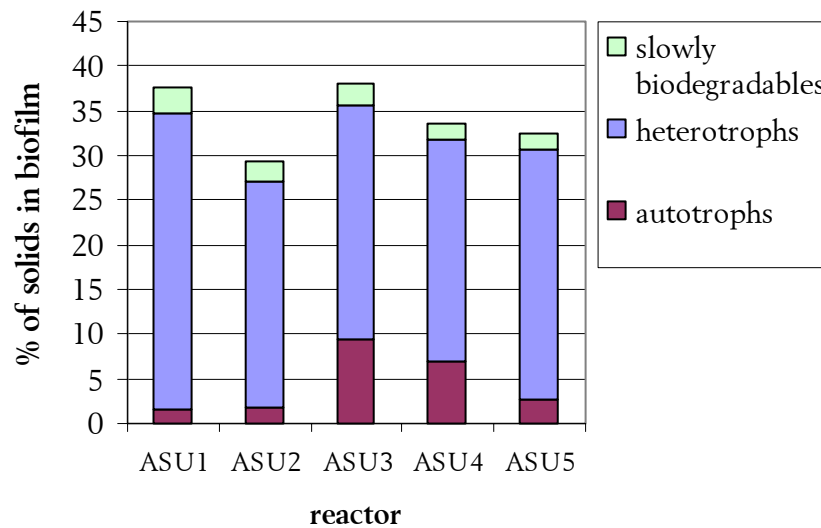


**Figure 10.12: Percentages of the different biofilm-sludge constituents in the suspended carrier reactors**

In the simulation with the DO controlled benchmark plant, the concentration of biodegradable COD, not including biomass, that was transferred to the oxic zone of the plant, was still 79.7 mg/l, despite the fact that the average nitrate nitrogen concentration in the second anoxic tank was still 4.1 mg/l. The COD leakage mainly took place in the form of slowly biodegradable material. This clearly shows that the influent biodegradables were not optimally used in the denitrification process. In the model description of the suspended carrier plant, only 65.5 mg/l of slowly biodegradable material leaked to the subsequent aerobic zone, while a nitrate nitrogen concentration as low as 1.0 mg/l was reached. This indicates an optimal use of the influent COD for nitrate reduction and the possibility to reach full denitrification at lower COD to nitrogen ratios. In fact, the denitrification in the second anoxic tank was limited by nitrate and no longer by the readily biodegradable COD.

### 10.5.3.3 Dissolved oxygen dependency of nitrification

When investigating the oxygen dependency of the nitrification in the suspended carrier plant, a weak point of the process design could be identified. When a DO concentration of 4 mg/l (instead of 5 mg/l) was selected in reactors 3 and 4, the nitrification activity dropped significantly due to oxygen limitation. As was shown above, even with full nitrification, all nitrate could be removed in the anoxic zone. When the nitrate supply to the anoxic zone was lower than normal, the COD that was not used in the anoxic zone leaked towards the aerobic zone.

In this situation, the advantage of the suspended carrier system, namely to have the different types of biomass separated in space, suddenly turns into a disadvantage. When COD leaks to the aerobic zone, only a limited amount of heterotrophic biomass is present there to aerobically degrade the COD influx. In a steady-state situation, the effluent biodegradable COD increased up to 75 mg/l. Even worse, nitrification was absent when the DO set point was set to 4 mg/l.

Although these results should be interpreted with care because of the absence of experimental data to support this finding, it is obvious that the dependency of the treatment efficiency on the DO concentration is of very big importance in this treatment system. It is of even greater importance here than in the case where carriers are only present in the aerobic phase. There, the sludge recycle makes sure that enough heterotrophic biomass is present in the aerobic zone to obtain sufficient COD removal when readily biodegradable COD leaks towards the aerobic zone.

#### 10.5.4 Dynamic performance evaluation

##### 10.5.4.1 Performance indexes

The dynamic performance evaluation was obtained during simulations with the *weather* files after obtaining a steady-state (Table 10.14). In this case too a different formula for the calculation of the aeration energy had to be derived. For a tank of 1100 m<sup>3</sup>, the formula becomes (AE in kWh/d):

$$AE(1100 \text{ m}^3) = \frac{24}{T} \int_{t_0}^{t_7 \text{ days}} \sum_{i=1}^{i=5} [0.2304 \cdot K_L a_i(t)^2 + 6.509 \cdot K_L a_i(t)] dt \quad (10.16)$$

where  $K_L a_i(t)$  is the mass transfer coefficient in the  $i^{\text{th}}$  aerated reactor at time  $t$  (h<sup>-1</sup>)

Table 10.14 shows that the effluent quality of the system is quite comparable or even slightly better than the classical activated sludge system. However, compared to this standard system, the behaviour of the system under storm conditions is rather strange. Under these conditions the effluent quality is significantly worse than under dry or rain weather conditions. This is not the case to this extent in the original benchmark plant. The worsening of the effluent quality has to do with a loss of nitrification activity under the storm weather condition. The first storm starts with a large loading peak. As described above, the substrate that is not needed for denitrification leaks towards the aerobic phase where it is only partly degraded and, more importantly, where it hampers nitrification. Also, when the loading peak comes in, the oxygen controllers can not keep the oxygen concentration above 4 mg/l (their set point is 5 mg/l). Consequently, the scenario outlined in paragraph 10.5.3.3 takes place and after this load shock the nitrification needs quite some time to recover. This can be seen in Figure 10.13.

The above indicates that the control of the oxygen supply to the system is of extreme importance to the performance of suspended carrier systems. Therefore, it has to be noted that the PI-control of the aeration was already rather stringent in this simulation study. The oxygen concentration under normal operating conditions did not drop below 4.3 mg/l. This way, a sudden disappearance of the nitrogen removal was not witnessed at dry weather conditions. However, these settings have as a consequence that the energy consumption for the aeration in this suspended carrier system is about three to four times as high as compared to the standard activated sludge nitrogen removal plant (Table 10.8) and about double the energy needed in a suspended carrier system where carriers are only present in the aerobic phase (Table 10.11).

As a last point in this comparison, the decrease of the sludge production can be studied. This decrease was due to the longer sludge retention times in the biofilm system as compared to the activated sludge

implementation. The low suspended solids concentrations in the mixed liquor also entails that the size of the secondary clarifier could be rather small.

**Table 10.14. Performance of the benchmark plant with suspended carriers in all phases**

	<i>Dry</i> (7d)	<i>Rain</i> (7d)	<i>Storm</i> (7d)
<i>Indexes</i>			
EQ (PU/d)	6113	7415	8409
PE (kWh/d)	318	318	318
AE (kWh/d)	23282	23025	21602
P <sub>sludge</sub> (kg/d)	1960	2200	2212
P <sub>total</sub> (kg/d)	2119	2490	2441

*Effluent constraint violations*

	<i>G</i> <i>#</i> <i>%T</i>			<i>G</i> <i>#</i> <i>%T</i>			<i>G</i> <i>#</i> <i>%T</i>		
SS <sub>e</sub>	8.96	0	0.0	12.35	0	0.0	11.16	2	5.24
N <sub>tot,e</sub>	13.77	18	14.75	12.10	18	7.96	16.34	5	32.94
S <sub>NH,e</sub>	3.66	7	26.70	2.55	6	18.62	7.78	4	42.75
COD <sub>e</sub>	48.80	0	0.0	43.00	0	0.0	51.03	0	0.0
BOD <sub>5,e</sub>	2.52	0	0.0	3.14	0	0.0	4.43	0	0.0

G = flow-weighted average values (in mg/l) over the period under study *T*; # = number of violations; %T = % time plant in violation.

#### 10.5.4.2 Economic analysis

Table 10.15 shows a comparison between the DO controlled benchmark and the suspended carrier plant. As already shown in Table 10.14, the overall effluent quality improved slightly. The average effluent concentrations decreased, as well as the time the effluent constraints were violated. This increased quality is also reflected in the cost for the effluent discharge. Also the cost for sludge disposal and the pumping costs decrease slightly. Since no settled sludge recycle is needed, the energy for pumping is lower as compared to the standard benchmark implementation.

The benefits summed up above are however no match for the increased aeration cost. Therefore, the total operational cost for the suspended carrier plant is significantly higher than the benchmark plant operational costs. On the other hand, the investment cost for the aeration basin is slightly lower since there is a possibility for volume reduction. The possible volume decrease of the secondary clarifier was not included here, since there was not enough data available on the settleability of the sludge in this suspended carrier implementation to adjust the parameters of the settler model accordingly. Also, the investment cost for the carriers and the grids to keep the carriers inside the tanks was not included in this comparison.

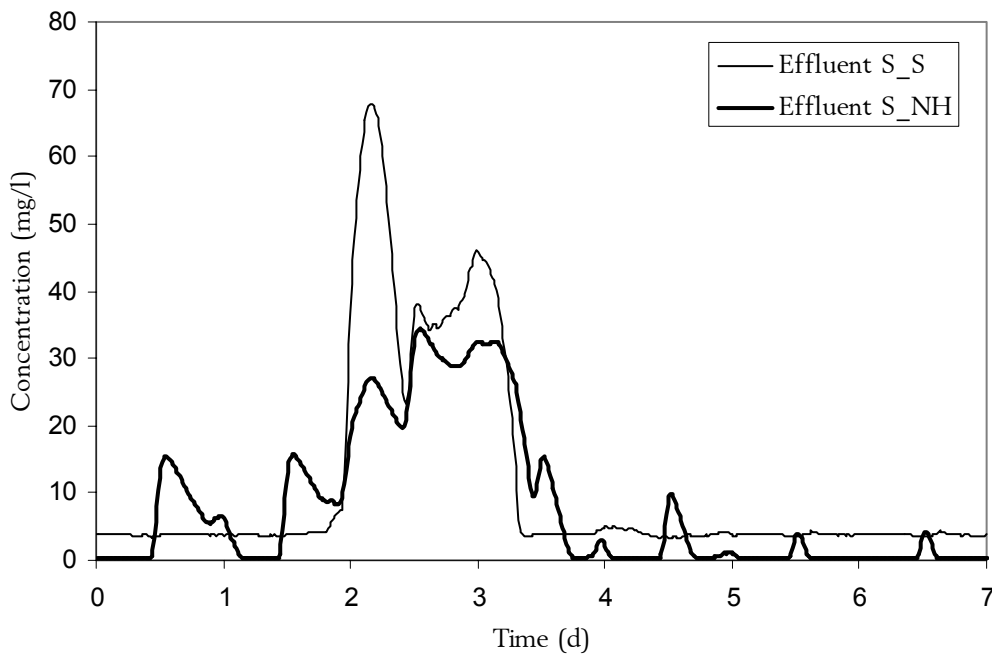


**Figure 10.13: Effluent ammonium nitrogen concentration compared to the concentration of readily biodegradable substrate in the effluent**

**Table 10.15. Economic comparison between the DO-controlled benchmark and the benchmark plant with carriers in the aerobic phase for nitrification**

	DO-controlled benchmark	Suspended carrier plant	difference
Operational costs (€/year)			
Effluent quality	397 350	365 617	- 31 733 (- 8.0%)
Pumping cost	10 600	7 950	+ 2 650 (- 25.0%)
Aeration cost	151 000	565 908	+ 414 908 (+ 275%)
Sludge disposal	182 000	159 300	- 22 700 (- 12.5%)
Investment cost (€)			
Aeration basin	653 407	575 627	- 77 780 (12.0%)

### 10.5.5 Conclusion

It is clear that suspended carrier technology is a valid alternative for standard activated sludge treatment techniques. However, the performance assessment showed that the operational cost of the suspended carrier plant is significantly higher than that of the standard benchmark plant. The slightly better effluent quality obtained by the suspended carrier plant is more than compensated by the higher aeration cost needed to obtain good nitrification results. Of course this conclusion is highly country specific, since electricity costs and effluent constraints and fines vary significantly, even within the European Union. Therefore, the performance assessment in non monetary units should be used as a basis for comparison in different countries.

It was shown that with relatively low COD to nitrogen ratios, still good nitrogen removal can be obtained in suspended carrier plants. This can also be accomplished in a smaller volume as compared to activated sludge technology. On the other hand, more investments will be needed in aeration

capacity and in control. The simulations showed that low oxygen concentrations - even for a limited period of time - can seriously hamper the performance of the plant.

## 10.6 Conclusions

The feasibility of attached growth processes for biological nitrogen removal has been evaluated using dynamic simulations. To this end, a simulation benchmark that was developed initially for the simulation and evaluation of operating and control strategies for activated sludge treatment plants has been modified and used. The benchmark served as a reference to compare the operating and part of the investments costs of attached growth processes to standard activated sludge treatment. To simulate the bacterial growth on suspended carriers, the Activated Sludge Model No 1 was coupled to a simplified mixed-culture biofilm model. This coupling was possible since the layout of the biofilm model avoids having to solve partial differential equations. This way, the calculation time for this type of application can be kept reasonably low.

Two types of attached growth processes were studied. In the first, carriers were only added to the aerobic zone of the plant in order to enhance nitrification in a relatively small volume and at low sludge retention times. It was noticed that the longer retention time of the biomass growing on the carriers stimulated nitrification. However, a rather strong dependency of the performance on the dissolved oxygen concentration was obvious, causing the required aeration energy to increase significantly. The effluent quality that was achieved, was worse than that of the benchmark plant. Mainly the relatively high reflux of oxygen to the anoxic zone limited full nitrogen removal. Also extra carrier surface area should be available for more nitrifiers to grow in the system. However, this would undo the volume saving that is seen as a major advantage of the suspended carrier plant layout. This plant layout is therefore only considered useful when external factors limit nitrification in an activated sludge treatment plant such as a limited suspended sludge concentration due to a small settler.

The next plant layout studied included the addition of carriers to all zones of the plant. In this system, the main goal is the physical separation of the heterotrophic and autotrophic biomass. The retention times of heterotrophs and autotrophs are different in this system and they are mainly present in the zones of the plant where they are active. Another advantage of the system that could be quantified using simulation is the limited leakage of readily biodegradable material from the anoxic zone to the aerobic zone of the plant. This entails that full nitrogen removal can be accomplished at lower C/N ratios in the influent. However, this plant layout is even more sensitive to the dissolved oxygen concentration in the aerobic zone. Therefore the oxygen control needs to be rather stringent and enough blower capacity should be available to preserve a sufficiently high oxygen concentration at high loading rates. If the DO concentration suddenly drops, nitrogen removal can be lost and will take some time to recover. However, when an attached growth system is operated well, an excellent effluent quality can be obtained.

# 11 Conclusions and perspectives

---

In the literature review, it became clear that a whole range of biofilm models is available, ranging from relatively simple one-dimensional models to comprehensive 3D descriptions of the biofilm structure in time and space. The first one-dimensional models mainly focussed on steady-state mass transport in the biofilm and could be solved analytically. More complex models included equations describing the species distribution in a biofilm and therefore resulted in partial differential equations. Finally 3D models can only be solved using dedicated hardware because of their computationally intensive nature.

Each of the above models has its value and its possible applications. It was not the aim of this thesis to promote one or the other model structure or complexity. The complexity of the model that is chosen should however be relevant for the application it is used for. High complexity models clearly have the advantage of including a lot of the available knowledge about biofilm processes. On the other hand, the high complexity of the model also increases the number of unknown parameters and the possible dependencies between them. As has been pointed out in the literature review, these factors make the accurate estimation of parameter values very difficult. Especially because of the difficult parameter estimation, it is hard to use these models for the prediction of the behaviour of processes in practice. Also, even for very complicated models, some biofilm processes – like attachment, detachment, the influence of higher organisms, ... – are still poorly understood and are described by empirical formulas. Based on these findings, combined with the required computational effort and time to solve highly complex models, it becomes clear they are too detailed for use in full-scale on-line applications.

In this thesis, a model was developed and applied that attempts to be a complexity compromise. It is relatively simple, since it is based on the analytical solution of the substrate profiles in the biofilm. This factor is very important for the application of the model in practical situations and in combination with other widely accepted models in wastewater treatment like Activated Sludge Model No 1 (Henze *et al.*, 1987). On the other hand, the model is able to calculate the conversion rates of processes in the biofilm performed by different biomass species. Thus, despite its simplifications, it can be used to describe processes occurring at different depths of the biofilm. In order to successfully use the model in applications for process optimisation, a simulation tool had to be available for its implementation and fast simulation.

## 11.1 The WEST simulator

Such a simulator is the recently developed WEST simulator (Hemmis NV, Kortrijk, Belgium) described in chapter 3. Indeed, to be able to use mathematical models, a good software tool to implement and simulate them is indispensable. One of the key features of WEST is its possibility to deal with multiple processes. In activated sludge wastewater treatment, the processes studied are the removal of organic matter, nitrogen and phosphorus, which are accomplished in a single system nowadays. In this work, WEST was also used to study treatment systems where these processes are simultaneously taking place in a biofilm and in the liquid phase. To enable this coupling, a powerful model base structure had to be developed, which plays a central role in WEST. In this model base,

models are described in MSL-USER (MSL stands for *model specification language*), a high level object-oriented declarative language. The model base is aimed at maximal re-use of existing knowledge and is therefore structured hierarchically. All re-usable knowledge – such as mass balances, physical units, default parameter values and applicable ranges – is thus defined centrally and can be re-used by an expert user to build new models. WEST has an open structure that allows the user to change existing models and define new ones as needed. The centrally defined knowledge is, however, also of great value for a non-expert who only uses the model base from within the graphical user interface, since the default values and range checking protect the user from erroneous simulation results. It is also crucial for the ease of implementation of new models that they can be implemented in a compact and surveyable form. Because of the hierarchical structure of the model base, models can directly be included in the model base using the matrix format (Petersen, 1965) selected by the IWA task group on mathematical modelling (Henze *et al.*, 1987). All other standard parts of a dynamic model such as the transport terms are re-used.

A second important feature of the WEST simulator that was extensively used in this thesis is its ability for graphical component-based modelling. A hierarchical graphical editor (HGE) is especially designed for the interactive composition of complex configurations from basic building blocks. From this graphical specification, together with the models chosen from the model base, a coupled model is produced. The graphical editor and the coupled model introduce a second level of hierarchy in WEST. Next to the hierarchical structure of the model base, aimed at maximal re-use of knowledge, also coupled models and their graphical representations can be re-used. The user can decide to add a coupled model to the model base and re-use it in yet another coupled model. This way, a model can be structured as a tree of coupled models and atomic models from the original model base. Again a maximal level of re-usability and transfer of knowledge is obtained here.

After constructing a coupled model, the WEST parser generates MSL-EXEC from this model for use in the experimentation environment. During this process, the syntax and the semantics of the MSL-USER model are checked to detect possible coding errors. Before the MSL-EXEC code can be used for simulations and optimisations in the experimentation environment, an extra compilation step is performed. This compilation guarantees code that is optimised for simulation performance and accuracy.

Although the compilation step is especially designed to obtain efficient and fast simulation code, an extra performance increase could be obtained by implementing integration algorithms that are especially designed for the integration of stiff systems. Certainly in case steady-state simulations are done, this could increase performance after the initial simulation steps.

## **11.2 Mixed-culture biofilm modelling: a complexity compromise**

### *11.2.1 Model structure and implementation*

The model base, which was initially oriented towards activated sludge models, was complemented with a new model for the description of biofilm systems. This model is described in chapter 3. Considering the remarks stated earlier on the complexity of biofilm models, a model was developed that attempts to be a complexity compromise. As already indicated before, it is relatively simple, since

it is based on the analytical solution of the substrate profiles in the biofilm. On the other hand, the model is able to calculate the conversion rates of processes in the biofilm performed by different biomass species. The main advantage of the model is the avoidance of the numerical solution of partial differential equations. This aspect makes the proposed model an attractive alternative to the existing complex models when emphasis is put more on fast predictions of system behaviour than on detailed understanding. The avoidance of partial differential equations also has the advantage of simplifying the connection of the model to other models widely used in wastewater treatment plant simulation. This can be done within standard wastewater treatment plant simulation software like WEST without adding extra software for the integration of PDE's.

The advantages listed above are obtained by decoupling the calculation of substrate diffusion into the biofilm from the computation of the conversion processes in the biofilm by using a two-step procedure that results in a fairly simple model structure. In reality, soluble substrate from the bulk liquid is transferred inside the biofilm and then transported further by means of molecular diffusion. The substrate is simultaneously utilised in the film by the bacteria for growth. In the model, this continuous process is split up into two steps. The first step of the procedure assumes a pseudo steady-state situation with respect to the diffusion in the biofilm. This entails that a steady-state in the biofilm substrate profile is assumed at any instance in time. This is possible because the characteristic time of the biofilm diffusion phenomena and, more general, the dynamics of the soluble components in the biofilm system are about one order of magnitude smaller than the time scale of reactions in the biofilm. In such steady-state situation, analytical solutions for the penetration depth of substrates can be calculated when assuming zero-order conversion rates in the biofilm. The result of the first step is an estimate of the fraction of each biomass species that is active in the present situation. In the second step of the procedure all conversion processes within the biofilm are computed dynamically. For the calculations of the conversion processes in the second step, the concepts formulated in the activated sludge model No 1 (Henze *et al.*, 1987) are followed as closely as possible. The simplified mixed-culture biofilm model is thus also expressed in the above mentioned Petersen matrix format. This obviously facilitates its implementation and the coupling of the model to well-accepted models for other unit processes in wastewater treatment.

In addition, two extended model descriptions were presented that can easily be implemented along with the original one. One of the assumptions of the original model states that soluble components that emerge from conversion processes inside the film are assumed to be subject of immediate out-diffusion at the surface of the biofilm. This assumption neglects the possible effect of the accumulation of soluble species inside the biofilm. The assumption already treated above states that an instantaneous steady-state profile is assumed. Together, these assumptions are in principle violating the mass balances during dynamic simulation. The first extension of the model accounts for the possible accumulation of soluble components in the biofilm and it thus guarantees a correct determination of the penetration depths. Also, the introduction of an external diffusional resistance was studied. Although considered not important in biofilm systems with a relatively turbulent liquid phase, it should be included in some cases where this resistance may be of great importance for the correctness of the model predictions. The implementation of the diffusional resistance did not substantially complicate the model as only the calculation of the penetration depths had to be adapted.

### *11.2.2 Recommendations for further model developments and calibration techniques*

During the research, some weaknesses of the model were identified. First of all, one should be careful when applying the model in situations where the substrate concentrations are low. As was shown in chapter 6, the model could successfully describe the concentration dynamics in the effluent of the pilot-scale filter. However, one should always be aware of the fact that at least in a part of this system, the use of zero-order kinetics might not be a reasonable assumption. In these cases, other reaction rates could be used as long as they give rise to analytical solutions for the substrate penetration depth, as this is inherent to the decoupling of diffusion and biokinetic reaction in this modelling approach. For example, when a first order reaction rate is used, the analytical calculation of the exact penetration depth becomes quite difficult, since the calculated concentration profiles only asymptotically approach zero when substrate is depleted in the biofilm. Therefore, rather than stating that the substrate conversion stops when substrate is completely depleted, a limiting non-zero substrate concentration should be chosen in order to model the competition between different processes in the biofilm. It should be noted here that even without the possibility of yielding analytical solutions, the decoupling of substrate diffusion and conversion can also be accomplished for Monod-type kinetics. However, the resulting PDE is then to be solved using shooting or finite element methods (Wik, 1999) significantly reducing the gain in calculation speed.

In short, the use of other reaction kinetics in the model would have complicated the model description and increased the computational effort. Moreover, it should be noted that in pilot-scale or full-scale reactors, the exact quantification of the order of reaction is not possible using the available measurement techniques, since substrate profiles in the biofilm and in the reactor are extremely hard to monitor. Therefore, such model changes were not studied in this thesis. However, as computational power increases every day, a modelling approach using Monod-kinetics might become feasible for use in process optimisation. The effort to obtain fast solvers for the resulting PDE's should therefore be continued and encouraged. For example, the WEST simulator has recently been extended with a solver for partial differential equations. WEST-PDE automatically discretises PDE models to models containing a restricted set of ordinary differential equations in so-called collocation points. Using such a solver, the homogeneous species distribution that is now an assumption of the model can be omitted. However, this would however again induce more complexity in the model description and it is therefore important to weigh the pros and cons of this extra complexity against each other before taking further development steps. Indeed, even using a homogeneous species distribution, in chapter 6 the competition between heterotrophic and autotrophic bacteria was successfully modelled and in chapter 7 a very good result was obtained describing the competition between aerobic and anoxic growth. Therefore, for the case studies in this thesis, no reason was seen for a substantial increase of the model complexity.

Still, care should be taken when using simplified models for process optimisation or even control purposes since over-simplified model structures and erroneous parameter values can be quite dangerous. First of all, when the model structure is not representative for the processes that govern the system dynamics in reality, parameter estimation algorithms or even manual trial-and-error calibration may come up with wrong parameter values. Also, in most cases where biological systems are modelled using mechanistic models, the majority of the parameter values are not identifiable

(Petersen, 2000). Already when using models for off-line optimisation, a lot of the effort must be devoted to the collection of experimental data and performing the calibration so as to obtain a reasonable parameter set. For these reasons, and maybe more than adding extra complexity to the model, substantial work should be done in the development of better calibration methods for biofilm models based on the relatively scarce measurements that are available. Only in the case where the model parameters can be regularly updated to detect and follow parameter changes as a result of process changes, on-line use of models in control will become possible.

## 11.3 Model applications in a pilot-scale trickling filter

### 11.3.1 Construction of the pilot-scale trickling filter

In order to test the model described above, a pilot-scale trickling filter was developed. The filter was constructed to allow the collection of experimental data on a fully characterised biofilm system.

The design of the unit allowed for the full characterisation of operational parameters and non-invasive on-line monitoring of the system was possible by means of an electronic balance and off-gas analysis measurement equipment that continuously monitored the off-gas of the filter for CO<sub>2</sub> and O<sub>2</sub>. The filter unit's dimensions were chosen to represent a cylindrical core taken from a full-scale unit. A plastic carrier medium (polypropylene) was chosen. The selected medium had a specific surface area of 220 m<sup>2</sup>/m<sup>3</sup>. Using the balance, an estimate of the total amount of biofilm in the filter and its thickness could be obtained. This information was used to follow the growth of the biofilm based on the substrate loading.

To characterise the filter's hydrodynamic behaviour, two tracer tests were conducted without and with biofilm. NaCl and Thioflavine-S were used as inert tracers. The hydraulic behaviour of the filter without biofilm could be described using an advection-dispersion model. If a biofilm was present, however, a CSBR (continuously stirred biofilm reactor) approach (Wik and Breitholtz, 1996) was found necessary to yield an optimal description of the hydraulics. In this approach each CSBR consists of a CSTR connected to a biofilm compartment by a diffusive link permitting diffusion of the tracer in and out of the biofilm compartment. For a good description of the pilot-scale filter, 7 CSBR's in series were needed. The volumes of the biofilm compartments of the CSBR's agreed well with the total biofilm mass recorded using the electronic balance.

Preliminary COD removal experiments showed that – although a high variability was noticed – the COD removal efficiency corresponded well with what could be expected for a filter with these dimensions and loading. Off-gas measurements showed that monitoring of the degree of nitrification in the filter was possible when operated at a lower influent loading rate.

The variability of the preliminary COD measurements during the start-up period was also caused by the high maintenance requirements of the filter, its high influent and effluent flows and its dimensions. When using such filter set-up in the future, some recommendations for a better design should be taken into account. The main recommendation, apart from optimising the influent distribution system and the gas collection, would be the use of a cross-flow carrier material instead of the random packing carrier material used in this study. Using this type of material, the chance to

suffer from shortcut flow in the reactor would be reduced, making the rings used for that purpose in the current filter unnecessary. This carrier material would make estimates of the wetted surface area in the filter easier and would therefore enable a more precise biomass thickness calculation. On the other hand, taking undisturbed biofilm samples from the reactor would no longer be possible in such a set-up.

### 11.3.2 *Modelling a load shift*

The pilot-scale trickling filter was used to investigate the dynamic model description of such a filter's behaviour. With this in mind, the filter was subjected to a load shift during a measurement campaign. During this campaign, analysis for the COD and nitrogen content of the water phase at different locations in the filter set-up were done. Also, the off-gas composition was analysed for oxygen and carbon dioxide. To be able to use the measurements, extra analyses of the inorganic carbon content of the liquid phase were needed as well as measurements of the *pH* in the filter.

The simplified mixed-culture biofilm model developed in this study was used to model the load shift. In order to respect the mass balances, the extended model based on the total masses of soluble components in the system was implemented. This model was further extended with a part for the description of the production and gas-liquid exchange of carbon dioxide based on the model developed by Spérandio and Paul (1997) and was subsequently integrated in the CSBR model describing the hydrodynamic behaviour of the filter. The initial approach to use the measured CODs/CODt relationship for the subdivision of the COD into the soluble and particulate model components did not produce good simulation results. From respiration tests with the synthetic wastewater from which the influent composition of the pilot scale trickling filter was derived, it was estimated that more than 50% of the total COD of the medium could be considered readily biodegradable (Boeije, 1999). Therefore, the  $S_s/\text{COD}_t$  was increased based on the hypothesis of bulk liquid hydrolysis in the filter.

The hydrolysis and biodegradation of particulate matter in biofilm systems is still a topic of vigorous discussion and should certainly be investigated further. Up to now, no model has been able to provide a mechanistic formulation of the attachment and hydrolysis of particulates in different biofilm process configurations. The model used here is not satisfactory either. Attachment and hydrolysis are modelled as first-order processes relative to the concentration of the particulates in the bulk liquid and in the biofilm respectively. Since even the molecular weight of starch is too high for this component to diffuse into the biofilm (Henze *et al.*, 1995), the study of the bacterial release of extracellular enzymes and the exact mechanism and place of the degradation of particulates deserves further investigation.

During the experiment, it could further be concluded that, following a drop in the loading of the filter system, the nitrification capacity increased due to a higher availability of oxygen for this process. The off-gas analysis measurements supplied extra information to calibrate the gas-liquid mass transfer coefficient. On top of that, the combined interpretation of the carbon dioxide and the inorganic carbon measurements together with the model calculations made it possible to find a leak in the off-gas collection system. After repairing this leak, it became clear that the model predictions were an accurate description of the filter's behaviour after the load shift. The start-up of nitrification could be followed using the model provided the decay coefficient for autotrophic biomass was sufficiently low

to assure a certain amount of autotrophs to stay in the system during the applied high loading conditions. The hypothesis that nitrifying biomass could survive prolonged periods with high loading in a trickling filter was confirmed with batch tests performed on carrier elements taken out of the filter.

A further investigation of the decay of autotrophic bacteria in biofilms should be performed. A “dormant” state of micro-organisms in starvation conditions has been reported in literature (Stevenson, 1978; Amy *et al.*, 1983) so that bacteria can successfully survive prolonged periods of starvation. Moreover, the survival and relatively fast re-activation of autotrophic bacteria in biofilm was also monitored by Wik (1999). Further research should be done to show if and to what extent this process is taking place in biofilms.

### 11.3.3 Nitrate addition to a highly loaded trickling filter system

Aerobic degradation in a trickling filter is mainly limited by the amount of oxygen that is transferred to the biofilm. It has been stated that the maximal oxygen uptake of biofilms is about  $10 \text{ g O}_2 \text{ m}^{-2}\text{d}^{-1}$  (see among others: Logan, 1993; Hinton and Stensel, 1994). This oxygen can be used for aerobic degradation of organic matter, and, if any is left after this conversion process, nitrification can proceed. A second pathway for the removal of organic matter is denitrification in anoxic zones of the biofilm. At high organic loading rates, providing the biofilm with an extra portion of electron acceptor could induce denitrification. This was tested, monitored and modelled in the pilot-scale trickling filter by adding a pulse of nitrate at high loading rate.

To facilitate the interpretation of the test results, ethanol was used as the sole carbon source in the influent. Also, the majority of inorganic carbon in the influent was stripped and *pH* control was implemented in the filter set-up. The test showed that denitrification could be induced by adding nitrate at high loading conditions and that this way a considerably increased substrate removal capacity could be obtained. The effluent COD concentration increased quite drastically after increasing the influent load to the filter. Also the production of  $\text{CO}_2$  from bioconversion processes increased, while no decrease of the  $\text{O}_2$  consumption was noticed. After adding the extra nitrate the effluent COD dropped, indicating the extra conversion capacity. Using the model, estimates of the extra capacity of the filter were made.  $54.3 \text{ g COD/d}$  were removed via the denitrification pathway on top of the  $206.1 \text{ g COD/d}$  removed via aerobic degradation. For this extra COD removal capacity,  $22.0 \text{ g NO}_3^- \text{-N/d}$  was used. Further investigations should focus on the feasibility of this operating strategy. First of all, for full-scale application, a measurement should be available to indicate whether the treatment process operates in an oxygen limited regime. To this end, an off-gas sensor could be used. In case the degradation process is found to be oxygen limited, the dosing of nitrate could then be started. In order to further regulate the amount of nitrate to be dosed, feed back control strategies based on the effluent load or the effluent nitrate concentration of the process could be used. Finally, the economic feasibility should be further studied based on the availability of a cheap nitrate source and a local analysis of the fines to be paid for the discharge of COD.

For the modelling of this experiment, the same model was used as for the modelling of the load shift. Only the effective diffusion constant of the biodegradable substrate in the biofilm had to be adjusted in order to obtain a good description of the measured results. It should however be noted that this

parameter was not identifiable from the previous experiments. The value found in this nitrate addition experiment should thus be considered to be more correct than the one initially used.

## 11.4 Modelling a full-scale industrial trickling filter system

At a wastewater treatment plant (WWTP) in Belgium, a project has been performed during the last years to demonstrate the application of on-line monitoring, modelling and process control in an industrial wastewater treatment (De Clercq *et al.*, 1999a; De Clercq *et al.*, 1999b; ; Devisscher *et al.*, 2000; Debusscher *et al.*, 2001; Demey *et al.*, 2001). In this part of the thesis, the modelling of the trickling filter process at this plant is described. Both its performance in terms of COD removal and the stripping of volatile organic compounds were studied.

### 11.4.1 Modelling COD removal

The process characteristics of the filters were quantified by means of a 5-day intensive measurement campaign with the use of an on-line respirometer complemented with on-line off-gas analysis. Using the respirometer, COD<sub>st</sub> measurements were conducted at the inflow and the outflow of the filters and the off-gas sensor was used to monitor the O<sub>2</sub> and CO<sub>2</sub> content of the off-gasses. To model the biodegradation in the filters, the simplified mixed-culture biofilm model introduced before was used. Again, the model was extended with equations for the production and the *pH*-dependent gas-liquid equilibrium for inorganic carbon (IC).

As in the pilot-scale trickling filter, the hydraulic behaviour of the trickling filter system was modelled based on the results of a tracer test (De Clercq *et al.*, 1999a). This test showed that the water phase in the filter could be modelled using two CSTR's in series. The gas mixing in the trickling filters was investigated by lowering the air flow through the filters halfway through the measurement campaign.

The calibrated model could follow the measured effluent and off-gas concentrations very closely. Other than was expected initially, the O<sub>2</sub> and CO<sub>2</sub> measurements revealed that the system was not always oxygen limited. In the model calibration the use of a very low value of the diffusion constant for readily biodegradable substrate was found to be the best means for describing the observed data. Alternative modelling approaches such as liquid film biodegradation and anaerobic degradation within the biofilm were investigated, but these could not account for sufficient COD removal to change the conclusions above.

As only a very limited amount of phosphate is available in the influent, the effect of the dosing of phosphate on the trickling filter system was studied. It could be noticed that the net phosphate uptake by the biofilm is very limited under normal operating conditions, since the phosphate dosing did not bring along better treatment efficiency. Apparently, phosphate can be recycled inside a full-grown biofilm, so the net phosphate demand is rather small. However, shortly after the start of the dosing, a clear effect on the off-gas measurements and the sludge production was noticed. This effect damped out in some days time and could only be modelled by temporarily increasing the yield coefficient for heterotrophic growth, making the oxygen consumption to decrease and the sludge production to increase.

Obviously, more research should be directed towards the nutrient dynamics in biofilm systems. It became clear from this study that the removal efficiency of a biofilm system does not necessarily drop significantly when a nutrient is only available in limited amounts in the system's influent. It is known that sulphur can be kept inside the biofilm in a cycle of sulphite oxidation and sulphate reduction (Lens *et al.*, 1995b). Probably nitrogen and phosphorus components too can be kept in the biofilm and be "recycled" after release from biomass decay. It has also been monitored before that the EPS fraction of biofilms seems to increase when phosphorus is limiting (Mohammed *et al.*, 1998). Since EPS is reported to be capable of adsorbing nutrients like amino acids and sugars (Flemming, 1995), such mechanism could possibly explain the good performance of this system under nutrient limitation. However, more investigation towards nutrient recycling in biofilm systems is necessary to be able to conclude if the temporary increase of the yield coefficient in the model is a good representation of reality or if the model structure is inadequate to simulate the real phenomena in the biofilm during this period.

#### 11.4.2 Modelling stripping of volatile organic compounds

Next to high COD and nitrogen concentrations, a considerable part of the chemicals in industrial wastewater is often highly volatile (*e.g.* solvents). The environmental impact of VOC's is high and since aeration is a basic process in aerobic biological treatment, there is a big risk for stripping of these volatile organic contaminants (VOC's) together with the air used for aeration (Melcer *et al.*, 1995). In trickling filters, stripping is likely to be the most important removal mechanism of volatile components, as VOC biodegradation is known to be low in systems with short retention times (Dobbs *et al.*, 1989).

In this part of the thesis, the VOC removal in the industrial wastewater treatment plant was monitored and modelled. The influent was highly loaded with volatile components. Therefore, environmental legislation enforced the construction of an off-gas treatment facility for the trickling filter system. The capital and operating cost and the efficiency of such facility are dependent on the air flow to be treated and the concentration of VOC's. A high removal efficiency of the most volatile components, typically chlorinated compounds in this case, in the trickling filter process was desired. This way, the washing out of volatile compounds to the activated sludge system, where they could strip into open air and hamper the biomass activity, could be prevented.

Two mathematical models describing the stripping of VOC's were developed. The first model used, was a model for the fate of individual chemicals that was built using the *SimpleBox* approach (van der Meent, 1993) combined with the existing steady-state biofilm diffusion/biodegradation model of Melcer *et al.* (1995). This new approach for chemical fate modelling in trickling filters was published in Boeije *et al.* (2000), where it was tested using experimental results for the surfactant LAS (Linear Alkylbenzene Sulfonate), which were obtained in the pilot-scale trickling filter described earlier in this thesis. The second model was a simple dynamic mass balance model, built on the basis of the results obtained with the steady-state model combined with the tracer test mentioned in paragraph 11.4.1.

Simulations with the non-equilibrium steady-state model showed that biodegradation as well as adsorption to suspended solids could be neglected for the volatile organics under study. Furthermore, based on the results of the tracer test, the hydrodynamic description of the original model (five layers

in the trickling filter) could be simplified down to a two-layer model. Scenario analysis with the simplified dynamic model built on the basis of these findings showed that stripping was virtually independent of the applied air flow rate. At high air flow, the total stripping efficiency only increased with a few percentages, resulting in a lower gas phase VOC concentration. In contrast to the steady state analyses, dynamic simulation revealed that immediately after changes in air flow rate, quite high flux and concentration peaks were to be expected. These peaks were of importance for the design of the off-gas treatment facility.

Using the findings of this research, the air flow through the trickling filters was lowered. On the one hand, as investigated during the modelling of the COD dynamics, the oxygen concentration in the off-gas was not significantly lower as compared to the high-flow case. An effect on the biodegradation was thus not to be expected. On the other hand, higher VOC concentrations and a lower off-gas flow rate were beneficial for the investment cost and the efficiency of the off-gas treatment facility. Furthermore, a fluctuating off-gas flow rate was avoided by blowing relatively clean off-gas from the sludge treatment unit into the trickling filters instead of transporting it directly to the off-gas treatment facility. Only the off-gas from the trickling filters is then treated in this facility so that a constant air flow and a relatively constant VOC concentration can be obtained.

This work showed that a simple model is in some case sufficient to obtain the necessary information so as to optimise the full-scale application of a process. On the other hand, the biodegradation and gas-liquid exchange mechanisms of volatile organics in filter systems are still subject to quite some fundamental research in the field of off-gas treatment by biofilter systems. In those cases, not the stripping of volatile organics is of importance, but rather the exchange of volatile chemicals from the gas phase to the liquid phase and their subsequent biodegradation in a biofilm. There, more complicated modelling approaches may be helpful to obtain the necessary insight in the process and its behaviour under changing process conditions.

## **11.5 Simulation of suspended-carrier biofilm systems**

As a last part of this thesis, suspended-carrier biofilm systems were studied. Qualitative steady-state analysis of this system already showed its interesting features (Yuan *et al.*, 2001). (i) More bacteria are maintained in the system, at high solids densities in the biofilm, (ii) both nitrifiers and denitrifiers are only present in the zones of the reactor where they are needed and (iii) in such a systems, most of the COD is kept in the biofilm. The COD leakage in the form of sludge flocs and cell COD is decreased. This leads to a better availability of influent COD to the denitrifiers.

In this chapter, the attached growth system described above was evaluated using dynamic simulations. The advantages of the system were validated quantitatively based on a simulation benchmark for activated sludge treatment systems (Spanjers *et al.*, 1998; Copp, 2001). To this end, this simulation benchmark was extended with the biofilm model introduced in this thesis. The Activated Sludge Model No 1 (Henze *et al.*, 1987) was coupled to a simplified mixed-culture biofilm model. This coupling was only possible since the layout of the biofilm model avoids having to solve partial differential equations and because of the similar matrix-representations of both models.

Two types of attached growth processes were studied. In the first, carriers were only added to the aerobic zone of the plant in order to enhance nitrification in a relatively small volume and at low sludge retention times. It was noticed that the longer retention time of the biomass growing on the carriers stimulated nitrification. However, a rather strong dependency of the performance on the dissolved oxygen concentration was obvious, causing the required aeration energy to increase significantly. The effluent quality that was achieved was worse than that of the benchmark plant. It was mainly the relatively high reflux of oxygen to the anoxic zone that limited full nitrogen removal. Also, extra carrier surface area should be available for more nitrifiers to grow in the system. However, this would undo the volume saving that is seen as a major advantage of the suspended carrier plant layout. This plant layout is therefore only considered useful when external factors limit nitrification in an activated sludge treatment plant such as a limited suspended sludge concentration due to a small settler.

The second plant layout studied included the addition of carriers to all zones of the plant. The main goal of this system is to physically separate the heterotrophic and autotrophic biomass. The simulation results showed that the retention times of heterotrophs and autotrophs were different and that autotrophs were mainly present in the zones of the plant where they were needed. Another advantage of the system that was qualitatively derived by Yuan *et al.* (2001) could also be confirmed and quantified using simulation. The leakage of readily biodegradable material from the anoxic zone to the aerobic zone of the plant was limited in the suspended carrier system. This entails that full nitrogen removal can be accomplished at lower C/N ratios in the influent. However, such plant layout is even more sensitive to the dissolved oxygen concentration in the aerobic zone. Therefore, oxygen control needs to be rather stringent and enough blower capacity should be available to preserve a sufficiently high oxygen concentration at high loading rates. If the DO concentration suddenly drops, nitrogen removal can be lost and can take up to several days to fully recover. This long recovery period is caused by the leaking of substrate from the anoxic phase to the aerobic phase when no nitrate is available for denitrification. Not only is the substrate only partly degraded there but, more importantly, it hampers the start-up of nitrification.

However, when an attached growth system is operated well, an excellent effluent quality can be obtained. Moreover, control can certainly show its value in such a system. A possible control strategy could be to regulate the aeration based on the ammonia concentration or the respiration rate in the aerobic zones of the plant. For example, in case the ammonia concentration would increase, a higher dissolved oxygen set point could be used to preserve nitrification in the aerobic zone and thus to safeguard nitrogen removal. Eventually, the performance of this control scheme could be augmented by incorporating feed forward control based on the influent loading of the plant. Another strategy could be to include aeration devices in the anoxic zone, so that nitrogen removal could recover much faster after a calamity.

It should be noted here that these conclusions were based on a simulation study only and should be interpreted with care. The conclusions drawn here should rather be seen as a good indication of the problems that could be encountered during operation. Research should certainly be devoted to the experimental validation of these results.

## 11.6 General conclusions

In this thesis, a biofilm model was developed and implemented that attempts to be a complexity compromise. In modelling biofilm processes, a compromise should be sought between the complexity needed to describe the dynamics of the process, the data available for calibration and the application the model is used for. The model presented is relatively simple, since it is based on the analytical solution of the substrate profiles in the biofilm. On the other hand, the model is able to calculate the conversion rates of processes in the biofilm performed by different biomass species. Despite its simplifications, it can thus be used to describe processes occurring at different depths of the biofilm.

The second part of this thesis was devoted to applications of the model in different situations. The calibration of the model was done using data obtained from pilot-scale and full-scale measurement campaigns. In the last chapter, a simulation study was conducted to investigate the operation of suspended carrier biofilm systems.

Although the model is rather simple, it still includes quite some conversion processes and a considerable set of parameters needs to be calibrated. A good dataset is indispensable for a successful calibration. To gather these data on pilot-scale and certainly on full-scale systems is quite a tedious task. Moreover, performing lab experiments to obtain estimates of individual parameters values is not always possible with biofilm systems. It was therefore decided to focus on a measurement technique that has up to now not been used in an extensive manner for model calibration in wastewater treatment. Off-gas analysis for oxygen and carbon dioxide can, together with classical analysis for COD and nitrogen compounds, deliver a dataset that is 'rich' enough for a good model calibration. In this thesis, these measurements were on occasion complemented with on-line measurements of total organic carbon (TOC) and respirometry.

Using this set of data, the model was calibrated such that it gave a reasonable description of the dynamics of the plants under study and that it could be used for further model applications like off-line process optimisation.

Chapter 9 digressed onto the optimisation of the design of an off-gas treatment facility for a full-scale trickling filter. Here, starting from a steady-state non-equilibrium model, a simple dynamic model was built that substantially contributed to the optimised design of the off-gas treatment.

As a last application, the simplified mixed-culture biofilm model was further used in a simulation study investigating suspended carrier biofilm systems. Although not supported with measurements, data from literature was found sufficient to obtain a realistic description of the dynamic behaviour of such systems and some vulnerabilities not reported in literature could be identified. It should be noted that no simulation studies could be found in literature describing the simultaneous degradation of organic matter in a biofilm and in the liquid phase in suspended carrier systems. This study can therefore be considered as the first application of such integrated modelling and simulation approach.

# References

---

- Alex, J., Beteau, J.F., Hellinga, C., Jeppsson, U., Marsili-Libelli, S., Pons, M.N., Spanjers, H. and Vanhooren, H. (1999) Benchmark for evaluating control strategies in wastewater treatment plants. In: *Proceedings ECC99*, Karlsruhe, Germany, August 31-September 3 1999.
- Amy, P.S., Pauling C. and Morita R.Y. (1983) Starvation-survival processes of a marine vibrio. *Appl. Environ. Microbiol.*, **45**, 1041-1048.
- Aravinthan, V., Takizawa, S., Fujita, K. and Komatsu, K. (1998) Factors affecting nitrogen removal from domestic wastewater using immobilized bacteria. *Wat. Sci. Tech.*, **38**(1), 193-202.
- Atkinson, B. and Davies, I.J. (1974) The overall reaction rate of substrate uptake by microbial films. Part I. A biological rate equation. *Trans. Inst. Chem. Eng.*, **52**, 248-259.
- ATV (1985) *Lehr- und handbuch der abwassertechnik, Bd. IV*. Ernst & Sohn.
- ATV (1989) *Standard ATV - A135E. Principles for the dimensioning of biological filters and biological contactors with connection values over 500 population equivalents*. Gesellschaft zur Förderung der Abwassertechnik e.V. (GFA), Hennef.
- Bird, R.B., Stewart, W.E. and Lightfoot, E.N. (1960) *Transport phenomena*. Wiley, New York.
- Bishop, P.L. (1997) Biofilm structure and kinetics. *Wat. Sci. Tech.*, **36**(1), 287-294.
- Bishop, P.L. and Kinner, N.E. (1986) Aerobic fixed-film processes. In: *Biotechnology: Microbial Degradations*, Vol. 8 (Ed: Schonborn, W.) VCH, Weinheim, pp. 113-176.
- Bishop, P.L., Zhang, T.C. and Fu, Y.C. (1995) Effects of biofilm structure, microbial distributions and mass transport on biodegradation processes. *Wat. Sci. Tech.*, **30**(1), 143-152.
- Boeije, G., Vanhooren, H. and Vanrolleghem, P.A. (2000) Development of a steady-state chemical fate model for trickling filters supported by measurements in a pilot-scale plant. *Environ. Sci. Technol.*, **34**, 4413-4417.
- Boeije, G.M. (1999) *Chemical fate prediction for use in geo-referenced environmental exposure assessment*. PhD Thesis, Faculty of Agricultural and Applied Biological Sciences, Ghent University, Ghent.
- Boeije, G.M., Corstanje, R., Rottiers, A. and Schowanek, D.R. (1998) Adaptation of the CAS test system and synthetic sewage for biological nutrient removal. Part I: Development of a new synthetic sewage. *Chemosphere*, **38**, 699-709.
- Bonarius, H.P.J., de Gooijer, C.D., Tramper, J. and Schmid, G. (1995) Determination of the respiration quotient in mammalian cell culture in bicarbonate buffered media. *Biotechnol. Bioeng.*, **45**, 524-535.
- Broenink, J.F. (1990) *Computer aided physical modeling and simulation: a bond graph approach*. PhD Thesis, University of Twente, Enschede, The Netherlands.
- Bryers, J.D. (1988) Modeling biofilm accumulation. In: *Physiological models in microbiology*, (Eds: Bazin, M. J. and Prosser, J. I.) FL: CRC, Boca Raton.
- Cao, Y.S. and Alaerts, G.J. (1995) Influence of reactor type and shear stress on aerobic biofilm morphology, population and kinetics. *Wat. Res.*, **29**, 107-118.
- Chang, H.T. and Rittmann, B. (1988) Comparative study of biofilm shear loss on different adsorptive media. *J. Water Pollut. Control Fed.*, **60**, 362-368.

- Characklis, W.G. and Marshall, K.C. (1990) *Biofilms*. Wiley, New York.
- Christiansen, P., Hollesen, L. and Harremoës, P. (1995) Liquid film diffusion on reaction rate in submerged biofilters. *Wat. Res.*, **29**, 947-952.
- Colasanti, R. (1992) Cellular automata models of microbial colonies. *Binary Computing and Microbiology*, **4**, 191.
- Cooney, M.J. and McDonalds, K.A. (1995) Optimal dynamic experiments for bioreactor model discrimination. *Appl. Microbiol. Biotechnol.*, **43**, 826-837.
- Copp, J.B. (2001) *The COST Simulation Benchmark: Description and Simulator Manual*. Office for Official Publications of the European Community, Luxembourg.
- Cox, H.H.J. and Deshusses, M.A. (1999) Chemical removal of biomass from waste air biotrickling filters: screening of chemicals of potential interest. *Wat. Res.*, **33**, 2383-2391.
- Cullen, A.C. and Frey, H.C. (1999) *Probabilistic techniques in exposure assessment. A handbook for dealing with variability and uncertainty in models and inputs*. Plenum, New York.
- de Beer, D. and Schramm, A. (1999) Micro-environments and mass transfer phenomena in biofilms studied with microsensors. *Wat. Sci. Tech.*, **39**, 173-178.
- de Beer, D., Schramm, A., Santegoeds, C.M. and Kuhl, M. (1997) A nitrite microsensor for profiling environmental biofilms. *Appl. Env. Microbiol.*, **63**, 973-977.
- de Beer, D. and Stoodley, P. (1995) Relation between the structure of an aerobic biofilm and transport phenomena. *Wat. Sci. Tech.*, **32**(8), 11-18.
- de Beer, D., Stoodley, P. and Lewandowski, Z. (1994) Liquid flow in heterogeneous biofilms. *Biotechnol. Bioeng.*, **44**, 636-641.
- De Clercq, B., Coen, F., Vanderhaegen, B. and Vanrolleghem, P.A. (1999a) Calibrating simple models for mixing and flow propagation in waste water treatment plants. *Wat. Sci. Tech.*, **19**, 61-69.
- De Clercq, B., Vanderhasselt, A., Vanderhaegen, B., Hopkins, L.N. and Vanrolleghem, P.A. (1999b) A model-based evaluation of control strategies for a clarifier at an industrial wastewater treatment plant. In: *Proceedings 8th IAWQ Conference on Design, Operation and Economics of Large Wastewater Treatment Plants*, Budapest, Hungary, September 6-9 1999.
- De heyder, B., Vanrolleghem, P.A., Van Langenhove, H. and Verstraete, W. (1997) Kinetic characterisation of microbial degradation of low water soluble gaseous compounds in batch experiments under mass transfer limited conditions. *Biotechnol. Bioeng.*, **55**, 511-519.
- Debusscher, D., Hopkins, L.N., Demey, D. and Vanrolleghem, P.A. (2000) Determining the potential benefits of controlling an industrial wastewater treatment plant. *Wat. Sci. Tech.* (in Press).
- Demey, D., Vanderhaegen, B., Liessens, J., Van Eyck, L. and Vanrolleghem, P.A. (2000) alidation and implementation of model based control strategies at an industrial wastewater treatment plant. *Wat. Sci. Tech.* (in Press).
- Devisscher, M., Harmand, J., Steyer, J.-P. and Vanrolleghem, P.A. (2000) Control design of an industrial equalization system - Handling system constraints, actuator faults and varying operating conditions. In: *Proceedings IFAC 4th Symposium on Fault Detection, Supervision and Safety for Technical Processes (SafeProcess2000)*, Budapest, Hungary, June 14-16 2000.
- Dobbs, R.A., Wang, L. and Govind, R. (1989) Sorption of toxic organic compounds on wastewater solids: correlation with fundamental properties. *Environ. Sci. Technol.*, **23**, 1092-1097.
- Dochain D. and Vanrolleghem P.A. (2001) *Modelling and Estimation in Wastewater Treatment Processes*. IWA Publishing, , London, UK. ISBN 1-900222-50-7 (in Press).

- Dold, P.L., Ekama, G.A. and Marais, G. (1980) A general model for the activated sludge process. *Prog. Wat. Technol.*, **12**, 47-77.
- Ellis, T.G., Barbeau, D.S., Smets, B.F. and Grady Jr, C.P.L. (1996) Respirometric technique for determination of extant kinetic parameters describing biodegradation. *Wat. Env. Res.*, **68**, 917-926.
- Flemming, H.-C. (1995) Sorption sites in biofilms. *Wat. Sci. Tech.*, **32**(8), 27-33.
- Fu, Y.C., Zhang, T.C. and Bishop, P.L. (1994) Determination of effective oxygen diffusivity in biofilms grown in a completely mixed biodrum reactor. *Wat. Sci. Tech.*, **29**(10-11), 455-462.
- Gantzer, C.J., Cunningham, A.B., Gujer, W., Gutekunst, B., Heijnen, J.J., Lightfoot, E.N., Odham, G., Rittmann, B.E., Rosenberg, E., Stolzenbach, K.D. and Zehnder, A.J.B. (1989) Exchange processes at the fluid-biofilm interface. In: *Structure and function of biofilms*, (Eds: Characklis, W. G. and Wilderer, P. A.) Wiley, New York.
- Gillot, S., De Clercq, B., Defour, D., Simoens, F., Gernaey, K. and Vanrolleghem, P.A. (1999) Optimisation of wastewater treatment plant design and operation using simulation and cost analysis. In: *Proceedings 72nd WEF Conference*, New Orleans, USA, October 9-13 1999.
- Gjaltema, A. (1996) *Biofilm development: growth versus detachment*. PhD Thesis, Delft University of Technology, Delft.
- Govind, R., Gao, C., Lai, L. and Tabak, H.H. (1997) Continuous, automated and simultaneous measurement of oxygen uptake and carbon dioxide evolution in biological systems. *Wat. Env. Res.*, **69**, 73-80.
- Grady Jr, C.P.L. and Lim, H. (1980) *Biological wastewater treatment. Theory and applications*. Marcel Dekker, New York.
- Grady Jr, C.P.L., Smets, B.F. and Barbeau, D.S. (1996) Variability in kinetic parameter estimates: a review of possible causes and a proposed terminology. *Wat. Res.*, **30**, 742-748.
- Grau, P., Sutton, P.M., Henze, M., Elmaleh, S., Grady, C.P., Gujer, W. and Koller, J. (1982) Recommended notation for use in the description of biological wastewater treatment processes. *Wat. Res.*, **16**, 1501-1505.
- Grijpspeerdt, K., Bogaert, H. and Verstraete, W. (1996) Design and verification of a model secondary clarifier for activated sludge. *J. Chem. Technol. Biotech.*, **67**, 404-412.
- Guyot, W., Henze, M., Mino, T. and van Loosdrecht M.C.M. (1999) Activated sludge model No. 3. *Wat. Sci. Tech.*, **39**(1), 183-193.
- Haemelinck, S. (2000) *Evaluatie van sturingsalgoritmen voor de verwijdering van stikstof uit afvalwater*. MSc Thesis, Faculty of Agricultural and Applied Biological Sciences, Ghent University, Ghent.
- Harmand, J., Steyer, J.P., Devisscher, M. and Vanrolleghem, P.A. (1999) Fuzzy supervisory control of an industrial waste water equalization system. In: *Proceedings 3rd World Multiconference on Systemics, Cybernetics and Informatics, 5th International Conference on Information Systems Analysis and Synthesis (SCI99/ISAS'99)*, Orlando, Florida, USA, July 31-August 4 1999.
- Harremoës, P. (1976) The significance of pore diffusion to filter denitrification. *J. Water Pollut. Control Fed.*, **48**, 377-388.
- Harremoës, P. (1978) Biofilm Kinetics. In: *Water Pollution Microbiology*, Vol. 2 (Ed: Michell) Wiley, New York, pp. 71-109.

- Hellinga, C., Vanrolleghem, P.A., van Loosdrecht, M.C.M. and Heijnen, J.J. (1996) The potentials of off-gas analysis for monitoring and control of waste water treatment plants. *Wat. Sci. Tech.*, **33**(1), 13-23.
- Hem, L.J., Rusten, B. and Ødegaard, H. (1994) Nitrification in a moving bed biofilm reactor. *Wat. Res.*, **28**, 1425-1433.
- Henze, M., Grady Jr, C.P.L., Gujer, W., Marais, G. and Matsuo, T. (1987) *Activated sludge model No. 1. Scientific and Technical Report No. 1*. IAWQ, London.
- Henze, M., Gujer, W., Mino, T. and van Loosdrecht, M.C.M. (2000) *Activated Sludge Models ASM1, ASM2, ASM2d and ASM3*. Scientific and Technical Report No. 9., IWA Publishing, London, UK.
- Henze, M., Harremoës, P., La cour Jansen, J. and Arvin, E. (1995) *Wastewater treatment. Biological and chemical processes*. Springer-Verlag, Berlin.
- Hermanowicz, S.W. (1998) A model of two-dimensional biofilm morphology. *Wat. Sci. Tech.*, **37**(4-5), 219-222.
- Hermanowicz, S.W., Schindler, U. and Wilderer, P.A. (1995) Fractal structure of biofilms: new tools for investigation of morphology. *Wat. Sci. Tech.*, **32**(8), 99-105.
- Hinton, S.W. and Stensel, H.D. (1994) Oxygen utilization of trickling filter biofilms. *J. Environ. Eng.*, **120**, 1284-1297.
- Horn, H. and Hempel, D.C. (1995) Mass transfer coefficients for an autotrophic and a heterotrophic biofilm system. *Wat. Sci. Tech.*, **32**(8), 199-204.
- Horn, H. and Hempel, D.C. (1997a) Growth and decay in an auto/heterotrophic biofilm. *Wat. Res.*, **31**, 2243-2252.
- Horn, H. and Hempel, D.C. (1997b) Substrate utilization and mass transfer in an autotrophic biofilm system: experimental results and numerical simulation. *Biotechnol. Bioeng.*, **53**, 363-371.
- Horn, H. and Telgmann, U. (1999) Simulation of tertiary denitrification with methanol in an upflow biofilter. In: *Proceedings IWA Conference on Biofilm Systems*, New York.
- Howell, J.A. and Atkinson, B. (1976) Sloughing of microbial film in trickling filters. *Wat. Res.*, **10**, 307-315.
- Iliuta, I., Iliuta, M.C. and Thyron, F.C. (1998) Gas-liquid mass transfer in trickle-bed reactors: gas-side mass transfer. *Chem. Eng. Technol.*, **20**, 589-595.
- Indrani, A.V. and Vangheluwe, H.L. (1998) *WEST++*, Transformation of a given PDE to a DAE using the orthogonal collocation method on finite elements. Internal Report, BIOMATH, Ghent University, Ghent.
- Jacquet, P. (1999) *Een globale kostenfunctie voor tuning en evaluatie van op respirometrie gebaseerde controle algoritmen voor actiefslibprocessen*. MSc Thesis, Faculty of Agricultural and Applied Biological Sciences, Ghent University, Ghent.
- Janning, K.F., Mesterton, K. and Harremoës, P. (1997) Hydrolysis and degradation of filtrated organic particulates in a biofilm reactor under anoxic and aerobic conditions. *Wat. Sci. Tech.*, **36**(1), 279-286.
- Janssen M., Hopkins L.N., Petersen B. and Vanrolleghem P.A. (2000) Reduction of an activated sludge process model to facilitate controller tuning. In: *Proceedings of the 14<sup>th</sup> European Simulation Multiconference*. Society for Computer Simulation International (SCS), Ghent, Belgium, May 23-26 2000.

- Jensen, M.S., Revsbech, N.P. and Nielsen, L.P. (1993) Microscale distribution of nitrification activity in sediment determined with a shielded microsensor for nitrate. *Appl. Env. Microbiol.*, **59**, 3287-3296.
- Jeppsson, U. (1996) *Modelling aspects of wastewater treatment processes*. PhD Thesis, Department of industrial and electrical engineering and automation, Lund Institute of Technology, Lund, Sweden.
- Khlebnikov, A., Samb, F. and Péringer, P. (1998) Use of a dynamic gassing-out method for activity and oxygen diffusion coefficient estimation in biofilms. *Wat. Sci. Tech.*, **37**(4-5), 171-175.
- Kissel, J.C., McCarty, P.L. and Street, R.L. (1984) Numerical simulation of mixed-culture biofilm. *J. Environ. Eng.*, **110**, 393-412.
- LaMotta, E.J. (1976) Internal diffusion and reaction in biological films. *Environ. Sci. Technol.*, **10**, 765-769.
- Lawrence, J.R., Korber, D.R., Hoyle, B.D., Costerton, J.W. and Caldwell, D.E. (1991) Optical sectioning of microbial biofilms. *J. Bacteriol.*, **173**, 6558-6567.
- Lazlo, J.A. and Silman, R.W. (1993) Cellular automata simulations of fungal growth on solid substrates. *Biotech. Adv.*, **11**, 621-633.
- Lens, P., Massone, A., Rozzi, A. and Verstraete, W. (1995a) Effect of sulfate concentration and scraping on aerobic fixed biofilm reactors. *Wat. Res.*, **29**, 857-870.
- Lens, P.N., De Poorter, M.P., Cronenberg, C.C. and Verstraete, W. (1995b) Sulfate reducing and methane producing bacteria in aerobic wastewater treatment systems. *Wat. Res.*, **29**, 871-880.
- Levenspiel, O. (1972) *Chemical reactor engineering. Second edition*. Wiley, New York.
- Lewandowski, Z., Altobelli, S.A. and Fukushima, E. (1993) NMR and microelectrode studies of hydrodynamics and kinetics in biofilm. *Biotechnol. Prog.*, **9**, 40-45.
- Lewandowski, Z. and Stoodley, P. (1995) Flow induced vibrations, drag force, and pressure drop in conduits covered with biofilm. *Wat. Sci. Tech.*, **32**(8), 19-26.
- Lewandowski, Z., Stoodley, P. and Altobelli, S. (1995) Experimental and conceptual studies on mass transport in biofilms. *Wat. Sci. Tech.*, **30**(1), 153-162.
- Lewandowski, Z., Stoodley, P., Altobelli, S. and Fukushima, E. (1994) Hydrodynamics and kinetics in biofilm systems - Recent advances and new problems. *Wat. Sci. Tech.*, **29**(10-11), 223-229.
- Livingston, A.G. and Chase, H.A. (1989) Modeling phenol degradation in a fluidized-bed reactor. *AIChE Journal*, **35**, 1980-1992.
- Logan, B.E. (1993) Oxygen transfer in trickling filters. *J. Environ. Eng.*, **119**, 1059-1076.
- Mackay, D. and Paterson, S. (1982) Fugacity revisited. *Environ. Sci. Technol.*, **16**, 654-660.
- Meirlaen, J., Huyghebaert, B., Sforzi, F., Benedetti, L. and Vanrolleghem, P.A. (2001) Fast, simultaneous simulation of the integrated urban wastewater system using mechanistic surrogate models. *Wat. Sci. Tech.*, **43**(7), 301-310.
- Melcer, H., Parker, W.J. and Rittmann, B.E. (1995) Modeling of volatile organic contaminants in trickling filter systems. *Wat. Sci. Tech.*, **30**(1), 95-104.
- Metcalf & Eddy, I. (1991) *Wastewater engineering. Treatment, disposal and reuse*. McGraw-Hill, New York.
- Mohammed, M.N., Lawrence, J.R. and Robarts, R.D. (1998) Phosphorus limitation of heterotrophic biofilms from the Fraser river, British Columbia, and the effect of pulp mill effluent. *Microbial Ecology*, **36**, 121-130.

- Morgenroth, E., van Loosdrecht, M.C.M. and Wanner, O. (2000) Biofilm models for the practitioner. *Wat. Sci. Tech.*, **41**(4-5), 509-512.
- Mueller, J.A., Paquin, J.L. and Famularo, J. (1980) Nitrification in rotating biological contactors. *J. Water Pollut. Control Fed.*, **52**, 688-710.
- Münch, E.v., Barr, K., Watts, S. and Keller, J. (2000) Suspended carrier technology allows upgrading high-rate activated sludge plants for nitrogen removal via process intensification. *Wat. Sci. Tech.*, **41**(4-5), 5-12.
- Namkung, E. and Rittmann, B.E. (1987) Modeling bisubstrate removal by biofilms. *Biotechnol. Bioeng.*, **29**, 269-278.
- Nelder J.A. and Mead R. (1964) A simplex method for function minimization. *Comp. J.*, **7**, 308-313.
- Nielsen, P.H. (1996) Adsorption of ammonium to activated sludge. *Wat. Res.*, **30**, 762-764.
- Noguera, D.R., Okabe, S. and Picioreanu, C. (1999) Biofilm modeling: present status and future directions. *Wat. Sci. Tech.*, **39**(7), 273-278.
- Noorman, H.J., Luijkx, G.C.A., Luyben, K.C.A.M. and Heijnen, J.J. (1992) Modeling and experimental validation of carbon dioxide evolution in alkalophilic cultures. *Biotechnol. Bioeng.*, **39**, 1069-1079.
- Perry, R.H. and Chilton, C.H. (1974) *Chemical engineers's handbook*. Mc-Graw-Hill, London.
- Petersen, B. (1999) *Wastewater and sludge characterisation - sensitivity study*. Internal Report, EPAS NV, Ghent, Belgium.
- Petersen, B. (2000) *Calibration, identifiability and optimal experimental design of activated sludge models*. PhD Thesis, Faculty of Agricultural and Applied Biological Sciences, Ghent University, Ghent.
- Petersen B., Gernaey K., Henze M. and Vanrolleghem P.A. (2001) Evaluation of an ASM1 model calibration procedure on a municipal-industrial wastewater treatment plant. *J. Hydroinformatics* (in Press).
- Petersen, E.E. (1965) *Chemical reaction analysis*. Prentice-Hall, Englewood Cliffs, New Jersey.
- Peyton, B.M. and Characklis, W.G. (1993) A statistical analysis of the effect of substrate utilization and shear stress on the kinetics of biofilm detachment. *Biotechnol. Bioeng.*, **41**, 728-735.
- Picioreanu, C., van Loosdrecht, M.C.M. and Heijnen, J.J. (1998a) Mathematical modeling of biofilm structure with a hybrid differential-discrete cellular automaton approach. *Biotechnol. Bioeng.*, **58**, 101-116.
- Picioreanu, C., van Loosdrecht, M.C.M. and Heijnen, J.J. (1998b) A new combined differential-discrete cellular automaton proach for biofilm modeling: Application for growth in gel beads. *Biotechnol. Bioeng.*, **57**, 718-731.
- Rauch, W., Aalderink, H., Krebs, K., Schilling, W. and Vanrolleghem, P.A. (1998) Requirements for integrated wastewater models driven by receiving water objectives. *Wat. Sci. Tech.*, **38**(11), 97-104.
- Rauch, W., Vanhooren, H. and Vanrolleghem, P.A. (1999) A simplified mixed-culture biofilm model. *Wat. Res.*, **33**, 2148-2162.
- Rauch W. and Vanrolleghem P.A. (1998) Modelling benthic activity in shallow eutrophic rivers. *Wat. Sci. Tech.*, **37**(3), 129-137.
- Reichert P., Borchardt D., Henze M., Rauch W., Shanahan P., and Somlyody L., Vanrolleghem P. (2001) River water quality model No. 1 (RWQM1). Scientific and Technical Report No. 12., IWA Publishing, London, UK.

- Reilly, P.M. and Patino-Leal, H. (1981) A Bayesian study of error-in-variables models. *Technometrics*, **23**, 221-231.
- Riefler, R.G., Ahlfeld, D.P. and Smets, B.F. (1998) Respirometric assay for biofilm kinetics estimation: parameter identifiability and retrievability. *Biotechnol. Bioeng.*, **57**, 35-45.
- Rittmann, B.E. (1982) The effect of shear stress on biofilm loss rate. *Biotechnol. Bioeng.*, **24**, 501-506.
- Rittmann, B.E. and Brunner, C.W. (1984) The nonsteady-state-biofilm process for advanced organics removal. *J. Water Pollut. Control Fed.*, **56**, 874-880.
- Rittmann, B.E., Crawford, L., Tuck, C.K. and Namkung, E. (1986) In situ determination of kinetic parameters for biofilms: isolation and characterization of oligotrophic biofilms. *Biotechnol. Bioeng.*, **28**, 1753-1760.
- Rittmann, B.E. and Manem, J.A. (1992) Development and experimental evaluation of a steady-state, multispecies biofilm model. *Biotechnol. Bioeng.*, **39**, 914-922.
- Rittmann, B.E. and McCarty, P.L. (1980a) Evaluation of steady-state-biofilm kinetics. *Biotechnol. Bioeng.*, **22**, 2359-2372.
- Rittmann, B.E. and McCarty, P.L. (1980b) Model of steady-state-biofilm kinetics. *Biotechnol. Bioeng.*, **22**, 2343-2357.
- Rousseau D., Verdonck F., Moerman O., Carrette R., Thoeye C., Meirlaen J. and Vanrolleghem P.A. (2001) Development of a risk assessment based technique for design/retrofitting of WWTPs. *Wat. Sci. Tech.*, **43**(7), 287-294.
- Royce, P.N. (1992) Effect of changes in the pH and carbon dioxide evolution rate on the measured respiratory quotient of fermentations. *Biotechnol. Bioeng.*, **40**, 1129-1138.
- Rozzi, A. and Massone, A. (1995) Residence time distribution analysis on biofilm reactors: an overview. *Med. Fac. Landbouww. Univ. Gent*, **60**, 2143-2153.
- Rusten, B. (1994) *Results from pre-denitrification of primary effluent using a moving bed biofilm pilot-plant at Guadalix, Spain*. Report Aquateam: Norwegian Water Technology Centre A/S.
- Rusten, B., Hellstrom, B.G., Hellstrom, F., Sehested, O., Skjelfoss, E. and Svendsen, B. (2000) Pilot testing and preliminary design of moving bed biofilm reactors for nitrogen removal at the FREVAR wastewater treatment plant. *Wat. Sci. Tech.*, **41**(4-5), 13-20.
- Rusten, B., Siljudalen, J.G. and Nordeidet, B. (1994) Upgrading to nitrogen removal with the KMT moving bed biofilm process. *Wat. Sci. Tech.*, **29**(12), 185-195.
- Saez, P.B. and Rittmann, B.E. (1992) Accurate pseudoanalytical solution for steady-state biofilms. *Biotechnol. Bioeng.*, **39**, 790-793.
- Siegrist, H. and Gujer, W. (1985) Mass transfer mechanisms in a heterotrophic biofilm. *Wat. Res.*, **19**, 1369-1378.
- Smets, B.F., Riefler, R.G., Lendenmann, U. and Spain, J.C. (1999) Kinetic analysis of simultaneous 2,4-dinitrotoluene and 6-DNT biodegradation in an aerobic fluidized-bed biofilm reactor. *Biotechnol. Bioeng.*, **63**, 642-653.
- Spanjers, H. and Vanrolleghem, P.A. (1995) Respirometry as a tool for rapid characterisation of wastewater and activated sludge. *Wat. Sci. Tech.*, **31**, 105-114.
- Spanjers, H., Vanrolleghem, P.A., Nguyen, K., Vanhooren, H. and Patry, G.G. (1998) Towards a simulation benchmark for evaluating respirometry-based control strategies. *Wat. Sci. Tech.*, **37**(12), 219-226.
- Spanjers, H., Vanrolleghem, P.A., Olsson, G. and Dold, P.L. (1996) *Respirometry in control of the activate sludge process: principles*. International Association on Water Quality, London.

- Spérandio, M. and Paul, E. (1997) Determination of carbon dioxide evolution rate using on-line gas analysis during dynamic biodegradation experiments. *Biotechnol. Bioeng.*, **53**, 243-252.
- Stevenson, L.H. (1978) A case for bacterial dormancy in aquatic systems. *Microbial Ecology*, **4**, 127-133.
- Stewart, P.S. (1993) A model for biofilm detachment. *Biotechnol. Bioeng.*, **41**, 111-117.
- Stewart, P.S. (1998) A review of experimental measurements of effective diffusive permeabilities and effective diffusion coefficients in biofilms. *Biotechnol. Bioeng.*, **59**, 261-272.
- Stoodley, P., de Beer, D. and Lewandowski, Z. (1994) Liquid flow in biofilm systems. *Appl. Env. Microbiol.*, **60**, 2711-2716.
- Struijs, J. (1996) *SimpleTreat 3.0: a model to predict the distribution and elimination of chemicals by sewage treatment plants*. Report nr. 719101025. National Institute of Public Health and Environmental Protection (RIVM), Bilthoven, The Netherlands.
- Takács, I., Patry, G.G. and Nolasco, D. (1991) A dynamic model of the clarification-thickening process. *Wat. Res.*, **25**, 1263-1271.
- Takors, R., Wiechert, W. and Weuster-Botz, D. (1997) Experimental design for the identification of macrokinetic models and model discrimination. *Biotechnol. Bioeng.*, **56**, 564-576.
- Tanuma, R., Shimizu, O., Takeda, K. and Tanji, N. (1981) Dissolved oxygen control using aeration exhaust gas. *Wat. Sci. Tech.*, **13**, 183-188.
- Tijhuis, L., van Loosdrecht, M.C.M. and Heijnen, J.J. (1994) Formation and growth of heterotrophic aerobic biofilms on small suspended particles in airlift reactors. *Biotechnol. Bioeng.*, **44**, 595-608.
- Tremblay, N. (2000) *Evaluation de la nitrification dans un biofiltre*. Rapport de Stage, Faculty of Agricultural and Applied Biological Sciences, Ghent University, Ghent.
- Trulear, M.G. and Characklis, W.G. (1982) Dynamics of biofilm processes. *J. Water Pollut. Control Fed.*, **54**, 1288-1301.
- Trybal, R.E. (1980) *Mass transfer operations*. McGraw-Hill, New York.
- Turakhia, M.H., Cooksey, K.E. and Characklis, W.G. (1983) Influence of a Ca-specific chelant on biofilm removal. *Appl. Env. Microbiol.*, **46**, 1236-1238.
- van der Meent, D. (1993) *SIMPLEBOX: a generic multimedia fate evaluation model*. Report nr. 672720001, National Institute of Public Health and Environmental Protection (RIVM), Bilthoven, The Netherlands.
- van Loosdrecht, M.C.M., Eikelboom, D., Gjaltema, A., Mulder, A., Tijhuis, L. and Heijnen, J.J. (1995) Biofilm structures. *Wat. Sci. Tech.*, **32**(8), 35-43.
- van Loosdrecht, M.C.M., Picioreanu, C. and Heijnen, J.J. (1997) A more unifying hypothesis for biofilm structures. *FEMS Microbiol. Ecol.*, **24**, 185-186.
- Van Vooren, L., Lessard, P., Ottoy, J.P. and Vanrolleghem, P.A. (1999) pH buffer capacity based monitoring of algal wastewater treatment. *Environ. Tech.*, **20**, 547-561.
- Vangheluwe, H.L., Claeys, F. and Vansteenkiste, G.C. (1998) The WEST++ wastewater treatment plant modelling and simulation environment. In: *10th European Simulation Symposium*, (Eds: Bergiela, A. and Kerckhoffs, E.) Society for Computer Simulation (SCS), Nottingham, UK.
- Vangheluwe, H.L. (2000). *Multi-Formalism Modelling and Simulation*. PhD Thesis, Faculty of Sciences. Ghent University. Ghent.
- Vanhooren, H. and Nguyen, K. (1996) *Development of a simulation protocol for evaluation of respirometry-based control strategies*. Report University of Gent and University of Ottawa.

- Vanrolleghem, P.A. and Gillot, S. (2001) Robustness and economic measured as control benchmark performance criteria. *Wat. Sci. Tech.* (in Press).
- Vanrolleghem, P.A., Jeppsson, U., Carstensen, J., Carlsson, B. and Olsson, G. (1996) Integration of WWT plant design and operation - A systematic approach using cost functions. *Wat. Sci. Tech.*, **34**(3-4), 159-171.
- Vanrolleghem, P.A., Kong, Z., Rombouts, G. and Verstraete, W. (1994) An on-line respirographic biosensor for the characterization of load and toxicity of wastewaters. *J. Chem. Technol. Biotech.*, **59**, 321-333.
- Vanrolleghem, P.A. and Van Daele, M. (1994) Optimal experimental design for structure characterization of biodegradation models: on-line implementation in a respirographic biosensor. *Wat. Sci. Tech.*, **30**(4), 243-253.
- Verbrugge, T. (1999) *Meting en dynamische modellering van het gedrag van micropolluenten in een trickling filter*. MSc Thesis, Faculty of Agricultural and Applied Biological Sciences, Ghent University, Ghent.
- Wanner, O. (1995) New experimental findings and biofilm modelling concepts. *Wat. Sci. Tech.*, **32**(8), 133-140.
- Wanner, O. and Gujer, W. (1986) A multispecies biofilm model. *Biotechnol. Bioeng.*, **28**, 314-328.
- Wanner, O. and Reichert, P. (1996) Mathematical modeling of mixed-culture biofilms. *Biotechnol. Bioeng.*, **49**, 172-184.
- Welander, U., Henrysson, T. and Welander, T. (1997) Nitrification of landfill leachate using suspended-carrier biofilm technology. *Wat. Res.*, **31**, 2351-2355.
- Welander, U., Henrysson, T. and Welander, T. (1998) Biological nitrogen removal from municipal landfill leachate in a pilot-scale suspended carrier biofilm process. *Wat. Res.*, **32**, 1564-1570.
- Wik, T. and Breitholtz C. (1996) Steady-state solutions of a two-species biofilm problem. *Biotechnol. Bioeng.*, **50**, 675-686.
- Wik, T. (1999) *On modeling the dynamics of fixed biofilm reactors*. PhD Thesis, Control Engineering Department - Department of Signals and Systems, Chalmers University of Technology, Göteborg, Sweden.
- Williamson, K. and McCarty, P.L. (1976) A model of substrate utilization by bacterial films. *J. Water Pollut. Control Fed.*, **48**, 9-24.
- Wimpenny, J.W.T. and Colasanti, R. (1997) A unifying hypothesis for the structure of microbial biofilms based on cellular automaton models. *FEMS Microbiol. Ecol.*, **22**, 1-16.
- Wolfram, S. (1984) Cellular automata as models of complexity. *Nature*, **311**, 419-424.
- Xia, F., Beyenal, H. and Lewandowski, Z. (1998) An electrochemical technique to measure local flow velocity in biofilms. *Wat. Res.*, **32**, 3631-3636.
- Yang, S. and Lewandowski, Z. (1995) Measurement of local mass transfer coefficients in biofilms. *Biotechnol. Bioeng.*, **48**, 737-744.
- Yegneswaran, P.K., Gray, M.R. and Thompson, B.G. (1990) Kinetics of CO<sub>2</sub> hydration in fermentors: pH and pressure effects. *Biotechnol. Bioeng.*, **36**, 92-96.
- Yuan, Z., Keller, J. and Lant, P. (2001) Optimization and control of nitrogen removal activated sludge processes: a review of recent developments. In: *Focus on Biotechnology. Vol 3: Biotechnology for the Environment*, Kluwer Academic Publishers, Dordrecht, The Netherlands.
- Zhang, M., Tay, J., Qian, Y. and Gu, X. (1998) Coke plant wastewater treatment by fixed biofilm system for COD and NH<sub>3</sub>-N removal. *Wat. Res.*, **32**, 519-527.

- Zhang, S. and Huck, P.M. (1996) Parameter estimation for biofilm processes in biological water treatment. *Wat. Res.*, **30**, 456-464.
- Zhang, T.C. and Bishop, P.L. (1994a) Density, porosity, and pore structure of biofilms. *Wat. Res.*, **28**, 2267-2277.
- Zhang, T.C. and Bishop, P.L. (1994b) Evaluation of tortuosity factors and effective diffusivities in biofilms. *Wat. Res.*, **28**, 2279-2287.

# Notation

---

$A$	area [ $L^2$ ]
$A_{electrode}$	the active surface of the micro-electrode [ $L^2$ ]
$A_F$	biofilm surface area [ $L^2$ ]
$a_{substr}$	specific surface of the substratum [ $L^2$ ]
$b_{(j)}$	specific decay rate of biomass (species $j$ ) [ $T^{-1}$ ]
$B_A$	hydraulic surface loading rate [ $L T^{-1}$ ]
$bCOD$	biodegradable chemical oxygen demand
$BOD$	biological oxygen demand
$B_V$	volumetric loading rate [ $M L^{-3}T^{-1}$ ]
$B_X$	sludge loading rate [ $M M^{-1}T^{-1}$ ]
$d$	thickness of a bulk liquid layer on top of the biofilm [ $L$ ]
$C_G$	molar concentration in the gas phase [ $mol L^{-3}$ ]
$C_L^{(sat)}$	molar (saturation) concentration in the liquid phase [ $mol L^{-3}$ ]
$COD$	chemical oxygen demand
$D_{(i)}$	diffusion coefficient of substrate ( $i$ ) in water [ $L^2 T^{-1}$ ]
$D_{f,(i)}$	(effective) diffusion coefficient of substrate ( $i$ ) in the biofilm [ $L^2 T^{-1}$ ]
$F$	Faraday constant ( $kC mol^{-1}$ )
$f_e$	local erosion or biofilm loss frequency
$F_e$	total biomass loss frequency
$f_c$	fraction of filter filled with carrier material
$f_j$	fraction of species $j$ in the total microbial mass
$(1 - f_d)$	fraction of the microbial mass that gives rise to inert particulates when decaying
$f_g$	fraction of filter pores filled with air
$f_l$	fraction of filter pores filled with water
$f_p$	fraction of inert material in biomass [ $M M^{-1}$ ]
$h$	mass transfer coefficient in the biofilm boundary layer [ $L T^{-1}$ or $T^{-1}$ ]
$H$	Henry's law constant ( $atm^{-1}M$ )
$i_{C,(i)}$	organic carbon concentration relative to the COD concentration of substrate ( $i$ ) [ $M M^{-1}$ ]
$i_X$	ammonium fraction in biomass [ $M M^{-1}$ ]
$I$	limiting current (A)
$J$	total transport in the biofilm [ $M L^{-2}T^{-1}$ ]
$J_B$	advective transport in the bulk liquid phase [ $M L^{-3}T^{-1}$ ]
$k$	reaction rate coefficient
$k_{at}$	attachment rate coefficient [ $M T^{-1}$ ]
$k_d$	rate of detachment [ $M T^{-1}$ ]
$k_{dt}$	detachment rate coefficient [ $M T^{-1}$ or (-)]
$k_{end}$	reaction rate for endogeneous metabolism [ $T^{-1}$ ]
$k_{gl}$	mass transfer coefficient for the gas and liquid interface [ $L T^{-1}$ ]
$k_h$	hydrolysis rate of hydrolysable substrate [ $T^{-1}$ ]
$k_r$	hydrolysis rate of hydrolysable soluble substrate [ $T^{-1}$ ]

$k_{0v}$	zero-order volumetric substrate consumption rate in the biofilm [ $M L^{-3}T^{-1}$ ]
$k_{0s}$	zero-order reaction rate, based on the surface area of a cylindrical pore in a biofilm [ $M L^{-2}T^{-1}$ ]
$k_{1/2a}$	half-order reaction rate, based on the total biofilm surface area [ $M^{1/2} L^{-1/2}T^{-1}$ ]
$K$	chemical equilibrium constant
$K_L a$	mass transfer coefficient between liquid phase and gas phase [ $T^{-1}$ ]
$K_b$	double 1 <sup>st</sup> order biodegradation rate constant [ $L^3 M^{-1}T^{-1}$ ]
$K_{S,(i)}$	half-saturation coefficient of substrate ( $i$ ) [ $M L^{-3}$ ]
$K_{ow}$	octanol-water partitioning constant,
$L$	biofilm thickness [L]
$M_{Fj}$	mass of a particulate component $j$ in the biofilm [M]
$M_{Oj}$	mass of a particulate component $j$ in the bulk liquid [M]
$M_j$	total mass of particulate substrate $j$ [M]
$M_{substr}$	total mass of substratum [M]
$MW$	molecular weight [ $M mol^{-3}$ ]
$n$	order of reaction
$n_e$	mols of transferred electrons in reaction
$n_p$	number of pores per surface area of biofilm
$n_x$	number of particulate components
$N_{int,(i)}$	mass flux of substrate ( $i$ ) through the liquid-biofilm interface [ $M L^{-2}T^{-1}$ ]
$N_s$	flux of VOC due to stripping from the liquid phase to the gas phase [ $M L^{-3}T^{-1}$ ]
$N_{tot}$	total transport flux over a cross section of a cylindrical pore in a biofilm [ $M L^{-2}T^{-1}$ ]
$N_{0,tot}$	total transport through the entrance of a cylindrical pore in a biofilm [ $M L^{-2}T^{-1}$ ]
$NO$	nitrate nitrogen
$q_m$	maximal specific substrate consumption rate [ $T^{-1}$ ]
$Q$	flow rate [ $L^3 T^{-1}$ ]
$Q_G$	gas flow rate ( $m^3/h$ )
$Q_L$	liquid flow rate ( $m^3/h$ )
$r_{(ij)}$	volumetric reaction rate (for the species $j$ with respect to the substrate $i$ ) [ $M L^{-3}T^{-1}$ ]
$r_{B(ij)}$	volumetric reaction rate (for the species $j$ with respect to the substrate $i$ ) with respect to the bulk volume [ $M L^{-3}T^{-1}$ ]
$r_{end}$	volumetric reaction rate for endogenous metabolism [ $M L^{-3}T^{-1}$ ]
$r_s$	reaction rate per unit of surface area [ $M L^{-2}T^{-1}$ ]
$r_{u(i)}$	volumetric reaction rate in the upper part of the biofilm [ $M L^{-3}T^{-1}$ ]
$r_{l(i)}$	volumetric reaction rate in the lower part of the biofilm [ $M L^{-3}T^{-1}$ ]
$r_{S,(i)}$	reaction rate of substrate ( $i$ ) in the biofilm [ $M L^{-3}T^{-1}$ ]
$r_{X,(j)}$	reaction rate of biomass species ( $j$ ) in the biofilm [ $M L^{-3}T^{-1}$ ]
$r_{\epsilon_l}$	rate of change of the liquid volume fraction in the biofilm [ $T^{-1}$ ]
$R$	radius of an idealised cylindrical pore in a biofilm [L]
$S_{(i)}$	concentration of substrate ( $i$ ) [ $M L^{-3}$ ]
$S_{0(i)}$	concentration of substrate ( $i$ ) in the bulk liquid phase [ $M L^{-3}$ ]
$S^*_{(i)}$	concentration of substrate ( $i$ ) at the liquid-biofilm interface [ $M L^{-3}$ ]
$S_{Ess,(i)}$	concentration of the $i^{\text{th}}$ not-essential but growth stimulating substrate [ $M L^{-3}$ ]
$S_{Sit,(i)}$	concentration of the $i^{\text{th}}$ essential substrate or nutrient [ $M L^{-3}$ ]

$S_{ea}$	concentration of electron acceptor [ $M L^{-3}$ ]
$S_{ed}$	concentration of electron donor [ $M L^{-3}$ ]
$S_{min}$	minimal substrate concentration that can sustain viable biofilm growth [ $M L^{-3}$ ]
SS	suspended solids concentration [ $M L^{-3}$ ]
$t$	time [T]
TKN	total Kjeldahl nitrogen
$(T)SS$	(total) suspended solids
$u$	flow velocity [ $L T^{-1}$ ]
$u_{at}$	advective velocity of the liquid-biofilm interface due to attachment [ $L T^{-1}$ ]
$u_{dt}$	advective velocity of the liquid-biofilm interface due to detachment [ $L T^{-1}$ ]
$u_F$	advective velocity of the liquid-biofilm interface not including attachment and detachment [ $L T^{-1}$ ]
$u_L$	advective velocity of the liquid-biofilm interface including attachment and detachment [ $L T^{-1}$ ]
$V_{max}$	maximal oxygen uptake rate ( $g O_2 m^{-3}d^{-1}$ )
$V$	volume [ $L^3$ ]
$V_G$	volume of the gas phase [ $L^3$ ]
$V_L$	volume of the liquid phase [ $L^3$ ]
$W$	covariance matrix of the experimental data
$X_{(j)}$	concentration of particulate component ( $j$ ) or biomass [ $M L^{-3}$ ]
$X_{(j)}^*$	concentration of particulate component ( $j$ ) or biomass at the liquid-biofilm interface [ $M L^{-3}$ ]
$X_F$	concentration of bacterial species in the biofilm as biomass per total biofilm volume [ $ML^{-3}$ ]
$X_B$	concentration of bacterial species in the biofilm as biomass per bulk liquid volume [ $ML^{-3}$ ]
$X_{max}$	the maximal attainable biomass concentration [ $M L^{-3}$ ]
$y_{model}$	vector of model predicted values.
$y_{obs}$	vector of observations
$Y_{(i)}$	yield coefficient for growth on substrate ( $i$ ) [ $M M^{-1}$ ]
$z_{(i)}$	penetration depth of substrate ( $i$ ) [L]

### Greek

$\beta_{(i)}$	active biofilm fraction or dimensionless penetration depth of substrate ( $i$ )
$\delta_{bl}$	thickness of the boundary layer [L]
$\varepsilon_l$	liquid volume fraction in the biofilm
$\varepsilon_{sj}$	volume fraction in the biofilm occupied by particles of type $j$
$\mu_{(j)}$	specific growth rate of biomass ( $j$ ) [ $T^{-1}$ ]
$\mu_{max}$	maximal specific growth rate [ $T^{-1}$ ]
$\nu_{(ij)}$	stoichiometric coefficient (for the species $j$ with respect to the substrate $i$ )
$\rho_{(j)}$	density of the particles (of type $j$ ) in the biofilm [ $M L^{-3}$ ]
$\rho_m$	mean biofilm density [ $M L^{-3}$ ]
$\sigma$	measure for the biofilm strength
$\tau$	fluid shear stress
$\varphi$	mass transport term [ $M T^{-1}$ ]
$\phi_H$	active fraction of aerobic heterotrophic degradation

$\phi_H^*$	active fraction of anoxic heterotrophic degradation
$\phi_H$	active fraction of autotrophic degradation
$\omega$	limiting substrate concentration [M L <sup>-3</sup> ]
$\zeta$	space coordinate in the biofilm perpendicular to the substratum surface [L]

**Subscripts**

<i>ast</i>	suffix denotes activated sludge tank
<i>clar</i>	suffix denotes clarifier
<i>at</i>	suffix denotes attachment
<i>dt</i>	suffix denotes detachment
<i>e</i>	suffix denotes effluent
<i>ed</i>	electron donor
<i>ea</i>	electron acceptor
<i>i</i>	suffix denotes substrates
<i>j</i>	suffix denotes species
<i>w</i>	suffix denotes waste
<i>B</i>	bulk liquid
<i>F</i>	biofilm
<i>G</i>	gas phase
<i>L</i>	liquid phase
<i>u</i>	upper layer of the biofilm
<i>l</i>	lower layer of the biofilm
<i>s</i>	solid phase
<i>A</i>	Autotrophic bacteria
<i>H</i>	Heterotrophic bacteria
<i>I</i>	inert substance
<i>P</i>	inert substance resulting from cell decay
<i>S</i>	biodegradable substance
<i>NH</i>	ammonium
<i>ND</i>	organic nitrogen
<i>NO</i>	nitrate

# Summary

---

In the literature review in chapter 2 of this thesis, it became clear that a whole range of biofilm models is available, ranging from relatively simple one-dimensional models to comprehensive 3D descriptions of the biofilm structure evolving in time and space. Each of these models has its value and its possible applications. The complexity of the model that is selected should however be relevant for the application it is used for. High complexity models clearly have the advantage of including a lot of the available knowledge about biofilm processes. However, they are too detailed for use in full-scale on-line applications. On the other hand, low complexity models are not able to describe all the dynamics of the system, since they are simplified.

In this thesis, a model was developed and applied that attempts to be a complexity compromise. The main advantage of the model is the avoidance of the numerical solution of partial differential equations. This was obtained by decoupling the calculation of substrate diffusion into the biofilm from the computation of the conversion processes in the biofilm by using a two-step procedure that resulted in a fairly simple model structure. This aspect makes the proposed model an attractive alternative to the existing complex models when emphasis is put more on fast predictions of system behaviour than on detailed understanding. Furthermore, it makes it more suitable for applications that combine it with widely accepted models for other wastewater treatment unit processes. Despite its relatively simple structure, the model is still able to calculate the conversion rates of processes in the biofilm performed by different biomass species. It can thus be used to describe processes occurring at different depths of the biofilm.

In addition to the original model, two extended model descriptions were developed. In the original model, an instantaneous steady-state profile for soluble substrates in the biofilm is used and soluble components emerging from conversion processes inside the film are assumed to be subject of immediate out-diffusion at the surface of the biofilm. Together, these assumptions are in principle violating the mass balances during dynamic simulation. The first extension of the model accounts for the possible accumulation of soluble components in the biofilm and it therefore guarantees a correct determination of the penetration depths. In the second extension, the introduction of an external diffusional resistance was studied. Although considered not important in biofilm systems with a relatively turbulent liquid phase, it should be included in some cases where this resistance may be of big importance for the correctness of the model predictions.

In order to successfully use the developed models in applications for process optimisation, the simulation tool WEST (Hemmis NV, Kortrijk, Belgium) was optimised and used. One of the key features of WEST is its possibility to integrate multiple processes. For example, in this work, WEST was used to study treatment systems where conversion processes are simultaneously taking place in a biofilm and in the liquid phase. To enable this coupling, a powerful model base structure was developed. This model base is aimed at maximal re-use of existing knowledge and is therefore structured hierarchically. Thanks to this structure, new models can be implemented using the compact matrix format (Petersen, 1965) selected by the IWA task group on mathematical modelling (Henze *et al.*, 1987).

In order to test the simplified mixed-culture biofilm model, a pilot-scale trickling filter was designed and built. The filter was constructed to allow the collection of experimental data on a fully characterised biofilm system. Non-invasive on-line monitoring of the filter was possible by means of an electronic balance and off-gas analysis measurement equipment that continuously monitored the off-gas of the filter for  $\text{CO}_2$  and  $\text{O}_2$ . To characterise the filter's hydrodynamic behaviour, two tracer tests were conducted in the absence and, later on, in the presence of biofilm. If a biofilm was present a CSBR (continuously stirred biofilm reactor) approach (Wik and Breitholtz, 1996) was found necessary to yield an adequate description of the hydraulics. For a good description of the pilot-scale filter, 7 CSBR's in series were needed.

This pilot-scale filter was first subjected to a pollutant load shift. During this experiment, it could be concluded that, following a drop in the loading of the filter system, the nitrification capacity increased due to a higher availability of oxygen for this process. The simplified mixed-culture biofilm model introduced in this thesis was used to model the load shift. To be able to use the off-gas measurement results in the model calibration, this model was further extended with a submodel for the description of the production and gas-liquid exchange of carbon dioxide. This submodel was based on the model developed by Spérandio and Paul (1997). The extended biofilm model was subsequently integrated in the CSBR model. The start-up of nitrification could be followed using the model, provided the decay coefficient for autotrophic biomass was sufficiently low to assure a certain amount of autotrophs to stay in the system during the high loading period.

In a second test, it was attempted to induce denitrification at high organic loading rates by adding nitrate. This test showed that denitrification could be induced and that this way a considerably increased substrate removal capacity could be obtained. During the addition of nitrate, the production of  $\text{CO}_2$  from bioconversion processes increased, while no decrease of the  $\text{O}_2$  consumption was noticed. For the modelling of this experiment, the model calibrated to describe the load shift was used. The model performed very well and furthermore it was possible to obtain a value for the effective diffusion constant of readily biodegradable substrate in the biofilm.

A second series of model applications was performed at an industrial wastewater treatment plant. More specifically, the performance in COD removal and the stripping of volatile organic compounds (VOC's) of the trickling filters were studied. To this end, the process characteristics of the filters were quantified by means of a 5-day intensive measurement campaign with the use of an on-line respirometer complemented with on-line off-gas analysis.

The model was calibrated and could follow the measured effluent and off-gas concentrations very closely. In contrast to what was initially expected, the  $\text{O}_2$  and  $\text{CO}_2$  measurements revealed that the system was not always oxygen limited. In the model calibration the use of a very low value of the diffusion constant for readily biodegradable substrate was found to be the best means for describing the observed data. As only a very limited amount of phosphate was available in the influent, the effect of the dosing of phosphate on the trickling filter system was studied too. It could be noticed that the net phosphate uptake by the biofilm was very limited under normal operating conditions, since the added phosphate dosing did not bring along better treatment efficiency. However, shortly after the start of the dosing, a clear effect on the off-gas measurement results and the sludge production was

seen. This effect damped out in some days time and could only be modelled by temporarily increasing the yield coefficient for heterotrophic growth, making the oxygen consumption to decrease and the sludge production to increase.

Next to high COD and nitrogen concentrations, a considerable part of the chemicals in the industrial wastewater was highly volatile. Therefore, the VOC removal in the industrial wastewater treatment plant was monitored and modelled. The capital and operating cost and the efficiency of a new off-gas treatment facility are dependent on the air flow to be treated and the concentration of VOC's. Two mathematical models describing the stripping of VOC's were developed. The first model was a model for the fate of individual chemicals that was built on the basis of the *SimpleBox* approach (van der Meent, 1993) combined with the existing steady-state biofilm diffusion/biodegradation model of Melcer *et al.* (1995). The second model was a simple dynamic model that was built on the basis of the results obtained with the steady-state model. These results showed that biodegradation and adsorption to suspended solids could be neglected for the volatile organics under study and that the model could further be simplified to a simple mass balance model for the gas-liquid exchange of the VOC's. Scenario analysis with the dynamic model showed that stripping was virtually independent of the applied air flow rate. The simulations, however, revealed that immediately after changes in air flow rate, quite high flux and concentration peaks were to be expected. Using the findings of this research, the air flow rate and the air flow pattern through the wastewater treatment plant were changed so as to obtain a lower overall air flow combined with a relatively constant VOC concentration. This way, the investment costs for the off-gas treatment facility could be substantially lowered.

As a last part of this thesis, suspended-carrier biofilm systems were studied. Qualitative steady-state analysis of these systems already showed its interesting features (Yuan *et al.*, 2001). In this thesis, these features were validated quantitatively based on a simulation benchmark for activated sludge treatment systems (Spanjers *et al.*, 1998; Copp, 2001). This simulation benchmark had to be extended with the biofilm model introduced before. The Activated Sludge Model No 1 (Henze *et al.*, 1987) had to be coupled to the simplified mixed-culture biofilm model. It should be noted that no simulation studies were found in literature describing the simultaneous degradation of organic matter in a biofilm and in the liquid phase by activated sludge flocs. This study can therefore be considered as the first application of such integrated modelling and simulation approach. Two types of attached growth processes were studied. In the first, carriers were only added to the aerobic zone of the plant in order to enhance nitrification in a relatively small volume and at low sludge retention times. It was noticed that the longer retention time of the biomass growing on the carriers stimulates nitrification. However, a rather strong dependency of the performance on the dissolved oxygen concentration was obvious, causing the required aeration energy to increase significantly. Moreover, the overall effluent quality that was achieved was worse than that of the benchmark plant.

The second plant layout studied included the addition of carriers to all zones of the plant. The simulation results again showed that the retention times of heterotrophs and autotrophs are different and that autotrophs are mainly present in the zones of the plant where they are needed. Also, the leakage of readily biodegradable material from the anoxic zone to the aerobic zone of the plant was limited. This entails that full nitrogen removal can be accomplished at lower C/N ratios in the influent. However, it was found that this plant layout is even more sensitive to the dissolved oxygen concentration in the aerobic zone. Therefore, in practical applications, the oxygen control needs to be

rather stringent and enough blower capacity should be available to preserve a sufficiently high oxygen concentration at high loading rates.

The above applications of a relatively simple mixed-culture biofilm model and a mass balance model for the gas-liquid exchange of volatile organics show that it is not always needed or even desired to use a complex model in order to obtain valuable simulation results. It can be concluded that, whenever using models for process optimisation, a compromise should be sought between the complexity needed to describe the dynamics of the process, the data available for calibration and the application the model is used for.

# Samenvatting

---

In het literatuuroverzicht in hoofdstuk 2 van deze thesis werd duidelijk dat een groot aantal biofilmmodellen beschikbaar is. Het gaat hierbij over relatief eenvoudige eendimensionele modellen enerzijds tot ingewikkelde driedimensionele beschrijvingen van de evolutie van de biofilmstructuur in plaats en tijd anderzijds. Elk van deze modellen heeft zijn toepassingsdomein. Bij het gebruik van een model moet de complexiteit ervan echter steeds relevant zijn voor de toepassing. Modellen met een hoge complexiteit hebben het voordeel een groot deel van de beschikbare kennis over biofilms te integreren. Ze zijn echter te gedetailleerd voor succesvolle on-line toepassingen op volle schaal. Aan de andere kant moet het duidelijk zijn dat modellen met een kleinere complexiteit niet alle dynamica van een biofilmsysteem kunnen beschrijven, precies door hun vereenvoudigingen.

In deze thesis werd daarom een model ontwikkeld dat een compromis poogt te zijn op het vlak van de complexiteit. Het grootste voordeel van het voorgestelde model is het vermijden van de numerieke integratie van partiële differentiaalvergelijkingen. Dit kon verwezenlijkt worden door het ontkoppelen van de berekening van de substraatdiffusie in de biofilm en de uitwerking van de conversieprocessen. Dit resulteerde in een procedure met twee stappen en een relatief eenvoudige modelstructuur. Door deze eenvoud is het model een aantrekkelijk alternatief voor de reeds bestaande complexe modelbeschrijvingen in gevallen waar meer nadruk wordt gelegd op een snelle voorspelling van de systeemdynamica dan op het verwerven van gedetailleerde kennis. Het model is verder ook meer geschikt voor toepassingen waarin het gekoppeld wordt met modellen die algemeen als standaard aanvaard worden bij het modelleren van andere eenheidsprocessen in de waterzuivering. Hierbij moet echter benadrukt worden dat, ondanks de eenvoudige modelstructuur, het steeds mogelijk blijft om conversiesnelheden te berekenen van processen die gebeuren door verschillende biomassagroepen in de biofilm. Het model kan dus nog steeds processen beschrijven die in verschillende lagen van de biofilm plaatsvinden.

Als aanvulling voor het oorspronkelijke model werden twee uitgebreide modellen ontwikkeld. In het oorspronkelijke model werd immers uitgegaan van een ogenblikkelijk *steady-state* concentratieprofiel voor opgeloste substraten in de biofilm. Ook werd aangenomen dat opgeloste componenten die het resultaat zijn van conversies in de biofilm onmiddellijk naar de vloeistoffase getransporteerd worden. Deze twee aannames schenden in principe de massabalans bij dynamische simulaties. De eerste uitbreiding van het model was er dan ook op gericht rekening te houden met de accumulatie van opgeloste substraten in de biofilm. Hierdoor werd een meer correcte berekening van de penetratiedieptes van deze substraten bekomen. Bij de tweede uitbreiding werd een externe diffusieweerstand aan het model toegevoegd. Wanneer de vloeistoffase in een biofilmreactor voldoende turbulent is, wordt deze weerstand over het algemeen overbodig geacht. In bepaalde gevallen is het echter wel noodzakelijk om correcte modelvoorspellingen te kunnen garanderen.

De simulatieomgeving WEST (Hemmis NV, Kortrijk, Belgium) werd in deze thesis gebruikt en geoptimaliseerd voor het aanwenden van de ontwikkelde modellen. Een van de belangrijke eigenschappen van WEST is de mogelijkheid om verschillende processen te integreren in een enkele simulatie. In dit werk werd WEST bijvoorbeeld gebruikt om zuiveringssystemen te beschrijven waar

conversies zowel in een biofilm als in de waterfase plaatsvinden. Om deze koppeling mogelijk te maken, moest een goede structuur voor de modellenbank uitgewerkt worden. Deze modellenbank is verder specifiek gericht op een maximaal hergebruik van bestaande kennis en heeft daarom een hiërarchische structuur. Mede door deze structuur is het mogelijk modellen te implementeren in de compacte matrixvorm (Petersen, 1965) die geselecteerd werd door de *task group on mathematical modelling* van de IWA (Henze *et al.*, 1987).

Om het vereenvoudigde biofilmmodel te kunnen testen werd een trickling filter gebouwd op pilotschaal. De filter werd zo geconstrueerd dat het verzamelen van gegevens mogelijk zou zijn op een volledig gekarakteriseerd biofilmsysteem. Onder andere werden *on-line* meetgegevens verzameld van de afvalgasconcentraties van CO<sub>2</sub> en O<sub>2</sub>. Verder werd ook het gewicht van de filter continu opgevolgd. Om het hydrodynamisch gedrag van de filter te karakteriseren, werden twee tracerstudies uitgevoerd. Hieruit bleek dat, na het ontwikkelen van de biofilm, de hydrodynamica het best beschreven kon worden met een CSBR (*continuously stirred biofilm reactor*) aanpak waarbij een biofilmcompartiment telkens gekoppeld wordt aan een ideaal gemengde reactor. 7 reactoren in serie waren nodig voor een goede beschrijving van de pilotschaal trickling filter.

De filter werd eerst onderworpen aan een plotse verlaging van de pollutenvracht. Tijdens dit experiment werd duidelijk dat de nitrificatiecapaciteit van de filter als gevolg hiervan steeg door een betere beschikbaarheid van zuurstof voor de autotrofe biomassa. Het vereenvoudigde biofilmmodel werd gebruikt om het experiment te beschrijven. Daartoe diende het model verder uitgebreid te worden met een model voor de productie en de gas-vloeistof overdracht van CO<sub>2</sub> om de resultaten van de *on-line* afgasanalyse te kunnen gebruiken voor het kalibreren van het model. Dit modelonderdeel werd gebaseerd op het model van Spérandio en Paul (1997). Na deze uitbreiding werd het model geïmplementeerd in het CSBR-model dat de hydrodynamica van de filter beschreef. Het opstarten van de nitrificatie werd goed beschreven op voorwaarde dat de afstervingscoëfficiënt van de autotrofe biomassa voldoende laag gehouden werd om aldus een hoeveelheid autotrofe biomassa in het systeem te bewaren gedurende de periode met hoge belasting.

Een tweede experiment was erop gericht denitrificatie te induceren in de filter door het toedienen van een extra hoeveelheid nitraat bij hoge belasting. Er bleek inderdaad dat hierdoor een grotere degradatiecapaciteit bereikt kon worden. Tijdens de toediening van nitraat verhoogde de productie van CO<sub>2</sub> uit bioconversie, terwijl geen merkbare daling van de zuurstofconsumptie opgemerkt werd. Het voor de belastingsverlaging gekalibreerde model kon ook met goed resultaat voor de beschrijving van dit experiment gebruikt worden. Het was verder mogelijk om een waarde voor de diffusieconstante van snel afbreekbaar substraat in de biofilm te bepalen.

Een tweede reeks modeltoepassingen gebeurde op een industriële waterzuiveringsinstallatie. Hier werd de COD verwijdering en het strippen van vluchtige organische componenten (VOC's) in de trickling filters onderzocht. De karakteristieken van het proces werden daarom bepaald door middel van een vijf dagen durende meetcampagne met het gebruik van een *on-line* respirometer samen met afvalgasanalyse.

Het vereenvoudigde biofilmmodel werd succesvol gekalibreerd met deze gegevens. In tegenstelling tot wat initieel was verwacht, brachten de zuurstof- en koolstofdioxidemetingen aan het licht dat het

systeem niet altijd zuurstofgelimiteerd was. Tijdens de kalibratie werd het gebruik van een zeer lage diffusieconstante voor snel afbreekbaar substraat geïdentificeerd als de beste methode om de metingen te beschrijven met het model. Verder was slechts een zeer kleine hoeveelheid fosfaat aanwezig in het influent. De mogelijkheden voor het doseren van fosfaat aan het systeem werden dan ook onderzocht. Het bleek dat de netto-opname van fosfaat in de biofilm klein was. Het toedienen van fosfaat verbeterde de COD verwijderingsefficiëntie van de filters immers niet merkbaar. Toch werd na de start van de toediening een plots effect op de afvalgasconcentraties en op de slibproductie opgemerkt. Dit effect ebde na enkele dagen weg en kon enkel beschreven worden door het tijdelijk verhogen van de slibopbrengstcoëfficiënt voor heterotrofe groei. Hierdoor verlaagde de zuurstofconsumptie maar steeg de slibproductie.

Naast de hoge COD en stikstofconcentraties, was een vrij groot deel van de chemicaliën in het industriële afvalwater sterk vluchtig. Daarom werd de verwijdering van VOC's in het trickling filtersysteem gemeten en gemodelleerd. De investering en de werkingskosten voor een afvalgasbehandeling zijn immers sterk afhankelijk van het gasdebiet en van de concentraties aan VOC's die behandeld moeten worden. Twee modellen werden ontwikkeld om de verwijdering van VOC's te beschrijven. Enerzijds werd een *steady-state* model ontwikkeld dat gebaseerd was op de *SimpleBox* aanpak (van der Meent, 1993) gecombineerd met het bestaande *steady-state* biofilm diffusie- en biodegradatiemodel van Melcer *et al.* (1995). Gebaseerd op de bevindingen verkregen door het toepassen van dit model, werd een eenvoudig dynamisch massabalansmodel opgesteld. Het bleek immers mogelijk te zijn de biodegradatie en de adsorptie aan gesuspendeerd materiaal van deze vluchtige organische componenten te verwaarlozen. Scenario-analyses met dit model toonden aan dat de efficiëntie van de VOC verwijdering nauwelijks afhankelijk was van het luchtdebiet. Anderzijds waren vrij hoge concentratie- en belastingspieken te verwachten indien een variabel luchtdebiet gebruikt zou worden. Gebaseerd op deze bevindingen werd het luchtdebiet en daarbij de volledige afzuiginstallatie aangepast. Hierdoor werd over het algemeen een lager luchtdebiet en een meer constante VOC concentratie naar de behandelingsinstallatie bekomen. Op deze manier konden de investeringskosten voor de afvalgasbehandeling vrij sterk gedrukt worden.

Als laatste onderdeel van deze thesis werden biofilmsystemen met dragers in suspensie onderzocht. Een kwalitatieve analyse van dergelijke systemen had reeds enkele interessante eigenschappen aangeduid (Yuan *et al.*, 2001). In deze thesis werden deze eigenschappen verder onderzocht met een simulatieprotocol voor de evaluatie van actief slibsystemen (Spanjers *et al.*, 1998; Copp, 2001). Daartoe werd dit protocol uitgebreid met het ontwikkelde vereenvoudigde biofilmmodel. In de literatuur werden geen toepassingen gevonden van een dergelijke aanpak voor de modellering en de simulatie van de gecombineerde biodegradatie van pollutanten in een biofilm en in actiefslibvlokken. Deze studie kan dan ook beschouwd worden als de eerste toepassing van zo'n geïntegreerde aanpak. Twee procesuitvoeringen werden onderzocht. In de eerste uitvoering werden enkel dragers toegevoegd in de aërobe zone om op die manier nitrificatie op gang te brengen in relatief kleine volumes en bij korte slibverblijftijden. De langere verblijftijd van de autotrofe biomassa op de dragers bracht inderdaad nitrificatie met zich mee. De performantie van het systeem bleek echter sterk afhankelijk te zijn van de concentratie aan opgeloste zuurstof. Hierdoor steeg de energiebehoefte voor de aëratie vrij sterk. Over het algemeen was de effluentkwaliteit echter toch slechter dan bij de basisuitvoering van het simulatieprotocol.

Wanneer dragers in alle zones van de installatie ingebracht werden, kon wel een betere effluentkwaliteit behaald worden. In dit systeem waren de slibverblijftijden van de heterotrofe en de autotrofe biomassa verschillend. De autotrofen waren ook enkel in belangrijke mate aanwezig in de zones waar ze nodig waren voor de nitrificatie. Verder werd ook een verminderde overdracht van afbreekbare COD van de anoxische naar de aërobe zone vastgesteld. Hierdoor kon een meer volledige stikstofverwijdering bekomen worden bij een nochtans vrij lage C/N verhouding van het influent. Deze uitvoering bleek echter nog meer gevoelig te zijn voor de zuurstofconcentratie in de aërobe zones van het systeem. Hierdoor moet in praktijktoepassingen zeker gezorgd worden voor een strikte controle van de zuurstofconcentratie en moet voldoende capaciteit aanwezig zijn om ook bij piekbelastingen een hoge zuurstofconcentratie te kunnen garanderen.

De hierboven beschreven toepassingen van het ontwikkelde biofilmmodel en het massabalansmodel voor de beschrijving van de verwijdering van vluchtige bestanddelen tonen aan dat het niet steeds noodzakelijk en gewenst is om een complex model te gebruiken voor het verkrijgen van bruikbare simulatieresultaten. Als algemeen besluit kan gesteld worden dat wanneer een model gebruikt wordt in een context van procesoptimalisatie, een compromis gevonden moet worden tussen de complexiteit die nodig is om het dynamisch gedrag van het proces te beschrijven, de aanwezige gegevens om het model te kalibreren en de uiteindelijke toepassing waarvoor het model gebruikt wordt.

# Curriculum Vitae

---

## Personalia

Henk Vanhooren  
Ieper, 10/09/1974  
Gehuwd met Els Verbeke

Aaigemstraat 55  
9000 Gent  
09.221.48.20  
henk.vanhooren@biomath.rug.ac.be

## Opleiding

1986-1992 Secundair onderwijs, Latijn-Wiskunde, Sint-Vincentiuscollege Ieper  
1992-1997 Bio-ingenieur in de Milieutechnologie, Universiteit Gent  
Scriptie: Optimalisatie van actiefslib- en biofilmwaterzuiveringsinstallaties door modellering en simulatie; begeleider Prof. Dr. ir. P.A. Vanrolleghem  
1997-2001 Doctoraat in de toegepaste biologische wetenschappen: Milieutechnologie  
Proefschrift: Modelbouw voor optimalisatie van biofilmwaterzuiveringsprocessen: een complexiteitscompromis

## Bijkomende opleidingen

Postacademische opleiding: Instituut voor Permanente Vorming, Universiteit Gent

2000 Moderne regel- en automatiseringstechnieken

In het kader van mijn doctoraatsopleiding volgde ik de volgende vakken

1998 Numerieke algoritmen met computertoepassingen: G. Vanden Berghe

1999 Identificatie van systemen: R. De Keyser

1999 Ethics and scientific research, an introduction: D. Holemans

2000 Adaptieve en zelflerende regelsystemen: R. De Keyser

2001 Bioinformatics, an introduction: W. Van Criekinge

## Werkervaring

1997-2000 Aspirant van het Fonds voor Wetenschappelijk Onderzoek - Vlaanderen  
Het onderzoek ter voorbereiding van het doctoraat werd uitgevoerd aan de Vakgroep Toegepaste wiskunde, Biometrie en Procesregeling (BIOMATH) van de Universiteit Gent

Vanaf 2001 EPAS NV (Eco Process Assistance), Venecoweg 19, B-9810 Nazareth  
(h.vanhooren@epas.be): Procesingenieur voor het implementeren van automatisatie- en controletoeepassingen in de milieusector

## Conferenties en studiedagen

### Congressen en symposia

- |                 |  |
|-----------------|--|
| 25-26 sept 1997 | 11th Forum for Applied Biotechnology, Gent (B)   |
| 8-10 okt 1998   | International Conference on Microbial Ecology of Biofilms, Lake Bluff, Illinois (USA)                                      |
| 22-23 sept 1999 | 13th Forum for Applied Biotechnology, Gent (B)   |
| 17-20 okt 1999  | 4th IWA Conference on Biofilm Systems, New York (USA)  |
| 10-12 apr 2000  | 4th International Symposium on Environmental Biotechnology: ISEB 4, Noordwijkerhout (NL)                                   |
| 3-7 jul 2000    | 1st World Water Congress of the International Water Association: Paris 2000, Paris (F)                                     |
| 18-20 sept 2000 | 5th International Symposium on Systems Analysis and Computing in Water Quality Management: WATERMATEX, Gent (B)            |
| 17-18 nov 2000  | Invited lecture at the Biofilm Club meeting: "Biofilms: Modelling and Analysis of Structure and Activity", Wageningen (NL) |
| 3-7 jun 2001    | 1st IWA (International Water Association) Conference on Instrumentation, Control and Automation: ICA 2001, Malmö (S)       |

### COST working group meetings

- |                |   |
|----------------|---|
| 10-12 ma 1999  | "Innovative Tools in Wastewater Treatment: LCA", Grenoble (F) |
| 27-29 aug 1998 | "Wastewater Treatment Benchmarking", Lund (S)                 |
| 23-24 apr 1998 | "Integrated Wastewater Management", Ljubljana (SL)            |
| 10-12 dec 1997 | "Characterisation of Wastewater", Amersfoort (NL)             |

### Nederlandse Vereniging voor Waterbeheer, NVA

- |             |   |
|-------------|---|
| 14 nov 1997 | Symposium/Workshop: "Modelleren in de toekomst"                     |
| 14 nov 1996 | Symposium: "Modelleren van rwzi's, de wereld rondom het IAWQ-model" |

## Publicaties

- Vanhooren, H. and Nguyen, K. (1996) Development of a simulation protocol for evaluation of respirometry-based control strategies. Report University of Gent and University of Ottawa.
- Spanjers, H., Vanrolleghem, P., Nguyen, K., Vanhooren, H. and Patry, G.G. (1997) Towards a simulation-benchmark for evaluating respirometry-based control strategies. In: Proceedings 7th international workshop on instrumentation, control and automation of water and wastewater treatment and transport systems. Brighton, UK, July 6-9 1997.
- Vanrolleghem, P.A., De Clercq, B. and Vanhooren, H. (1997) RWZI Modellen: Basisprincipes. In: Postacademisch Onderwijs Cursus Regelen en Besturen van Actief-slibinstallaties. Delft, The Netherlands, October 28-30 1997.
- Vanhooren, H., Vanrolleghem, P., De Clercq, B. and Coen, F. (1997) Hydraulics as a starting point for the calibration of wastewater treatment plants. In: Cost-682 Working Group Meeting. Amersfoort, The Netherlands, December 10-11 1997.

- Vanrolleghem, P.A., Benchiheb, Y. and Vanhooren, H. (1998) Economic optimisation of wastewater treatment plant design and operation through modelling. In: Proceedings Waste Decision '98. Narbonne, France, February 10-11 1998.
- Rauch, W., Vanhooren, H. and Vanrolleghem, P. (1999) A simplified mixed-culture biofilm model. *Water Research*, **33**, 2148-2162.
- Alex, J., Beteau, J.F., Hellinga, C., Jeppsson, U., Marsili-Libelli, S., Pons, M.N., Spanjers, H., Vanhooren, H. (1999) Benchmark for evaluating control strategies in wastewater treatment plants. In: Proceedings ECC99, Karlsruhe, Germany, August 31 - September 3 1999.
- Vanhooren, H., Boeije, G., Accoe, F. and Vanrolleghem, P.A. (1999) Non-invasive and continuous monitoring of a pilot-scale trickling filter: weight, off-gas and hydraulic characterization. In: Proceedings of the IAWQ Conference on Biofilm Systems. New York, USA, October 17-20 1999.
- Vanhooren, H., Boeije, G., Accoe, F. and Vanrolleghem, P.A. (1999) Non-invasive and continuous monitoring of a pilot-scale trickling filter: Weight, off-gas and hydraulic characterization. *Med. Fac. Landbouww. Univ. Gent*, **64**(5), 217-221.
- Boeije, G., Vanhooren, H. and Vanrolleghem, P.A. (2000) Development of a steady-state chemical fate model for trickling filters supported by measurements in a pilot-scale plant. *Environmental Science and Technology*, **34**, 4413-4417.
- Vanhooren, H., Demey, D., Vannijvel, I. and Vanrolleghem, P.A. (2000) Monitoring and modelling an industrial trickling filter using on-line off-gas analysis and respirometry. *Water Science and Technology*, **41**(12), 139-148.
- Vanhooren, H., Vanderhaegen, B. and Vanrolleghem, P.A. (2000) Modelling stripping of volatile organics in an industrial trickling filter system. In: Proceedings 1st World Congress of the International Water Association. Paris, France, July 3-7 2000.
- Vanhooren, H., De Pauw, D., Gillot, S., Demey, D., Vannijvel, I. and Vanrolleghem, P.A. (2000) Adequate complexity for biofilm systems modelling. *Med. Fac. Landbouww. Univ. Gent*, **65**(4), 39-44.
- Vanhooren, H., Verbrugge, T., Boeije, G., Demey, D. and Vanrolleghem, P.A. (2001) Adequate model complexity for scenario analysis of VOC stripping in a trickling filter. *Water Science and Technology*. **43**(7), 29-38.
- Vanhooren, H., Yuan, Z. and Vanrolleghem, P.A. (2001) Performance evaluation of nitrogen removal suspended-carrier biofilm systems using dynamic simulation. In: Proceedings 3rd IWA International Specialized Conference on Microorganisms in Activated Sludge and Biofilm Processes. Rome, Italy, June 13-15 2001.

## Vrijetijdsbesteding

- In 1996 behaalde ik mijn diploma trompet en instrumentaal ensemble met grote onderscheiding. Ook nu nog ben ik een actief trompettist, ik speel als 1e en solo-trompet in verschillende ensembles.
- Sinds enkele jaren volg ik regelmatig danscursussen, van klassiek tot latijns-amerikaans.

- Tijdens mijn studententijd had ik een druk socio-cultureel leven. Daar heb ik een hoop communicatieve vaardigheden aan overgehouden. Team-work en time-management zijn voor mij dus geen vage begrippen.
  - ✓ Vanaf 1991 tot 1998 was ik actief als monitor in de jeugdbeweging KSA. In 1992 behaalde ik het attest van monitor in het jeugdwerk. In 1996 kwam daar het attest van instructeur bovenop. Vanaf 1993 tot en met 1996 was ik hoofdmonitor van de KSA-afdeling in Kemmel met ongeveer 160 leden.
  - ✓ Vanaf 1992 was ik lid van de studentenvereniging KUC (Katholiek Universitair Centrum). In het academiejaar 1994-'95 was ik vice-preses en coördinator van de introductiedagen voor eerstejaarsstudenten.

## **Interesses**

- Milieuproblematiek in het algemeen, vooral waterbeheer en ruimtelijke ordening
- Mathematische modellering van biologische systemen om die systemen beter te begrijpen en te doorgronden en om een beter procesdesign en een betere procesvoering en -controle mogelijk te maken
- Kunst en muziek, zowel actief (instrument bespelen, dans, ...) als passief (concerten, opera, ...)